Design Rules for Characteristics of Heat Flow in Welding on Thick Plates using Asymptotics and Blending

by

Ying Wang

A thesis submitted in partial fulfillment of the requirements for the degree of

Doctor of Philosophy

in

Materials Engineering

Department of Chemical and Materials Engineering
University of Alberta

Abstract

The problem of moving heat sources is central to a wide range of industrial fields, including welding, surface heat treatment and additive manufacturing. However, there are few general and easily applicable solutions to predict critical thermal characteristics of heat flow such as the cooling rate and dimensions of the heat affected zone, which have a decisive effect on the metallurgical and mechanical properties of the workpiece. Design rules in the form of asymptotes and correction factors have been obtained for the first time to predict critical thermal characteristics in welding and other moving heat source processes.

Design rules are presented for 13 critical thermal characteristics based on Rosenthal's point heat source model. Related thermal characteristics are: maximum isotherm width and its location, leading and trailing lengths of isotherm, centerline heating rate and cooling rate, peak temperature and its gradient at the maximum width, aspect ratio of isotherms, melting efficiency, cooling time from 800°C to 500°C, solidification time, thickness of the heat affected zone, and modification criteria to account for the effect of joint preparation. Dimensional analysis suggests that all dimensionless characteristics depend on a single dimensionless parameter that captures all possible cases. This dimensionless number is the Rykalin number (Ry), except for the dimensionless maximum temperature, which depends on the distance from the centerline. Ry can be interpreted as a Peclet number, and it reflects the effect of advection relative to conduction. The obtained design rules are accurate to within 7% of the exact analytical solutions.

Although the point heat source model captures isotherm characteristics for all

values of Ry, it cannot provide reliable estimations in the vicinity of the heat source because of the singularity at the origin, which is intrinsic to the assumption of point heat source. For the first time, design rules for the peak temperature and the penetration depth have been obtained based on a moving Gaussian surface heat source on a thick substrate. In dimensionless form, peak temperature depends on the dimensionless distribution parameter. Penetration depth depends on two dimensionless quantities: Ry and the dimensionless heat distribution parameter. Conventional blending techniques are extended to multiple dimensionless groups. Correction factors associated with the heat distribution parameter have been developed to improve the accuracy of point heat source solutions. The maximum error of estimation from the exact solution is below 0.19% for the peak temperature and 9.7% for the penetration depth. Prediction of peak temperature and the penetration depth is accurate within the range of validity of the assumptions in the moving Gaussian surface source model. The obtained design rules have an excellent agreement with published measurements and simulation data for various processes and material systems.

This research has addressed the problems associated with applying sophisticated numerical simulations that are often challenging for practitioners to use and empirical expressions that can hardly be generalized to other processes due to the lack of theoretical foundation. Derived from the first principles, the obtained design rules are general and capable of reflecting quantitative effects of operating parameters (e.g., power and velocity of the heat source) on resulting thermal characteristics. They are simple enough to be calculated with a calculator or spreadsheet and can also verify numerical models. The systematic methodology of asymptotic analysis and blending can be extended to other disciplines besides welding.

Preface

All materials included in this thesis comprise the candidate's research under the supervision of Prof. Patricio Mendez. This research has been funded by Natural Sciences and Engineering Research Council (NSERC) of Canada (NSERC RGPIN 4892 and NSERC RGPIN-2019-05981), Canadian Welding Bureau (CWB) Welding Foundation/NSERC (NSERC CRDPJ 544277-19), Apollo Clad/NSERC (NSERC CRDPJ 462535-13) and Group Six Technologies/MITACS (MI MA IT09825).

Chapter 1 is an introduction of this research based on two written materials authored or co-authored by the candidate. The first is a paper published as Mendez, P.F., Lu, Y. and Wang, Y., 2018. Scaling analysis of a moving point heat source in steady-state on a semi-infinite solid. Journal of Heat Transfer, 140(8). The second document is the candidacy report submitted to the Associate Chair-Graduate Program for which the candidate was the primary author.

Chapter 2 is a peer-reviewed conference paper published as Wang, Y., Lu, Y., Grams, M., Cesaro, A. and Mendez, P.F., 2019. Asymptotics and Blending in the Modeling of Welding. Mathematical Modelling of Weld Phenomena 12, pp.907-32. Yi Lu contributed to the development of methodology (section of 5.4, 5.5 and 5.6), and he was listed as one of the coauthors for his contributions. Mitchell Grams wrote Case C as one of the case studies to support the applicability of the proposed methodology to predict the thermal stress field produced by a moving point heat source. Alejandro Hintze Cesaro wrote Case B as one of the case studies where the proposed methodology of asymptotes and blending was applied to predict the maximum hardness in the heat affected zone (HAZ). Dr. Patricio Mendez was the

supervisory author.

Chapter 3 is published as Wang, Y., Lu, Y. and Mendez, P.F., 2019. Scaling expressions of characteristic values for a moving point heat source in steady state on a semi-infinite solid. International Journal of Heat and Mass Transfer, 135, pp.1118-1129. Yi Lu contributed to the conceptualization and the generation of schematics and curves for correction factors. He is a co-author of the paper for his contributions. Prof. Patricio Mendez was the supervisory author.

Chapter 4 is submitted to the International Journal of Heat and Mass Transfer as Wang, Y., Lu, Y., and Mendez, P.F., 2021. Prediction of Peak Temperature under a Moving Gaussian Surface Heat Source. Yi Lu contributed to the conceptualization and mathematical formulation, and therefore he was listed as a co-author. Prof. Patricio Mendez was the supervisory author.

Chapter 5 is submitted to the International Journal of Thermal Sciences as Wang, Y., and Mendez, P.F., 2021. Penetration Depth under a Moving Gaussian Surface Heat Source on a Thick Substrate. Prof. Patricio Mendez was the supervisory author.

Prof. Patricio Mendez provided valuable advice for the methodology, validation and data interpretation. He proofread all publications before submission. Because the format of this thesis is paper-based, chapters 2 to chapter 5 consist of published papers as listed above.

To Louie, I am forever grateful for your unconditional love, support, and company. I am so fortunate to have experienced this unique period of life with you.

Acknowledgements

Throughout the research and writing process of this thesis, I have received a great deal of help, inspiration and support.

I would like first to thank Dr. Patricio Mendez. The story of my Ph.D. started from the summer internship in 2014 when I spent two months in the Canadian Centre for Welding and Joining (CCWJ) working on moving heat source problems. Since then, Patricio has been my advisor in research, a mentor in coursework, and a role model in life. As an advisor, Patricio is willing to do whatever it takes to open doors and expand possibilities for me. I learned a lot, not only about an elegant approach to solve engineering problems, but also how to think deep and independently to apply what we know to change the world. We have spent much time together working on papers, solving equations and preparing for heat transfer class. He is the main reason for me to land a career in engineering after graduation. It is my privilege and fortunate to have this opportunity to pursue my Ph.D. degree under his supervision.

I would like to acknowledge our lovely lab members and CCWJ alumni for their collaboration and support. I would particularly like to single out our alumni Dr. Gentry Wood (star engineer in Apollo Clad) and Steven Borle (Materials/Welding engineer in Group Six Technologies). I have known Gentry since my internship in 2014, and since then, he is my motivator and role model. Working with Gentry is never boring. He has the magic to explain abstract concepts and theory in an intuitively understanding way. As one of the first Chinese students in the lab, English was challenging for me at the beginning of my stay, but I can always get help from Gentry. In 2017, through a Mitacs awarded program, I spent six months in Group Six

Technologies applying my Ph.D. work to improve the productivity in laser cladding processes. This internship would never work out without Steven. As a mentor, Steven is always patient and helpful. Special thanks to Goetz, Mitch, Ale, Dima, Syed, Vivek and my Chinese friends Jason, Huan, Fan and Zhaoyang for a cherished time we are working together in CCWJ and happy group events that have rest my mind outside of research. I am so fortunate to have been surrounded by a group of smart and kind people. The vocation and working ethics of all of you always motivate me to strive to be better.

Last but not least, biggest thanks to my loving partner, Louie, to whom this work is dedicated to. You are always there for me. Five years of my Ph.D. life have shaped me into a better person. All my self-improvements would not have been the same without your understanding and encouragement.

Table of Contents

1 Introduction **1**

1.1 Background 1

1.2 Literature Review 4

1.3 Methodology of Asymptotic Analysis and Blending 10

1.4 Objectives 16

1.5 Thesis Outline 17

References 19

2 Asymptotics and Blending in the Modeling of Welding **23**

2.1 Abstract 23

2.2 Introduction 24

2.3 MRCF: Minimal Representation and Correction Factor 27

2.3.1 Important concepts and notation in MRCF 28

2.4 Foundations of Blending Techniques 29

2.5 Development of Correction Factors 30

2.6 1D Blending 31

2.6.1 Standard 1D Blending 32

2.6.2 1D Blending of Non-Crossing Asymptotics 33

2.6.3 1D Blending of Constant Asymptotics 34

2.6.4 Asymptotes with Changes in the Sign 36

2.6.5 Addition of Intermediate Terms 37

2.6.6 An Extension of 1D Blending: Parametric 1D Blending 38

2.7 Challenges beyond 1D Blending 39
2.8 Case Studies 40
2.9 Conclusions 53
2.10 Appendix: Notation 54
References 56

3 Scaling Expressions of Characteristic Values for a Moving Point Heat Source in Steady State on a Semi-Infinite Solid 59

3.1 Abstract 59
3.2 Introduction 61
3.3 Maximum Isotherm Width $y_{\max}$ and its location $x_{\max}$ 63
3.4 Trailing Length of Isotherm x_{b} 65
3.5 Centerline Cooling Rate $\dot{T}_{\mathrm{b}}$ 66
3.6 Leading Length of Isotherm x_{f} 68
3.7 Centerline Heating Rate $\dot{T}_{\mathrm{f}}$ 70
3.8 Maximum Temperature $T_{\max}$ 71
3.9 Gradient of Maximum Temperature $dT_{\max}/dy$ 72
3.10 Aspect Ratio A_R 73
3.11 Melting Efficiency η_{m} 75
3.12 Cooling Time $t_{8/5}$ 78
3.13 Solidification Time at Centerline t_{sl} 78
3.14 Thickness of the Heat Affected Zone Δy_{HAZ} 80
3.15 Effect of Joint Preparation Geometry 81
3.16 Discussion 84
3.17 Conclusions 86
References 87

4 Prediction of Peak Temperature under a Moving Gaussian Surface Heat Source 94

4.1 Abstract . . . 94
4.2 Introduction . . . 96
4.3 Governing Equation . . . 98
4.4 Normalization and Dimensional Analysis . . . 99
4.5 Asymptotic Analysis, Blending and Correction Factors . . . 100
4.6 Scaling Analysis of Peak Temperature $T_{\max}$ . . . 102
4.7 Scaling Analysis of Maximum Distribution Parameter $\sigma_{\max}$ . . . 107
4.8 Scaling Analysis of the Location of Peak Temperature $x_{\max}$ . . . 109
4.9 Experimental Validation . . . 114
4.10 Example of Application . . . 116
4.11 Discussion . . . 118
4.12 Conclusions . . . 120
References . . . 122
4.A Derivation of Asymptotic Behaviors . . . 125
4.B Data Collected from the Literature Survey . . . 130

5 Penetration Depth under a Moving Gaussian Surface Heat Source on a Thick Substrate 131

5.1 Abstract . . . 131
5.2 Introduction . . . 133
5.3 Mathematical Formulation . . . 135
5.4 Methodology of Asymptotic Analysis and Blending . . . 136
5.4.1 Normalization . . . 137
5.4.2 Blending of Asymptotic Solutions . . . 139
5.5 Asymptotic Analysis and Blending of Maximum Isotherm Depth . . . 141
5.5.1 Asymptotic Analysis of Maximum Isotherm Depth . . . 141
5.5.2 1D blending in Contiguous Regimes . . . 142
5.5.3 Blended Equation Applicable to all Regimes . . . 145

5.6 Experimental Validation 149
5.7 Example of Application 152
5.8 Discussion 153
5.9 Conclusions 154
References 156
5.A Location of $z^*_{\max}$ in Regime V and VI 159
5.A.1 Regime VI Ry $\to 0$, $\sigma^*/\sigma^*_{\max} \to 1$ 160
5.A.2 Regime V Ry $\to \infty$, $\sigma^*/\sigma^*_{\max} \to 1$ 161
5.B Data Collected from the Literature 164

6 Conclusions and Future Work **165**
6.1 Conclusions 165
6.2 Future Work 169

Appendix A: MATLAB Codes **183**
A.1 Calculating the peak temperature induced by a moving Gaussian surface source 183
A.2 Calculating the maximum isotherm depth under a moving Gaussian surface source 186

Appendix B: Supporting figures for blending results in Chapter 3 **191**
B.1 Asymptotes, error map and correction factors for the maximum temperature at y^*_c 191
B.2 Asymptotes, error map and correction factors for the gradient of maximum temperature 195
B.3 Asymptotes, error map and correction factors for aspect ratio of isotherms 199
B.4 Asymptotes, error map and correction factors for melting efficiency . 203

List of Tables

2.1 Variables used in Chapter 2 with the units and description 54

3.1 Variables used in Chapter 3 with the units and description 60

3.2 Summary of characteristic values and correction factors for welding on thick plates 93

4.1 Variables used in Chapter 4 with the units and description 95

4.2 The laser absorptivity, heat distribution parameter, thermal properties, processing parameters and reported peak temperature used in the validation. 130

5.1 Variables used in Chapter 5 with the units and description 132

5.2 The heat source efficiency, heat distribution parameter, thermal properties, processing parameters and the maximum isotherm depth reported in the validation. 164

6.1 Summary of thermal characteristics and correction factors derived from a moving point heat source model. 168

6.2 Summary of thermal characteristics and correction factors derived from a moving Gaussian surface source model. 169

List of Figures

1.1 Point heat source moving with constant velocity on a semi-infinite solid 5

2.1 Costs of simulation, prototypes, and design rules. For the aerospace industry, a prototype is much more expensive than simulations. For welding, a prototype is often cheaper than simulations, resulting in trial-and-error approaches. Design rules are much less expensive than simulations, and should enable a design approach where it is seldom done currently. 26

2.2 Comparison between Equation 2.12 and Equation 2.13. The solid line is $u_c^*(\{\Pi\}) = 1 + \frac{1}{2}[1 + \tanh(\Pi)]$, and the dash line represents $u_c^*(\{\Pi\}) = 1 + \frac{1}{2}\left[1 + \frac{\pi}{2}\arctan\left(\frac{\pi}{2}\Pi\right)\right]$. Two constant asymptotics are 1 and 2,respectively. The center point $\Pi = 0$ and its slope is the same for both functions but the dash line is less steep than the solid line. . 36

2.3 Correction factors for maximum isotherm width $y_{\max}$ [96] 45

2.4 Characteristic hardness in HAZ as a function of cooling time between 800°C and 500°C [160]. 46

3.1 Characteristic values of isotherm $T = T_c$ for a moving point heat source on a semi-infinite solid 64

3.2 Dimensionless leading length as a function of Ry. The exact solution and the approximation of Equation 3.28 overlap within the thickness of the line. 69

3.3 Aspect ratio of the isotherm $T = T_c$ for different Ry values under a moving point heat source on a semi-infinite solid 75
3.4 Schematic of V-groove joint preparation (a), and single bevel joint preparation (b) 83

4.1 Dimensionless peak temperature T^*_{max} as a function of dimensionless heat source distribution parameter σ^*. 103
4.2 Relative error of blending for dimensionless peak temperature as a function of dimensionless heat source distribution parameter σ^* for the optimal value $n = -1.946$. The error tends to zero for both high and low σ^*. 104
4.3 Maximum error for dimensionless peak temperature as a function of blending parameter n. Minimized maximum error is 0.19% at the optimal value $n = -1.946$. 105
4.4 Correction factors to estimate peak temperature. For $\sigma^* < \sigma^*_{VI} = 0.1480$ or $\sigma^* > \sigma^*_V = 3.098$, the maximum error of directly using asymptotic is less than 10%. The correction factors cross over at $\sigma^*_c = 0.6638$. 106
4.5 Dimensionless maximum distribution parameter of the heat source as a function of T^*. 108
4.6 Correction factors to estimate the maximum distribution parameter. For $T^* < T^*_V = 0.3960$ or $T^* > T^*_{VI} = 8.994$, the maximum error of directly using simple formulas is less than 10%. The correction factors cross over at $T^*_c = 1.887$. 110
4.7 Dimensionless location of peak temperature x^*_{max} as a function of dimensionless heat source distribution parameter σ^*. 111
4.8 Relative error of blending for the location of peak temperature as a function of dimensionless heat source distribution parameter σ^* near the optimal value $n = -0.9347$. 112

4.9 Maximum error for the location of peak temperature as a function of blending parameter n. Minimized maximum error is 0.47% at the optimal value $n = -0.9347$. 113

4.10 Correction factors of two simple formulas to estimate the location of peak temperature. For $\sigma^* < \sigma^*_{\mathrm{VI}} = 0.07089$ or $\sigma^* > \sigma^*_{\mathrm{V}} = 8.532$, the maximum error of directly using simple formulas is less than 10%. The correction factors cross over at $\sigma^*_c = 0.7650$. 115

4.11 Comparison of explicit blending solution Equation 4.21 with published data for peak temperature in laser processing. 117

4.12 Plot of the integrand $\exp[f(\theta)]$ at $\sigma^* = 1000$, $x^* = -1000$, $y^* = 0$ over $[0, \frac{\pi}{2})$. $\exp[f(\theta)]$ increases with increasing θ until $\theta_{\max}$ and then decreases exponentially. Interval over $[0, \delta)$ where $\theta_{\max} \ll \delta \ll 1$, contributes the most part of the integral. 126

4.13 Plot of the integral in Equation 4.34 ($\int_0^\infty \exp\left\{-\frac{1}{2}\left[\left(\sqrt{\sigma^*}\theta\right)^2 + \frac{x^*}{\sigma^*}\right]^2\right\} d\left(\sqrt{\sigma^*}\theta\right)$) as a function of x^*/σ^*. When x^*/σ^* = -0.7650, the integral reaches its maximum of $I_m = 1.280$. 128

5.1 Dependence of dimensionless isotherm depth $z^*_{\max}$ on $\sigma^*/\sigma^*_{\max}$ in Regime II and VI. For a given Ry, $z^*_{\max}$ decreases with increasing $\sigma^*/\sigma^*_{\max}$. When $\sigma^* = 0$, $z^*_{\max}$ converges to the solution of a point heat source. The asymptote in Regime II and Regime VI shown by the dashed line and dotted line are derived from asymptotic analysis of Equation 5.12. 143

5.2 Dependence of dimensionless isotherm depth $z^*_{\max}$ on Ry in Regime V and VI. The asymptotes in Regime V and Regime VI are derived from asymptotic analysis of Equation 5.12. The exact solution and its blended counterpart are undistinguishable in this graph. 145

5.3 Error map of Equation 5.30 as a function of $\sigma^*/\sigma^*_{\max} \leq 0.9$ and Ry $\leq$ 1000. When $n_1 = -1.465$, $n_2 = -1.960$, $n_3 = -3.223$, $n_4 = -2.459$, the maximum error is below 9.7% compared to the exact analytical solution. Within area bounded by dash lines, using asymptotes only yields an error smaller than 10% compared to the analytical solution. 148

5.4 Comparison of a point heat source solution with published data for the maximum isotherm depth. 151

5.5 Validation of the blended expression for a Gaussian heat source (Equation 5.30) against published experimental data for the maximum isotherm depth. 152

B.1 Dimensionless maximum temperature as a function of y_c^* 191

B.2 Blending error for the maximum temperature as a function of y_c^* for exponents n at or near the optimal value 192

B.3 Maximum blending error for the maximum temperature as a function of blending parameter n 193

B.4 Correction factors for the maximum temperature 194

B.5 Dimensionless gradient of maximum temperature as a function of Ry 195

B.6 Blending error for the gradient of maximum temperature as a function of Ry for exponents n at or near the optimal value 196

B.7 Maximum blending error for the gradient of maximum temperature as a function of blending parameter n 197

B.8 Correction factors for the gradient of maximum temperature 198

B.9 Aspect ratio of isotherms as a function of Ry 199

B.10 Blending error for aspect ratio of isotherms as a function of Ry for exponents n at or near the optimal value 200

B.11 Maximum blending error for aspect ratio of isotherms as a function of blending parameter n 201

B.12 Correction factors for aspect ratio of isotherms 202
B.13 Melting efficiency as a function of Ry 203
B.14 Blending error for melting efficiency as a function of Ry for exponents n at or near the optimal value 204
B.15 Maximum blending error for melting efficiency as a function of blending parameter n 205
B.16 Correction factors for melting efficiency 206

Chapter 1

Introduction

1.1 Background

Welding is a common fabrication process of permanently joining two pieces of components into one and has widespread applications across several industrial sectors to make metal parts, tools, machines and equipment used in construction and manufacturing plants as a reliable and inexpensive joining method. From a microscopic point of view, welding can be defined as the processes of making atoms (or ions, molecules) from separate components close enough to share bonds under the combined action of heat and pressure, sometimes with an intermediate or filler metal[101].

Welding processes can be categorized into three types according to distinctive mechanisms, diffusion welding (diffusion), solid-state welding (plastic deformation), and liquid welding (melting). For instance, in fusion welding, one of the liquid welding processes, a fraction of base materials, edges or surfaces typically, is heated up to melting by various sources of energy. Since the emergence of welding as a manufacturing process in the late nineteenth century with the development of arc welding and oxy-fuel welding, various advanced welding methods such as electric resistance welding (ERW), shielded metal arc welding (SMAW), gas metal arc welding (GMAW), submerged arc welding (SAW), flux-cored arc welding (FCAW) have been developed.

Typical thermal cycles in welding contain several time intervals as follows. The temperature remains at the ambient temperature (or preheat) before the supply of

heat. Once the heat arrives at the point of interest, the temperature rises rapidly until it reaches the melting point of the substrate and then cools down to the initial temperature at a rate dependent on process parameters and thermal-physical properties of the substrate [101]. A large number of parameters relative to involved physics such as heat and mass transfer, fluid dynamics, electromagnetism, thermodynamics make welding very difficult to understand at an intuitive level. Practical questions about heat flows in welding are not easily answered by existing knowledge; for example, the question "what is the size of a weld by a given set of welding parameters?" is difficult to answer, even as a rough approximation. Similar questions are: "what are temperature cycles occurring during welding under given welding conditions" (have a decisive influence on the quality of weld), "what is the maximum temperature?" (important in almost all applications and materials systems). In all these cases, the answers depend on the welding conditions (typically the preheat, heat from the source, heat dissipation to the environment, the chemistry of the base material, and travel speed of the heat source). The answers are not the same for different types of welds or welding processes.

Design rules in the form of simple formula and correction factors abound in heat transfer and fluid dynamics, such as calculating stress concentration in solid mechanics and fluid dynamic drag. However, there are very few of these design rules in the field of materials processing. Current codes and standards are material-specific or process-specific. One of the most commonly used codes, American Welding Society (AWS) D1.1, was specifically developed for welded structure made from the commonly used carbon and low-alloy constructional steels[9]. One consequence is that the answers to practical questions provided by these codes or standards are difficult to be extended or synthesized into basic rules applicable for another case of different weld material despite that they all respond to very similar heat transfer phenomena. A compilation of design rules applicable to general welding conditions and materials is essential at the initial design stage to save time and effort in trial-and-error tests.

A good example of design rules is the following formula in European Union standards [18] to estimate cooling time $t_{8/5}$, which is defined as the time it takes for the weld metal to cool from 800°C to 500°C and typically used as a metric of cooling rate in the welding of steels:

$$t_{8/5} = \frac{q}{2\pi kU} \times \left(\frac{1}{T_{500} - T_0} - \frac{1}{T_{800} - T_0} \right) \tag{1.1}$$

where q is the net heat absorbed by the base material, U is the travelling speed of the heat source, k is the thermal conductivity of the substrate, and T_0 is the ambient temperature. T_{500} and T_{800} is 500°C and 800°C, respectively. Equation 1.1 is modified with the appropriate shape factors for unalloyed and low alloyed steels with a different joint preparation:

$$t_{8/5} = (6700 - 5T_0) \times \frac{q}{U} \times \left(\frac{1}{T_{500} - T_0} - \frac{1}{T_{800} - T_0} \right) \times F$$

The relationship between the welding conditions and the cooling time $t_{8/5}$ can be described in closed-form as a simple formula (Equation 1.1), which is the solution to the most idealized case and a correction factor F to capture the effects of different joint geometries. For example, $F = 1$ for a run on plate weld, and $F = 0.9$ for a butt weld [18]. The empirical term, $(6700 - 5T_0)$, is added to take account of the variations on the value of thermal conductivity with temperature. However, source of the empirical term and the applicability of Equation 1.1 are not identified in European Union standards.

The ultimate goal of this research is to develop a set of design rules in the standardized form of simple formula and correction factors that can predict (or reasonably estimate) important weld properties valid for general welding procedures with different alloys, process conditions and operating parameters. This research will significantly reduce the money and effort put in the trial and error stage and provide general guidance for the satisfactory production and control of welds.

1.2 Literature Review

Heat flow studying and modelling is essential in welding research to describe and understand the effects of welding parameters, such as preheat, heat input and travelling speed on the heat distribution, which directly impacts the properties and qualities of welds [37, 108]. There are numerous publications in the thermal modelling of welding and other manufacturing processes, such as surface heat treatment and additive manufacturing [42, 48, 73, 76, 84, 96, 100, 126, 128, 157]. Because of constraints in length, only appropriate literature where derivations, examples, and comprehensive literature surveys are treated in great detail will be briefly reviewed.

Moving Point Heat Source

Starting from the 1930s and continued to the 1960s, the theory of moving heat source model was introduced and expanded for general treatments of metals by Rosenthal [126–128], Boulton [17] and Rykalin [131], but that had been solved before in 1904 by Wilson [154] and in 1923 by Roberts [125] for the case of mass transfer. The model is illustrated in Figure 1.1 and consists of a point heat source of intensity q moving in steady state along a straight line (x-axis) with constant velocity U on the flat surface of a semi-infinite solid with constant thermophysical properties.

Assumptions

Assumptions involved in the point heat source model are an infinitesimal size of heat source, quasi-steady state, infinitely thick plate, constant travel speed and heat intensity, no change in physical state and constant thermal conductivity and diffusivity.

- Point heat source

  The temperature value is infinity as the heat is approximated as a single concentrated point on the plate surface. Rosenthal and Schmerber [129] cautioned the application of this 3D model and the obtained temperature solution for lo-

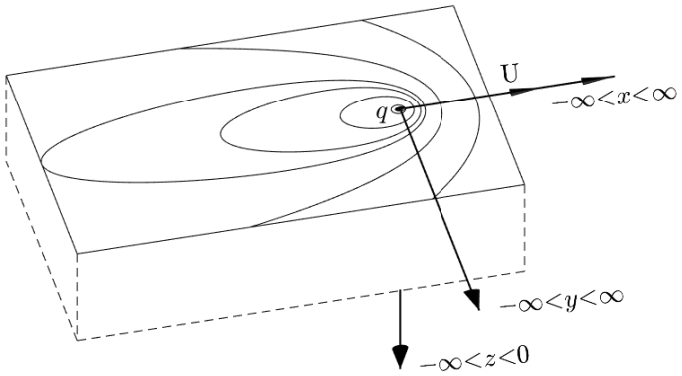

Figure 1.1: Point heat source moving with constant velocity on a semi-infinite solid

cations in the vicinity of the heat source of less than a few millimetres ($\approx$ 6 to 8 mm) based on their measurements of seven temperature isotherms in welding of mild steel with thermocouples. The singularity is not observed in practical systems, and preliminary study [36, 67] has indicated that the application of a distributed heat source can improve the accuracy of prediction for area near the heat source. A circular Gaussian distributed surface source which includes the additional parameter of heat distribution parameter σ would be used as the next step in complexity beyond a point heat source.

- Quasi-steady state

  A complete welding process can be divided into three intervals by sequence: the initial transient stage, quasi-stationary state, and the transient termination state. The quasi-steady state is a steady state condition to the moving heat source and develops quickly after the initiation and before the termination of the heat source. The time required to reach the quasi-steady state is in the order of seconds for the common arc welding processes [72, 144]. No change in the size or shape of the isotherms can be noticed if an observer stationed at the

location of the heat source. This assumption can be justified experimentally when the length of the weld is long compared to the extent of heat.

- Infinitely thick plate

  The assumption is valid for a small bead-on-weld pass deposited on thick material, such as most root pass welds, single or multipass welds with partial penetration in arc welding processes [66]. Numerical results show that the temperature distribution of the area close to the centre of the weld is determined by three-dimensional heat flow [109]. Following this work, a criterion to distinguish between thick or thin plates is proposed in [84].

- Constant travel speed and the heat intensity

  The thermal power from the heat source absorbed by the solid can be estimated based on the nominal power of the heat source and thermal efficiency. For the case of arc welding, the heat absorbed by the substrate can be estimated as $q = \eta V I$, where V and I are the voltage and current of the welding process.

- No change of physical state in the substrate

  The physical state of the base material remains solid during the processes, i.e., there is no melting of the substrate. Absorption of latent heat at the front of the weld pool and its release at the rear is not considered. For typical structural steel, the Stefan number, defined as the ratio of sensible heat to latent heat, is approximately 3 [102]. For the case of steels in typical welding conditions, it was demonstrated in [86, 147] that solidification and solid-state phase transformations cause only small departures on the prediction of maximum isotherm width.

- Adiabatic surface: no convection or radiation heat loss

  The heat dissipation on the plate surface to the external atmosphere in convection or radiation is usually considered negligible. Experimental work by

Tekriwal and Mazumder [139] estimated that the heat loss due to convection is less than 5% of the total amount of heat involved. A criterion to ignore surface heat loss within 10% error compared to Rosenthal's thin plate solution is proposed in [83].

- Constant thermal conductivity and diffusivity of the substrate

  In reality, these thermal properties vary considerably with temperature and particularly, thermal conductivity is also sensitive to the composition of the base material. A closed-form solution to the temperature distribution is difficult to obtain considering variable thermal properties with temperature. Effective values of thermal properties can be used to mitigate the influence of temperature dependence. They can be calculated as average values for both the thermal conductivity and specific heat over the range from room temperature to the melting point [129], or values of thermophysical properties that correspond to some intermediate temperature [72, 73, 139].

Model Refinement and Validation

Hess [57] proposed a modification of the cooling rate given by fitting Rosenthal's solution with the experimental measurements of the cooling curves under various welding conditions. Grosh [54] derived an analytical solution for temperature distribution of a moving point heat source on the substrate with a linear dependence of thermal properties on temperature. Adams [3] proposed an empirical relationship for centreline cooling rate and peak temperature distribution as functions of geometric, thermal and welding variables based on Rosenthal's moving point heat source model. It confirmed that the cooling rate is not sensitive to the distance from the weld centreline. Centreline cooling rate is only 5% to 10% higher than that in the weld HAZ and can be therefore treated as the representative of the cooling rate in the entire weld region [67]. The same conclusion can also be found in [61, 69]. Jackson [64]

provided an extension of Rosenthal's solution and obtained the temperature field in an infinite slab with phase changes. Myers [108] summarized a comprehensive review on Rosenthal's moving point theory and found that reasonably good predictions can be made for the width of the heat-affected zone, and trends of cooling rates can be well predicted.

Among the all the experimental validations of Rosenthal's thick solution, Christensen's work [22] was especially thorough, and validated the exact solution for the case of welding using many characteristic values in common with those presented here (experiments tested $y_{\max}$ both as width and depth, $x_{\max}$, $x_{\mathrm{f}} - x_{\mathrm{b}}$, $x_{\max} - x_{\mathrm{b}}$, $T_{\max}$, $\dot{T}_{\mathrm{b}}$) and put experimental measurements in dimensionless form to validate multiple welding processes and materials over wide ranges of heat input. The reference temperature considered was the melting temperature, which is beyond the range of validity of the model, and the results were still consistent with the model. Predictions for width, trailing length, and cooling rate are typically useful for engineering purposes, while the predictions for leading length at the melting temperature tend to be underestimated because the size of the heat source is typically larger than the leading length. An estimate of weld penetration is also typically unreliable because convection in the molten metal plays a significant role. Remarkably, Rosenthal's idealized solution was proved to be effective despite its simplicity.

Malmuth [86] presented mathematical solutions for thermal cycles and weld geometry by considering the effect of the latent heat of fusion and concluded that the latent heat has negligible effects on the maximum bead width and penetration. A similar conclusion was made in [147] by solving the free boundary problem of conduction and taking account of the emission and absorption of the latent heat. Nunes [114] proposed an extended Rosenthal weld model, taking account the effects of phase changes by thermal dipoles and circulations in the weld pool by thermal quadrupoles. The obtained temperature field may be represented approximately in multi-polar expansion form. Eagar and Tsai [36] developed a solution to the size of

weld pools induced by a travelling two-dimensional Gaussian distributed heat source on a semi-infinite plate as a function of process parameters and material properties, and the agreement with experiments was improved over the original Rosenthal model. Niles [112] reported that an increase in travel speed or current level results in an increase in melting efficiency in GTAW processes. This relationship was correlated quantitatively by Okada [115] based on Rosenthal's moving point heat source model. The maximum melting efficiency is 36.8% at high travel speeds for three-dimensional heat flow. Fuerschbach [44] proposed a dimensionless parameter that correlated well with the measured melting efficiencies and developed a simple monomial equation for melting efficiency of three-dimensional heat flow empirically, which was later adopted by DuPont [33, 34] and achieved a good representation of his experimental results, where single pass welds of 308 stainless steel were deposited on a 6.4-mm-thick A36 steel substrate. Fuerschbach [43] used dimensionless parameters (Ry number and Ch number) to relate the size of a laser weld to the net heat absorbed by the substrate with thermal properties chosen at the liquidus temperature. The proposed empirical expression achieved excellent correlation with the melting efficiency of continuous power laser welding.

Myhr and Grong [109] established dimensionless maps numerically as a general outline to predict temperature distributions of a moving heat source on plates of different thickness and thermal properties. The accuracy of the maps was tested against in situ thermocouple measurements and numerical analysis of stringer bead welds. Fuerschbach [45] used the moving point heat source model to calculate the effective values of thermal conductivity and diffusivity by least square fitting and generated useful dimensionless parameters (including the Ry number studied in this research analytically) to compare with the experimental data. The generation of dimensionless parameters is remarkable because it allows direct comparisons between experimental data collected from different welding conditions. Poorhaydari [121] modified Rosenthal's thick solution to estimate the cooling rate with a weighting factor developed

empirically from the width of the HAZ to account for the effect of intermediate plate thickness.

1.3 Methodology of Asymptotic Analysis and Blending

The methodology of asymptotic analysis and blending is well suited for multiphysics and multicoupled problems. It has been widely applied in many engineering disciplines such as heat transfer and fluid dynamics [123]. It focuses on characteristic values, not every point in the domain, and consists of a simple formula derived from a simplified problem and correction factors for the neglected phenomena in the simplified problem. The methodology of asymptotic analysis and blending consists of six steps in general [96, 100, 149]:

1. List all physics considered relevant.

2. Identify dominant factors. Identification of dominant factors can be investigated analytically, experimentally, numerically or conceptually based on engineering understanding and experience. When an exact solution is available, dominant factors can be identified directly from asymptotic analysis of the analytical solution, which is the case of the moving heat source problems solved in this thesis. Another example of analytical approaches is the order of magnitude scaling analysis (OMS) by comparing the order of dimensionless groups revealing the relative significance of different phenomena [91]. Another approach is to postulate dominant factors when the exact solution is unknown and check for self-consistency in Step 4 [100].

3. Solve approximate problem considering only dominant factors to obtain a simple formula, typically in the form of power laws.

4. Check for self-consistency.

5. Compare predictions to "reality", where "reality" are characteristic values from experiments or numerical simulations.

6. Create correction factors

The maximum width of isotherm produced by a moving point heat source on a thick plate is used here as an example to illustrate these six steps in detail. Asymptotes and correction factors were developed considering the following analytical temperature field as the "reality" [65, 128, 154]:

$$T(x, y, z) = T_0 + \frac{q}{2\pi kr} \exp\left[-\frac{U}{2\alpha}(r + x)\right] \tag{1.2}$$

where x, y and z constitute the independent spatial variables and r is the radial coordinate defined as $r = \sqrt{x^2 + y^2 + z^2}$. The heat source is considered stationary and the substrate moves in the $-x$ direction. The temperature, $T = T(x, y, z)$, is the dependent variable and also depends on the problem parameters. U is the velocity of the heat source relative to the substrate. q is the thermal power from the heat source absorbed by the solid, k and α is the thermal conductivity and diffusivity of the substrate, respectively. T_0 is the ambient temperature.

Equation 1.2 is a reasonable representation of welding under a wide range of operating parameters and materials, often termed as the "Rosenthal thick plate solution". The singularity at the origin ($r = 0$) is a consequence of the point heat source assumption.

Equation 1.2 can be rewritten in a normalized form as:

$$T^* = \frac{1}{r^*} \exp\left(-r^* - x^*\right) \tag{1.3}$$

where

$$T^* = \frac{4\pi k\alpha\,(T - T_0)}{qU} \tag{1.4}$$

$$x^* = \frac{Ux}{2\alpha} \tag{1.5}$$

$$y^* = \frac{Uy}{2\alpha} \tag{1.6}$$

$$z^* = \frac{Uz}{2\alpha} \tag{1.7}$$

$$r^* = \frac{Ur}{2\alpha} \tag{1.8}$$

where the * superscript indicates a dimensionless quantity. The methodology of asymptotic analysis and blending is now applied to illustrate how asymptotes to simplified problems can be combined with a constant blending parameter to obtain a closed-form solution with high accuracy.

Step 1: List All Physics Considered Relevant. The list must include dominant physics and may include secondary phenomena. Phenomena that are considered especially relevant in this example include conduction in the solid substrate, advection caused by the motion of heat source, surface heat losses via convection and radiation, latent heat associated with phase changes, electromagnetic, fluid dynamics, surface physics, and many more.

Step 2: Identify dominant factors. Assumptions in the point heat source model on a thick plate instinctively indicate two dominant factors: conduction in the workpiece and advection by the motion of the heat source. The following physics are considered secondary:

- Point heat source assumption: the shape and heat flux distribution of the heat source have negligible effects on the temperature field.
- Infinitely thick plate: the effect of plate thickness is secondary.

- Adiabatic surfaces: surface heat losses through convection and radiation are considered negligible.

- No phase transformations: phase transformations from solid to liquid have little effect on the resulting isotherms.

- Constant thermal properties: temperature dependence of thermal conductivity and diffusivity has little effect on the temperature profile.

Two dominant physics establishes two asymptotic regimes: Regime I, where advection dominates and Regime II, where conduction dominates. The division of regimes is not sharp, and it can be determined where a dominant factor has the same magnitude as the largest secondary term [100, 148]. These asymptotic regimes yield simple expressions for the characteristic values, usually in the form of power laws. The vicinity near the separations of asymptotic regimes is the "intermediate regimes".

Dimensional analysis states that a problem can be described with dimensionless groups, and the number of these groups is fewer than that of parameters plus system variables [100]. The number of dimensionless groups in a problem is given by the number of magnitudes with dimension minus the number of independent units involved and minus one when the temperature is not measured in absolute terms [152]. Equation 1.2 involves nine magnitudes with units: x, y, and z, temperature $T(x, y, z)$, T_0, q, k, U, and α and four independent units for the magnitude with dimension: m, kg, s, °C. Because all temperatures in the case have an arbitrary zero, the number of dimensionless groups is $9-4-1=4$. Three of them can be associated with independent dimensionless groups x^*, y^* and z^*, one with the dependent variable $T^*(x^*, y^*, z^*)$.

The dimensionless maximum isotherm width $y^*_{\max}$ of the isotherm at the temperature of interest $T = T_c$ depends only on one dimensionless group. It is important to keep in mind that T_c is an additional parameter that constrains the temperature field $T(x, y, z)$ to a constant value. Equation 1.3 involves four degrees of freedoms (DOFs), related to the four independent dimensionless groups (x^*, y^*, z^*, T^*). One

constraint is $T = T_c$. The definition of $y^*_{\max}$ contains two more constraints: $z^* = 0$, and $y^*_{\max} = \max(y^*)$, leaving only one DOF. This DOF can be assigned to the Rykalin number (Ry) proposed by Fuerschbach [43]:

$$\mathrm{Ry} = \frac{qU}{4\pi k\alpha\,(T_c - T_0)} \tag{1.9}$$

Ry relates the effect of advection caused by the motion of the heat source relative to conduction in the solid substrate. Therefore, a high Ry value can be interpreted as a "fast heat source" where advection dominates over conduction. A low Ry value can be interpreted as a "slow heat source" with heat transfer dominated by conduction [96, 148, 149].

Step 3: Solve approximate problem considering dominant factors Approximate problems are often obtained manually, and recent progress has contributed algorithms to implement the solving process with commercialized software. There are four typical approaches to obtain a solution to an approximate problem [100]. The approach of asymptotics of closed-form expressions is employed here because the analytical temperature field is available.

Asymptotic analysis of Equation 1.3 yields the following power laws [96, 148, 149]:

$$\widehat{y^*}_{\max_{\mathrm{I}}}(\mathrm{Ry}) = \sqrt{\frac{2\mathrm{Ry}}{\mathrm{e}}} \qquad \text{for Regime I (fast)} \tag{1.10}$$

$$\widehat{y^*}_{\max_{\mathrm{II}}}(\mathrm{Ry}) = \mathrm{Ry} \qquad \text{for Regime II (slow)} \tag{1.11}$$

where the symbol $\widehat{\ }$ indicates that the magnitude is an asymptotic approximation.

Step 4: Check for self-consistency. In this simple and uncoupled example, self-consistency is easy to check. Because only two physics are considered as the dominant phenomena, it is assured that when one physic dominates the system behaviour, the other one is negligible. For complex cases where three or more phenomena are coupled, it is necessary to check that secondary physics is of secondary magnitude compared to the dominant ones. This can be done by calculating the value of secondary

physics using estimated characteristic values and comparing with the magnitude of the dominant physics.

Step 5: Compare predictions to "reality". Derived from the analytical temperature field under a moving point source on a thick plate, the "reality" used here to calibrate the deviations from the idealized behaviour is the maximum isotherm width calculated from Equation 1.2 numerically.

The obtained asymptotes for each asymptotic regime are less accurate in intermediate values (Ry=O(1)). For these intermediate values, an explicit and accurate solution can be obtained using the blending functions proposed by Churchill and Usagi [23, 26]. A blending function proposed for the dimensionless maximum isotherm width is:

$$y^*{}_{\max}(\mathrm{Ry}) \approx \widehat{y^*}^{+}_{\max}(\mathrm{Ry}) = \left[\widehat{y^*}_{\max_{\mathrm{I}}}(\mathrm{Ry})^n + \widehat{y^*}_{\max_{\mathrm{II}}}(\mathrm{Ry})^n\right]^{1/n} \tag{1.12}$$

where n is the blending parameter and the $^+$ superscript indicates improvement over the asymptotic approximations. Equation 1.12 remains the exact asymptotic behaviour for both asymptotic regimes for any finite value of n. The error is not zero for intermediate values of Ry and is defined as:

$$\text{error} = \ln \frac{\widehat{y^*}^{+}_{\max}}{y^*{}_{\max}} \tag{1.13}$$

The definition of error is consistent with [91, 93, 98]. It can generate comparable magnitudes for large errors, especially convenient for power-law functions.

The blending parameter n was determined using a minimax optimization approach as detailed in [96]. When $n = -1.731$, the maximum error of Equation 1.12 compared to the analytical solution over the whole domain of Ry is less than 0.7236%.

Step 6: Create correction factors. Equation 1.12 can also be used to create correction factors that extend the usefulness of the asymptotic expressions. The correction factors $f_{y_{\max_{\mathrm{I}}}}(\mathrm{Ry})$ and $f_{y_{\max_{\mathrm{II}}}}(\mathrm{Ry})$ for the characteristic value $y_{\max}$ have the

following expressions [96]:

$$y_{\max} \approx \widehat{y}^{+}_{\max} = \widehat{y}_{\max_{\mathrm{I}}} \left\{ 1 + \left[\frac{\widehat{y^*}_{\max_{\mathrm{II}}}(\mathrm{Ry})}{\widehat{y^*}_{\max_{\mathrm{I}}}(\mathrm{Ry})} \right]^{n} \right\}^{1/n} = \widehat{y}_{\max_{\mathrm{I}}} f_{y_{\max_{\mathrm{I}}}}(\mathrm{Ry}) \qquad \text{for Regime I (fast)} \tag{1.14}$$

$$y_{\max} \approx \widehat{y}^{+}_{\max} = \widehat{y}_{\max_{\mathrm{II}}} \left\{ 1 + \left[\frac{\widehat{y^*}_{\max_{\mathrm{II}}}(\mathrm{Ry})}{\widehat{y^*}_{\max_{\mathrm{I}}}(\mathrm{Ry})} \right]^{-n} \right\}^{1/n} = \widehat{y}_{\max_{\mathrm{II}}} f_{y_{\max_{\mathrm{II}}}}(\mathrm{Ry}) \quad \text{for Regime II (slow)} \tag{1.15}$$

Equations 1.14 and 1.15 are exactly equivalent and they are the same approximation to the exact solution, but based on different starting regimes. As Ry approaches infinity (Regime I), $f_{y_{\max_{\mathrm{I}}}}(\mathrm{Ry})$ tends to 1 and for Ry approaching 0, $f_{y_{\max_{\mathrm{II}}}}(\mathrm{Ry})$ tends to 1. The value of n for Equations 1.14 and 1.15 are the same as for Equation 1.12.

Substituting the two asymptotics (Equation 1.10 and Equation 1.11) into Equation 1.14 and Equation 1.15, the following expression for the correction factors of the maximum isotherm width are obtained [96]:

$$f_{y_{\max_{\mathrm{I\text{-}II}}}}(\mathrm{Ry}) = \left[1 + \left(\sqrt{\frac{\mathrm{eRy}}{2}} \right)^{\pm n} \right]^{1/n} \tag{1.16}$$

where the exponent +n corresponds to Regime I, and -n corresponds to Regime II. The maximum error of approximation is always smaller than 0.7236% at the optimal value of $n = -1.731$.

1.4 Objectives

The ultimate objective of this research is to develop a set of design rules for welding on thick plates in the form of simple formula and correction factors to predict critical thermal characteristics of interest to practitioners and engineers. The following objectives have been fulfilled:

- Establish a general and rigorous methodology of asymptotics and blending to model materials processing with a focus on dimensional analysis and characteristic values.

- Identify critical thermal characteristics of interest to engineers and develop design rules in the form of simple formula and correction factors based on the most idealized analytical model in welding: a moving point heat source on an infinitely thick plate (Rosenthal's thick plate solution).

- Establish design rules for the peak temperature of the workpiece based on the moving Gaussian distributed surface heat source model to quantify the role of heat distribution parameter. Validate the obtained design rules against published experimental measurements and simulation data.

- Establish a closed-form design rule to predict the penetration depth under a moving Gaussian surface source and develop a correction factor for the heat distribution parameter. Validate the applicability of the obtained design rules against experimental measurements and simulation results from the literature.

1.5 Thesis Outline

An outline of each chapter included in this thesis (excluding the introduction) is listed below:

- Chapter 2 describes a novel methodology of asymptotic and blending that has never been applied in the field of welding to predict critical thermal characteristics values of heat flow in the modelling of welding. The proposed methodology has the applicability to correlate experimental measurements, numerical simulations, or theoretical values.

- Chapter 3 lists design rules for 13 critical characteristic values of heat flow in welding using the methodology proposed in Chapter 2. Simple formula and correction factors have been derived based on Rosenthal's thick plate solution. The design rules developed in dimensionless form have only one dependence on

a dimensionless group, the Rykalin number (Ry). All design rules are accurate to within 7% of the exact analytical solutions.

- Chapter 4 presents an application of the methodology of asymptotic analysis and blending to predict the peak temperature rise and its location and the maximum distribution parameter to reach a certain peak temperature based on a moving Gaussian distributed surface heat source model. The obtained expressions remain the exact asymptotic behaviour in asymptotic regimes. The maximum error of approximation in the domain is 0.19%, and 0.47% for the peak temperature and its location, 1.4% for the maximum feasible heat distribution parameter. The proposed design rules have an excellent agreement with experimental and simulation data collected from the literature for a wide range of processes and materials.

- Chapter 5 presents a correction factor associated with the heat distribution parameter to improve the accuracy of prediction for the maximum isotherm depth. Based on a moving Gaussian surface source model, the dimensionless isotherm depth depends on Ry and the dimensionless heat distribution parameter, σ^*. Conventional blending techniques have been extended to blend functions dependent on two dimensionless groups. The maximum error compared to the analytical solution is smaller than 9.7%. Despite the considerable simplifications instinct in the employed analytical model, the obtained design rules are accurate, at least as accurate as measurements.

- Chapter 6 is a summary of the main findings in this thesis, conclusions, and recommendations for future work.

- Appendix includes supporting figures and Matlab codes for the related thermal characteristics.

References

[3] C. M. Adams, "Cooling Rates and Peak Temperatures in Fusion Welding," *Welding Journal*, vol. 37, no. 5, pp. 210–215, 1958.

[9] AWS D1.1/D1.1M:2015, *Structural Welding Code–Steel*. the United States of America: American Welding Society, 2015.

[17] N. S. Boulton and H. E. Lance-Martin, "Residual Stresses in Arc Welded Plates.," in *Proceedings of the Institution of Mechanical Engineers*, 1936, pp. 295–347.

[18] BS EN 1011-2:2001, *Welding–Recommendations for Welding of Metallic Materials–Part 2: Arc Welding of Ferritic Steels*. London: British Standards Institution, 2001.

[22] N. Christensen, Davies, V. de L., and K. Gjermundsen, "Distribution of Temperatures in Arc Welding," *British Welding Journal*, vol. 12, no. 2, pp. 54–75, 1965.

[23] S. W. Churchill and R. Usagi, "A general expression for the correlation of rates of transfer and other phenomena," *AIChE Journal*, vol. 18, no. 6, pp. 1121–1128, 1972, ISSN: 15475905.

[26] S. W. Churchill and R. Usagi, "A Standardized Procedure for the Production of Correlations in the Form of a Common Empirical Equation," *Industrial & Engineering Chemistry Fundamentals*, vol. 13, no. 1, pp. 39–44, 1974.

[33] J. N. DuPont, "Solidification of an Alloy 625 Weld Overlay," *Metallurgical and Materials Transactions A*, vol. 27A, no. 11, pp. 3612–3620, 1996.

[34] J. N. DuPont and A. R. Marder, "Thermal Efficiency of Arc Welding Processes," *Welding Journal-Including Welding Research Supplement*, vol. 74, no. 12, 406s–416s, 1995.

[36] T. W. Eagar and N. S. Tsai, "Temperature Fields Produced by Traveling Distributed Heat Sources," *Welding Journal*, vol. 62, no. 12, pp. 346–355, 1983, ISSN: 00432296.

[37] K. E. Easterling, *Introduction to the physical metallurgy of welding*. Butterworth Heinemann, 1992, p. 270.

[42] E. Friedman, "Thermomechanical Analysis of the Welding Process Using the Finite Element Method," *Journal of Pressure Vessel Technology*, vol. 97, no. 3, pp. 206–213, 1975.

[43] P. W. Fuerschbach, "Measurement and Prediction of Energy Transfer Efficiency in Laser Beam Welding," *Welding Journal, Research Supplement*, vol. 75, no. 1, pp. 24–34, 1996.

[44] P. W. Fuerschbach and G. A. Knorovsky, "A Study of Melting Efficiency in Plasma Arc and Gas Tungsten Arc Welding," *Welding Journal*, vol. 70, no. 11, pp. 287–297, 1991.

[45] P. W. Fuerschbach and G. R. Eisler, "Determination of Material Properties for Welding Models by Means of Arc Weld Experiments," in *6th Intl. Trends in Welding Research*, Pine Mountain, Georgia, 2002.

[48] J. Goldak, A. Chakravarti, and M. Bibby, "A New Finite Element Model for Welding Heat Sources," *Metallurgical Transactions B*, vol. 15, no. 2, pp. 299–305, 1984, ISSN: 03602141.

[54] R. J. Grosh, E. A. Trabant, and G. A. Hawkins, "Temperature Distribution in Solids of Variable Thermal Properties Heated by Moving Heat Sources," *Quarterly of Applied Mathematics*, vol. 13, no. 2, pp. 161–167, 1955.

[57] W. F. Hess, L. L. Merrill, E. F. Nippes, and A. P. Bunk, "The Measurement of Cooling Rates Associated with Arc Welding and Their Application to the Selection of Optimum Welding Conditions," *Welding Journal*, vol. 22, no. 9, pp. 377–422, 1943.

[61] M. Inagaki, "Welding Conditions of Steels and Cooling Time near the Fusion Line (Report 1)," *Journal of the Japan Welding Society*, vol. 27, no. 12, pp. 716–722, 1958.

[64] F Jackson, "Moving Heat Sources With Change of Phase," *Journal of Heat Transfer*, vol. 87, no. 3, pp. 329–332, 1965.

[65] J. C. Jaeger, "Moving Sources of Heat and the Temperature of Sliding Contacts," *Proceeding of the Royal Society of New South Wales*, vol. 76, pp. 203–224, 1942.

[66] C. L. Jenney and A. O'Brien, *Welding Handbook, Volume 1 - Welding Science and Technology (9th Edition)*. American Welding Society (AWS), 2001.

[67] P. Jhaveri, W. G. Moffatt, and C. M. Adams, "The Effect of Plate Thickness and Radiation on Heat Flow in Welding and Cutting," *Welding Journal, Research Supplement*, vol. 41, no. 1, pp. 12–16, 1962.

[69] T. Kasuya and N. Yurioka, "Prediction of Welding Thermal History by a Comprehensive Solution," *Welding Journal*, vol. 72, no. 3, pp. 107–115, 1993.

[72] R Komanduri and Z. B Hou, "Thermal Analysis of the Arc Welding Process : Part I . General Solutions," *Metallurgical and Materials Transactions B*, vol. 31, no. 6, pp. 1353–1370, 2000.

[73] R. Komanduri and Z. B. Hou, "Thermal analysis of the laser surface transformation hardening process," *International Journal of Heat and Mass Transfer*, vol. 44, no. 15, pp. 2845–2862, 2001, ISSN: 0017-9310.

[76] S. Kou, D. K. Sun, and Y. P. Le, "A fundamental study of laser transformation hardening," *Metallurgical Transactions A*, vol. 14, no. 3, pp. 643–653, 1983.

[83] Y. Lu and P. F. Mendez, "The effect of surface heat losses on isotherm trailing length and cooling rate," 2021.

[84] Y. Lu, Y. Wang, and P. F. Mendez, "Width of thermal features induced by a 2-d moving heat source," *International Journal of Heat and Mass Transfer*, vol. 156, p. 119 793, 2020.

[86] N. D. Malmuth, W. F. Hall, B. I. Davis, and C. D. Rosen, "Transient Thermal Phenomena and Weld Geometry in GTAW," *Welding Journal, Research Supplement*, vol. 53, no. 9, pp. 388–400, 1974.

[91] P. F. Mendez and T. W. Eagar, "Order of Magnitude Scaling: A Systematic Approach to Approximation and Asymptotic Scaling of Equations in Engineering," *Journal of Applied Mechanics*, vol. 80, no. 1, p. 011 009, 2013, ISSN: 0021-8936.

[93] P. F. Mendez, "Characteristic Values in the Scaling of Differential Equations in Engineering," *Journal of Applied Mechanics, Transactions ASME*, vol. 77, no. 6, 2010, ISSN: 00218936.

[96] P. F. Mendez, Y. Lu, and Y. Wang, "Scaling Analysis of a Moving Point Heat Source in Steady- State on a Semi-Infinite Solid," *Journal of Heat Transfer*, vol. 140, no. 8, p. 081 301, 2018.

[98] P. F. Mendez and F. Ordonez, "Scaling Laws from Statistical Data and Dimensional Analysis," *Journal of Applied Mechanics, Transactions ASME*, vol. 72, no. 5, pp. 648–657, 2005, ISSN: 00218936.

[100] P. Mendez, "Reduced order models for welding and solidification processes," in *IOP Conference Series: Materials Science and Engineering*, IOP Publishing, vol. 861, 2020, p. 012 003.

[101] R. W. Messler Jr, *Principles of welding: processes, physics, chemistry, and metallurgy*. New York: John Wiley & Sons, 2004.

[102] J. Miettinen, "Calculation of Solidification-Related Thermophysical Properties for Steels," *Metallurgical and Materials Transactions B*, vol. 28, no. 2, pp. 281–297, 1997.

[108] P. S. Myers, O. A. Uyehara, and G. L. Borman, "Fundamentals of Heat Flow in Welding," *Welding Research Council Bulletin*, no. 123, pp. 1–46, 1967.

[109] O. R. Myhr and Ø. Grong, "Dimensionless Maps for Heat Flow Analyses in Fusion Welding," *Acta Metallurgica Et Materialia*, vol. 38, no. 3, pp. 449–460, 1990, ISSN: 09567151.

[112] R. W. Niles and C. E. Jackson, "Weld Thermal Efficiency of the GTAW Process," *Welding Journal*, vol. 54, no. 1, pp. 25–32, 1975.

[114] A. C. Nunes, "An Extended Rosenthal Weld Model," *Welding Journal, Research Supplement*, vol. 62, no. 6, pp. 165–170, 1983.

[115] A. Okada, "Application of Melting Efficiency Welding and its Problems," *Journal of the Japan Welding Society*, vol. 46, no. 2, pp. 53–61, 1977.

[121] K. Poorhaydari, B. M. Patchett, and D. G. Ivey, "Estimation of Cooling Rate in the Welding of Plates with Intermediate Thickness," *Welding Journal*, vol. 84, no. 10, 149–s–155–s, 2005.

[123] D. Rivas and S. Ostrach, "Scaling of Low-Prandtl-Number Thermocapillary Flows," *International Journal of Heat and Mass Transfer*, vol. 35, no. 6, pp. 1469–1479, 1992.

[125] O. F. T. Roberts, "The Theoretical Scattering of Smoke in a Turbulent Atmosphere," *Proceedings of the Royal Society of London. Series A, Containing Papers of a Mathematical and Physical Character*, vol. 104, no. 728, pp. 640–654, 1923.

[126] D. Rosenthal, "The Theory of Moving Sources of Heat and Its Application to Metal Treatments," *Transactions of the A.S.M.E.*, vol. 68, pp. 849–866, 1946.

[127] D. Rosenthal, "Etude Théorique du Régime Thermique Pendant La Soudure à L'Arc," in *Comptes Rendus (2eme Congres National des Sciences)*, 1935, pp. 1277–1292.

[128] D. Rosenthal, "Mathematical Theory of Heat Distribution During Welding and Cutting," *Welding Journal*, vol. 20, no. 5, pp. 220–234, 1941.

[129] D. Rosenthal and R. Schmerber, "Thermal Study of Arc Welding. Experimental Verification of Theoretical Formulas.," *The Welding Journal*, vol. 17, no. 4, pp. 2–8, 1938.

[131] N. N. Rykalin, *Calculation of Heat Flow in Welding*. Moscow: Mashgis, 1951.

[139] P Tekriwal and J Mazumder, "Finite Element Analysis of Three-Dimensional Transient Heat Transfer in GMA Welding," *Welding Journal, Research Supplement*, vol. 67, no. 7, pp. 150–156, 1988.

[144] C. L. Tsai, "Heat Flow in Fusion Welding," *Welding, Brazing, and Soldering, ASM Handbook, ASM International*, vol. 6, pp. 7–18, 1993.

[147] M. Ushio, T. Ishimura, F. Matsuda, and Y. Arata, "Theoretical Calculation on Shape of Fusion Boundary and Temperature Distribution around Moving Heat Source (Report I)," *Transactions of JWRI*, vol. 6, no. 1, pp. 1–6, 1977.

[148] Y Wang, Y Lu, M Grams, A Cesaro, and P. Mendez, *Asymptotics and blending in the modeling of welding*, 2019.

[149] Y. Wang, Y. Lu, and P. F. Mendez, "Scaling expressions of characteristic values for a moving point heat source in steady state on a semi-infinite solid," *International Journal of Heat and Mass Transfer*, vol. 135, pp. 1118–1129, 2019.

[152] T. Washio and H. Motoda, "Extension of Dimensional Analysis for Scale-types and its Application to Discovery of Admissible Models of Complex Processes," in *International Workshop on Similarity Method*, 1999, pp. 129–147.

[154] H. A. Wilson, "On Convection of Heat," *Proceedings of the Cambridge Philosophical Society*, vol. 12, pp. 406–423, 1904.

[157] G. D. Wood, "Heat and mass transfer aspects of coaxial laser cladding and its application to nickel-tungsten carbide alloys," PhD thesis, University of Alberta, 2017.

Chapter 2

Asymptotics and Blending in the Modeling of Welding

2.1 Abstract

Important welding questions are often easy to ask and difficult to answer. For example, the question "what is the width of the weld?" is essential for understanding the strength of a weld, but it is currently answered through trial and error, or through sophisticated numerical modeling. In this work, it is proposed that there is a third approach based on a deep understanding of physics, and a basic command of mathematics. From the point of view of the practitioner, the answer can be approximated using formula, tables, and graphs of great generality. In this approach, the aspect of interest of the weld is reduced to its minimal representation, neglecting all secondary physical phenomenon. Mathematically, this corresponds to an asymptotic regime. In contrast with other asymptotic techniques such as perturbation analysis, in the proposed methodology, blending techniques are applied. The advantage of these blending techniques is that they approach the exact solutions (typically within a few percentage points) but involve only a few constants that are suitable to be transmitted in print. Much of the existing work on heat transfer outside welding is summarized in this form, but the approach has not been applied to welding yet. Some welding problems are outside the range of standard blending techniques, and an extension of the techniques will be discussed. The application of this approach will also be discussed

using the width of the weld and other related problems.

2.2 Introduction

The complexity of an engineering problem can be decomposed into the complexity of its physics, which can be assessed by the number of parameters related to the physics of the problem, and the complexity of its geometry, given by the number of parameters necessary to capture the shape of the problem [140]. In the field of welding, the geometry of welding processes (e.g. bead geometry and joint preparation) is generally not complex; however, the large number of parameters relative to relevant physics such as heat and mass transfer, fluid dynamics, electromagnetism, thermodynamics, as well as their tight coupling make welding very difficult to understand at intuitive level and more complex than most other engineering fields.

Typically, there are three approaches to analyze welding problems: trial and error (making a prototype), numerical simulation and design rules. Trial and error is the most common and reliable way in welding procedure development as it is capable of producing the reality with complex geometries and provides direct measurements from experiments. However, case-by-case results of specific processes are difficult to be synthesized for the next trial or extended to new operating parameters. The horizontal axis in Fig. 2.1 is the cost of making a prototype and the vertical axis represents the total cost.

Sophisticated computer simulations are cost effective in the fields such as aerospace and nuclear industry where the prototype is time-consuming and expensive to make. In welding, running a weld may cost on the order of one to thousand dollars and within this range of cost, making a prototype or trial and error usually costs much less money than developing or implementing a comprehensive simulation. Numerical models excel at dealing with the complexity of geometries, but implementing multicoupled physics is often challenging.

Design rules (the red horizontal line in Fig. 2.1) can significantly lower costs, and

enable a design approach to welding procedures which are usually done by trial and error. Typically, the design rules can be expressed in the form of simple formulae and correction factors. The simple formulae are the asymptotic solutions to ideal case and their correction factors are developed to capture the departures from the ideal cases.

Instead of considering every point in the space-time domain, the target of the design rules is to predict the characteristic values such as a maximum velocity, or maximum temperature. The concept of characteristic values was discussed in detail in [93] to normalize the governing equations into proper magnitudes and it is typically chosen as the maximum absolute value of the function of interest. Asymptotic analysis and blending do not present convergence problems and they are well suited for multiphysics problems.

The use of design rules can provide guidelines for follow-up tests and significantly reduce the money and effort put in the trial and error stage. There are very few of these design rules in the field of welding; for example, the practical question "what is the resulting width of a weld bead by a given set of parameters" is difficult to be answered quickly within the existing knowledge.

Expressions in explicit form which are general, accurate, easy-to-calculate are convenient for transmission and amenable to be used by practitioners in industry. This paper proposes a systematic methodology based on asymptotics and blending techniques to develop a set of formulae in standardized form (asymptotics and correction factors) that can predict (or estimate reasonably) important weld properties valid for general welding procedures with different alloys, process conditions and operating parameters. The predictions sought would target the size of the weld pool, heating and cooling rates, melting efficiencies, etc., such that they could be coupled with metallurgical and performance models.

The systematic methodology advocated here to obtain engineering formulas of interest can be roughly summarized as a six-step procedure call the Minimal Representation and Correction Factors (MRCF) [92]. MRCF considers the dominant

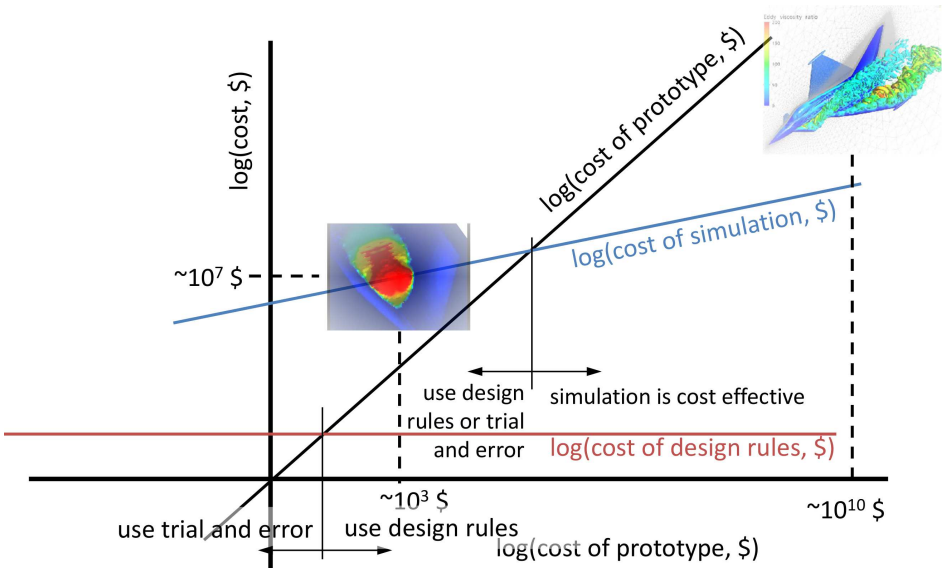

Figure 2.1: Costs of simulation, prototypes, and design rules. For the aerospace industry, a prototype is much more expensive than simulations. For welding, a prototype is often cheaper than simulations, resulting in trial-and-error approaches. Design rules are much less expensive than simulations, and should enable a design approach where it is seldom done currently.

phenomena and the deviations from the ideal case using the exact analytical solutions, experimental measurements or results from numerical models. Once a complex multicoupled problem is minimally represented by its dominant mechanisms, explicit, closed-form expressions can be developed.

Blending techniques will be applied to extend the asymptotic solutions to the whole domain of dimensionless groups capturing the characteristic values of interest. Blending has been widely applied in many disciplines such as heat transfer [24, 25], including moving heat sources [96], mass transfer [40], and fluid dynamics [35]. With blending, correction factors can be rigorously derived to capture the deviation from asymptotic behavior and define the validity of the asymptotics. Blending techniques and their extension are the main focus of this paper.

2.3 MRCF: Minimal Representation and Correction Factor

The approach presented here for asymptotic analysis of engineering problems is the Minimal Representation and Correction Factor (MRCF). It was first proposed in [92] and has been successfully implemented to construct general expressions for thermal characteristics of moving heat sources in [96, 156]. The MRCF approach consists of the following six steps:

1. List all physics considered relevant
2. Identify dominant factors
3. Solve approximate problem considering only dominant factors (Minimal Representation)
4. Check for self-consistency
5. Compare predictions to "reality"
6. Create correction factors

The minimal representation of a problem corresponds to the formulation of the problem with parameters such that all secondary phenomena become negligible. There are various techniques for obtaining the minimal representation. They can be roughly divided into manual and computational techniques. Manual Asymptotics include "Informed" Dimensional Analysis: generate dimensionless groups based on knowledge about system [43, 44, 104–106, 130], Inspectional Analysis: dimensionless groups from normalized equations[22, 55, 124, 161], Order of Magnitude/Balancing Techniques [13, 31, 77]. Computational Asymptotics include Statistical analysis/data mining[95, 98, 122], and analysis of the Governing equations[92, 93, 159]

The MRCF is an iterative approach of identifying dominant phenomena and solve the simple solutions of this minimal represented problem by considering only domi-

nant factors and characteristic values of the simplified problem can be addressed by asymptotics to capture the behavior of the system for combinations of parameters that result in the same dominant phenomena (which is called a Regime). Thus, a multicoupled complex problem will be decomposed into its minimal representation of the dominant mechanisms. The dominant factors are typically unknown and need ingenuity and expertise to make a reasonable postulation. The advantage of the MRCF is that this iterative process transverses all possible choice of dominant factors and self-consistency is checked for the obtained results to assure the neglected phenomenon are secondary. Departure from the reality caused by the neglect of secondary phenomenon will be accounted by the correction factors, which capture the deviation from the ideal solutions. Correction factors can be calibrated with experimental numerical results to account for secondary phenomena not considered explicitly.

2.3.1 Important concepts and notation in MRCF

Because of the complexity of the concepts involved in MRCF, careful notation is essential. We will call here $\{U\}$ the set of dependent variables with elements $u(\{X\}, \{P\})$, where $\{X\}$ is the set of independent variables, and $\{P\}$ is the set of problem parameters.

When the parameters of an engineering problem change, the resulting characteristic values will be influenced even if the independent variables remain unchanged. Thus, the set of problem parameters $\{P\}$ is also included as arguments of the solution functions. Accordingly, u_{c} represents the characteristic value of $u(\{X\}, \{P\})$.

For the sake of greater generality, normalization will be applied to transform relevant variables into dimensionless form and thus, results in different units or from different operating parameters can be generalized and compared within the same scale. The magnitude $\widehat{u}_{\mathrm{c,i}}$ is the asymptotic behavior of $u_{\mathrm{c}}(\{P\})$ in Regime i (e.g. Regime I, Regime II) where the value of the dimensionless groups based on parameters

is asymptotically large or small. Very often, the asymptotic behavior has power-law dependence on the dimensionless groups.

In normalized form, $u^*(\{X^*\},\{\Pi\})$ is the dimensionless dependent variable where $\{X^*\}$ is the set of normalized independent variables, and $\{\Pi\}$ is a set of independent dimensionless groups based only on the problem parameters. $u_c^*(\{\Pi\})$ is the characteristic value of $u^*(\{X^*\},\{\Pi\})$. Similarly, $\widehat{u^*}_{c,i}(\{\Pi\})$ is the asymptotic behavior of $u_c^*(\{\Pi\})$ in Regime i (often in the form of a power law).

Dimensional analysis indicates that a problem can be captured by a set of n dimensionless groups, where $n = m - k$, m is the number of independent physical magnitudes involved in the problem, and k is the set of independent reference units of the problem [19]. Typically, the functional dependence between the characteristic value targeted (u_c) and the dimensionless groups is monotonic, thus the number of regimes is two per dimensionless group (close to zero, and close to infinity, then the number of regimes n_r is:

$$n_r = 2^n \tag{2.1}$$

2.4 Foundations of Blending Techniques

Blending is the general description of a family of techniques of interpolation between two asymptotic solutions. In this work, the focus is on techniques that use a very small number of parameters (typically one or two). The advantage is that they are very easy to communicate and implement. Surprisingly, in many practical cases these techniques have a very small error (typically few percentage points) against the exact solution they are interpolating.

The oldest technique of interest for this work was first described by Acrivos [1, 2] for the rate of heat and mass transfer in several laminar boundary layer flows and was later extended and generalized by Churchill and Usagi [23, 26] as the CUE (Churchill-Usagi equation).

In this work we will use the notation $\mathcal{B}$ to represent the blending of asymptotics

$\widehat{u^*}_{\mathrm{c,i}}(\{\Pi\})$, corresponding to regime i (Regime I, Regime II, etc.) using the set of blending parameters $\{B\}$, thus:

$$u^*_{\mathrm{c}}(\{\Pi\}) \approx \widehat{u^*_{\mathrm{c}}}^{+}(\{\Pi\}) = \mathcal{B}\left(\widehat{u^*}_{\mathrm{c,I}}(\{\Pi\}), \widehat{u^*}_{\mathrm{c,II}}(\{\Pi\}), \widehat{u^*}_{\mathrm{c,III}}(\{\Pi\}) \ldots \{B\}\right) \tag{2.2}$$

where the symbol $\widehat{\ }$ indicates that the magnitude is an asymptotic approximation and the $^+$ superscript represents the improvement over the asymptotics after blending.

There are several approaches to determine the set of blending constants $\{B\}$ and the minimax optimum procedure [96] applied in this paper is used to determine the optimum set of blending constants which minimizes the maximum error defined as:

$$\text{max error} = \max_{\Pi}\left[\ln \frac{\widehat{u^*_{\mathrm{c}}}^{+}(\{\Pi\})}{u^*_{\mathrm{c}}(\{\Pi\})}\right] \tag{2.3}$$

where $u^*_{\mathrm{c}}(\{\Pi\})$ is the target dimensionless characteristic value, which can be an exact analytical solution, experimental measurements or numerical simulation results. The maximum value is explored over the whole domain of $\{\Pi\}$, and the minimum is explored over the blending parameters $\{B\}$.

Equation 2.3 has the advantage of revealing the comparable magnitudes for large errors and it is equivalent to the definition of relative error when the error is small. The set of blending constants $\{B\}$ needs be determined only once for each blending function.

One essential property of the blending function $\mathcal{B}$ is that it shares the asymptotic behavior of the original function:

$$u^*_{\mathrm{c}}(\{\Pi\}) \to \widehat{u^*}_{\mathrm{c,i}}(\{\Pi\}) \text{ when } \{\Pi\} \to \{\Pi\}_i \text{ (Regime i)}$$

2.5 Development of Correction Factors

Based on the blending of Equation 2.2, correction factors can be established for each asymptotic regime to capture the departure of the blended approximation from

asymptotic behavior. In dimensionless form:

$$u_{\mathrm{c}}^{*}(\{\Pi\}) \approx \widehat{u}_{\mathrm{c,i}}^{*^{+}}(\{\Pi\}) = \widehat{u^{*}}_{\mathrm{c,i}}(\{\Pi\})\mathcal{B}\left(\frac{\widehat{u^{*}}_{\mathrm{c,I}}(\{\Pi\})}{\widehat{u^{*}}_{\mathrm{c,i}}(\{\Pi\})}, \frac{\widehat{u^{*}}_{\mathrm{c,II}}(\{\Pi\})}{\widehat{u^{*}}_{\mathrm{c,i}}(\{\Pi\})}, \frac{\widehat{u^{*}}_{\mathrm{c,III}}(\{\Pi\})}{\widehat{u^{*}}_{\mathrm{c,i}}(\{\Pi\})} \ldots \{B\}\right)$$
$$= \widehat{u^{*}}_{\mathrm{c,i}}\, f_{u_{\mathrm{c,i}}}(\Pi) \qquad \text{for Regime i} \tag{2.4}$$

and its dimensional counterpart:

$$u_{\mathrm{c}}(\{\Pi\}) \approx \widehat{u}_{\mathrm{c,i}}^{+}(\{\Pi\}) = \widehat{u}_{\mathrm{c,i}}(\{\Pi\})\mathcal{B}\left(\frac{\widehat{u}_{\mathrm{c,I}}(\{\Pi\})}{\widehat{u}_{\mathrm{c,i}}(\{\Pi\})}, \frac{\widehat{u}_{\mathrm{c,II}}(\{\Pi\})}{\widehat{u}_{\mathrm{c,i}}(\{\Pi\})}, \frac{\widehat{u}_{\mathrm{c,III}}(\{\Pi\})}{\widehat{u}_{\mathrm{c,i}}(\{\Pi\})} \ldots \{B\}\right)$$
$$= \widehat{u}_{\mathrm{c,i}}\, f_{u_{\mathrm{c,i}}}(\Pi) \qquad \text{for Regime i} \tag{2.5}$$

where the i^{th} term inside the correction factor is equal to 1 and the set of blending constants $\{B\}$ is the same as in Equation 2.2 and $f_{u_{\mathrm{c,i}}}(\Pi)$ is a shorthand notation for the blending function that leads to correction factors. In the shorthand notation, the set of blending parameters is not stated explicitly, but it is present.

As the blending function $\mathcal{B}$ maintains the asymptotic behavior of the original function, the value of the correction factor $f_{u_{\mathrm{c,i}}}(\Pi)$ tends to the value of 1 or at the same order as 1 in its corresponding Regime i:

$$f_{u_{\mathrm{c,i}}}(\Pi) \to 1 \text{ when } \{\Pi\} \to \{\Pi\}_i \text{ (Regime i)}$$

Equations 2.4 and 2.5 capture the deviation of the blended approximation from the asymptotic behavior. These equations can also be used to determine the range of validity of the asymptotic equations for a given acceptable error, and can also be used to account for systematic errors from the mathematical treatment of the asymptotics, or random errors from the physics caused by neglected secondary phenomenon. The correction factors developed are explicit and can typically be calculated with a handheld calculator or a spreadsheet.

2.6 1D Blending

When the target function depends on only one dimensionless group, the system has two asymptotic regimes (Equation 2.1). Thus, according to Equation 2.4:

$$u_{\mathrm{c}}^{*}(\{\Pi\}) \approx \widehat{u}_{\mathrm{c}}^{*^{+}}(\{\Pi\}) = \mathcal{B}\left(\widehat{u^{*}}_{\mathrm{c,I}}(\{\Pi\}), \widehat{u^{*}}_{\mathrm{c,II}}(\{\Pi\}), \{B\}\right) \tag{2.6}$$

Blending in 1D (when blending depends on only one dimensionless group) is the simplest case and the basis of the extension of blending to more complex scenarios. Standard 1D blending was treated in [1, 2, 23, 26]; however, these studies could not account for the case when the asymptotes did not cross. Also, the standard blending technique could result in high errors when the functions involved are not power laws.

2.6.1 Standard 1D Blending

In the case where the two asymptotic solutions are known and intersect with each other only once, the two asymptotes can be blended with only one blending constant (in this case $\{B\} = \{n\}$):

$$u_{\mathrm{c}}^{*}(\{\Pi\}) \approx \widehat{u_{\mathrm{c}}^{*}}^{+}(\{\Pi\}) = \left[\widehat{u^{*}}_{\mathrm{c,I}}(\{\Pi\})^{n} + \widehat{u^{*}}_{\mathrm{c,II}}(\{\Pi\})^{n}\right]^{1/n} \tag{2.7}$$

where the optimal value of n needs to be determined only once for each blending function. A sufficient (more restrictive than necessary) condition to permit the use of Equation 2.7 is that the target function is monotonous on its dependence on the dimensionless group. A vast number of engineering problems have an asymptotic behavior in the form of power laws. Equation 2.7 can also be used to create the correction factors $f_{u_{\mathrm{c,I}}}(\Pi)$ (based on asymptotic in Regime I) and $f_{u_{\mathrm{c,II}}}(\Pi)$ (based on asymptotic in Regime II) as follows:

$$f_{u_{\mathrm{c,I}}}(\Pi) = \mathcal{B}\left(1, \frac{\widehat{u^{*}}_{\mathrm{c,II}}(\{\Pi\})}{\widehat{u^{*}}_{\mathrm{c,I}}(\{\Pi\})}, n\right) = \left\{1 + \left[\frac{\widehat{u^{*}}_{\mathrm{c,II}}(\{\Pi\})}{\widehat{u^{*}}_{\mathrm{c,I}}(\{\Pi\})}\right]^{n}\right\}^{1/n} \tag{2.8}$$

$$f_{u_{\mathrm{c,II}}}(\Pi) = \mathcal{B}\left(\frac{\widehat{u^{*}}_{\mathrm{c,I}}(\{\Pi\})}{\widehat{u^{*}}_{\mathrm{c,II}}(\{\Pi\})}, 1, n\right) = \left\{1 + \left[\frac{\widehat{u^{*}}_{\mathrm{c,II}}(\{\Pi\})}{\widehat{u^{*}}_{\mathrm{c,I}}(\{\Pi\})}\right]^{-n}\right\}^{1/n} \tag{2.9}$$

Equations 2.8 and 2.9 are exactly equivalent and they capture the difference between the blended approximation and different starting asymptotic expressions. They tend to the exact value of 1 in their corresponding limits for all finite values of n. The value of n for Equations 2.8 and 2.9 are the same as for Equation 2.7.

Standard 1D blending provides a new paradigm to obtain a general solution over the whole domain in terms of simple, known, limiting solutions with minimal degree

of explicit empiricism, which is typically caused by the additional introduction of the blending constants $\{B\}$. Equation 2.7 is a canonical expression for the formulation of correlating equations and has the advantage of simplicity, generality, inherent accuracy, and convergence to theoretical solutions in the limits. Nevertheless, it must be applied with an understanding of its restrictions. It can not represent processes with irregular transition in the non-asymptotic part and Equation 2.7 only applies for the situation where asymptotes in the limiting regimes have a single intersection. What's more, the asymptotic solutions must be free of singularities because the existence of singularity will persist and disrupt the prediction even though the singularity occurs outside asserted range of the asymptote [23, 26].

2.6.2 1D Blending of Non-Crossing Asymptotics

Equation 2.7 is not applicable for non-crossing asymptotics. For any finite positive value of n, the blended result will always be the asymptotic of larger magnitude and the smaller asymptotic would be chosen as the approximation for any negative value n.

A modified blending technique is proposed here to extend the applicability of Equation 2.7, by applying a factor $\exp(a\Pi^b)$ to either of the asymptotes to force the two asymptotics to have a single intersection. This approach is useful for asymptotic behavior weaker than exponential; for example, it can not be used in the case such as a Γ function. The 1D blending function for non-crossing asymptotics has the following expression:

$$\begin{aligned} u_{\mathrm{c}}^*(\{\Pi\}) \approx \widehat{u_{\mathrm{c}}^*}^+(\{\Pi\}) &= \mathcal{B}\left(\widehat{u^*}_{\mathrm{c,I}}(\{\Pi\}), \widehat{u^*}_{\mathrm{c,II}}(\{\Pi\}), \{n, a, b\}\right) \\ &= \left\{\widehat{u^*}_{\mathrm{c,I}}(\{\Pi\})^n + \left[\widehat{u^*}_{\mathrm{c,II}}(\{\Pi\})\exp(a\Pi^b)\right]^n\right\}^{1/n} \end{aligned} \tag{2.10}$$

where in this case, $\{B\} = \{n, a, b\}$.

The reason of choosing exponential function as the form of modification factor is due to its simplicity and that its dependence on the dimensionless group is stronger

than any power law or other common functional relationships in engineering design. The sign of the coefficient a determines the type of the modification factor: when $a > 0$, the modification factor is always larger than 1 while for $a < 0$, the modification factor $\exp(a\Pi^b)$ varies within the interval of $(0, 1]$. Both the sign and the magnitude of b matter as the modification factor has increasing dependence on the independent variable for $ab > 0$ while for the case of $ab < 0$, it decreases as the independent variable increases. An appropriate magnitude of b should be chosen to ensure the modified asymptote intersects the other. With a suitable selection of the blending constants $\{n, a, b\}$, the modified asymptote still maintains its asymptotic behaviour, while the exponential term changes its intermediate behavior such that the two asymptotes intersect. A similar approach was made in [40] to obtain a general correlation of three functions, with the applied modification factor using $b = 1$.

2.6.3 1D Blending of Constant Asymptotics

Many phenomena demonstrate the asymptotic behaviour of two limiting solutions of different constant values, for example, in the field of welding, the maximum hardness of the heat affected zone [6, 160] and in heat transfer, the temperature distribution of a slab heated on both surfaces at different constant temperatures. Although the treatment of non-crossing asymptotes could apply to constant asymptotics, a specific treatment of this particular problem results in convenient solutions of smaller complexity.

The following three blending functions are explored:

$$
\begin{aligned}
u_{\mathrm{c}}^{*}(\{\Pi_1\}) \approx \widehat{u_{\mathrm{c}}^{*}}^{+}(\{\Pi_1\}) &= \mathcal{B}\left(\widehat{u^{*}}_{\mathrm{c,I}}, \widehat{u^{*}}_{\mathrm{c,II}}, \{a_1, b_1\}\right) \\
&= \widehat{u^{*}}_{\mathrm{c,I}} + \frac{\widehat{u^{*}}_{\mathrm{c,II}} - \widehat{u^{*}}_{\mathrm{c,I}}}{2}\left(1 + \frac{1 - a_1\Pi_1^{b_1}}{1 + a_1\Pi_1^{b_1}}\right) \qquad (2.11) \\
u_{\mathrm{c}}^{*}(\{\Pi_2\}) \approx \widehat{u_{\mathrm{c}}^{*}}^{+}(\{\Pi_2\}) &= \mathcal{B}\left(\widehat{u^{*}}_{\mathrm{c,I}}, \widehat{u^{*}}_{\mathrm{c,II}}, \{a_2, b_2\}\right) \\
&= \widehat{u^{*}}_{\mathrm{c,I}} + \frac{\widehat{u^{*}}_{\mathrm{c,II}} - \widehat{u^{*}}_{\mathrm{c,I}}}{2}\left[1 + \tanh\left(a_2\Pi_2 + b_2\right)\right] \qquad (2.12) \\
u_{\mathrm{c}}^{*}(\{\Pi_3\}) \approx \widehat{u_{\mathrm{c}}^{*}}^{+}(\{\Pi_3\}) &= \mathcal{B}\left(\widehat{u^{*}}_{\mathrm{c,I}}, \widehat{u^{*}}_{\mathrm{c,II}}, \{a_3, b_3\}\right) \\
&= \widehat{u^{*}}_{\mathrm{c,I}} + \frac{\widehat{u^{*}}_{\mathrm{c,II}} - \widehat{u^{*}}_{\mathrm{c,I}}}{2}\left[1 + \frac{2}{\pi}\arctan\left(a_3\Pi_3 + b_3\right)\right] \qquad (2.13)
\end{aligned}
$$

where Π_1, Π_2, Π_3 represents three different blending expressions, not implying multi-variable dependence, and $\{a_1, b_1\}$, $\{a_2, b_2\}$, $\{a_3, b_3\}$ are the corresponding sets of blending constants. Equations 2.11, 2.12, and 2.13 converge to exact asymptotics in both regimes for all finite values of $\{a, b\}$. Equation 2.11 is consistent with the correlation method proposed by Churchill [26] when only limiting values are known by replacing the constant asymptotic behaviour of either regime with a postulated functional dependence (typically power functions) and then blending the constructed function with constant asymptotic in the other regime with a blending exponent n. Equation 2.11 is the special case with $n = 1$. Equation 2.11 and Equation 2.12 are essentially equivalent with the transformation of variables: $\Pi_2 = -\frac{1}{2}\ln(\Pi_1)$, $a_2 = -\frac{1}{2}b_1$ and $b_2 = -\frac{1}{2}\ln(a_1)$.

The two blending constants $\{a, b\}$ capture the two degrees-of-freedom of the functional behaviour after blending: the location of the midpoint $u_{\mathrm{c}}^{*}(\Pi) = \left(\widehat{u^{*}}_{\mathrm{c,I}} + \widehat{u^{*}}_{\mathrm{c,II}}\right)/2$ and the slope of tangent at the midpoint, $\frac{\mathrm{d}\widehat{u_{\mathrm{c}}^{*}}^{+}(\{\Pi\})}{\mathrm{d}\Pi}$, which represents the steepness of the transformation between the two asymptotics.

The differences in the form of the three blending expressions make them applicable for different scenarios. The main difference between Equation 2.11 and Equation 2.12 is the domain, which is $(0, \infty)$ of Equation 2.11, and $(-\infty, \infty)$ of Equation 2.12. Equation 2.12 and Equation 2.13 share the same domain of $(-\infty, \infty)$ and but the

curvature is different, with the same slope at the value of 1 and the same location of midpoint, Equation 2.13 is less sharp than Equation 2.12 as shown in Figure 2.2.

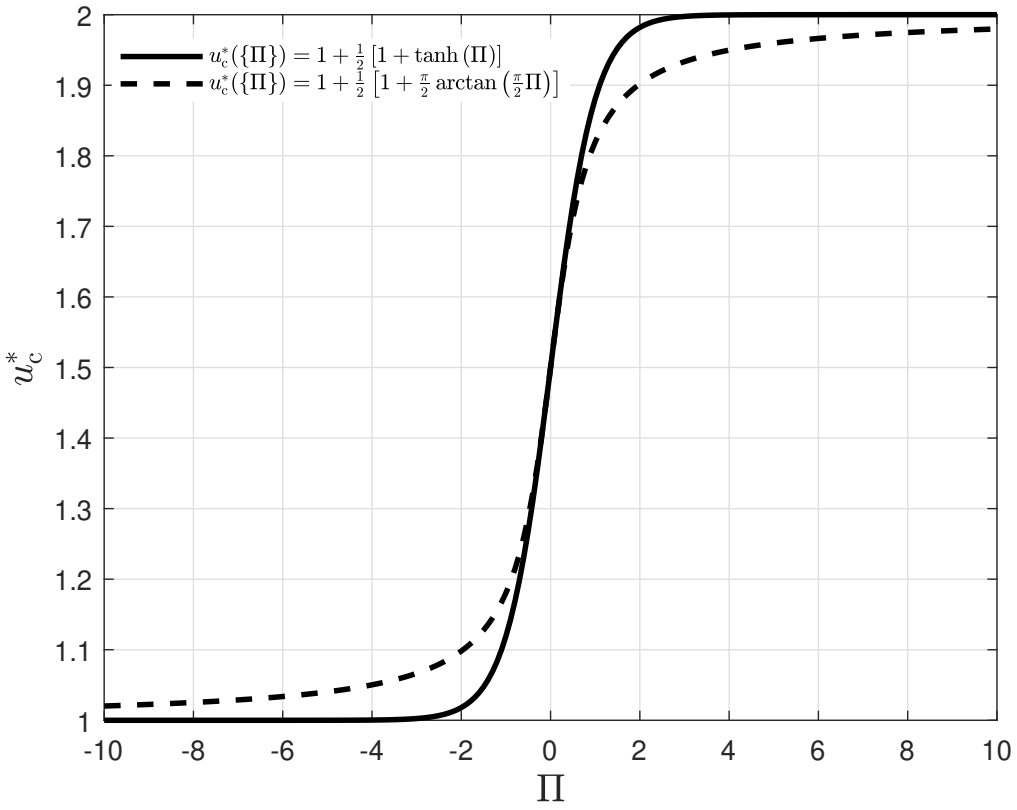

Figure 2.2: Comparison between Equation 2.12 and Equation 2.13. The solid line is $u_c^*(\{\Pi\}) = 1 + \frac{1}{2}[1 + \tanh(\Pi)]$, and the dash line represents $u_c^*(\{\Pi\}) = 1 + \frac{1}{2}\left[1 + \frac{\pi}{2}\arctan\left(\frac{\pi}{2}\Pi\right)\right]$. Two constant asymptotics are 1 and 2,respectively. The center point $\Pi = 0$ and its slope is the same for both functions but the dash line is less steep than the solid line.

2.6.4 Asymptotes with Changes in the Sign

The blending techniques proposed require that all asymptotes are positive over the whole domain; however, in some cases the asymptotic function might be negative outside its range of asymptotic validity. For example, when the asymptotic behavior towards infinity is logarithmic (e.g. $\widehat{u^*}_{c,\Pi}(\{\Pi\}) = \ln(\Pi)$ as $\Pi \to \infty$), the asymptotic tends to minus infinity as Π tends to zero, which is invalid for the techniques proposed. One possible solution in this case is replacing the asymptote $\ln(\Pi)$ with $\ln(1 + \Pi)$,

such that asymptotic behavior keeps unaffected as $\ln(1+\Pi) \approx \ln(\Pi)$, when $\Pi \to \infty$ and the modified expression is always positive over the whole domain of $(0, \infty)$.

2.6.5 Addition of Intermediate Terms

The blending function Equation 2.7 guarantees the limiting solutions in asymptotic regions and estimates values of the intermediate region by optimization of the blending constant n. For power-law functions, this approach is simple and accurate; however, when the functions to be blended are not power-laws, such as logarithmic or exponential functions, Equation 2.7 converges very slowly towards small errors. When convergence is slow, the blending error is small at unrealistically large or small orders of magnitude. An alternative approach is proposed here to deal with these functions while preserving simplicity and accuracy. To improve the accuracy of estimation in the intermediate regime, an additive term $G(\Pi)$ can be introduced as:

$$u_{\mathrm{c}}^*(\{\Pi\}) \approx \widehat{u_{\mathrm{c}}^*}^+(\{\Pi\}) = \left[\widehat{u^*}_{\mathrm{c,I}}(\Pi)^n + \widehat{u^*}_{\mathrm{c,II}}(\Pi)^n + G(\Pi)^n\right]^{1/n} \tag{2.14}$$

where the choice of $G(\Pi)$ is flexible as long as it does not change the asymptotic behavior, i.e., for the case of $n > 0$, $G(\Pi) \ll \widehat{u^*}_{\mathrm{c,I}}(\Pi)$ as $\Pi \to \infty$, and $G(\Pi) \ll \widehat{u^*}_{\mathrm{c,II}}(\Pi)$ as $\Pi \to 0$. Although the blended result could be more accurate with a sophisticated $G(\Pi)$, the format of $G(\Pi)$ should be as simple as possible to minimize the number of involved blending constants.

The added term can be interpreted as the departure between normal blending equation and the exact value of the intermediate regime, or the "asymptote" of the intermediate regime. As the absolute value of blending constant n is typically of the order of magnitude of 1, it is reasonable to set the blending parameter $n = \pm 1$ to reduce the number of optimization variables to two. These variables can be optimized by the proposed minimax optimum procedure of minimizing the maximum error defined in Equation 2.3. The sign of n is chosen based on the asymptotic solutions. When both asymptotes are the lower bounds in their corresponding regimes, $n = 1$

while the dependent variable, $u_c^*(\{\Pi\})$, has a decreasing power of Π, $n = -1$.

For the case of two power asymptotes, the additive term can be chosen in the form of power law as $G(\Pi) = a\Pi^b$, with blending constants $\{B\} = \{a, b, \pm 1\}$. Denoting the two power asymptotes as $\widehat{u^*}_{c,I}(\Pi) = c_I \Pi^{d_I}$ and $\widehat{u^*}_{c,II}(\Pi) = c_{II}\Pi^{d_{II}}$, the exponent of the additive term b has to be set between d_I and d_{II} to make sure $G(\Pi)$ is negligible in the asymptotic regions. It is not clear in what cases this approach is more accurate than Equation 2.7. One obvious difference is that this approach needs to optimize two variables instead of one.

For the case of logarithmic asymptotes (e.g. $\widehat{u^*}_{c,II}(\{\Pi\}) = \ln(\Pi)$), $G(\Pi) = a\Pi^b$ fails in maintaining asymptotic behavior, because $\ln(\Pi)$ is always smaller than power laws when Π tends to infinity, no matter the value of exponent. In this case, additive term $G(\Pi)$ can be expressed in the fractional form as $G(\Pi) = a\Pi/(b + \Pi)$ instead with blending constants $\{B\} = \{a, b, \pm 1\}$, such that the additive term can be smaller than the logarithmic asymptote in the limiting regime when $\Pi \to \infty$.

2.6.6 An Extension of 1D Blending: Parametric 1D Blending

Some problems involve multiple dimensionless groups, so they are not 1D blending problems. However, when the some dimensionless groups have a reduced range of variation, they can be considered as another parameter in the blending problem, as opposed to another dimensionless group to be blended. For example, solid mechanics problems involve the dimensionless parameter ν (Poisson's ratio), which is seldom far from 0.3 for most engineering materials. In this case, it is convenient to consider ν as a constant instead of performing blending over unrealistic values.

This approach is especially valuable when the dimensionless groups that can be considered as parameters is such that blending can be reduced to 1D.

2.7 Challenges beyond 1D Blending

The 1D blending describes many engineering problems concerning to one independent variable with much rigor and elegance, however, in some cases, the secondary factors play a significant role and are not negligible indeed, for example, welding on a plate of medium thickness[109, 121], or where the size of a Gaussian distributed heat source can not be neglected [36]. It is necessary to develop a series of practical and systematic 2D blending methods on the basis of current 1D blending theory.

In normalized form, 2D blending problem can be defined as $u_{\mathrm{c}}^{*}\left(\Pi_1, \Pi_2\right)$, where u_{c}^{*} is the target characteristic value dependent on two dimensionless variables $\{\Pi\} = \{\Pi_1, \Pi_2\}$. The 2D blending problem can also be addressed with an equivalent expression in implicit form: $F\left(u_{\mathrm{c}}^{*}, \{\Pi\}\right) = F\left(u_{\mathrm{c}}^{*}, \Pi_1, \Pi_2\right) = 0$, which could be one equation or a group of equations associated with problem parameters. The general strategy to construct 2D blending is to decompose the 2D blending problem into several 1D blending branches, where 1D blending theory is well-developed, and then combine the solved 1D blending equation of each branch to assemble the solution to 2D problem.

Asymptotes in 2D problems are typically derived with limitation theorems, but the limitation theorems of two variable or multi-variable functions are much more complex than functions of single dependence. The complexity includes but not restrict to the division of limiting regimes, different types of asymptotics, relationship between double limits and iterated limits, and so on. The decomposition of 2D blending into 1D blending problems and the assembly of 2D blending solution based on 1D blending functions have high demand on mathematical skills and are never trivial. The simplest case of 2D blending is that the target function $u_{\mathrm{c}}^{*}\left(\Pi_1, \Pi_2\right)$ is assumed variable separable over its entire domain, which means $u_{\mathrm{c}}^{*}\left(\Pi_1, \Pi_2\right) = v\left(\Pi_1\right) \cdot w\left(\Pi_2\right)$, and the 2D blending could be directly split into two 1D blending functions of $v\left(\Pi_1\right)$ and $w\left(\Pi_2\right)$. Thus the assembled 2D blending is in form of the product of both 1D blending equation $\widehat{u_{\mathrm{c}}^{*}}^{+}\left(\Pi_1, \Pi_2\right) = \widehat{v}^{+}\left(\Pi_1\right) \cdot \widehat{w}^{+}\left(\Pi_2\right)$, where $\widehat{v}^{+}\left(\Pi_1\right)$ $\widehat{w}^{+}\left(\Pi_2\right)$ are

relatively simple and easily tractable with in 1D blending theory proposed in this paper. Systematic 2D blending methods to obtain general estimation of the target characteristic value in terms of asymptotics and correction factors with high accuracy are the focus of current research.

2.8 Case Studies

Four case studies are be presented to demonstrate the application of MRCF approach. Target characteristic values of interest are expressed in terms of asymptotics (simple case solutions in the extreme cases) and the type of the blending approach for each case will be identified and applied to generate correction factors in explicit form.

Case A: Estimation of Maximum Bead Width Based on Rosenthal 3D Model

Step 1: List all physics considered relevant

Relevant physics involved in the shape of the weld pool include heat transfer, heat dissipation on the surface to the environment, convective flow, the effects of fluid dynamics and so on. It is impossible to list all relevant mechanisms but the dominant phenomenon and the best practice is to list typical and essentially relevant approximations, which can be suggested by published papers and experimental observations.

Step 2: Identify dominant factors

For the case of the maximum bead width, the dominant mechanism is postulated as heat transfer via conduction and the classic Rosenthal 3D model [126, 128] was utilized to calculate thermal characteristics which assumes the heat source as a point moving with constant velocity in a straight line on the surface of the semi-infinite base materials with constant thermal properties. Heat dissipation on the mental surface, convective flow, and the effects of fluid dynamics are neglected as secondary phenomenon. This Rosenthal 3D model assumes the heat source as a infinitely small

point(which is actually not), and considers everything as solid by neglecting the effect of fluid dynamics and phase changes. What' more, it only focuses on the conduction within the solid base metal and the advection due to the relative motion between the heat source and the substrate without considering the effects of convective heat transfer in the molten metal and heat dissipation to the external environment (convection and radiation). Due to the huge simplifications, this idealized model and the obtained estimations must check self-consistency which will be discussed in step 4.

Step 3: Solve approximate problem considering only dominant factors (Minimal Representation)

Starting from the Fourier's law and the boundary conditions of the moving system, the simplified problem has been solved in [96] and the obtained analytical solution of the temperature field has the following expression:

$$T(x, y, z) = T_0 + \frac{q}{2\pi kr} \exp\left[-\frac{U}{2\alpha}(r + x)\right] \tag{2.15}$$

where q is the net thermal power absorbed by the base material, k is the thermal conductivity of the base material, and T_0 is the temperature of the substrate far from the heat source or the preheat temperature. In welding, the power q is estimated as the product of nominal power of the heat source and its thermal efficiency.

Equation 2.15 provides the value of temperature for each point in the domain with a singularity at $r = 0$, which is the location of the point heat source and the temperature value there is infinite. It is the theoretical solution of the temperature field as a function of position to the simplified welding problem by considering conduction as the dominant mechanism. However, in practical applications, temperatures of interest always appear as known conditions, for example, melting temperature and the A_1, A_3 where phase transformations typical occur are readily known beforehand. Characteristic values which capture the essence of thermal history such as maximum bead width and the location where it occurs are unknown and difficult to obtain.

In this idealized model, dependent variable is the temperature $\{U\} = \{T\}$, and

there are three spatial independent variables $\{X\} = \{x, y, z\}$, and five parameters $\{P\} = \{T_0, q, k, U, \alpha\}$. The characteristic value of interest is the maximum isotherm width: $u_c(\{P\}) = y_{\max}$. After normalization and dimensional analysis of Equation 2.15, the conclusion is that if we denote the temperature value of the isotherm under consideration as $T = T_c$, the dimensionless characteristic values associated with $T = T_c$ depend only on one dimensionless group (more details can be found in [96]): The Rykalin number (Ry), first proposed by Fuerschbach [45] and has the following expression in terms of parameters:

$$\mathrm{Ry} = \frac{qU}{4\pi k\alpha\left(T_c - T_0\right)} \tag{2.16}$$

where the constant of $1/4\pi$ is added to simplify the final expressions detailed below.

All dimensionless characteristic values associated with an isotherm $T = T_c$ can be captured with functions depending only on Ry, thus the set of independent dimensionless groups based only on parameters turns into $\{\Pi\} = \{\mathrm{Ry}\}$ and the dimensionless characteristic value $u_c^*(\{\Pi\}) = y_{\max}^*(\{\Pi\})$ can be expressed with sole dependence on Ry as $y_{\max}^*(\mathrm{Ry})$. As Ry is the only one dimensionless group necessary to capture all characteristic values, the number of asymptotic regimes is given by $2^1 = 2$ and they are Regime I, corresponding to large values of Ry ("fast heat source" where advection dominates over conduction), and Regime II, corresponding to small values of Ry ("slow heat source" with heat transfer dominated by conduction) and the two asymptotics can be represented as $\widehat{u^*}_{\mathrm{c,I}}(\{\Pi\}) = \widehat{y^*}_{\max_{\mathrm{I}}}(\mathrm{Ry})$ and $\widehat{u^*}_{\mathrm{c,II}}(\{\Pi\}) = \widehat{y^*}_{\max_{\mathrm{II}}}(\mathrm{Ry})$, respectively. These asymptotic regimes yield simple expressions for the characteristic values, usually in the form of power laws. Asymptotic analysis of Equation 2.15 yields the following two asymptotics of the dimensionless maximum isotherm width dependent only on Ry [96]:

$$\widehat{y^*}_{\max_{\mathrm{I}}}(\mathrm{Ry}) = \sqrt{\frac{2\mathrm{Ry}}{\mathrm{e}}} \qquad \text{for Regime I (fast)} \tag{2.17}$$

$$\widehat{y^*}_{\max_{\mathrm{II}}}(\mathrm{Ry}) = \mathrm{Ry} \qquad \text{for Regime II (slow)} \tag{2.18}$$

Step 4: Check for self-consistency

As Equation 2.15 comes directly from the postulated model, the validity of calculations based on Equation 2.15 (Equation 2.17 and 2.18) will remain in the limit of the validity of this model itself. The self-consistency of this idealized model has been accomplished by comparison with experiments as it is impossible to prove the accuracy of the Rosenthal 3D model from the mathematical point of view. Christensen in the 1960s has done a series of experiments to test the validity of this Rosenthal 3D model [22] of different operating parameters and materials. It has shown that despite of the great simplifications, the model by considering conduction and advection as the dominant phenomena can still generate reasonable results for points far away from the heat source at temperatures below the melting temperature.

Step 5: Compare predictions to "reality"

Equations 2.17 and 2.18 are less accurate for intermediate values (Ry=O(1)). As the obtained two asymptotics are in the form of power laws, Standard 1D Blending method is applicable for this case. For the non-asymptotic region, simple and accurate expressions can be obtained with Equation 2.7.

Substitute Equation 2.17 and 2.18 into Equation 2.7, the blended function of the maximum isotherm width in dimensionless form is obtained:

$$y^*_{\max}(\mathrm{Ry}) \approx \widehat{y^*}^{+}_{\max}(\mathrm{Ry}) = \left[\widehat{y^*}_{\max_{\mathrm{I}}}(\mathrm{Ry})^n + \widehat{y^*}_{\max_{\mathrm{II}}}(\mathrm{Ry})^n\right]^{1/n} \tag{2.19}$$

The optimal blending constant n was determined using a minimax approach with two nested optimizations as detailed in [96]. With Rosenthal 3D model and the resulting temperature field, the "reality" used here to calibrate the deviations from the idealized behavior is the maximum value of the isotherm width calculated from Equation 2.15 numerically. When n is equal to -1.7312, the maximum error over the whole domain of Ry is less than 0.7236%.

Step 6: Create correction factors

Substituting the two asymptotics $\widehat{u^*}_{\mathrm{c,I}}(\{\Pi\}) = \widehat{y^*}_{\max_{\mathrm{I}}}(\mathrm{Ry})$ and $\widehat{u^*}_{\mathrm{c,II}}(\{\Pi\}) =$

$\widehat{y^*}_{\max_{\text{II}}}(\text{Ry})$ into Equations 2.8 and 2.9, the following expression for the correction factors are obtained:

$$f_{y_{\max}}(\text{Ry}) = \left[1 + \left(\sqrt{\frac{\text{eRy}}{2}}\right)^{\pm n}\right]^{1/n} \qquad \begin{matrix} + \text{ for Regime I (fast)} \\ \\ - \text{ for Regime II (slow)} \end{matrix} \tag{2.20}$$

where the exponent $+n$ corresponds to Regime I, and $-n$ corresponds to Regime II. The minimax error is always smaller than 0.7236% at the optimal value of n=-1.7312.

Correction factors based on both asymptotics are plotted in Figure 2.3 and the reflected symmetry is consistent with Equation 2.20 as expected. They can also be used to check the validity of both asymptotics. The intersection of the correction factors, $\text{Ry}_c = 0.7359$, can be considered as the rough divider of the two asymptotic regions: Regime I, Regime II and the intermediate region (the vicinity of Ry_c) where the typically the maximum departure occurs.

Case B: Predictions of the Maximum Hardness of the HAZ

One of the major challenges in the welding industry is predicting the maximum hardness of the heat affected zone that depends the chemical composition and the welding parameters. During the 1970s and the 1980s, many empirical models (based on statistical regression of experimental data) were proposed to address this problem [69, 160]. Although each proposed model is different, they all treat the problem with a similar nature using asymptotic values to obtain a hardness value as a function of the cooling rate.

Basically, the hardness of a specific point on heat affected zone depends on the present microstructures and their volume fraction. At the same time, the type and amount of each microstructure is a function of the thermal history and chemical composition. In the case, the characteristic value of interest is the the maximum hardness of the HAZ, and many variables can be discarded as the assumptions are

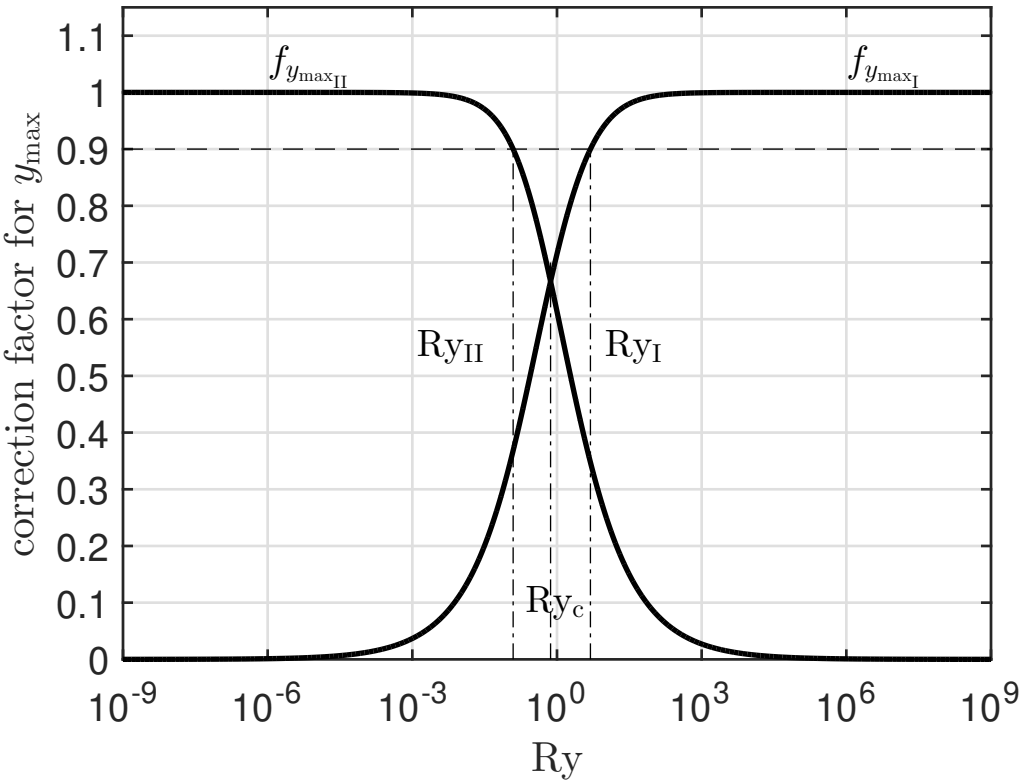

Figure 2.3: Correction factors for maximum isotherm width $y_{\max}$ [96]

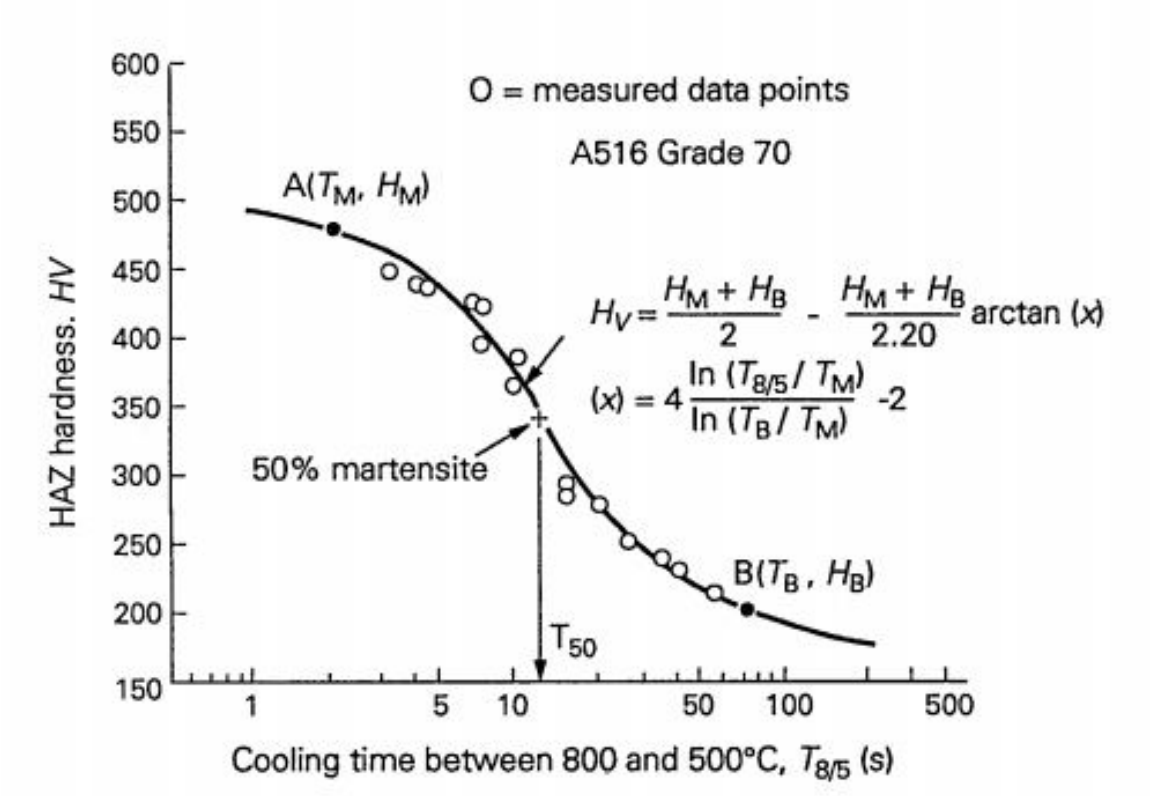

Figure 2.4: Characteristic hardness in HAZ as a function of cooling time between 800°C and 500°C [160].

made. For example, austenitization peak temperature, which plays an important role in the kinetics of austenite decomposition, can be assumed to be equal for all cases by considering that the maximum hardness will be found adjacent to the fusion line where the peak temperature is maximum, very close to the fusion temperature (i.e in the coarse grain heat affected zone). By making this simplification, hardness can be written down as a function of the cooling rate at 700 °C (or cooling time, $t_{8/5}$), and the nominal chemical composition of the welded plate.

One clear example of using asymptotes to address this problem is given by Yurioka's model [160] and a proposed Continuous Cooling Transformation Structure Hardness (CCTSH) curve is represented in Figure 2.4. In this case, the maximum hardness in HAZ depends only on the cooling time between 800°C and 500°C . With only one dependence on the cooling time, there are in total two regimes and the char-

acteristic points given by the hardness upper (H_M) and lower limits (H_B) and their characteristic times are used to develop a equation able to predict the hardness value for any time between τ_M and τ_B.

Upper and lower hardness asymptotes are easy to picture when this problem is addressed, if the different possible microstructures are considered. The upper limit is directly related with the hardness of the martensite, which means $\widehat{u}_{\mathrm{c,II}} = H_M$. No other microstructure is harder than the fresh martensite obtained from cooling from the austenite region with cooling rates higher than a critical value τ_M. On the other hand, the lower limit can be quite more complicated to picture, since different criteria used by the author. However, the main idea resides on using a lower limit, $\widehat{u}_{\mathrm{c,I}} = H_B$, that represents a microstructure with no martensite, τ_B. After the formulation of the two limiting constant hardness values empirically, a blended expression in the form of Equation 2.13 was proposed:

$$HV = \frac{H_M + H_B}{2} - \frac{H_M - H_B}{2.2} \arctan x \tag{2.21}$$

where x is defined as:

$$x(\mathrm{rad}) = 4\frac{\log \frac{t_{8/5}}{\tau_M}}{\log \frac{t_B}{\tau_M}} - 2$$

It is important to remark that, when blending two constant asymptotics (point A and B in Figure 2.4), Equation 2.13 must be applied with a understanding of its applicable scope as for cooling times that are not between τ_M and τ_B, Equation 2.21 is not applicable. Equation 2.11 and Equation 2.12 can also be applied for this case and there are many other types of functions proposed by different authors.

Case C: Thermal Stress Field in the Vicinity of a Moving Point Heat Source

Step 1: List all physics considered relevant

The thermal stress field produced by a non-uniform temperature field surrounding

a moving point heat source is of significant interest in welding research due to the implications for the size and magnitude of the residual stress field. This example will focus on estimation of the thermal stresses produced by a moving heat source in a thin-plate (i.e. 2D material). The characteristic values (u_c) which are of primary interest in the analysis of thermal stresses are the longitudinal stress ($\sigma_{x,c}$) and transverse stress ($\sigma_{y,c}$) produced by some critical temperature change (ΔT_c).[1] The dimensionless form ($u_c^* = \{\sigma_x^*, \sigma_y^*\}$) of the characteristic values is obtained by normalizing with respect to the product of the elastic modulus (E), coefficient of thermal expansion (a), and critical temperature change (ΔT_c):

$$\{u_c^*\} = \{\sigma_{x,c}^*, \sigma_{y,c}^*\} = \{\sigma_{x,c}/(Ea\Delta T_c), \sigma_{y,c}/(Ea\Delta T_c)\}$$

The mathematical formulation for the thermal stress field in a 2D plane composed of a homogeneous, isotropic, linear elastic material involves a total of six dependent variables, three independent variables and six fixed parameters. The dependent variables are: $\{U\} = \{\epsilon_x, \epsilon_y, \gamma_{xy}, \sigma_x, \sigma_y, \tau_{xy}\}$

which represent the x, y, and shear components of the strain and stress fields; the independent variables are:

$$\{X\} = \{\Delta T, x, y\}$$

where ΔT is the temperature field at a given location (x,y) in a 2D cartesian plane; and the parameters are:

$$\{P\} = \{\Delta T_c, x_c, y_c, E, G, a\}$$

where ΔT_c is some characteristic temperature change, x_c is the maximum length of the characteristic temperature isotherm, y_c is the maximum width of the characteristic temperature isotherm, G is the shear modulus of the material, E is the elastic modulus of the material, and a is the linear coefficient of thermal expansion.

Step 2: Identify dominant factors

Applying the Buckingham Π theory, it is found that there can only be exactly

[1] by convention stresses/strains oriented parallel to the heat source movement (i.e. x direction) are termed longitudinal, and stresses/strains oriented perpendicular to heat source movement (i.e. y direction) are referred to as transverse

two independent dimensionless groups in this analysis. Any 2 dimensionless groups that form an independent set may be selected. In this example, the dimensionless parameters are chosen as:

$\{\Pi\} = \{E/G, x_c/y_c\}$

where E/G is the ratio of the elastic modulus to shear modulus which can be equivalently expressed in terms of the Poisson's ratio (ν) as $E/G = 2(1+\nu)$ and $x_c/y_c = \text{Æ}$ is defined as the aspect ratio of the critical isotherm ΔT_c.

Note that in this example, since there are two dimensionless groups (G/E and Æ), there will be four asymptotic regimes:

- Regime I: $\text{Æ} \to \infty, E/G \to 0$
- Regime II: $\text{Æ} \to 1, E/G \to 0$
- Regime III: $\text{Æ} \to \infty, E/G \to \infty$
- Regime IV: $\text{Æ} \to 1, E/G \to \infty$

Note that the lower asymptotic value of the aspect ratio Æ is 1, which corresponds to a perfectly circular temperature isotherm (i.e. an infinitely slow or stationary heat source).

For all isotropic materials it is necessary that $-1 \leq \nu \leq 0.5$[51], which constrains the allowable range of the modulus ratio to $0 \leq E/G \leq 3$. For all commonly welded metallic materials, Poisson's ratio is approximately $\nu = 0.3$ and the modulus ratio is approximately $E/G = 2.6$. Since for all practical problems, the modulus ratio is relatively small in Regime I and Regime II , which are of practical interest.

Step 3: Solve approximate problem considering only dominant factors (Minimal Representation)

The asymptotic solutions for the dimensionless stresses in Regime I are [49]:

$$\widehat{\sigma^*}_{x,\text{c,I}} = 1$$

$$\widehat{\sigma^*}_{y,\text{c,I}} = 1/\text{Æ}^2$$

and the corresponding dimensional stress values are:

$$\widehat{\sigma}_{x,\mathrm{c,I}} = aE\Delta T_c$$

$$\widehat{\sigma}_{y,\mathrm{c,I}} = aE\Delta T_c/\text{Æ}^2$$

Analytical expressions for the asymptotic solutions of the dimensionless stresses in Regime II will have the general form:

$$\widehat{\sigma^*}_{x,\mathrm{c,II}} = \widehat{\sigma^*}_{x,\mathrm{c,II}}(\{\text{Æ}, \nu\})$$

$$\widehat{\sigma^*}_{y,\mathrm{c,II}} = \widehat{\sigma^*}_{y,\mathrm{c,II}}(\{\text{Æ}, \nu\})$$

Step 4: Check for self-consistency

For single-pass full-penetration welding of plain carbon and low-alloy steel, the aspect ratio is expected to vary between 2 - 20 depending on the welding process. Although the asymptotic equations may provide reasonable estimates in some of these cases, it is clearly an issue of practical interest necessary to obtain estimates of the characteristic stresses at intermediate values of the aspect ratio. The asymptotic blending technique provides a powerful and convenient method to develop a closed form equation for estimating the stresses at these intermediate values.

Step 5 and 6: Compare predictions to "reality" and create correction factors

In this case, the standard approach for 1D asymptotic blending may be applied with only one minor modification. Although the asymptotic solutions in Regime I depend only on Æ, this will not necessarily be the case in Regime II. If the asymptotic expressions in Regime II are found to depend on the value of Poisson's ratio, it will be necessary to optimize the value of the set of blending constants $\{B\}$ over a range of typical values of ν (ex. 0.25-0.35) using Parametric 1D blending. In this case, the value of ν is treated as a parameter and the optimization for the 1D blending coefficients is evaluated in the 2D space defined by $1 < \text{Æ} < \infty$ and ν is around the value of 0.3. The 1D parametric blending technique provides a simple and powerful alternative to full 2D blending in 2-parameter systems where the range of one parameter is relatively restricted.

Although significant challenges are associated with obtaining experimental measurements of thermal stresses, the "reality" for the critical stress at a selection of intermediate values used in the optimization may be readily obtained from finite-element analysis (FEA). A limited number of experimental measurements may then be performed to validate the final solution and aid in the development of additional correction factors for secondary effects.

Case D: Maximum Temperature in Friction Stir Welding (FSW)

Step 1: List all physics considered relevant

Relevant physics involved in FSW are the plastic flow near the pin and the generated heat, heat conduction into the base material, heat loss to the environment, inertial factors, kinematics and forces related in the deformation.

Step 2: Identify dominant factors

For the case of FSW, the dominant factors are identified as the heat diffusion in a localized soft layer in [99, 140]. Four groups of competing phenomena are considered: heat diffusion vs. heat advection, kinematics of rotational flow vs. translational flow, thickness of the soft shear layer vs. the radius of the pin and the peak temperature jump caused by shoulder vs. the contribution of plastic area around the pin. Among the four groups, dominant factors are identified as the heat diffusion, rotational flow, thickness of the shear layer and the dominance of the pin on peak temperature. Self consistency will be checked for the secondary factors in step 4 by comparing the obtained expression for maximum temperature against experiments published in literature.

Step 3: Solve approximate problem considering only dominant factors (Minimal Representation)

The problem is greatly simplified to its minimal representation by considering only dominant factors listed above. The target characteristic value is the maximum

temperature developed during process can be expressed as $u_c = T_s$ and asymptotics obtained have the following form[99]:

$$\widehat{T}_s = T_0 + \Delta T_{\mathrm{m}} \left[\frac{3}{2} \frac{\eta_s}{AB\Delta T_{\mathrm{m}}} \left(\frac{\eta K_0}{\Delta T_0} \right)^{n-1} \left(\frac{a^2 \tau_{\mathrm{R}}}{k} \right)^{n} \omega^{n+1} \right]^{\frac{1}{2}} \tag{2.22}$$

where T_s is the maximum temperature achieved at the pin-shear layer interface, T_0 is the temperature at the interface between shear layer and the base plate, $\Delta T_{\mathrm{m}} = T_m - T_0$ and T_m is the melting temperature of the substrate, η_s is the efficiency which considers mechanical energy converted into heat, excluding the mechanical energy accumulated in the form of dislocations, A is the constant of constitutive behavior of the alloy and η is the total efficiency of the process, accounts for energy stored in the form of dislocations in the shear layer and heat lost to the tool, K_0 is the Modified Bessel function of second kind and 0 order, $\Delta T_0 = T_0 - T_\infty$, a is the pin radius, τ_{R} is the reference shear stress of the alloy, k is the thermal conductivity of the alloy at T_0 and ω is the angular velocity of rotation of the pin.

Step 4: Check for self-consistency

All predictions based on the minimally represented problem must be checked for self-consistency. For the case of FSW, Equation 2.22 was evaluated by comparing the effect of assumed secondary factors on the accuracy of the estimation. The relative magnitude of the selected secondary factor can be represented by its value to that of the dominant factors. In this way, a value of 1 indicates that the secondary factor is of similar magnitude than the dominant factor. Very small values on the horizontal axis correspond to the self-consistent regime, while high values correspond to inconsistent cases in which the factors considered secondary are actually larger than the dominant factors. There are four independent dimensionless groups that characterize the secondary phenomena $\{\Pi\} = \{\mathrm{Pe}, V/\omega\hat{\delta}, \hat{\delta}/a, (T_p - T_\infty)/(T_s^+ - T_\infty)\}$

Step 5: Compare predictions to "reality"

Equation 2.22 must be validated through comparisons with reality. In summary, three factors considered secondary (advective heat transfer, pin translation on max-

imum temperature and shoulder heat input on the peak temperature in FSW) have been proved indeed secondary for the vast majority of cases in [99, 140], and that for those valid cases, Equation 2.22 predicts the proper order of magnitude and dependence on process parameters. However, the approximation by considering the shear layer thickness on peak temperature as secondary phenomena is not always valid, and correction factors for the estimation of maximum temperature are necessary. The 4D blending problem can be simplified into Parametric Blending of one dependence: $\{\Pi\} = \{\mathrm{Pe}, V/\omega\hat{\delta}, \hat{\delta}/a, (T_p - T_\infty/T_s^+ - T_\infty)\} \approx \{\hat{\delta/a}\}$

Step 6: Create correction factors

In this FSW case, systematic errors in the math and physics can be accounted for by the correction factor in Standard 1D blending form with blending constants $\{B\} = \{C_1, C_2, C_3\}$:

$$f_T^+ = C_1 \left(1 + C_2 \frac{\hat{\delta}}{a}\right)^{C_3}$$

Blending constant C_1 takes care of the systematic error in the mathematics while C_2 and C_3 are used to account for the secondary phenomena. When C_1=0.764, C_2=0.259, and C_3=-0.857, optimal match between Equation 2.22 and the published experimental values has been achieved with 12% standard deviation.

2.9 Conclusions

Design rules in the form of a simple formula (asymptotic behavior of the simplified problem by considering only dominant mechanisms) and correction factors which capture the deviation from the ideal cases are proposed. This approach is of much help to solve complex multiphysics problems such as welding and is based on a six-step framework we termed Minimal Representation and Correction Factor (MRCF). The formulation of the design rules makes it convenient to couple them to represent multi-coupled phenomena and embed them in numerical models and control systems. It is shown through examples that the technique of blending has wide applicability

for correlating experimental or numerical data or theoretical values for processes with known asymptotic solutions.

The proposed blending theory extends the applicability of standard blending approaches to obtain general, accurate and explicit expressions in terms of known asymptotic solutions and blending constants determined with a systematic optimization procedure. The blending expressions are also used to develop correction factors that capture the deviations from ideal cases.

Blending is also useful in summarizing isolated experimental results and numerical data from simulation. The general and systematic formulation can be extended to other multi-coupled phenomena besides welding.

2.10 Appendix: Notation

Table 2.1: Notation

Symbols	Description
Variables	
a	Blending constant
b	Blending constant
f	Correction factors
k	Number of independent reference units
m	Number of independent physical magnitudes
n	Blending exponent
n_r	Number of regimes
u	Dependent variable and related function
v	Varaible separated function of u
w	Varaible separated function of u
B	Blending constants
F	Implicit Function

Continued on next page

Table 2.1 – continued from previous page

Symbols	Description
P	Problem parameter
X	Independent variable
U	Dependent variable
Π	Independent dimensionless groups
$\mathcal{B}$	Blending functions
Superscripts	
*	Normalized value
$\widehat{\ }$	Asymptotic behavior
$^+$	Blended approximation
Subscripts	
I	Corresponding to Regime I
II	Corresponding to Regime II
III	Corresponding to Regime III
i	Regime i
c	Characteristic values
Others	
$\{\cdots\}$	Set

References

[1] A. Acrivos, "On the Solution of the Convection Equation in Laminar Boundary Layer Flows," *Chemical Engineering Science*, vol. 17, no. 6, pp. 457–465, 1962.

[2] A. Acrivos, "A Rapid Method for Estimating the Shear Stress and the Separation Point in Laminar Incompressible Boundary-Layer Flows," *Journal of the Aerospace Sciences*, vol. 27, no. 4, pp. 314–315, 1960.

[6] Y. Arata, K. Nishiguchi, T. Ohji, and N. Kohsai, "Weldability Concept on Hardness Prediction (Materials, Metallurgy, Weldability)," *Transactions of JWRI*, vol. 8, no. 1, pp. 43–52, 1979.

[13] A. Bejan, *Convection Heat Transfer*. Hoboken, New Jersey: John Wiley & Sons, Inc., 2013.

[19] E. Buckingham, "On Physically Similar Systems; Illustrations of the Use of Dimensional Equations," *Physical Review*, vol. 4, no. 4, pp. 345–376, 1914, ISSN: 0031899X. arXiv: `arXiv:1011.1669v3`.

[22] N. Christensen, Davies, V. de L., and K. Gjermundsen, "Distribution of Temperatures in Arc Welding," *British Welding Journal*, vol. 12, no. 2, pp. 54–75, 1965.

[23] S. W. Churchill and R. Usagi, "A general expression for the correlation of rates of transfer and other phenomena," *AIChE Journal*, vol. 18, no. 6, pp. 1121–1128, 1972, ISSN: 15475905.

[24] S. W. Churchill, "Comprehensive Correlating Equations For Heat, Mass and Momentum Transfer in Fully Developed Flow in Smooth Tubes," *Industrial & Engineering Chemistry Fundamentals*, vol. 16, no. 1, pp. 109–116, 1977.

[25] S. W. Churchill and H. H. S. Chu, "Correlating Equations for Laminar and Turbulent Free Convection From a Vertical Plate," *International Journal of Heat and Mass Transfer*, vol. 18, no. 11, pp. 1323–1329, 1975.

[26] S. W. Churchill and R. Usagi, "A Standardized Procedure for the Production of Correlations in the Form of a Common Empirical Equation," *Industrial & Engineering Chemistry Fundamentals*, vol. 13, no. 1, pp. 39–44, 1974.

[31] J. A. Dantzig and C. L. Tucker, *Modeling in Materials Processing*. Cambridge, England: Cambridge University Press, 2001, p. 384.

[35] F. Durst, S. Ray, B. Ünsal, and O. A. Bayoumi, "The Development Lengths of Laminar Pipe and Channel Flows," *Journal of Fluids Engineering*, vol. 127, no. 6, pp. 1154–1160, 2005.

[36] T. W. Eagar and N. S. Tsai, "Temperature Fields Produced by Traveling Distributed Heat Sources," *Welding Journal*, vol. 62, no. 12, pp. 346–355, 1983, ISSN: 00432296.

[40] P. S. Fedkiw and J. Newman, "Mass-Transfer Coefficients in Packed Beds at Very Low Reynolds Numbers," *International Journal of Heat and Mass Transfer*, vol. 25, no. 7, pp. 935–943, 1982.

[43] P. W. Fuerschbach, "Measurement and Prediction of Energy Transfer Efficiency in Laser Beam Welding," *Welding Journal, Research Supplement*, vol. 75, no. 1, pp. 24–34, 1996.

[44] P. W. Fuerschbach and G. A. Knorovsky, "A Study of Melting Efficiency in Plasma Arc and Gas Tungsten Arc Welding," *Welding Journal*, vol. 70, no. 11, pp. 287–297, 1991.

[45] P. W. Fuerschbach and G. R. Eisler, "Determination of Material Properties for Welding Models by Means of Arc Weld Experiments," in *6th Intl. Trends in Welding Research*, Pine Mountain, Georgia, 2002.

[49] M. Grams and P. F. Mendez, "Quantification of root pass residual stresses in pipeline girth welds," in *Fabtech/AWS Annual Meeting*, 2017.

[51] G. N. Greaves, A. L. Greer, R. S. Lakes, and T. Rouxel, "Poisson's ratio and modern materials," *Nat Mater*, vol. 10, no. 11, pp. 823–837, 2011, ISSN: 1476-1122.

[55] X. He, P. W. Fuerschbach, and T. DebRoy, "Heat Transfer and Fluid Flow during Laser Spot Welding of 304 Stainless Steel," *Journal of Physics D: Applied Physics*, vol. 36, no. 12, pp. 1388–1398, 2003.

[69] T. Kasuya and N. Yurioka, "Prediction of Welding Thermal History by a Comprehensive Solution," *Welding Journal*, vol. 72, no. 3, pp. 107–115, 1993.

[77] W. B. Krantz, *Scaling Analysis in Modeling Transport and Reaction Processes: A Systematic Approach to Model Building and the Art of Approximation*. New York: John Wiley & Sons, 2007.

[92] P. F. Mendez, K. E. Tello, and S. S. Gajapathi, "Generalization and communication of welding simulations and experiments using scaling analysis," in *9th International Conference on Trends in Welding Research*, vol. 1, Chicago, Illinois, USA: ASM International, 2012, pp. 249–258.

[93] P. F. Mendez, "Characteristic Values in the Scaling of Differential Equations in Engineering," *Journal of Applied Mechanics, Transactions ASME*, vol. 77, no. 6, 2010, ISSN: 00218936.

[95] P. F. Mendez, R. Furrer, R. Ford, and F. Ordóñez, "Scaling Laws as a Tool of Materials Informatics," *JOM*, vol. 60, no. 3, pp. 60–66, 2008.

[96] P. F. Mendez, Y. Lu, and Y. Wang, "Scaling Analysis of a Moving Point Heat Source in Steady- State on a Semi-Infinite Solid," *Journal of Heat Transfer*, vol. 140, no. 8, p. 081 301, 2018.

[98] P. F. Mendez and F. Ordonez, "Scaling Laws from Statistical Data and Dimensional Analysis," *Journal of Applied Mechanics, Transactions ASME*, vol. 72, no. 5, pp. 648–657, 2005, ISSN: 00218936.

[99] P. F. Mendez, K. E. Tello, and T. J. Lienert, "Scaling of Coupled Heat Transfer and Plastic Deformation around the Pin in Friction Stir Welding," *Acta Materialia*, vol. 58, no. 18, pp. 6012–6026, 2010, ISSN: 1359-6454.

[104] P. E. Murray, "Stability of Droplets in Gas Metal Arc Welding," *Science and Technology of Welding and Joining*, vol. 5, no. 4, pp. 221–226, 2000.

[105] P. E. Murray, "Selecting Parameters for GMAW Using Dimensional Analysis," *Welding Journal*, vol. 81, no. 7, pp. 125–131, 2002.

[106] P. E. Murray and A. Scotti, "Depth of Penetration in Gas Metal Arc Welding," *Science and Technology of Welding and Joining*, vol. 4, no. 2, pp. 112–117, 1999.

[109] O. R. Myhr and Ø. Grong, "Dimensionless Maps for Heat Flow Analyses in Fusion Welding," *Acta Metallurgica Et Materialia*, vol. 38, no. 3, pp. 449–460, 1990, ISSN: 09567151.

[121] K. Poorhaydari, B. M. Patchett, and D. G. Ivey, "Estimation of Cooling Rate in the Welding of Plates with Intermediate Thickness," *Welding Journal*, vol. 84, no. 10, 149–s–155–s, 2005.

[122] K. Rajan, C. Suh, and P. F. Mendez, "Principal Component Analysis and Dimensional Analysis as Materials Informatics Tools to Reduce Dimensionality in Materials Science and Engineering," *Statistical Analysis and Data Mining*, vol. 1, no. 6, pp. 362–371, 2009.

[124] A. Robert and T. DebRoy, "Geometry of Laser Spot Welds from Dimensionless Numbers," *Metallurgical and Materials Transactions B*, vol. 32, no. 5, pp. 941–947, 2001.

[126] D. Rosenthal, "The Theory of Moving Sources of Heat and Its Application to Metal Treatments," *Transactions of the A.S.M.E.*, vol. 68, pp. 849–866, 1946.

[128] D. Rosenthal, "Mathematical Theory of Heat Distribution During Welding and Cutting," *Welding Journal*, vol. 20, no. 5, pp. 220–234, 1941.

[130] G. G. Roy, R. Nandan, and T. DebRoy, "Dimensionless Correlation to Estimate Peak Temperature during Friction Stir Welding," *Science and Technology of Welding and Joining*, vol. 11, no. 5, pp. 606–608, 2006.

[140] K. Tello, U. Duman, and P. Mendez, "Scaling Laws for the Welding Arc, Weld Penetration and Friction Stir Welding," in *Trends in Welding Research, Proceedings of the 8th International Conference*, 2009, pp. 172–181.

[156] G. Wood, S. A. Islam, and P. F. Mendez, "Calibrated expressions for welding and their application to isotherm width in a thick plate," *Soldagem & Inspeção*, vol. 19, no. 3, pp. 212–220, 2014.

[159] K. M.-k. Yip, "Model Simplification by Asymptotic Order of Magnitude Reasoning," *Artificial Intelligence*, vol. 80, no. 2, pp. 309–348, 1996.

[160] N. Yurioka, O. Makoto, K. Tadashi, and C. Harry, "Prediction of HAZ Hardness of Transformable Steels," *Metal Construction*, vol. 19, no. 4, 217R–223R, 1987.

[161] W. Zhang, C. H. Kim, and T. DebRoy, "Heat and Fluid Flow in Complex Joints during Gas Metal Arc Welding ? Part I : Numerical Model of Fillet Welding," *Journal of Applied Physics*, vol. 95, no. 9, pp. 5210–5219, 2004.

Chapter 3

Scaling Expressions of Characteristic Values for a Moving Point Heat Source in Steady State on a Semi-Infinite Solid

3.1 Abstract

Engineering expressions for characteristic values of a moving point heat source on a semi-infinite solid are presented. Related characteristic values are: maximum isotherm width and its location, leading and trailing lengths of isotherm, centerline heating rate and cooling rate, maximum temperature and its gradient at maximum width, aspect ratio of isotherms, melting efficiency, cooling time from 800 °C to 500 °C (often used for studying steels), solidification time, the thickness of zone affected by the heat source, and modification criteria to account for the effect of joint preparation. All engineering expressions proposed are accurate to within 7% of the exact analytical solutions, and are obtained with a systematic approach. Dimensional analysis indicates that the expressions developed depend on a single dimensionless parameter that captures all possible cases. This dimensionless number is typically the Rykalin number (Ry), which characterizes three dimensional heat flow induced by a moving point heat source. The obtained engineering equations are of great practical value for very diverse fields where moving heat sources are involved, and are simple enough to

be calculated with a calculator or spreadsheet.

Table 3.1: Notation

Variables	**Unit**	**Description**
A_R	1	Aspect ratio of isotherm
c_p	$\mathrm{J\,kg^{-1}\,K^{-1}}$	Specific heat
k	$\mathrm{W\,m^{-1}\,K^{-1}}$	Thermal conductivity
q	W	Power of heat source absorbed by substrate
r	m	Distance from the heat source
Ry	1	Rykalin number
St	1	Stefan number
t	s	Time
t_sl	s	Solidification time at centerline
$t_{8/5}$	s	Cooling time from 800°C to 500°C
T	K	Temperature
T_0	K	Initial temperature
T_c	K	Temperature of interest
T_HAZ	K	Temperature of edge of HAZ
T_max	K	Maximum temperature
$\dot{T}_\mathrm{b}$	$\mathrm{K\,s^{-1}}$	Centerline cooling rate
$\dot{T}_\mathrm{f}$	$\mathrm{K\,s^{-1}}$	Centerline heating rate
dT_max/dy	$\mathrm{K\,m^{-1}}$	Gradient of maximum temperature
U	$\mathrm{m\,s^{-1}}$	Travel speed of moving heat source
W_0	-	Lambert function
x, y, z	m	Cartesian coordinates
x_b	m	Trailing length of isotherm
x_f	m	Leading length of isotherm
x_max	m	Location of maximum isotherm width

Continued on next page

Table 3.1 – continued from previous page

Variables	Unit	Description
$y_{\max}$	m	Maximum isotherm width
Δy_{HAZ}	m	Thickness of the affected zone
Greek symbols		
α	$\mathrm{m^2\,s^{-1}}$	Thermal diffusivity
η_{m}	1	Melting efficiency
ϕ	$^\circ$	Actual heat flow angle
ρ	$\mathrm{kg\,m^{-3}}$	Density
Superscripts		
*		Dimensionless value
$\widehat{\ }$		Asymptotic behavior
$^+$		Correction for intermediate values
$\dot{\text{symbol}}$		Time derivative
Subscripts		
I		Corresponding to Regime I
II		Corresponding to Regime II

3.2 Introduction

This paper applies the methodology of scaling analysis, asymptotic analysis, and correction factors based on blending techniques to the calculation of 13 technologically relevant characteristic values of moving point heat sources (represented in Figure 3.1) associated with the isotherm $T(x, y, z) = T_{\mathrm{c}}$. The method of analysis is explained in detail in [96] where the maximum isotherm width and its location ($y_{\max}$ and $x_{\max}$) were analyzed as demonstration examples. This paper focuses on 6 new primary characteristic values, and 5 secondary characteristic values associated with the primary ones. The primary characteristic values studied are: the trailing length of isotherm

x_{b}, the leading length of isotherm x_{f}, the centerline cooling rate $\dot{T}_{\mathrm{b}}$, the centerline heating rate $\dot{T}_{\mathrm{f}}$, the maximum temperature of a point in the cross section $T_{\max}$ and the transverse temperature gradient at the maximum isotherm width $dT_{\max}/dy$. The secondary characteristic values are the aspect ratio A_R of the chosen isotherm (indicating how elongated it is), the melting efficiency η_{m} (in this case as a rough approximation useful to estimate the dilution of filler metal in welding), cooling time from 800°C to 500°C ($t_{8/5}$, a standard metric of rate of cooling in the welding of steels), solidification time t_{sl}, (the time interval for the base material to solidify over a range of temperature) and the separation between the maximum width of two isotherms Δy_{HAZ} (useful to assess thickness of the heat affected zone in welding). The cylindrical symmetry of the idealized problem formulation also enables the generalization of results to other geometries with cylindrical symmetry, such as edges, corners, and bevels.

The methodology employed here is based on the solution for a moving point heat source in quasi-stationary state on a semi-infinite solid presented in [125, 126, 154], and typically called "Rosenthal solution"

$$T(x, y, z) = T_0 + \frac{q}{2\pi k r} \exp\left[-\frac{U}{2\alpha}(r + x)\right] \tag{3.1}$$

where x, y, and z are the independent variables illustrated in Figure 3.1, q is the intensity of the point heat source, k is the thermal conductivity of the substrate, T_0 is the temperature of the substrate far from the heat source, U is the velocity of the heat source relative to the substrate, and α is the thermal diffusivity of the substrate. The radial coordinate r is defined in relation to the independent variables as $r = \sqrt{x^2 + y^2 + z^2}$. Equation 3.1 can be rewritten in normalized form as

$$T^* = \frac{1}{r^*} \exp\left(-r^* - x^*\right) \tag{3.2}$$

where

$$T^* = \frac{4\pi k\alpha\,(T - T_0)}{qU} \tag{3.3}$$

$$x^* = \frac{Ux}{2\alpha} \tag{3.4}$$

$$y^* = \frac{Uy}{2\alpha} \tag{3.5}$$

$$z^* = \frac{Uz}{2\alpha} \tag{3.6}$$

$$r^* = \frac{Ur}{2\alpha} \tag{3.7}$$

In Equations 3.3-3.7 the * superscript indicates a dimensionless quantity. Dimensional analysis indicates that for a selected isotherm $T = T_c$, all dimensionless characteristic values depend only on the Rykalin number (Ry) [97]

$$\mathrm{Ry} = \frac{qU}{4\pi k\alpha\,(T_c - T_0)} \tag{3.8}$$

A high Ry value can be interpreted as a "fast heat source," and a low Ry value as a "slow heat source." In the following sections, closed-form expressions of characteristic values in high and low Ry asymptotic regimes are presented, and blending functions are used to provide estimates at the intermediate regime with high accuracy and simplicity. The blending then becomes the basis of correction factors suitable for engineering applications. Finally, engineering expressions suitable for use by practitioners are presented.

3.3 Maximum Isotherm Width $y_{\max}$ and its location $x_{\max}$

The maximum isotherm width is a parameter of much practical value, since it can be measured from cross sections of samples. Temperatures of relevance include the melting temperature (for the case of welding) and the austenitization temperature (for the case of moving heat sources on steel). Explicit estimates and associated correction factors were derived in [97]. For maximum isotherm width, the asymptotic

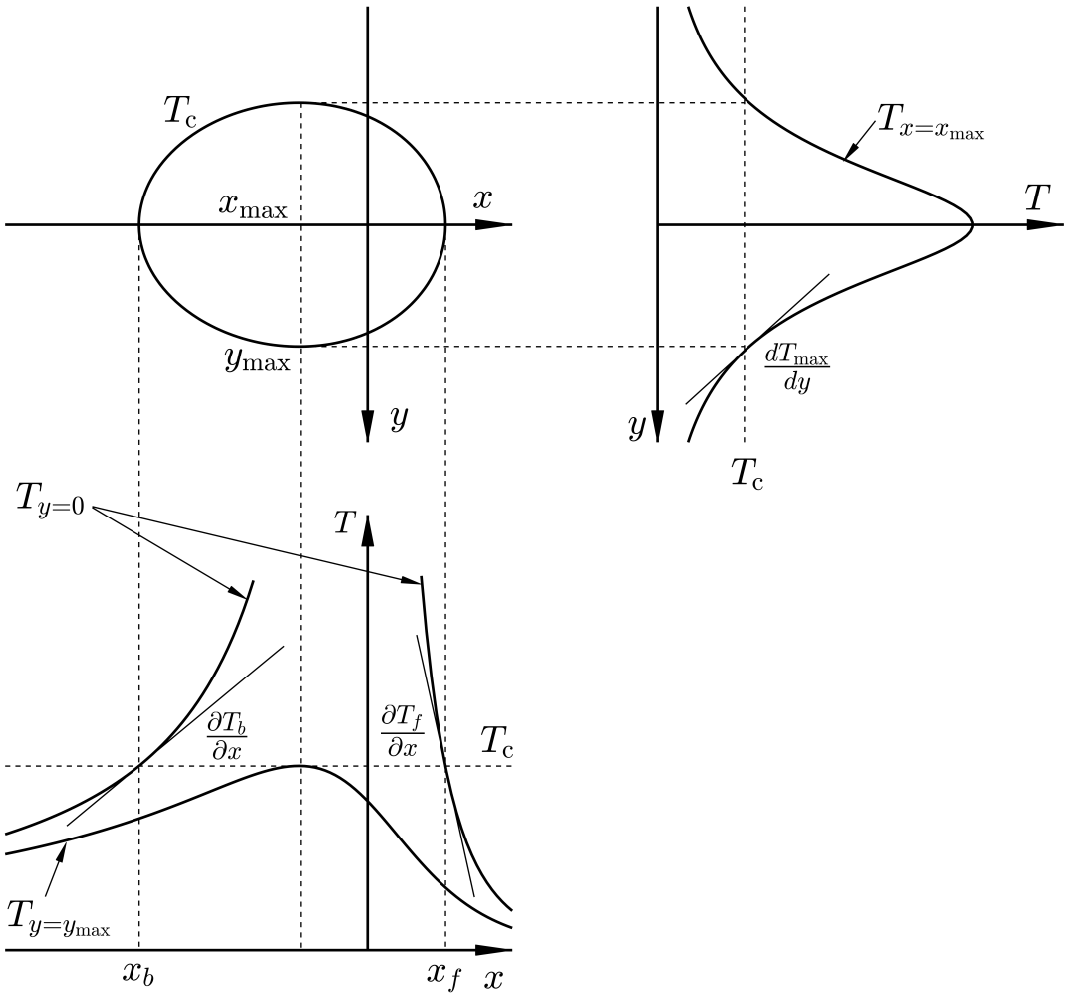

Figure 3.1: Characteristic values of isotherm $T = T_{\mathrm{c}}$ for a moving point heat source on a semi-infinite solid

behavior in dimensionless form is

$$\widehat{y^*}_{\max_{\mathrm{I}}}(\mathrm{Ry}) = \sqrt{\frac{2\mathrm{Ry}}{\mathrm{e}}} \qquad \text{for Regime I (fast)} \tag{3.9}$$

$$\widehat{y^*}_{\max_{\mathrm{II}}}(\mathrm{Ry}) = \mathrm{Ry} \qquad \text{for Regime II (slow)} \tag{3.10}$$

and the corresponding practical engineering expressions with correction factors are

$$\widehat{y}^{+}_{\max} = \widehat{y}_{\max_{\mathrm{I}}} f_{y_{\max_{\mathrm{I}}}}(\mathrm{Ry}) = \sqrt{\frac{2}{\pi \mathrm{e}} \frac{\alpha q}{Uk\left(T_{\mathrm{c}} - T_0\right)}}\; f_{y_{\max_{\mathrm{I}}}}(\mathrm{Ry}) \quad \text{for Regime I (fast)} \tag{3.11}$$

$$\widehat{y}^{+}_{\max} = \widehat{y}_{\max_{\mathrm{II}}} f_{y_{\max_{\mathrm{II}}}}(\mathrm{Ry}) = \frac{1}{2\pi} \frac{q}{k\left(T_{\mathrm{c}} - T_0\right)}\; f_{y_{\max_{\mathrm{II}}}}(\mathrm{Ry}) \qquad \text{for Regime II (slow)} \tag{3.12}$$

$$f_{y_{\max_{\mathrm{I\text{-}II}}}}(\mathrm{Ry}) = \left[1 + \left(\sqrt{\mathrm{eRy}/2}\right)^{\pm n}\right]^{1/n} \qquad n = -1.731 \tag{3.13}$$

where the value of the exponent n was determined through the optimization process described in [97]. For the location of maximum isotherm width, the asymptotic behavior in dimensionless form is

$$\widehat{x}^{*}_{\max_{\mathrm{I}}}(\mathrm{Ry}) = -\frac{\mathrm{Ry}}{\mathrm{e}} \qquad \text{for Regime I (fast)} \tag{3.14}$$

$$\widehat{x}^{*}_{\max_{\mathrm{II}}}(\mathrm{Ry}) = -\mathrm{Ry}^2 \qquad \text{for Regime II (slow)} \tag{3.15}$$

resulting in the following practical engineering expressions

$$\widehat{x}^{+}_{\max} = \widehat{x}_{\max_{\mathrm{I}}} f_{x_{\max_{\mathrm{I}}}}(\mathrm{Ry}) = -\frac{q}{2\pi \mathrm{e} k\left(T_{\mathrm{c}} - T_0\right)} f_{x_{\max_{\mathrm{I}}}}(\mathrm{Ry}) \qquad \text{for Regime I (fast)} \tag{3.16}$$

$$\widehat{x}^{+}_{\max} = \widehat{x}_{\max_{\mathrm{II}}} f_{x_{\max_{\mathrm{II}}}}(\mathrm{Ry}) = -\frac{2U}{\alpha}\left[\frac{q}{4\pi k\left(T_{\mathrm{c}} - T_0\right)}\right]^2 f_{x_{\max_{\mathrm{II}}}}(\mathrm{Ry}) \quad \text{for Regime II (slow)} \tag{3.17}$$

$$f_{x_{\max_{\mathrm{I\text{-}II}}}}(\mathrm{Ry}) = \left[1 + (\mathrm{eRy})^{\pm n}\right]^{1/n} \qquad n = -0.9990 \tag{3.18}$$

In Equations 3.13 and 3.18, the positive sign corresponds to Regime I ($f_{y_{\max_{\mathrm{I}}}}$, $f_{x_{\max_{\mathrm{I}}}}$), and the negative sign corresponds to Regime II ($f_{y_{\max_{\mathrm{II}}}}$, $f_{x_{\max_{\mathrm{II}}}}$).

3.4 Trailing Length of Isotherm x_{b}

The trailing length of an isotherm, x_{b}, is the length of the "hot tail" trailing the heat source. In the case of welding, the trailing length of the isotherm of melting tem-

perature estimates the length of the molten tail (which is often protected with inert gases of limited reach). The trailing length, together with the maximum isotherm width, are geometrical parameters often used to characterize the shape of the melt pool in welding and laser cladding [56, 81], and has been used as a variable in electron beam manufacturing (EBM) processes [38, 136]. For the problem formulation captured by Equation 3.2, x_{b}^{*} is calculated by solving the equation at the centerline ($y^{*}=0$, $z^{*}=0$), and $T=T_{\mathrm{c}}$. This equation has two roots; x_{b}^{*} is the negative root, while the positive root is x_{f}^{*}, which will be discussed later. For both roots, the exact solution is in closed form, and covers the whole range of Ry from Regime I (Ry$\rightarrow 0$) through Regime II (Ry$\rightarrow \infty$); therefore, asymptotic approximations and blending are not necessary. In dimensionless form, the expression of x_{b}^{*} is

$$x_{\mathrm{b}}^{*}(\mathrm{Ry}) = -\mathrm{Ry} \qquad \text{Regime I (fast) and II (slow)} \tag{3.19}$$

where the $\widehat{\ }$ symbol is not used because the above equation is an exact expression, not an asymptotic approximation. The corresponding engineering expression with units is obtained by replacing Equation 3.4 and Equation 3.8 into Equation 3.19, obtaining

$$x_{\mathrm{b}} = -\frac{q}{2\pi k\left(T_{\mathrm{c}}-T_{0}\right)} \qquad \text{Regime I (fast) and II (slow)} \tag{3.20}$$

3.5 Centerline Cooling Rate $\dot{T}_{\mathrm{b}}$

The centerline cooling rate, $\dot{T}_{\mathrm{b}}$, is one of the most important characteristic values associated with moving heat sources, and in most practical cases, the centerline cooling rate is representative of the cooling rate of the whole area affected by the heat source [3, 57]. The centerline cooling rate is crucial to determine the microstructure and mechanical properties such as hardness and strength in metals. For example, for the case of steels, for a given composition and austenite grain size, their hardness is almost completely determined by the cooling rate at a temperature near the transformation temperature (approximately 700°C) [50, 62].

To calculate the rate of temperature variation at a particular point in the substrate (which is moving relative to the heat source), the concept of material derivative is needed

$$\frac{DT}{Dt} = \frac{\partial T}{\partial t} - U\frac{\partial T}{\partial x} \tag{3.21}$$

where $\partial T/\partial t = 0$ in the pseudo-steady state of the problem formulation. Equation 3.21, together with Equations 3.3 and 3.4 yield the following normalization for time t

$$t^* = \frac{U^2 t}{2\alpha} \tag{3.22}$$

resulting in

$$\frac{DT^*}{Dt^*} = -\frac{\partial T^*}{\partial x^*} \tag{3.23}$$

The derivative $\partial T^*/\partial x^*$ at the centerline is directly derived from Equation 3.2. Similarly to the case of x_b, an exact closed-form solution covers the whole range of Ry and neither asymptotic approximations nor blending are necessary. In dimensionless form

$$\left.\frac{DT^*}{Dt^*}\right|_\mathrm{b} (\mathrm{Ry}) = -\mathrm{Ry}^{-2} \qquad \text{Regime I (fast) and II (slow)} \tag{3.24}$$

The corresponding engineering expression with units can be obtained by replacing Equation 3.3, Equation 3.8 and Equation 3.22 into Equation 3.24

$$\dot{T}_\mathrm{b} = -\frac{2\pi k U (T_\mathrm{c} - T_0)^2}{q} \qquad \text{Regime I (fast) and II (slow)} \tag{3.25}$$

Equation 3.25 is identical to the expressions presented in [3, 128], and it has been widely used in practice in applications such as welding[52], laser processing[59, 63], and many other more. Empirical approximations based on modifications of this formula have been proposed in[14, 61, 121, 138]; for example, a modification of the exponent of temperature difference as follows [61, 138]

$$\dot{T}_\mathrm{b} \propto (T_\mathrm{c} - T_0)^n \tag{3.26}$$

where the proposed value of n for the welding of steels is approximately 1.8, very close to the theoretical value of 2. This modified exponent captures in a rough form the physical effects beyond the limitations of Rosenthal's model (finite heat source, latent heat, non-insulated surface, convection in the melt, etc.). It is remarkable that the extremely idealized Rosenthal model yields a dependence on temperature so close to what is seen in practice.

3.6 Leading Length of Isotherm x_f

The leading length of an isotherm, x_f, is an indication of how far the heat travels by conduction (and against advection) ahead of the heat source. If the melting isotherm is considered, x_f is a metric of how much the molten bead "leads" the heat source. The leading length is of much technological relevance in welding, laser cladding, and additive manufacturing [119, 120].

As mentioned in the discussion of x_b^*, x_f^* involves solving Equation 3.2 for $T = T_\mathrm{c}$ at the centerline, but in this case, using the positive root. The exact solution can be expressed in a simple form using the Lambert W_0 function and covers the whole range of Ry; therefore, no blending or correction functions are necessary.

$$x_\mathrm{f}^*(\mathrm{Ry}) = \frac{1}{2} W_0\left(2\mathrm{Ry}\right) \qquad \text{Regime I (fast) and II (slow)} \tag{3.27}$$

The Lambert function is implemented into common scientific software such as Matlab, Maple, Mathematica, and online calculation tools such as WolframAlpha. Although the Lambert function is non-elementary, it can be approximated using elementary functions 3.28 [12] as shown below

$$\widehat{W_0}(x) \approx (1+\epsilon)\ln\left\{\frac{1.2x}{\ln\left[\frac{2.4x}{\ln(1+2.4x)}\right]}\right\} - \epsilon\ln\left[\frac{2x}{\ln\left(1+2x\right)}\right] \tag{3.28}$$

where $\epsilon \approx 0.46$, and the relative error is below $2\times\ 10^{-3}$.

The dimensional engineering expression for leading length can be obtained by re-

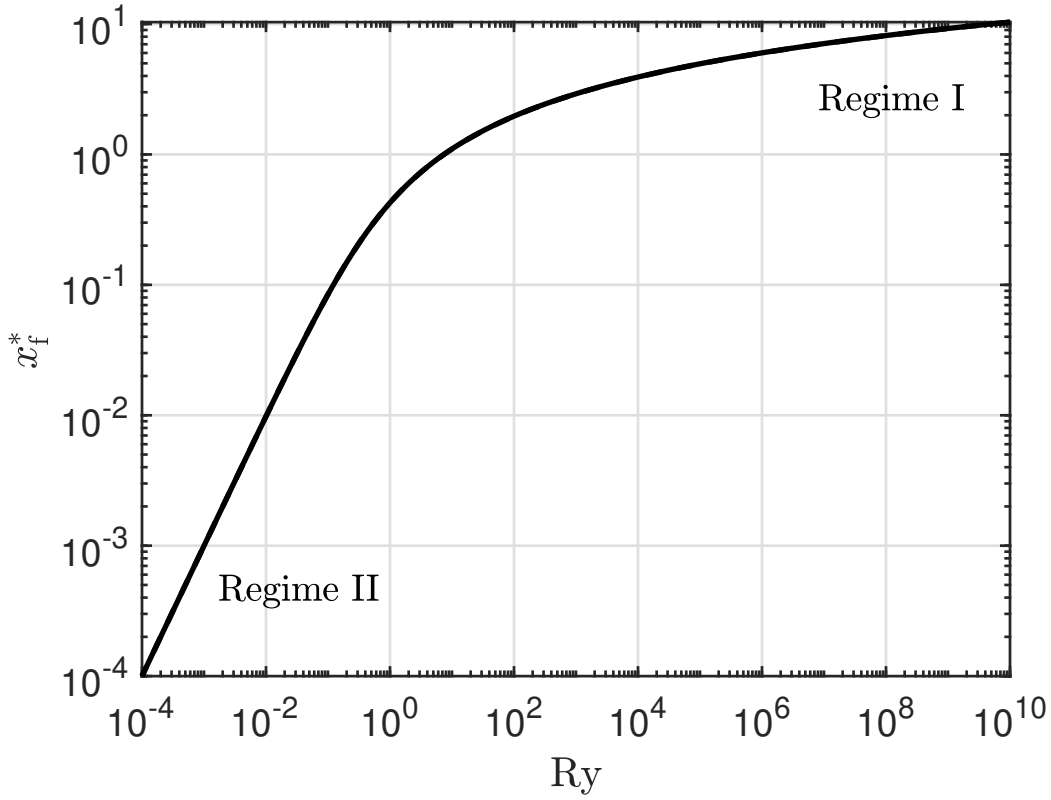

Figure 3.2: Dimensionless leading length as a function of Ry. The exact solution and the approximation of Equation 3.28 overlap within the thickness of the line.

placing Equation 3.4 into Equation 3.27, obtaining

$$x_{\mathrm{f}} = \frac{\alpha}{U} W_0 \left[\frac{qU}{2\pi k\alpha \left(T_{\mathrm{c}} - T_0\right)} \right] \qquad \text{Regime I (fast) and II (slow)} \qquad (3.29)$$

3.7 Centerline Heating Rate $\dot{T}_{\mathrm{f}}$

The centerline heating rate ahead of the heat source, $\dot{T}_{\mathrm{f}}$, is relevant to understand phase transformations in thermal processes. For example, during heating, steels experience a phase transformation from ferrite to austenite around 700°C (The temperature at which the transformation starts depends on the alloy, and it is called A_{C1}, and the temperature at which the transformation is complete A_{C3}). Both temperatures are significantly affected by the heating rate, and in the ignorance of the rate of heating, these temperatures are assumed to be those measured in near-equilibrium conditions, resulting in predictions of transformed region larger than seen in reality. Another example of relevance of the heating rate is the case of welding of Zn-coated steels. The Zn coating tends to evaporate ahead of the weld, preventing porosity in the weld; however, if the rate of heating is faster than the rate of evaporation, Zn might remain on the surface and become entrapped in the melt, causing porosity.

The centerline heating rate $\dot{T}_{\mathrm{f}}$ shares the same derivation process as centerline cooling rate $\dot{T}_{\mathrm{b}}$. The temperature evolution at the leading length of an isotherm when the heat source approaches is also captured by Equation 3.23. The exact solution can be calculated in exact form using the first derivative of Lambert W function [29], and it covers the whole range of Ry, so neither asymptotic approximations nor blending are necessary. In dimensionless form, the expression of DT^*/Dt^* is

$$\left.\frac{DT^*}{Dt^*}\right|_{\mathrm{f}} = \frac{2}{\mathrm{Ry}} \left[\frac{1}{W_0\left(2\mathrm{Ry}\right)} + 1 \right] \qquad \text{Regime I (fast) and II (slow)} \qquad (3.30)$$

The corresponding engineering expression with units can be obtained by replacing Equation 3.3, Equation 3.8, and Equation 3.22 into Equation 3.30

$$\dot{T}_{\mathrm{f}} = \frac{U^2 \left(T_{\mathrm{c}} - T_0\right)}{\alpha} \left[\frac{1}{W_0\left(2\mathrm{Ry}\right)} + 1 \right] \qquad \text{Regime I (fast) and II (slow)} \qquad (3.31)$$

3.8 Maximum Temperature $T_{\max}$

The maximum temperature reached at a given point in a cross section gives an indication of possible phase changes, phase transformations, thermodynamic effects, or practical defects that might happen. With the cylindrical symmetry of the formulation used, any point on the cross section is equivalent to a point on the surface ($z^* = 0$) at the same radial distance from the centerline $y^* = y_c^*$. In this case, the target characteristic value $T_{\max}^*$ depends only on the dimensionless group y_c^*, rather than Ry as in the previous cases. The reason is that dimensionless temperature T^* and Ry are directly related by $T_c^* = 1/\text{Ry}$; therefore, this case can be interpreted as the reverse of the calculation of $y_{\max}^*(\text{Ry})$ studied in [97]. The location of the maximum temperature at $y^* = y_c^*$ is $x^* = x_{\max}^*$, such that $x_{\max}^* = x_{\max}^*(y_c^*)$. This way, $\max\left[T^*(x^*, y_c^*, 0)\right] = T^*(x_{\max}^*, y_c^*, 0) = T_{\max}^*(y_c^*)$. Asymptotic analysis of Equation 3.2 yields the following power laws for Regime I (fast) and Regime II (slow)

$$\widehat{T^*}_{\max_{\text{I}}}(y_c^*) = \frac{2}{\text{e}y_c^{*2}} \qquad \text{for Regime I (fast)} \tag{3.32}$$

$$\widehat{T^*}_{\max_{\text{II}}}(y_c^*) = \frac{1}{y_c^*} \qquad \text{for Regime II (slow)} \tag{3.33}$$

Equation 3.32 is in agreement with the expression derived by Adams in [3] for fast welds. Adams expression, despite an apparent attempt at blending, breaks down for slow welds. The blending techniques detailed in [97] result in the following correction factors

$$f_{T_{\max_{\text{I-II}}}}(y_c^*) = \left[1 + \left(\frac{\text{e}y_c^*}{2}\right)^{\pm n}\right]^{1/n} \qquad \begin{matrix} +n \text{ for Regime I (fast)} \\ -n \text{ for Regime II (slow)} \end{matrix} \tag{3.34}$$

The optimal value of n for Equation 3.34 is n = -1.246, with an error always less than 3.880%. The crossover point for the correction factors is $y_c^* = 0.7363$. Asymptotic expressions without correction factors result in an error less than 10% for $y_{c_{\text{I}}}^* > 2.809$ or $y_{c_{\text{II}}}^* < 0.1050$ in their corresponding regimes.

The corresponding engineering expression with units can be obtained by replacing Equation 3.8 into Equations 3.32 and 3.33 and combining with Equation 3.3

$$\widehat{T}^{+}_{\max} = \widehat{T}_{\max_{\mathrm{I}}} f_{T_{\max_{\mathrm{I}}}}(y^*_{\mathrm{c}}) = T_0 + \frac{2\alpha q}{\mathrm{e}\pi k U {y_{\mathrm{c}}}^2} f_{T_{\max_{\mathrm{I}}}}(y^*_{\mathrm{c}}) \qquad \text{for Regime I (fast)} \tag{3.35}$$

$$\widehat{T}^{+}_{\max} = \widehat{T}_{\max_{\mathrm{II}}} f_{T_{\max_{\mathrm{II}}}}(y^*_{\mathrm{c}}) = T_0 + \frac{q}{2\pi k y_{\mathrm{c}}} f_{T_{\max_{\mathrm{II}}}}(y^*_{\mathrm{c}}) \qquad \text{for Regime II (slow)} \tag{3.36}$$

3.9 Gradient of Maximum Temperature $dT_{\max}/dy$

The gradient of maximum temperature is a useful intermediate step to approximate the distance between two important temperatures that can be identified in a cross section, for example, this gradient can be used to estimate the thickness of the heat affected zone (HAZ) in welding. Because the HAZ is typically thin, the error of using the gradient instead of the exact subtraction is typically negligible. The advantage of using the gradient instead of subtracting the maximum widths corresponding to the two target temperatures is that the gradient yields a power-law answer, which is convenient to see intuitively the interplay of parameters.

The dimensionless form of the gradient of maximum temperature can be analyzed by expanding the derivative of $T^*_{\max} = T(x^*_{\max}(y^*), y^*, 0)$, and evaluating it at point $(x^*_{\max}, y^*_{\mathrm{c}}, 0)$

$$\frac{dT^*_{\max}}{dy^*} = \frac{\partial T^*}{\partial x^*}\frac{dx^*_{\max}}{dy^*} + \frac{\partial T^*}{\partial y^*} \tag{3.37}$$

where $\partial T^*/\partial x^* = 0$ at $x = x^*_{\max}$, by definition; therefore $dT^*_{\max}/dy^* = dT^*/dy^*$ yielding the following power laws

$$\left.\widehat{\frac{dT^*_{\max}}{dy^*}}\right|_{\mathrm{I}} (\mathrm{Ry}) = -\sqrt{2\mathrm{e}}\,\mathrm{Ry}^{-\frac{3}{2}} \qquad \text{for Regime I (fast)} \tag{3.38}$$

$$\left.\widehat{\frac{dT^*_{\max}}{dy^*}}\right|_{\mathrm{II}} (\mathrm{Ry}) = -\,\mathrm{Ry}^{-2} \qquad \text{for Regime II (slow)} \tag{3.39}$$

with the following correction factors

$$f_{dT_{\max}/dy|_{\mathrm{I,II}}}(\mathrm{Ry}) = \left[1 + \left(\sqrt{\frac{1}{2\mathrm{eRy}}}\right)^{\pm n}\right]^{1/n} \qquad \begin{matrix} +n \text{ for Regime I (fast)} \\ -n \text{ for Regime II (slow)} \end{matrix} \tag{3.40}$$

The optimal value of n for Equation 3.40 is $n = 3.079$, with an error always less than 6.141%. The crossover point for the correction factors is $\mathrm{Ry_c} = 0.1839$. Asymptotic expressions without correction factors result in an error smaller than 10% for $\mathrm{Ry_I} > 0.3897$ or $\mathrm{Ry_{II}} < 0.05530$ in their corresponding regimes.

The corresponding engineering expression with units can be obtained by replacing Equation 3.5 into Equations 3.38 and 3.39, and combining with Equation 3.3

$$\widehat{\frac{dT_{\max}}{dy}}^{+} = \left.\widehat{\frac{dT_{\max}}{dy}}\right|_{\mathrm{I}} f_{dT_{\max}/dy|_{\mathrm{I}}}(\mathrm{Ry}) = -\sqrt{\frac{2\mathrm{e}\pi kU}{\alpha q}}(T_{\max} - T_0)^{\frac{3}{2}} f_{dT_{\max}/dy|_{\mathrm{I}}}(\mathrm{Ry}) \quad \text{for Regime I (fast)} \tag{3.41}$$

$$\widehat{\frac{dT_{\max}}{dy}}^{+} = \left.\widehat{\frac{dT_{\max}}{dy}}\right|_{\mathrm{II}} f_{dT_{\max}/dy|_{\mathrm{II}}}(\mathrm{Ry}) = -\frac{2\pi k}{q}(T_{\max} - T_0)^2 f_{dT_{\max}/dy|_{\mathrm{II}}}(\mathrm{Ry}) \qquad \text{for Regime II (slow)} \tag{3.42}$$

3.10 Aspect Ratio A_R

The aspect ratio of an isotherm is a metric of how elongated the isotherm is, and because it depends only on Ry, the aspect ratio is also a proxy for Ry. In many practical applications, such as welding, key isotherms are visible; for example the melting isotherm can be observed easily, and the isotherm of 600°C is often seen in steels as the line at which the steel starts to turn red hot; this way, a simple observation becomes a practical assessment of travel speed. Previous attempts at obtaining an explicit expression were made in [120] using a polynomial fitting over a limited range of speeds, and a linear correlation for slow speeds. The aspect ratio, A_R, is defined as the ratio of isotherm length $(x_{\mathrm{f}} - x_{\mathrm{b}})$ to isotherm width $(2y_{\max})$

$$A_R = \frac{x_{\mathrm{f}} - x_{\mathrm{b}}}{2y_{\max}} = \frac{x^*_{\mathrm{f}} - x^*_{\mathrm{b}}}{2y^*_{\max}} \tag{3.43}$$

Asymptotic analysis of Equation 3.43 yields the following power laws for Regime I and Regime II

$$\widehat{A_{R\mathrm{I}}}(\mathrm{Ry}) = \sqrt{\frac{\mathrm{eRy}}{8}} \qquad \text{for Regime I (fast)} \tag{3.44}$$

$$\widehat{A_{R\mathrm{II}}}(\mathrm{Ry}) = 1 \qquad \text{for Regime II (slow)} \tag{3.45}$$

The aspect ratio of 1 in Regime II is consistent with the spherical symmetry of the pure conduction problem when there is no motion of the heat source. The correction factors using blending are the following

$$f_{A_{R\mathrm{I,II}}}(\mathrm{Ry}) = \left[1 + \left(\sqrt{\frac{8}{\mathrm{eRy}}}\right)^{\pm n}\right]^{1/n} \qquad \begin{matrix} +n \text{ for Regime I (fast)} \\ -n \text{ for Regime II (slow)} \end{matrix} \tag{3.46}$$

The optimal value of n for Equation 3.46 is $n = 1.904$, with an error always less than 1.994%. The crossover point for the correction factors is $\mathrm{Ry}_c = 2.943$. Asymptotic expressions without correction factors result in an error less than 10% for $\mathrm{Ry_I} > 19.07$ or $\mathrm{Ry_{II}} < 0.6756$ in their corresponding regimes. The corresponding engineering expression with units can be obtained by replacing Equation 3.8 into Equations 3.44 and 3.45 to obtain

$$\widehat{A_R}^{+} = \widehat{A_{R\mathrm{I}}} f_{A_{R\mathrm{I}}}(\mathrm{Ry}) = \sqrt{\frac{\mathrm{e}qU}{32\pi k\alpha\left(T_\mathrm{c} - T_0\right)}} f_{A_{R\mathrm{I}}}(\mathrm{Ry}) \quad \text{for Regime I (fast)} \tag{3.47}$$

$$\widehat{A_R}^{+} = \widehat{A_{R\mathrm{II}}} f_{A_{R\mathrm{II}}}(\mathrm{Ry}) = f_{A_{R\mathrm{II}}}(\mathrm{Ry}) \quad \text{for Regime II (slow)} \tag{3.48}$$

Figure 3.3 presents the aspect ratio as a function of Ry, and displays the isotherms corresponding to Ry equals to 0.01, 1, 10 and 100, showing how the isotherm becomes progressively more elongated with Ry.

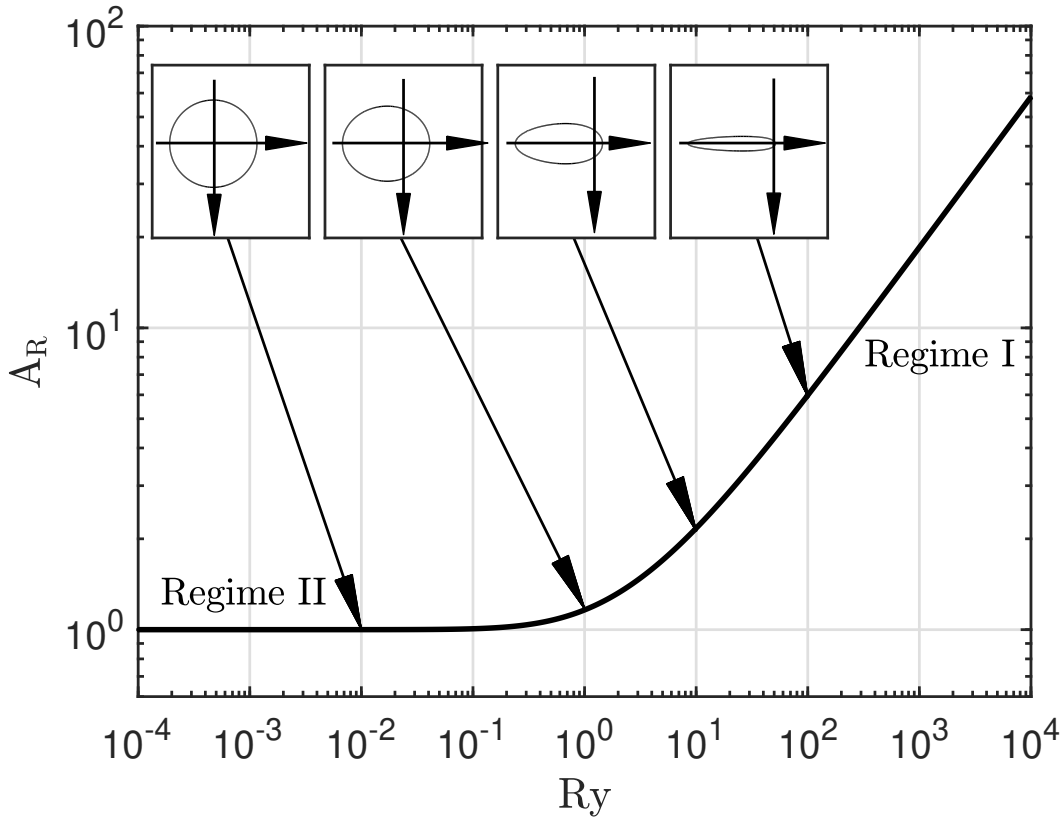

Figure 3.3: Aspect ratio of the isotherm $T = T_c$ for different Ry values under a moving point heat source on a semi-infinite solid

3.11 Melting Efficiency η_m

Melting efficiency η_m is a magnitude defined for fusion welding processes, in which melting is essential to accomplish the joining operation. The superheat above melting is unnecessary for joining, and in the ideal case, the molten material reaches the melting point but does not exceed it, leaving the rest of the substrate unaffected. For a given cross section of a weld, a lower melting efficiency implies that more heat will affect the substrate, resulting in distortions, residual stresses, and grain coarsening. When the welding process involves a filler material, different melting efficiencies can result in different mixtures of filler and base material in the melt (dilution). Dilution is a critical factor in the welding of wear-resistant overlays [16], the welding of carbon to

stainless steels [10, 11] and the welding of aluminum [28]. Beyond welding, if critical temperatures other than melting are considered, the melting efficiency is an applicable parameter to other relevant thermal processes. For example, if the characteristic temperature considered is the austenitization temperature, the adapted concept of melting efficiency yields insight into the excess heat applied and potential distortions and residual stresses in laser or flame heat treating.

The melting efficiency is defined as the energy used to reach melting relative to the total energy deposited from the heat source, and it can be approximated using Rosenthal's model, acknowledging its limitations, especially the lack of proper accounting for latent heat. Despite its limitations, the conclusions obtained are qualitatively correct, and quantitatively not far from reality as shown by previous studies on melting efficiency [34, 44, 112, 115]. Some rough corrections can be used to improve the calculations, such as using an average specific heat which includes the effect of latent heat.

For the model considered, the volumetric energy to reach melting is given by $\rho c_{\mathrm{p}}(T_{\mathrm{m}} - T_0)$, where ρ, c_{p}, and T_{m} are the density, specific heat, and melting temperature of the substrate respectively. The cross section of fusion zone has a cross sectional area of $\frac{\pi}{2} y^2_{\mathrm{max,m}}$, where $y_{\mathrm{max,m}}$ is the maximum width of the isotherm of melting temperature. The melting efficiency can then be calculated as

$$\eta_{\mathrm{m}} = \frac{\rho c_{\mathrm{p}}(T_{\mathrm{m}} - T_0) U \frac{\pi}{2} y^2_{\mathrm{max,m}}}{q}$$

which can be rewritten using Equations 3.8 and 3.5 as

$$\eta_{\mathrm{m}} = \frac{1}{2} \frac{{y^*}^2_{\mathrm{max,m}}}{\mathrm{Ry}_{\mathrm{m}}} \tag{3.49}$$

where Ry_{m} correspond to T_{m}. Replacing the asymptotic expressions for $\widehat{y}^{+}_{\mathrm{max}}$ from [97] into Equation 3.49 yields the following power laws

$$\widehat{\eta}_{\mathrm{m_I}}(\mathrm{Ry}) = \frac{1}{\mathrm{e}} \qquad \text{for Regime I (fast)} \tag{3.50}$$

$$\widehat{\eta}_{\mathrm{m_{II}}}(\mathrm{Ry}) = \frac{\mathrm{Ry}}{2} \qquad \text{for Regime II (slow)} \tag{3.51}$$

The blending expressions for η_{m} are based on those for $y^*_{\max}$, resulting in

$$f_{\eta_{\mathrm{m_{I,II}}}}(\mathrm{Ry}) = \left[1 + \left(\frac{\mathrm{eRy}}{2}\right)^{\pm n}\right]^{1/n} \qquad \begin{array}{l} +n \text{ for Regime I (fast)} \\ -n \text{ for Regime II (slow)} \end{array} \tag{3.52}$$

The optimal value of n for Equation 3.52 is n = -0.8655, with an error always less than 1.450%. The crossover point for the correction factors is $\mathrm{Ry}_c = 0.7359$. Asymptotic expressions without correction factors result in an error smaller than 10% for $\mathrm{Ry}_c > 11.85$ or $\mathrm{Ry}_c < 0.05388$ in their corresponding regimes.

Equation 3.50 indicates that for the model considered, the melting efficiency reaches a maximum value of 36.79% for very fast heat sources, but it never approaches 100%. This is a consequence of the superheat inside the molten region and the gradients on the substrate outside the molten region. Equation 3.51 indicates that for slow welds, the heat lost by conduction reduces the melting efficiency significantly.

Equations 3.50 and 3.51 suggest that the melting efficiency is never zero, regardless of the power of the heat source; however, experience indicates that for weak heat sources sometimes there is no melting and the melting efficiency should be zero. This discrepancy is a consequence of the model being based on a point heat source reaching infinite temperature at the point of application, regardless of the power of the heat source. More sophisticated models that account for distributed heat sources such as [36] are needed to capture this phenomenon correctly, and are the focus of current research.

The corresponding engineering expressions with units can be obtained by replacing Equation 3.8 into Equations 3.50 and 3.51, obtaining

$$\widehat{\eta}^{+}_{\mathrm{m}} = \widehat{\eta}_{\mathrm{m_I}} f_{\eta_{\mathrm{m_I}}}(\mathrm{Ry}) = \frac{1}{\mathrm{e}} f_{\eta_{\mathrm{m_I}}}(\mathrm{Ry}) \qquad \text{for Regime I (fast)} \tag{3.53}$$

$$\widehat{\eta}^{+}_{\mathrm{m}} = \widehat{\eta}_{\mathrm{m_{II}}} f_{\eta_{\mathrm{m_{II}}}}(\mathrm{Ry}) = \frac{qU}{8\pi k\alpha\,(T_{\mathrm{m}} - T_0)} f_{\eta_{\mathrm{m_{II}}}}(\mathrm{Ry}) \qquad \text{for Regime II (slow)} \tag{3.54}$$

3.12 Cooling Time $t_{8/5}$

The characteristic value $t_{8/5}$ is typically used as a metric of cooling rate in the welding of steels, and it is defined as the time it takes for the centerline to cool from 800°C to 500°C. For steels, austenite decomposition occurs in this temperature range, resulting in a variety of microstructural constituents such as ferrite, pearlite, bainite, and martensite, depending on the cooling rate [75]. Similar to cooling rate $\dot{T}_{\mathrm{b}}$, cooling time $t_{8/5}$ is also insensitive to the location in the vicinity of weld centerline [61, 69].

For a fixed point on the centerline, the time to cool from 800°C to 500°C, is the time it takes for the heat source to travel the distance between the trailing length x_{b} of the 800°C and 500°C isotherms; thus

$$t_{8/5} = \frac{1}{U}\Delta x_{\mathrm{b}}\bigg|_{500}^{800} = \frac{q}{2\pi k U}\left(\frac{1}{T_{500}-T_0} - \frac{1}{T_{800}-T_0}\right) \tag{3.55}$$

The time $t_{8/5}$ can be approximated as

$$t_{8/5} \approx -\frac{1}{\dot{T}_{\mathrm{b,i}}}\Delta T\bigg|_{500}^{800} = \frac{q\,(T_{800}-T_{500})}{2\pi k U (T_{\mathrm{i}}-T_0)^2} \tag{3.56}$$

where $\dot{T}_{\mathrm{b,i}}$ is the cooling rate evaluated at a temperature T_{i} intermediate between 500°C and 800°C. This equation is equivalent to that presented in [128]. Typically, the error is small for any T_{i}, and it is shown in the Appendix that Equation 3.56 is exact when

$$T_{\mathrm{i}} - T_0 = \sqrt{(T_{800}-T_0)(T_{500}-T_0)} \qquad (T_{\mathrm{i}} = 632°\mathrm{C} \text{ for } T_0 = 20°\mathrm{C}) \tag{3.57}$$

The parameters q and U appear combined and never independently in the calculation of $t_{8/5}$ Equation 3.55 (and also in the determination of cooling rate). For this reason, in practice only the ratio q/U termed "linear heat input" is typically used, and embodied in codes and standards such as [7, 9, 18, 30]

3.13 Solidification Time at Centerline $t_{\mathbf{sl}}$

The model used here can be extended to capture aspects of phase transformations when their presence does not affect significantly the solution. For the case of steels in

typical welding conditions, it was demonstrated in [147] that solidification and solid-state phase transformations cause only small departures from the exact solution shown in Equation 3.1. To deal with phase transformations, an enthalpy-based formulation is convenient. In the original solution, the hypothesis of constant properties means that the enthalpy formulation and the temperature formulation are equivalent, and enthalpy variations can be calculated based on temperature variations. This way, in the original formulation of the problem, it is possible to state the following rate of enthalpy loss at the trailing length of the weld based on Equation 3.25

$$\left.\frac{Di}{Dt}\right|_{\mathrm{b}} = -\frac{2\pi k c_{\mathrm{p}} U (T_{\mathrm{c}} - T_0)^2}{q} \qquad \text{Regime I (fast) and II (slow)} \tag{3.58}$$

where i is enthalpy per unit mass, and c_{p} is the effective specific heat considered constant in Rosenthal's formulation, and for this reason is not necessary to attribute it to solid or liquid. Because phase transformations have a small effect on the solution, this rate of enthalpy loss can be used to estimate the time associated with the dissipation of enthalpy from a phase transformation. For the case of solidification, the latent heat of solidification i_{sl} would take a time t_{sl} to be dissipated, which can be estimated as

$$t_{\mathrm{sl}} = -\frac{i_{\mathrm{sl}}}{Di/Dt|_{\mathrm{b}}} = \frac{q i_{\mathrm{sl}}}{2\pi k c_{\mathrm{p}} U (T_{\mathrm{m}} - T_0)^2} \qquad \text{Regime I (fast) and II (slow)} \tag{3.59}$$

where T_{m} ("melting temperature") is a temperature representative of the solidification. Because of the approximate nature of the calculation, it is not possible to give an exact number; however, solidification typically happens over a relatively narrow range of temperatures, and for practical calculations it can be considered that T_{m} is an intermediate between the liquidus and solidus temperature of the alloy in question. Equation 3.59 has also been presented in [80, 101] and has been applied in[33, 113] to study nonequilibrium solidification conditions. The dimensionless counterpart of Equation 3.59 is

$$t^*_{\mathrm{sl}} = \frac{\mathrm{Ry}}{\mathrm{St}} \qquad \text{Regime I (fast) and II (slow)} \tag{3.60}$$

where time is normalized according to Equation 3.22, Ry is considered at T_{m}, and St is the Stefan number

$$\mathrm{St} = \frac{c_{\mathrm{p}}\left(T_{\mathrm{m}} - T_0\right)}{i_{\mathrm{sl}}} \tag{3.61}$$

For typical structural steel, the Stefan number is approximately 3 [102]. The analysis above can be extended to other phase transformations such as austenite decomposition, and Equation 3.58 could be the basis to extend the calorimetry analysis of phase transformations of [46, 68] to in-situ analysis of transformations in welding and surface heat treating.

3.14 Thickness of the Heat Affected Zone Δy_{HAZ}

The heat affected zone (HAZ) is an extremely important concept in welding and thermal cutting of all metals, and it is defined as the layer of material surrounding the fusion line that is affected by the heat. In steels, it typically corresponds to the material that was exposed to temperatures between slightly below the beginning of austenitization ($\mathrm{A}_{c,1}$) and melting (T_{m}) [75]. The microstructures in the HAZ are typically undesirable, and a narrower HAZ can often enable welds that would not have been performed acceptably otherwise.

Mathematically, the thickness of the heat affected zone can be defined as

$$\Delta y_{\mathrm{HAZ}} = y_{\mathrm{HAZ,m}} - y_{\mathrm{max,m}} \tag{3.62}$$

where $y_{\mathrm{max,HAZ}}$ is the width of the isotherm T_{HAZ} that marks the edge of the HAZ; for example $\mathrm{A}_{c,1}$ in steels, and $y_{\mathrm{max,m}}$ is the width of the melting isotherm (T_{m}, marking the width of the weld). Substituting T_{HAZ} and T_{m} into Equations 3.11 and 3.12 results in the following predictions for thickness of the HAZ

$$\Delta y_{\mathrm{HAZ}} = \sqrt{\frac{2\alpha q}{\pi \mathrm{e} k U}}\left[\frac{f_{y_{\mathrm{max_I}}}(\mathrm{Ry}_{T_{\mathrm{HAZ}}})}{\sqrt{T_{\mathrm{HAZ}} - T_0}} - \frac{f_{y_{\mathrm{max_I}}}(\mathrm{Ry}_{T_{\mathrm{m}}})}{\sqrt{T_{\mathrm{m}} - T_0}}\right] \quad \text{for Regime I (fast)} \tag{3.63}$$

$$\Delta y_{\mathrm{HAZ}} = \frac{q}{2\pi k}\left[\frac{f_{y_{\mathrm{max_{II}}}}(\mathrm{Ry}_{T_{\mathrm{HAZ}}})}{T_{\mathrm{HAZ}} - T_0} - \frac{f_{y_{\mathrm{max_{II}}}}(\mathrm{Ry}_{T_{\mathrm{m}}})}{T_{\mathrm{m}} - T_0}\right] \quad \text{for Regime II (slow)} \tag{3.64}$$

For a relatively thin HAZ, its thickness approximated also as

$$\Delta y_{\text{HAZ}} \approx -\frac{1}{dT_{\max}/dy|_i}\Delta T\Big|_{T_{\text{HAZ}}}^{T_{\text{m}}} = \sqrt{\frac{q\alpha}{2\text{e}\pi kU}}\frac{T_{\text{m}}-T_{\text{HAZ}}}{(T_{\text{i}}-T_0)^{\frac{3}{2}}} \quad \text{for Regime I (fast)} \tag{3.65}$$

$$\Delta y_{\text{HAZ}} \approx -\frac{1}{dT_{\max}/dy|_i}\Delta T\Big|_{T_{\text{HAZ}}}^{T_{\text{m}}} = \frac{q\,(T_{\text{m}}-T_{\text{HAZ}})}{2\pi k(T_{\text{i}}-T_0)^2} \quad \text{for Regime II (slow)} \tag{3.66}$$

where $dT_{\max}/dy|_i$ is the gradient of maximum temperature in a cross section evaluated at a temperature T_{i} intermediate between T_{HAZ} and T_{m}. Typically, the error is small for any T_{i}, and using the expression derived in the Appendix, Equation 3.65 and Equation 3.66 is exact when

$$T_{\text{i}}-T_0 = \left[\sqrt{(T_{\text{HAZ}}-T_0)(T_{\text{m}}-T_0)}\frac{\sqrt{T_{\text{HAZ}}-T_0}+\sqrt{T_{\text{m}}-T_0}}{2}\right]^{2/3} \quad \text{for Regime I (fast)} \tag{3.67}$$

$$T_{\text{i}}-T_0 = \sqrt{(T_{\text{HAZ}}-T_0)(T_{\text{m}}-T_0)} \quad \text{for Regime II (slow)} \tag{3.68}$$

Typical values for plain carbon steel are T_{HAZ} ≈750°C and T_{m} ≈1500°C, and for a starting temperature T_0 =20°C, this results in T_{i} =1070°C for Regime I, and a very similar T_{i} =1059°C for Regime II (11°C apart). In comparison, the arithmetic mean of temperatures results in $T_{\text{i}} = (T_{\text{HAZ}}+T_{\text{m}})/2$ =1125°C (55°C and 66°C above the exact intermediate temperatures). Given the simplicity of calculation of intermediate temperature for Regime II, and how it also represents the intermediate temperature in Regime I much closer than the arithmetic mean, it is practical (and typically accurate) to use Equation 3.68 for all values of Ry when estimating an intermediate temperature when using a temperature gradient to estimate the width of the HAZ.

3.15 Effect of Joint Preparation Geometry

Equation 3.1 has symmetry of revolution around the x-axis. The implication of this symmetry is that the problem formulation is the same for other configurations with symmetry of revolution such as a full solid, or a wedge of angle ϕ with its edge along

the x-axis (which is a good representation of a beveled weld joint preparation in a thick plate). All problems with the same "angular heat intensity" defined as q/ϕ will have the same solution; for the case of a semi-infinite solid, $\phi = 180°$. The formulae presented above for a semi-infinite solid can be applied without additional mathematical error to the other related problems replacing the heat intensity q with an "effective heat intensity" q_{eff} that accounts for the different angle covered in the cylindrical symmetry.

$$q_{\text{eff}} = \frac{180°}{\phi} q \tag{3.69}$$

where ϕ is in degrees. A particular practical application of this extended analysis is weld joint preparations, for which the analysis is valid as long as the isotherm of interest (T_{c}) is well inside the beveled edges, and far from the edge where the bevel meets the top surface of the plate. For example, for the 75°V-groove joint preparation shown in Figure 3.4a, assuming that the heat is divided evenly between the two halves of the joint preparation, all formulae derived above are applicable when q is replaced by $q_{\text{eff}} = (q/2) \times (180°/52.5°) = 1.714q$. The division by 2 is because only half of the heat goes to each plate, and the 52.5°correspond to the angle covered by the solid for each plate (52.5°=90°-75°/2). Predicted cooling time from 800°C to 500°C, $t_{8/5}$, and cooling rate $\dot{T}_{\text{b}}$ at 650°C in root pass welding of steel plates with the groove joint preparation are in agreement with general experience[5].

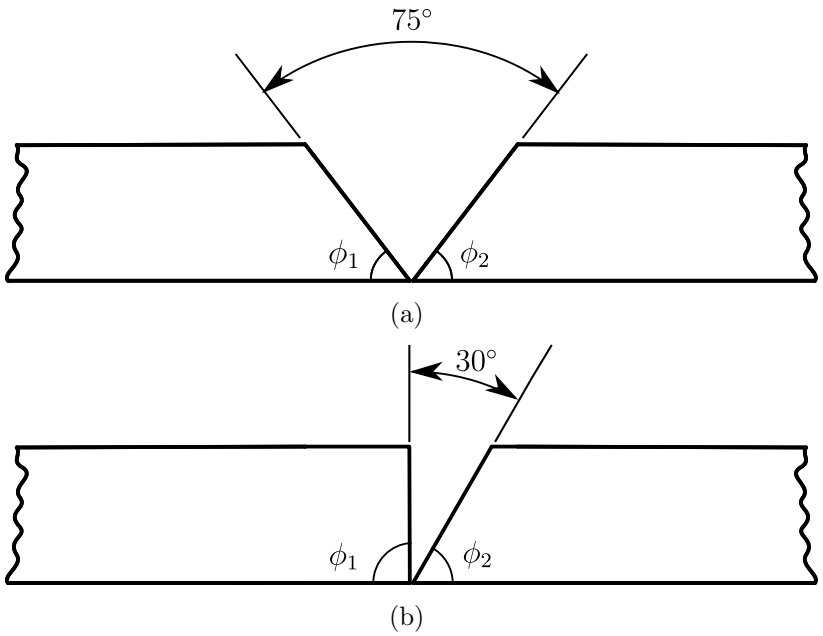

Figure 3.4: Schematic of V-groove joint preparation (a), and single bevel joint preparation (b)

For the case in which the two sides of a joint have different preparation, such as the single bevel groove joint of Figure 3.4b, the distribution of heat is typically not even between the two sides. If the same characteristic values (e.g. cooling rate or width of melting isotherm) are desirable for both sides of the joint, the effective heat intensity should be the same on both sides, resulting in a distribution of heat proportional to the wedge angle of each side

$$\frac{q_j}{q} = \frac{\phi_j}{\phi_1 + \phi_2} \tag{3.70}$$

where $j = 1, 2$ identifies each side of the joint, such that q_1 and q_2 are the amounts of heat on each side of the joint, and ϕ_1 and ϕ_2 are their corresponding wedge angles. For example, for the 30°single bevel of Figure 3.4b, $\phi_1 = 90°$ for the square side, and $\phi_2 = 60°$ for the beveled side, resulting in $q_1 = 0.6q$ and $q_2 = 0.4q$. In this case, if similar properties are desired for both sides of the joint, the partition of heat for welding should be 60% on the square side, and 40% on the beveled side. This partition is typically accomplished in practice by making an asymmetric weave

and/or having different dwell times on each side during the weave. The width of the weave is small, of the order of the width of the molten metal, and a weaved weld is typically considered a straight line in practice. Equation 3.70 can be of much help in anticipating the different dwell times needed.

3.16 Discussion

The results presented here are novel, with the main difference with previous attempts is the use of blending techniques to provide explicit solutions for the entire range of parameters; this had never been accomplished before. Another important difference is the identification of a single dimensionless group that determines all characteristic values (instead of two as in [22]). This dimensionless group is typically the Rykalin number, which had been proposed before [44] based on the analysis of experiments, but had not been adopted by the community.

The expressions developed are based on fundamental principles, are simple and general, and are within 7% of the exact solution. Such combination is desirable, and uncommon. For values of Ry larger than 20 or smaller than 1/20, the correction factors account for less than 10% and can be omitted; in these cases, the final expressions are even simpler. Many practical applications, such as heat sources based on lasers and electron beams are consistently at Ry much larger than 20. The mathematical analysis is proven in detail in this work; however, the next obvious question is whether the exact solution (Equation 3.1) is close enough to reality for the expressions presented to be of practical use.

The accuracy of the exact solution has been validated through intensive testing [22, 53, 108–111, 131] and numerical analysis [32, 118, 147, 151]. The effect of variable materials properties and latent heat was analyzed numerically in [147], where it was shown that these effects resulted in variations below 10% in the trailing length.

Christensen's work [22] was especially thorough, and validated the exact solution for the case of welding using many characteristic values in common with those pre-

sented here (experiments tested $y_{\max}$ both as width and depth, $x_{\max}$, $x_{\mathrm{f}}-x_{\mathrm{b}}$, $x_{\max}-x_{\mathrm{b}}$, $T_{\max}$, $\dot{T}_{\mathrm{b}}$). The validation considered multiple welding processes and materials. The reference temperature considered was the melting temperature, which is beyond the range of validity of the model, and the results were still consistent with the model. The predictions for width, trailing length, and cooling rate are typically useful for engineering purposes, while the predictions for leading length for the melting temperature tend to be underestimates, because the size of the heat source is typically larger than the leading length. Estimate of weld penetration is also typically unreliable because convection in the molten metal plays a significant role. It is remarkable that Rosenthal's idealized solution was proved to be effective despite of its simplicity.

The accuracy of the expressions presented here is limited by the limitations of the exact solution. Some of this limitations can be overcome in practical ways. The limitation of constant thermophysical properties can be addressed in a practical way by using effective values, such as those proposed in [45]. The limitation of a point heat source can be addressed with the consideration of distributed heat sources, which would add precision and physical meaning with as little as a single extra parameter (dimensionless size of the heat source). The limitation of considering only conduction can be addressed by accounting for the effect of fluid flow as in [123], which would add two dimensionless groups (Prandtl number and Marangoni number). The consideration of infinite thickness of the substrate can be addressed by blending with the 2D solutions for moving heat sources (often called the "thin plate solution"). The challenge in this case is that blending must be extended to asymptotic behaviors beyond power laws and to two or more dimensionless groups. Blending under these conditions is beyond the capabilities of [23, 26]. All these are current focus of intense research.

The ultimate goal of the estimates and correction factors presented here is to serve as accurate predictors of actual processes, in a similar way that moving heat source equations from [62] are used in [133]. In these references, the asymptotic solutions

are modified with empirical correction factors. These empirical modifications are not based on fundamental analysis, resulting in two important drawbacks: first, these modifications are valid only for the materials and processes used in the calibrations, and second, the range of parameters for which these calibrations are valid is not clearly defined.

3.17 Conclusions

Equations for characteristic values are listed in Table 3.2, including maximum isotherm width and its location, leading and trailing lengths of the isotherm, centerline heating and cooling rates, maximum temperature and its gradient, aspect ratio of isotherm, cooling time $t_{8/5}$, solidification time, thickness of the affected zone, and modification coefficient for joint preparation geometry. As a general rule of thumb, for $\mathrm{Ry} < 1/20$ or $\mathrm{Ry} > 20$, the asymptotic solutions alone yield an error below 10% for all listed characteristic values. Key characteristics of isotherms produced by a given set of experimental parameters can be calculated with ubiquitous means such as scientific calculators or spreadsheets. In addition to predictive estimations, the engineering expressions also enhance intuition and reflect quantitative effects of different process parameters and their combination on resulting thermal conditions. The methodology and engineering expressions obtained can be applied into a number of processes and materials in different disciplines since they capture the inherent essence of complex physical phenomena based on fundamental physics.

Acknowledgments

The authors wish to acknowledge funding support from the Natural Sciences and Engineering Research Council of Canada (NSERC), and the China Scholarship Council (CSC). Student scholarships from the American Welding Society and the Canadian Welding Association Foundation were gratefully received.

References

[3] C. M. Adams, "Cooling Rates and Peak Temperatures in Fusion Welding," *Welding Journal*, vol. 37, no. 5, pp. 210–215, 1958.

[5] O. M. Akselsen and G. Sagmo, "Technical Report STF34 A89147," Sintef-Division of Metallurgy, Trondheim(Norway), Tech. Rep., 1989.

[7] ASME Section IX: Boiler and Pressure Vessel Code, *Qualification Standard for Welding and Brazing Procedures, Welders, Brazers, and Welding and Brazing Operators*. New York: American Society of Mechanical Engineers, 2010.

[9] AWS D1.1/D1.1M:2015, *Structural Welding Code–Steel*. the United States of America: American Welding Society, 2015.

[10] A. Bahrami and D. K. Aidun, "Modeling of Carbon Steel-Duplex Stainless Steel GTA Weld Pool," *Welding Journal*, vol. 93, no. 7, 262s–270s, 2014.

[11] E. J. Barnhouse and J. C. Lippold, "Microstructure/Property Relationships in Dissimilar Welds between Duplex Stainless Steels and Carbon Steels," *Welding Journal, Research Supplement*, vol. 77, no. 12, 477s–487s, 1998.

[12] D. A. Barry, J. Parlange, L. Li, H. Prommer, C. J. Cunningham, and F. Stagnitti, "Analytical Approximations for Real Values of the Lambert W - function," *Mathematics and Computers in Simulation*, vol. 53, pp. 95–103, 2000.

[14] H. K.D. H. Bhadeshia, L. E. Svensson, and B. Gretoft, "A Model for the Development of Microstructure in Low-Alloy Steel (Fe-Mn-Si-C) Weld Deposits," *Acta Metallurgica*, vol. 33, no. 7, pp. 1271–1283, 1985.

[16] S. D. Borle, I. Le Gall, and P. F. Mendez, "Primary Chromium Carbide Fraction Control with Variable Polarity SAW," *Welding Journal*, vol. 94, no. January, pp. 1–7, 2015.

[18] BS EN 1011-2:2001, *Welding–Recommendations for Welding of Metallic Materials–Part 2: Arc Welding of Ferritic Steels*. London: British Standards Institution, 2001.

[22] N. Christensen, Davies, V. de L., and K. Gjermundsen, "Distribution of Temperatures in Arc Welding," *British Welding Journal*, vol. 12, no. 2, pp. 54–75, 1965.

[23] S. W. Churchill and R. Usagi, "A general expression for the correlation of rates of transfer and other phenomena," *AIChE Journal*, vol. 18, no. 6, pp. 1121–1128, 1972, ISSN: 15475905.

[26] S. W. Churchill and R. Usagi, "A Standardized Procedure for the Production of Correlations in the Form of a Common Empirical Equation," *Industrial & Engineering Chemistry Fundamentals*, vol. 13, no. 1, pp. 39–44, 1974.

[28] N. Coniglio, C. E. Cross, T. Michael, and M. Lammers, "Defining a Critical Weld Dilution to Avoid Solidification Cracking in Aluminum," *Welding Journal*, vol. 87, no. 8, 237s–247s, 2008.

[29] R. M. Corless, G. H. Gonnet, D. E. G. Hare, D. J. Jeffrey, and D. E. Knuth, "On the Lambert W function," *Advances in Computational Mathematics*, vol. 5, no. 1, pp. 329–359, 1996.

[30] CSA W59–13, *Welded Steel Construction (Metal Arc Welding)*. Canada: Canadian Standards Association, 2013.

[32] D. Darmadi, J. Norrish, and A. K. Tieu, "Analytic and finite element solutions for temperature profiles in welding using varied heat source models," *World Academy of Science, Engineering and Technology*, vol. 81, pp. 154–162, 2011.

[33] J. N. DuPont, "Solidification of an Alloy 625 Weld Overlay," *Metallurgical and Materials Transactions A*, vol. 27A, no. 11, pp. 3612–3620, 1996.

[34] J. N. DuPont and A. R. Marder, "Thermal Efficiency of Arc Welding Processes," *Welding Journal-Including Welding Research Supplement*, vol. 74, no. 12, 406s–416s, 1995.

[36] T. W. Eagar and N. S. Tsai, "Temperature Fields Produced by Traveling Distributed Heat Sources," *Welding Journal*, vol. 62, no. 12, pp. 346–355, 1983, ISSN: 00432296.

[38] J. W. Elmer, W. H. Giedt, and T. W. Eagar, "The Transition from Shallow to Deep Penetration during Electron Beam Welding," *Welding Journal, Research Supplement*, vol. 69, no. 5, 167s–176s, 1990.

[44] P. W. Fuerschbach and G. A. Knorovsky, "A Study of Melting Efficiency in Plasma Arc and Gas Tungsten Arc Welding," *Welding Journal*, vol. 70, no. 11, pp. 287–297, 1991.

[45] P. W. Fuerschbach and G. R. Eisler, "Determination of Material Properties for Welding Models by Means of Arc Weld Experiments," in *6th Intl. Trends in Welding Research*, Pine Mountain, Georgia, 2002.

[46] J. W. Gibbs, C. Schlacher, A. Kamyabi-Gol, P. Mayr, and P. F. Mendez, "Cooling Curve Analysis as an Alternative to Dilatometry in Continuous Cooling Transformations," *Metallurgical and Materials Transactions A*, vol. 46A, no. 1, pp. 148–155, 2015.

[50] B. A. Graville, "Weld Cooling Rates and Heat-Affected Zone Hardness in a Carbon Steel," *Welding Journal, Research Supplement*, vol. 52, no. 9, 377s–385s, 1973.

[52] M. L. Greeff and M. d. Toit, "Looking at the Sensitization of 11-12 % Chromium EN 1.4003 Stainless Steels during Welding," *Welding Journal*, vol. 85, no. 11, 243s–251s, 2006.

[53] D. Grewell and A. Benatar, "Modeling Heat Flow For A Moving Heat Source To Describe Scan Micro-Laser Welding," in *ANTEC*, 2003, pp. 1045–1050.

[56] K. Heller, S. Kessler, F. Dorsch, P. Berger, and T. Graf, "Analytical Description of the Surface Temperature for the Characterization of Laser Welding Processes," *International Journal of Heat and Mass Transfer*, vol. 106, pp. 958–969, 2017.

[57] W. F. Hess, L. L. Merrill, E. F. Nippes, and A. P. Bunk, "The Measurement of Cooling Rates Associated with Arc Welding and Their Application to the Selection of Optimum Welding Conditions," *Welding Journal*, vol. 22, no. 9, pp. 377–422, 1943.

[59] W. Hofmeister, M. Griffith, M. Ensz, and J. Smugeresky, "Solidification in Direct Metal Deposition by LENS Processing," *The Journal of The Minerals, Metals & Materials Society*, vol. 53, no. 9, pp. 30–34, 2001.

[61] M. Inagaki, "Welding Conditions of Steels and Cooling Time near the Fusion Line (Report 1)," *Journal of the Japan Welding Society*, vol. 27, no. 12, pp. 716–722, 1958.

[62] M. Inagaki, H. Nakamura, and A. Okada, "Studies of Cooling Processes in the Cases of Welding with Coated Electrode and Submerged Arc Welding," *Journal of the Japan Welding Society*, vol. 34, no. 10, pp. 1064–1075, 1965.

[63] J. C. Ion, *Laser Processing of Engineering Materials: Principles, Procedure and Industrial Application*. Butterworth-Heinemann, Oxford: Elsevier, 2005.

[68] A. T. A. Kamyabi-Gol and P. F. Mendez, "The Evolution of the Fraction of Individual Phases During a Simultaneous Multiphase Transformation from Time – Temperature Data," *Metallurgical and Materials Transactions A*, vol. 46, no. 2, pp. 622–638, 2015.

[69] T. Kasuya and N. Yurioka, "Prediction of Welding Thermal History by a Comprehensive Solution," *Welding Journal*, vol. 72, no. 3, pp. 107–115, 1993.

[75] S. Kou, *Welding Metallurgy*, 2nd ed. Hoboken, New Jersey: John Wiley & Sons, Inc., 2003, pp. 234–235.

[80] T. J. Lienert, S. S. Badu, T. A. Siewert, and V. L. Acoff, *ASM Handbook*, ser. Volume 06A Welding Fundamentals and Processes. Materials Park, Ohio: ASM International, 2011.

[81] W. Liu and J. N. DuPont, "Effects of Melt-Pool Geometry on Crystal Growth and Microstructure Development in Laser Surface-Melted Superalloy Single Crystals . Mathematical Modeling of Single-Crystal Growth in a Melt Pool (Part I)," *Acta Materialia*, vol. 52, no. 16, pp. 4833–4847, 2004.

[96] P. F. Mendez, Y. Lu, and Y. Wang, "Scaling Analysis of a Moving Point Heat Source in Steady- State on a Semi-Infinite Solid," *Journal of Heat Transfer*, vol. 140, no. 8, p. 081 301, 2018.

[97] P. F. Mendez, Y. Lu, and Y. Wang, "Scaling Analysis of a Moving Point Heat Source in Steady-State on a Semi-Infinite Solid," *Journal of Heat Transfer*, vol. 140, no. 8, p. 081 301, 2018.

[101] R. W. Messler Jr, *Principles of welding: processes, physics, chemistry, and metallurgy*. New York: John Wiley & Sons, 2004.

[102] J. Miettinen, "Calculation of Solidification-Related Thermophysical Properties for Steels," *Metallurgical and Materials Transactions B*, vol. 28, no. 2, pp. 281–297, 1997.

[108] P. S. Myers, O. A. Uyehara, and G. L. Borman, "Fundamentals of Heat Flow in Welding," *Welding Research Council Bulletin*, no. 123, pp. 1–46, 1967.

[109] O. R. Myhr and Ø. Grong, "Dimensionless Maps for Heat Flow Analyses in Fusion Welding," *Acta Metallurgica Et Materialia*, vol. 38, no. 3, pp. 449–460, 1990, ISSN: 09567151.

[110] O. R. Myhr and Ø. Grong, "Process Modelling Applied to 6082-T6 Aluminium Weldments–II. Applications of Model," *Acta Metallurgica et Materialia*, vol. 39, no. 11, pp. 2703–2708, 1991.

[111] N. T. Nguyen, A. Ohta, K. Matsuoka, N. Suzuki, and Y. Maeda, "Analytical Solutions for Transient Temperature of Semi-Infinite Body Subjected to 3-D Moving Heat Sources," *Welding Journal, Research Supplement*, vol. 78, no. August, 265s–274s, 1999.

[112] R. W. Niles and C. E. Jackson, "Weld Thermal Efficiency of the GTAW Process," *Welding Journal*, vol. 54, no. 1, pp. 25–32, 1975.

[113] F. F. Noecker II and J. N. DuPont, "Microstructural Development and Solidification Cracking Susceptibility of Cu Deposits on Steel : Part I," *Journal of Materials Science*, vol. 42, no. 2, pp. 495–509, 2007.

[115] A. Okada, "Application of Melting Efficiency Welding and its Problems," *Journal of the Japan Welding Society*, vol. 46, no. 2, pp. 53–61, 1977.

[118] W. Perret, C. Schwenk, and M. Rethmeier, "Comparison of Analytical and Numerical Welding Temperature Field Calculation," *Computational Materials Science*, vol. 47, no. 4, pp. 1005–1015, 2010, ISSN: 0927-0256.

[119] P. Peyre, P. Aubry, R. Fabbro, R. Neveu, and A. Longuet, "Analytical and Numerical Modelling of the Direct Metal Deposition Laser Process," *Journal of Physics D: Applied Physics*, vol. 41, no. 2, p. 025 403, 2008.

[120] A. J. Pinkerton and L. Li, "Modelling the Geometry of a Moving Laser Melt Pool and Deposition Track via Energy and Mass Balances," *Journal of Physics D: Applied Physics*, vol. 37, no. 14, pp. 1885–1895, 2004.

[121] K. Poorhaydari, B. M. Patchett, and D. G. Ivey, "Estimation of Cooling Rate in the Welding of Plates with Intermediate Thickness," *Welding Journal*, vol. 84, no. 10, 149–s–155–s, 2005.

[123] D. Rivas and S. Ostrach, "Scaling of Low-Prandtl-Number Thermocapillary Flows," *International Journal of Heat and Mass Transfer*, vol. 35, no. 6, pp. 1469–1479, 1992.

[125] O. F. T. Roberts, "The Theoretical Scattering of Smoke in a Turbulent Atmosphere," *Proceedings of the Royal Society of London. Series A, Containing Papers of a Mathematical and Physical Character*, vol. 104, no. 728, pp. 640–654, 1923.

[126] D. Rosenthal, "The Theory of Moving Sources of Heat and Its Application to Metal Treatments," *Transactions of the A.S.M.E.*, vol. 68, pp. 849–866, 1946.

[128] D. Rosenthal, "Mathematical Theory of Heat Distribution During Welding and Cutting," *Welding Journal*, vol. 20, no. 5, pp. 220–234, 1941.

[131] N. N. Rykalin, *Calculation of Heat Flow in Welding*. Moscow: Mashgis, 1951.

[133] P. Seyffarth, B. Meyer, and A. Scharff, *Grosser Atlas Schweiss-ZTU-Schaubilder*, ser. Fachbuchreihe Schweisstechnik. Düsseldorf: Deutscher Verlag für Schweisstechnik, 1992, p. 175.

[136] E. Soylemez, J. L. Beuth, and K. Taminger, "Controlling Melt Pool Dimensions over a Wide Range of Material Deposition Rates in Electron Beam Additive Manufacturing," in *Proceedings of 21st Solid Freeform Fabrication Symposium, Austin, TX, Aug*, 2010, pp. 571–582.

[138] L. E. Svensson, B. Gretoft, and H. K.D. H. Bhadeshia, "An Analysis of Cooling Curves from the Fusion Zone of Steel Weld Deposits," *Scandinavian Journal of Metallurgy*, vol. 15, no. 97, pp. 97–103, 1986.

[147] M. Ushio, T. Ishimura, F. Matsuda, and Y. Arata, "Theoretical Calculation on Shape of Fusion Boundary and Temperature Distribution around Moving Heat Source (Report I)," *Transactions of JWRI*, vol. 6, no. 1, pp. 1–6, 1977.

[151] Y. Wang and J. Lin, "Characterization of the Laser Cleaving on Glass Sheets with a Line-Shape Laser Beam," *Optics & Laser Technology*, vol. 39, no. 5, pp. 892–899, 2007.

[154] H. A. Wilson, "On Convection of Heat," *Proceedings of the Cambridge Philosophical Society*, vol. 12, pp. 406–423, 1904.

Appendix: Relationship between the derivatives and variations in power-law asymptotic regimes

Consider a problem in which the characteristic values depend on a single dimensionless group Π (in this paper, the single dimensionless group is typically Ry). Consider also two characteristic values with power-law dependence on Π

$$u_{\mathrm{c}}(\Pi) = A\Pi^m \tag{3.71}$$

$$v_{\mathrm{c}}(\Pi) = B\Pi^n \tag{3.72}$$

There is an intermediate value of Π for which the following calculation is exact

$$\left.\frac{du_{\mathrm{c}}}{dv_{\mathrm{c}}}\right|_{\Pi_{\mathrm{i}}} = \frac{u_{\mathrm{c}}(\Pi_2) - u_{\mathrm{c}}(\Pi_1)}{v_{\mathrm{c}}(\Pi_2) - v_{\mathrm{c}}(\Pi_1)} \tag{3.73}$$

where Π_1 and Π_2 are two separate values and Π_i is the intermediate value sought. To calculate the value of Π_i where Equation 3.73 is exact, we can analyze the derivative and the ratio of variations

$$\left.\frac{du_\mathrm{c}}{dv_\mathrm{c}}\right|_{\Pi_\mathrm{i}} = \left.\frac{du_\mathrm{c}/d\Pi}{dv_\mathrm{c}/d\Pi}\right|_{\Pi_\mathrm{i}} = \frac{A}{B}\frac{m}{n}\Pi_\mathrm{i}^{m-n} \tag{3.74}$$

$$\frac{\Delta u_\mathrm{c}}{\Delta v_\mathrm{c}} = \frac{A}{B}\frac{\Pi_2^m - \Pi_1^m}{\Pi_2^n - \Pi_1^n} \tag{3.75}$$

Combining Equations 3.73 through 3.75 results in the following value for Π_i, for which the derivative and the ratio of variations give exactly the same result

$$\Pi_\mathrm{i} = \left(\frac{n}{m}\frac{\Pi_2^m - \Pi_1^m}{\Pi_2^n - \Pi_1^n}\right)^{\frac{1}{m-n}} \tag{3.76}$$

This expression is exact only for power-law asymptotic regimes, but it is still a useful approximation for intermediate regimes. As an example of application of Equation 3.76, consider the case of cooling rate and $t_{8/5}$, where $\Pi = \mathrm{Ry}$, $u_\mathrm{c} = T_\mathrm{b}^*$, and $v_\mathrm{c} = x_\mathrm{b}^*$. From Equation 3.3, we obtain $m = -1$, from Equation 3.19, $n = 1$, resulting in

$$\mathrm{Ry_i} = \left(-\frac{\mathrm{Ry}_2^{-1} - \mathrm{Ry}_1^{-1}}{\mathrm{Ry}_2 - \mathrm{Ry}_1}\right)^{\frac{1}{-1-1}} = \sqrt{\mathrm{Ry}_1\mathrm{Ry}_2} \tag{3.77}$$

which becomes Equation 3.57 when the definition of Ry is used.

Table 3.2: Summary of characteristic values and correction factors for welding on thick plates

Variable	Regime	Asymptotic	Correction factor	n	Error[%]	Eq.
$y_{\max}$	I	$\sqrt{\frac{2}{\pi e}\frac{\alpha q}{kU\left(T_c-T_0\right)}}$	$\left[1+\left(\sqrt{\frac{\mathrm{eRy}}{2}}\right)^n\right]^{\frac{1}{n}}$	-1.73	0.7	3.11
	II	$\frac{1}{2\pi}\frac{q}{k\left(T_c-T_0\right)}$	$\left[1+\left(\sqrt{\frac{\mathrm{eRy}}{2}}\right)^{-n}\right]^{\frac{1}{n}}$			3.12
$x_{\max}$	I	$-\frac{q}{2\pi e k\left(T_c-T_0\right)}$	$\left[1+(\mathrm{eRy})^n\right]^{\frac{1}{n}}$	-1.00	1.9	3.16
	II	$-\frac{2U}{\alpha}\left[\frac{q}{4\pi k\left(T_c-T_0\right)}\right]^2$	$\left[1+(\mathrm{eRy})^{-n}\right]^{\frac{1}{n}}$			3.17
x_b	I and II	$-\frac{q}{2\pi k\left(T_c-T_0\right)}$				3.20
$\dot{T}_b$	I and II	$-\frac{2\pi kU(T_c-T_0)^2}{q}$				3.25
x_f	I and II	$\frac{\alpha}{U}W_0\left[\frac{qU}{2\pi k\alpha\left(T_c-T_0\right)}\right]$				3.29
$\dot{T}_f$	I and II	$\frac{U^2\left(T_c-T_0\right)}{\alpha}\left[\frac{1}{W_0\left(2\mathrm{Ry}\right)}+1\right]$				3.31
$T_{\max}$	I	$T_0+\frac{2\alpha q}{e\pi kU{y_c}^2}$	$\left[1+\left(\frac{eUy_c}{4\alpha}\right)^n\right]^{\frac{1}{n}}$	-1.25	3.9	3.35
	II	$T_0+\frac{q}{2\pi k y_c}$	$\left[1+\left(\frac{eUy_c}{4\alpha}\right)^{-n}\right]^{\frac{1}{n}}$			3.36
$dT_{\max}/dy$	I	$-\sqrt{\frac{2e\pi kU}{q\alpha}}(T_m-T_0)^{\frac{3}{2}}$	$\left[1+\left(\sqrt{\frac{1}{2\mathrm{eRy}}}\right)^n\right]^{\frac{1}{n}}$	3.08	6.1	3.41
	II	$-\frac{2\pi k}{q}(T_m-T_0)^2$	$\left[1+\left(\sqrt{\frac{1}{2\mathrm{eRy}}}\right)^{-n}\right]^{\frac{1}{n}}$			3.42
A_R	I	$\sqrt{\frac{eqU}{32\pi k\alpha\left(T-T_0\right)}}$	$\left[1+\left(\sqrt{\frac{8}{\mathrm{eRy}}}\right)^n\right]^{\frac{1}{n}}$	1.90	2.0	3.47
	II	1	$\left[1+\left(\sqrt{\frac{8}{\mathrm{eRy}}}\right)^{-n}\right]^{\frac{1}{n}}$			3.48
η_m	I	$\frac{1}{e}$	$\left[1+\left(\frac{\mathrm{eRy}}{2}\right)^n\right]^{\frac{1}{n}}$	-0.87	1.4	3.53
	II	$\frac{qU}{8\pi k\alpha\left(T_m-T_0\right)}$	$\left[1+\left(\frac{\mathrm{eRy}}{2}\right)^{-n}\right]^{\frac{1}{n}}$			3.54
$t_{8/5}$	N/A	$\frac{q}{2\pi kU}\left(\frac{1}{T_{500}-T_0}-\frac{1}{T_{800}-T_0}\right)$				3.55
$t_{8/5}$	N/A	$t_{8/5}\approx\frac{q\left(T_{800}-T_{500}\right)}{2\pi kU(T_i-T_0)^2}$				3.56
		$T_i-T_0=\sqrt{(T_{800}-T_0)(T_{500}-T_0)}$			*	3.57
t_{sl}	N/A	$\frac{qi_{sl}}{2\pi c_p U(T_m-T_0)^2}$				3.59
Δy_{HAZ}	I	$\sqrt{\frac{2\alpha q}{\pi ekU}}\left[\frac{f_{y_{\max_I}}(\mathrm{Ry}_{T_{\mathrm{HAZ}}})}{\sqrt{T_{\mathrm{HAZ}}-T_0}}-\frac{f_{y_{\max_I}}(\mathrm{Ry}_{T_m})}{\sqrt{T_m-T_0}}\right]$	$\left[1+\left(\sqrt{\frac{\mathrm{eRy}}{2}}\right)^n\right]^{\frac{1}{n}}$	-1.73	0.7	3.63
	II	$\frac{q}{2\pi k}\left[\frac{f_{y_{\max_{II}}}(\mathrm{Ry}_{T_{\mathrm{HAZ}}})}{T_{\mathrm{HAZ}}-T_0}-\frac{f_{y_{\max_{II}}}(\mathrm{Ry}_{T_m})}{T_m-T_0}\right]$	$\left[1+\left(\sqrt{\frac{\mathrm{eRy}}{2}}\right)^{-n}\right]^{\frac{1}{n}}$			3.64
Δy_{HAZ}	I	$\Delta y_{\mathrm{HAZ}}\approx\sqrt{\frac{q\alpha}{2e\pi kU}}\frac{T_m-T_{\mathrm{HAZ}}}{(T_i-T_0)^{\frac{3}{2}}}$	$\left[1+\left(\sqrt{\frac{1}{2\mathrm{eRy}}}\right)^n\right]^{\frac{1}{n}}$	3.08	6.1	3.65
		$T_i-T_0=\left[\sqrt{(T_{\mathrm{HAZ}}-T_0)(T_m-T_0)}\frac{\sqrt{T_{\mathrm{HAZ}}-T_0}+\sqrt{T_m-T_0}}{2}\right]^{2/3}$			*	3.67
	II	$\Delta y_{\mathrm{HAZ}}\approx\frac{q\left(T_m-T_{\mathrm{HAZ}}\right)}{2\pi k(T_i-T_0)^2}$	$\left[1+\left(\sqrt{\frac{1}{2\mathrm{eRy}}}\right)^{-n}\right]^{\frac{1}{n}}$	3.08	6.1	3.66
		$T_i-T_0=\sqrt{(T_{\mathrm{HAZ}}-T_0)(T_m-T_0)}$			*	3.68

* using these intermediate temperatures the calculation using the derivative is exactly the same as that using differences

Chapter 4

Prediction of Peak Temperature under a Moving Gaussian Surface Heat Source

4.1 Abstract

This paper presents a systematic scaling analysis of a steady-state temperature field under a Gaussian distributed surface heat source on a semi-infinite solid. Dimensionless maximum temperature and its location are functions dependent only on the heat source distribution parameter (σ^*). Maximum temperature and its location are determined for the first time in closed-form over the entire range of σ^*. The maximum error of estimation from the exact solution is below 0.19% for the peak temperature and 1.4% for its location. The methodology employed consists of normalization, dimensional analysis, asymptotic analysis, and blending techniques. Comparisons of the proposed equations are conducted with experimental data. The expressions obtained can be calculated using a calculator or a basic spreadsheet and are useful for engineers to verify numerical models.

Table 4.1: Notation

Variables	Unit	Description
d	m	Thickness of the substrate
I_m	1	Asymptotic constant $I_m = 1.280$
k	$\mathrm{W\,m^{-1}\,K^{-1}}$	Thermal conductivity of the substrate
q	W	Power absorbed by substrate
t	s	Time
T	K	Temperature
T_0	K	Initial temperature or preheat
T_c	K	Temperature of interest
T_max	K	Peak temperature
U	$\mathrm{m\,s^{-1}}$	Travel speed of the moving heat source
x, y, z	m	Cartesian coordinates
x_max	m	Location of peak temperature
Greek symbols		
α	$\mathrm{m^2\,s^{-1}}$	Thermal diffusivity of the substrate
σ	m	Standard deviation of a Gaussian function
σ_max	m	Maximum heat source distribution parameter
Superscripts		
*		Dimensionless value
$\widehat{\ }$		Asymptotic behavior
$^+$		Improvement over asymptotic approximation
Subscripts		
V		Regime V of broad heat sources
VI		Regime VI of concentrated heat sources

Continued on next page

Table 4.1 – continued from previous page

Variables	Unit	Description
Acronyms		
DOF		Degree of Freedom
GTAW		Gas Tungsten Arc Welding
SAW		Submerged Arc Welding

4.2 Introduction

The modelling of temperature fields is required to predict dimension of isotherms, microstructures, residual stresses and distortions of workpiece in a number of industrial applications including cutting [70, 134], tribology [60, 107, 143], welding [126, 128, 131], heat treatments [74, 76], and additive manufacturing [141, 155]. Previous analyses based on the classic point heat source model have been performed to predict isotherm characteristics such as width and length of isotherms, cooling and heating rate [82, 84, 96, 149]. Although the point heat source model can capture isotherm characteristics over several orders of magnitude, it cannot provide an estimate of maximum temperature because of the singularity at the origin, intrinsic to the model [22, 32, 109].

The answer to the practical question "What is the peak temperature of the substrate?" is essential in many processes, especially heat treatment and additive manufacturing of materials sensitive to temperatures[4, 94]. Real-time monitoring of the temperature field by thermal image processing requires specialized equipment and necessary training to set up [39], and it is plagued by uncertainties such as radiative emissivity, interference by radiation from the arc or laser, and the presence of surface contaminants and surface oscillations in the case of melting.

First-order predictions of the maximum surface temperature have been obtained for square uniform, circular uniform and parabolic heat sources using a heuristic (but

not systematic) methodology over a range of Peclet number from 0.01 to 20 [143], and uniform and parabolic moving heat sources of several geometries were studied using dimensional analysis and blending in [107]. A power-law approximation for the onset of surface melting under a top-hat (uniform rectangle) heat source was determined by least square regression of simulation data [76]; however, the range of validity of the proposed power-law was not identified.

A variety of models were developed to improve the accuracy of predictions [36, 47, 73, 88, 111, 117]. Among all these refinements, the Gaussian heat source model is a widely applied surface heat source model with close resemblance to the heat distribution in arc welding [146] and laser processes [15]. By using a Gaussian heat distribution, the obtained temperature distribution has no singularities [27, 36] and it is proven to be more accurate than the point-heat source theory to predict dimensions of isotherms and thermal profile in the vicinity of heat source [36, 84, 146]. Despite previous investigations on peak temperature problems, no explicit, accurate expressions exist to predict the peak temperature under a moving Gaussian distributed heat source applicable to a broad range of processes and materials.

This paper presents for the first time such explicit and accurate expressions to predict the peak temperature rise and its location in the workpiece scanned by a Gaussian distributed heat source. Asymptotic analysis was employed to derive asymptotic solutions in closed-form for the extreme cases of broad and concentrated heat sources. Blending functions [23, 84, 149] were applied to extend rigorously the usefulness of the asymptotic expressions to intermediate cases, developing correction factors for each asymptotic regime. The resulting asymptotics are in power-law form, making the resulting blended equations and correction factors easy to calculate in a calculator or spreadsheets.

4.3 Governing Equation

The moving Gaussian heat source model describes a Gaussian distributed heat source moving along a straight line (x-axis) at a constant velocity U on the surface of a semi-infinite substrate. Thermophysical properties of the substrate are assumed independent of temperatures. In an Eulerian coordinate frame, where the heat source is stationary, and the substrate moves in the $-x$ direction, the governing equation can be written as:

$$\frac{\partial^2 T}{\partial x^2} + \frac{\partial^2 T}{\partial y^2} + \frac{\partial^2 T}{\partial z^2} + \frac{U}{\alpha}\frac{\partial T}{\partial x} = 0 \tag{4.1}$$

where x, y and z are the independent variables. The temperature, $T = T(x, y, z)$, is the dependent variable, and α is the thermal diffusivity of the substrate.

The boundary conditions for Equation 4.1 are:

$$\frac{\partial T}{\partial z} = \frac{q}{2\pi k\sigma^2}\exp\left(-\frac{x^2+y^2}{2\sigma^2}\right) \quad \text{For} \quad z = 0 \tag{4.2}$$

$$T \to T_0 \quad \text{For} \quad x^2 + y^2 + z^2 \to \infty \tag{4.3}$$

where q is the heat absorbed by the substrate, k is the thermal conductivity of the substrate, and T_0 is the initial temperature or preheat. The distribution parameter σ is the standard deviation of Gaussian function. For problems such as welding, typical values of σ varies from 1 mm (for the case of GTAW) to 7 mm (for the case of SAW) [146]. The solution to Equation 4.1 with boundary conditions in equations 4.2 and 4.3 is [27, 36]:

$$T = T_0 + \frac{q\alpha^{\frac{1}{2}}}{2k\pi^{\frac{3}{2}}}\int_0^\infty \frac{t^{-\frac{1}{2}}}{2\alpha t + \sigma^2}\cdot \exp\left(-\frac{x^2 + 2xtU + U^2t^2 + y^2}{4\alpha t + 2\sigma^2} - \frac{z^2}{4\alpha t}\right) dt \tag{4.4}$$

4.4 Normalization and Dimensional Analysis

The original equations are transformed to their dimensionless counterparts by normalization. In this case, Equation 4.4 can be rewritten in a normalized form as:

$$T^* = \frac{1}{\sqrt{2\pi}} \int_0^\infty \frac{t^{*-\frac{1}{2}}}{t^* + \sigma^{*2}} \cdot \exp\left(-\frac{x^{*2} + 2t^*x^* + t^{*2} + y^{*2}}{2t^* + 2\sigma^{*2}} - \frac{z^{*2}}{2t^*} \right) dt^* \tag{4.5}$$

Equation 4.6 and Equation 4.7 describe the dimensionless time and distribution parameter in terms of dimensional parameters:

$$t^* = \frac{U^2 t}{2\alpha} \tag{4.6}$$

$$\sigma^* = \frac{U\sigma}{2\alpha} \tag{4.7}$$

where t has the physical meaning of time elapsed since the start of the application of the moving heat source. The current steady-state calculations, involve a range of time between 0 and infinity.

Equations 4.8 to 4.11 are the dimensionless temperature, dimensionless coordinates x^*, y^* and z^*:

$$T^* = \frac{4\pi k\alpha \left(T_c - T_0\right)}{qU} \tag{4.8}$$

$$x^* = \frac{Ux}{2\alpha} \tag{4.9}$$

$$y^* = \frac{Uy}{2\alpha} \tag{4.10}$$

$$z^* = \frac{Uz}{2\alpha} \tag{4.11}$$

where T_c is the temperature of interest, such as melting temperature or austenization temperature in the heat affected zone of ferritic steels.

In Equation 4.6-Equation 4.11, the * superscript indicates a dimensionless quantity. Equation 4.5 involves five dimensionless groups: three independent variables x^*, y^*, and z^*, dimensionless distribution parameter σ^* and the dependent variable

$T^*(x^*, y^*, z^*, \sigma^*)$. The dimensionless time t^* is a variable of integration and the steady state temperature field has no time dependence.

Using variable substitution method $\theta = \arctan(\sqrt{t^*}/\sigma)$, Equation 4.5 can be rewritten as Equation 4.12 such that the improper integral is converted to a proper one, saving much effort in computation.

$$T^* = \frac{2}{\sqrt{2\pi}\sigma^*} \int_0^{\frac{\pi}{2}} \exp\left\{ -\frac{1}{2} \left[\sigma^{*2} \left(\cos^2\theta + \frac{1}{\cos^2\theta} - 2 \right) + \frac{\cos^2\theta \left(x^{*2} + y^{*2} \right)}{\sigma^{*2}} + 2x^* \left(1 - \cos^2\theta \right) + \frac{z^{*2}\cos^2\theta}{\sigma^{*2}(1-\cos^2\theta)} \right] \right\} d\theta \tag{4.12}$$

The number of dimensionless groups is consistent with the number expected from applying dimensional analysis theory [19]. Equation 4.4 involves ten magnitudes with units: three independent variables x, y, and z, the dependent variable $T(x, y, z, \sigma)$, heat source distribution parameter σ, and five problem parameters T_0, q, k, U, and α. There are four independent units for the magnitude with dimension (m, kg, s, °C). Because there is no temperature that must be measured in absolute values, the number of dimensionless groups should minus one [152], obtaining $10 - 4 - 1 = 5$.

The dimensionless form of peak temperature and its location depend only on one dimensionless group. Considering the dimensionless peak temperature ($T^*_{\max}$), Equation 4.5 involves five independent dimensionless groups (x^*, y^*, z^*, σ^*, T^*). One constraint is Equation 4.5, leaving only four dimensionless degrees of freedom. The definition of $T^*_{\max}$ involves three more constraints: $y^* = 0$, $z^* = 0$, and $T^*_{\max} = \max(T^*)$, leaving only one free dimensionless group. For practical reasons, the remaining degree of freedom is assigned to the dimensionless distribution parameter σ^*.

4.5 Asymptotic Analysis, Blending and Correction Factors

The value of σ^* varies from zero to infinity, defining two asymptotic regimes for the dimensionless variables, which will be named following the conventions determined in[84, 96]: Regime V, corresponding to large values of σ^* (broad heat source), and

Regime VI, corresponding to small values of σ^* (concentrated heat source). Asymptotic analysis of Regime V and Regime VI yields explicit power-law expressions for peak temperature and its location.

For the dimensionless peak temperature $T^*_{\max}(\sigma^*)$, the associated asymptotic expression for Regime V is $\widehat{T^*}_{\max_{\mathrm{V}}}(\sigma^*)$, and for Regime VI is $\widehat{T^*}_{\max_{\mathrm{VI}}}(\sigma^*)$. In this notation, the symbol $\widehat{\ }$ indicates that the magnitude is an asymptotic approximation.

The power-law asymptotic expressions obtained for each asymptotic regime are less accurate in the intermediate regime, when σ^*=O(1). For intermediate values of σ^*, general and accurate expressions can be obtained using the traditional blending technique [23]. For the case of peak temperature:

$$T^*{}_{\max}(\sigma^*) \approx \widehat{T^*}^{+}_{\max} = \left[\widehat{T^*}^{n}_{\max_{\mathrm{V}}} + \widehat{T^*}^{n}_{\max_{\mathrm{VI}}}\right]^{1/n} \tag{4.13}$$

where n is the blending parameter and the $^+$ superscript indicates that the expression is the result of blending. The error of approximation is not zero for intermediate values of σ^*, and it has the same definition as [96]:

$$\text{error} = \ln \frac{\widehat{T^*}^{+}_{\max}}{T^*{}_{\max}} \tag{4.14}$$

The blending parameter n is determined with a numerical optimization procedure described in [96]. It needs to be determined only once for each blending function. For many practical cases, the absolute value of n is typically of the order of 1.

The blending results can be used to generate explicit correction factors to extend the validity of asymptotic expressions. For the peak temperature, Equation 4.13 can be rearranged to yield

$$\begin{aligned} T_{\max} \approx \widehat{T}^{+}_{\max} &= \widehat{T}_{\max_{\mathrm{V}}} \left\{1 + \left[\frac{\widehat{T^*}_{\max_{\mathrm{VI}}}(\sigma^*)}{\widehat{T^*}_{\max_{\mathrm{V}}}(\sigma^*)}\right]^{n}\right\}^{1/n} \\ &= \widehat{T}_{\max_{\mathrm{V}}} f_{T_{\max_{\mathrm{V}}}}(\sigma^*) \text{ For Regime V (large Ry, wide source)} \end{aligned} \tag{4.15}$$

$$\begin{aligned} T_{\max} \approx \widehat{T}^{+}_{\max} &= \widehat{T}_{\max_{\mathrm{VI}}} \left\{1 + \left[\frac{\widehat{T^*}_{\max_{\mathrm{VI}}}(\sigma^*)}{\widehat{T^*}_{\max_{\mathrm{V}}}(\sigma^*)}\right]^{-n}\right\}^{1/n} \\ &= \widehat{T}_{\max_{\mathrm{VI}}} f_{T_{\max_{\mathrm{VI}}}}(\sigma^*) \text{ For Regime VI (small Ry, wide source)} \end{aligned} \tag{4.16}$$

where $f_{T_{\max_{\mathrm{V}}}}(\sigma^*)$ corresponds to Regime V and $f_{T_{\max_{\mathrm{VI}}}}(\sigma^*)$ to Regime VI. As σ^* approaches infinity, Regime V, $f_{T_{\max_{\mathrm{V}}}}(\sigma^*)$ tends to 1 and when σ^* approaches 0 in Regime VI, $f_{T_{\max_{\mathrm{VI}}}}(\sigma^*)$ tends to 1. The value of n for Equations 4.15 and 4.16 are the same as for Equation 4.13.

4.6 Scaling Analysis of Peak Temperature $T_{\max}$

The magnitude $T_{\max}$ is the maximum temperature that the base material reaches under a Gaussian distributed surface heat source, and $T^*_{\max}$ is its dimensionless counterpart. The determination of $T_{\max}$ requires a numerical calculation to find the maximum for each point in the centerline, and its dependence on σ^* is illustrated in Figure 4.1. The asymptotic behaviors at large and small σ^* are straight lines in log-log scale, resulting from their power-law behavior.

Asymptotic analysis of Equation 4.5, detailed in the Appendix, yields the following power laws:

$$\widehat{T^*}_{\max_{\mathrm{V}}}(\sigma^*) = \sqrt{\frac{2}{\pi}} I_m \, \sigma^{*-1.5} \quad \text{For Regime V (large Ry, wide source)} \tag{4.17}$$

$$\widehat{T^*}_{\max_{\mathrm{VI}}}(\sigma^*) = \sqrt{\frac{\pi}{2}} \, \sigma^{*-1} \quad \text{For Regime VI (small Ry, wide source)} \tag{4.18}$$

where $I_m = 1.280$. The blending expression for $\widehat{T}^+_{\max}(\sigma^*)$ is given by Equation 4.13. Replacing the expressions for $\widehat{T^*}_{\max_{\mathrm{V}}}(\sigma^*)$ and $\widehat{T^*}_{\max_{\mathrm{VI}}}(\sigma^*)$ into Equations 4.15 and 4.16, the following expressions for the correction factors are obtained:

$$f_{T_{\max_{\mathrm{V\text{-}VI}}}}(\sigma^*) = \left[1 + \left(\frac{\pi\sqrt{\sigma^*}}{2I_m}\right)^{\pm n}\right]^{1/n} \tag{4.19}$$

where the exponent $+n$ corresponds to Regime V, and $-n$ corresponds to Regime VI. The error of Equation 4.19 as a function of σ^* was calculated using Equation 4.14 for three values of n as illustrated in Figure 4.2. The error of approximation approches zero in both ends because asymptotic behavior in extreme cases are exactly captured

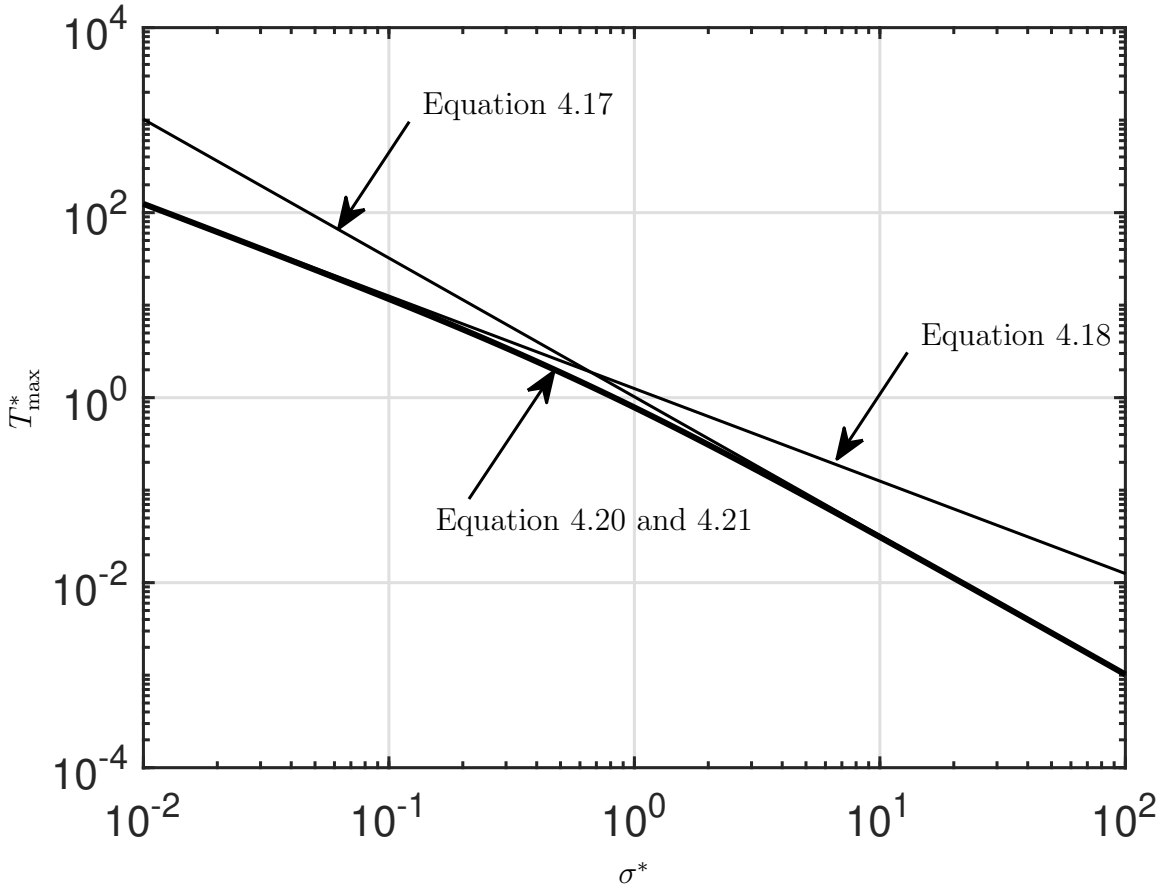

Figure 4.1: Dimensionless peak temperature $T^*_{\max}$ as a function of dimensionless heat source distribution parameter σ^*.

by the blending function.

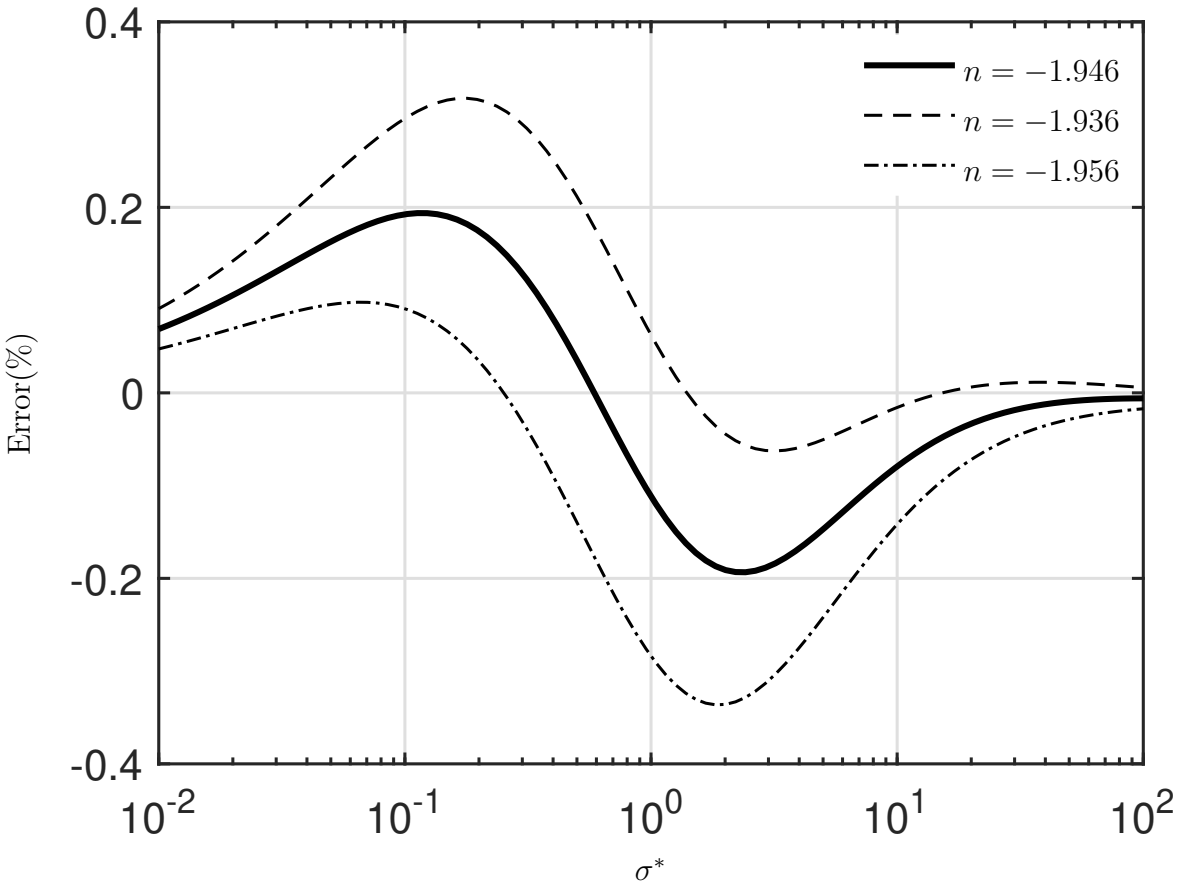

Figure 4.2: Relative error of blending for dimensionless peak temperature as a function of dimensionless heat source distribution parameter σ^* for the optimal value $n = -1.946$. The error tends to zero for both high and low σ^*.

Figure 4.3 illustrates the variation in maximum absolute value of error as a function of n over all σ^*. The sharp minimum indicated by the dash line is because the maximum error can be positive (for n smaller than the optimum), or negative (for n lager than the optimum). For the optimal value n = -1.946, the minimax error is 0.19%.

Correction factors for both regimes (Equation 4.19) are illustrated in Figure 4.4. These correction factors based on blending have an error smaller than 0.19 % com-

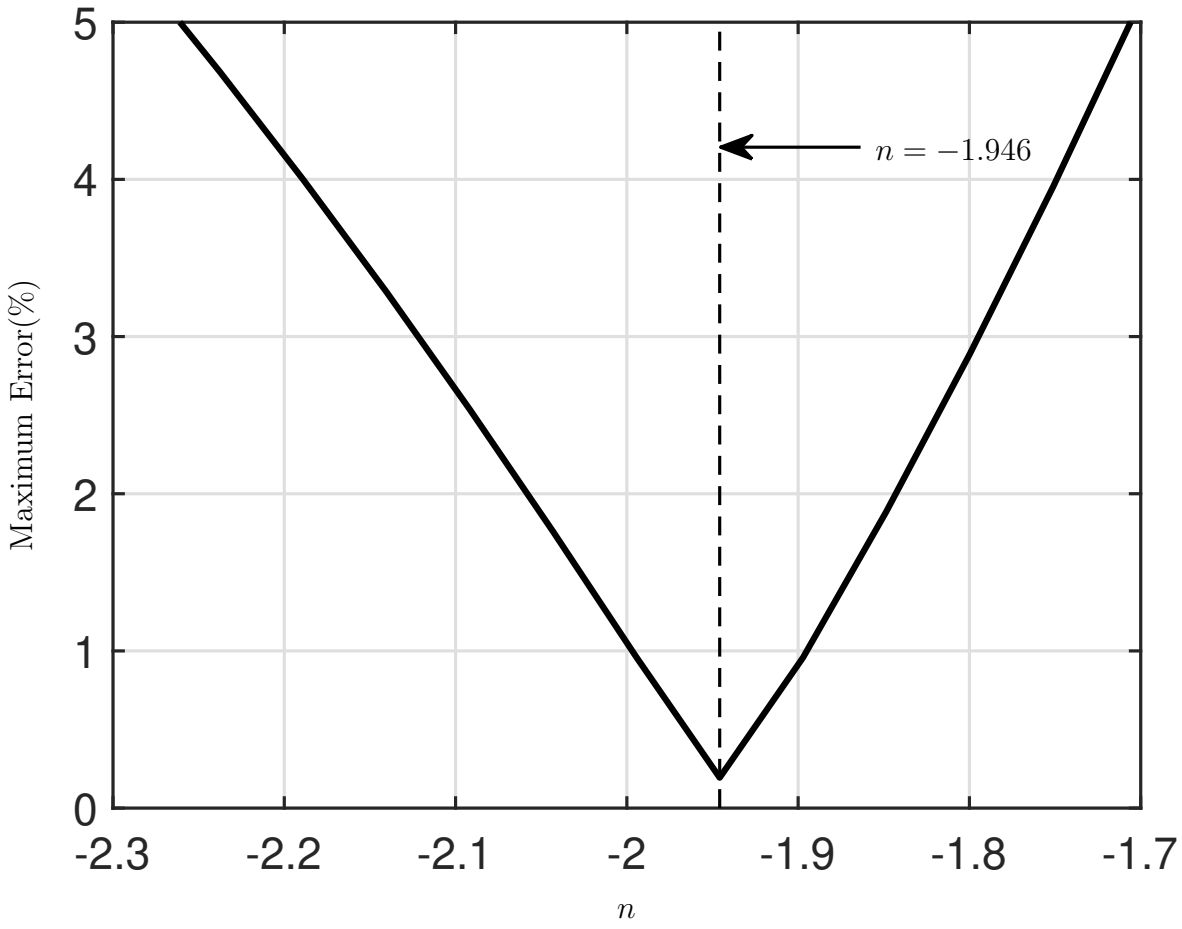

Figure 4.3: Maximum error for dimensionless peak temperature as a function of blending parameter n. Minimized maximum error is 0.19% at the optimal value $n = -1.946$.

pared with the exact solution for any value of σ^*. The correction factors tend to a constant of 1 (no correction needed) in their corresponding asymptotic regimes, and they cross over at $\sigma_c^* = 0.6638$. The magnitude σ_c^* can be considered as a divider between Regime V and Regime VI, with the understanding that in the vicinity of σ_c^* the situation is actually intermediate between both regimes.

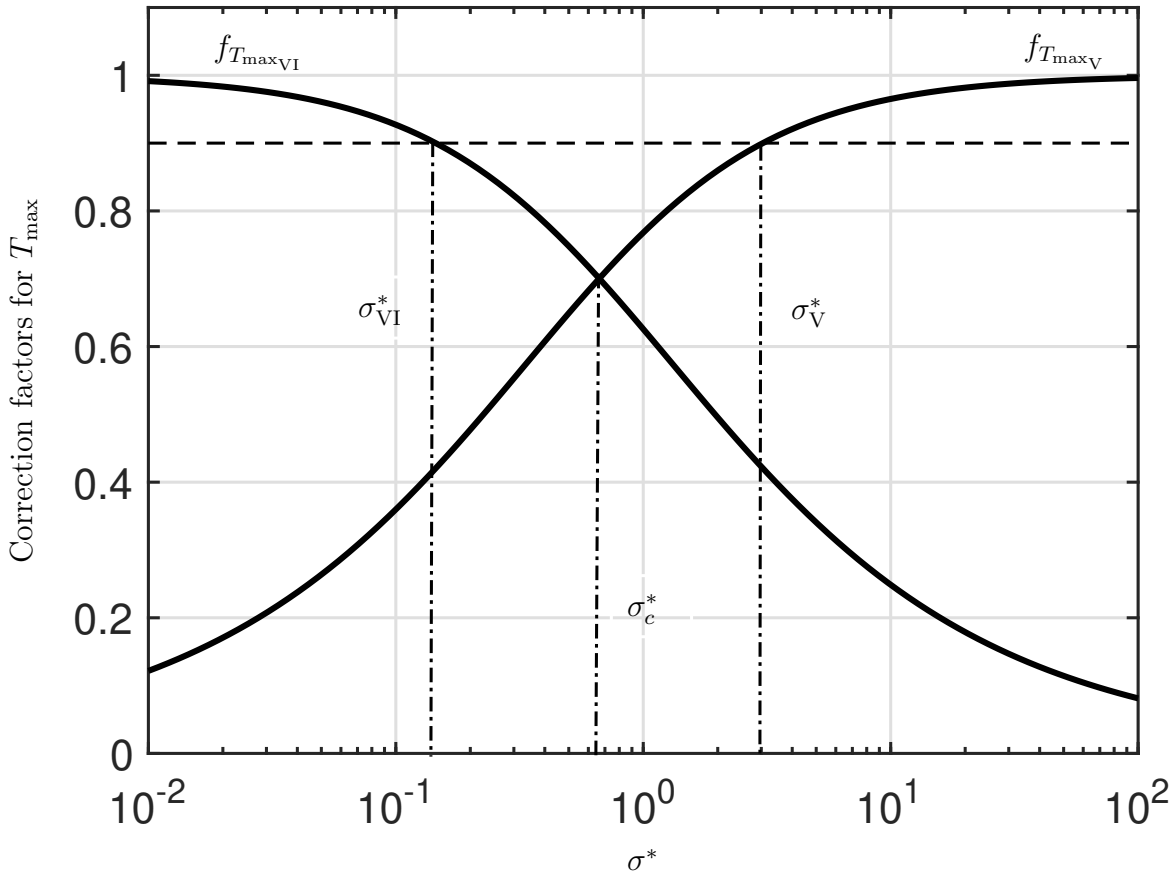

Figure 4.4: Correction factors to estimate peak temperature. For $\sigma^* < \sigma^*_{\mathrm{VI}} = 0.1480$ or $\sigma^* > \sigma^*_{\mathrm{V}} = 3.098$, the maximum error of directly using asymptotic is less than 10%. The correction factors cross over at $\sigma^*_c = 0.6638$.

Choosing the right asymptotic expression, but neglecting the correction factors results in an error smaller than 10 % for $\sigma^* > \sigma^*_{\mathrm{V}} = 3.098$ or $\sigma^* < \sigma^*_{\mathrm{VI}} = 0.1480$ in their corresponding regimes. The heuristic proposed before [96, 149] is also valid for this case: that when the blending variable (in this case σ^*) is outside the range

defined by $20^{\pm 1}$, the error in neglecting the correction factors is below 10%.

Engineering expressions (with units) for the peak temperature under a Gaussian distributed heat source on a semi-infinite solid can be obtained by replacing Equation 4.7 into Equations 4.17 and 4.18, and combining with Equation 4.8, obtaining

$$\widehat{T}^{+}_{\max} = T_0 + \left(\widehat{T}_{\max_{\mathrm{V}}} - T_0\right) f_{T_{\max_{\mathrm{V}}}}(\sigma^*) =$$
$$T_0 + \tfrac{qI_m}{\pi k\sigma}\sqrt{\frac{\alpha}{\pi\sigma U}}\; f_{T_{\max_{\mathrm{V}}}}(\sigma^*) \text{ For Regime V (large Ry, wide source)} \tag{4.20}$$
$$\widehat{T}^{+}_{\max} = T_0 + \left(\widehat{T}_{\max_{\mathrm{VI}}} - T_0\right) f_{T_{\max_{\mathrm{VI}}}}(\sigma^*) =$$
$$T_0 + \tfrac{q}{2\pi k\sigma\sqrt{2\pi}}\; f_{T_{\max_{\mathrm{VI}}}}(\sigma^*) \text{ For Regime VI (small Ry, wide source)} \tag{4.21}$$

4.7 Scaling Analysis of Maximum Distribution Parameter $\sigma_{\max}$

In some practical cases, a peak temperature of the substrate is the target, and what needs to be calculated is the maximum size of the heat sorce that can reach this temperature; for example, when substrate melting must be assured to avoid debonding in laser cladding and powder-deposition additive manufacturing processes, or to achieve austenization in laser hat treating [76]. For any given temperature T^*, there is a maximum distribution parameter $\sigma^*_{\max}$, above which the target temperature cannot be reached.

To abtain a blended expression of $\sigma^*_{\max}$, equations 4.17 and 4.18 can be rewritten as:

$$\widehat{\sigma^*}_{\max_{\mathrm{V}}}(T^*) = \left(\sqrt{\frac{2}{\pi}}\frac{I_m}{T^*}\right)^{2/3} \quad \text{For Regime V (large Ry, wide source)} \tag{4.22}$$
$$\widehat{\sigma^*}_{\max_{\mathrm{VI}}}(T^*) = \sqrt{\frac{\pi}{2}}\frac{1}{T^*} \quad \text{For Regime VI (small Ry, wide source)} \tag{4.23}$$

where $I_m = 1.280$, which is the same asymptotic constant in Equation 4.17.

The blending equation for $\widehat{\sigma^*}^{+}_{\max}$ has the following expression:

$$\widehat{\sigma^*}^{+}_{\max} = \left\{\left[\left(\sqrt{\tfrac{2}{\pi}}\frac{I_m}{T^*}\right)^{2/3}\right]^n + \left(\sqrt{\tfrac{\pi}{2}}\frac{1}{T^*}\right)^n\right\}^{1/n} \tag{4.24}$$

with an optimal blending parameter $n = -2.397$ and maximum error of 1.4%. Asymptotics of the dimensionless maximum heat distribution parameter in both regimes (Equation 4.22 and Equation 4.23) and the blending equation (Equation 4.24) are

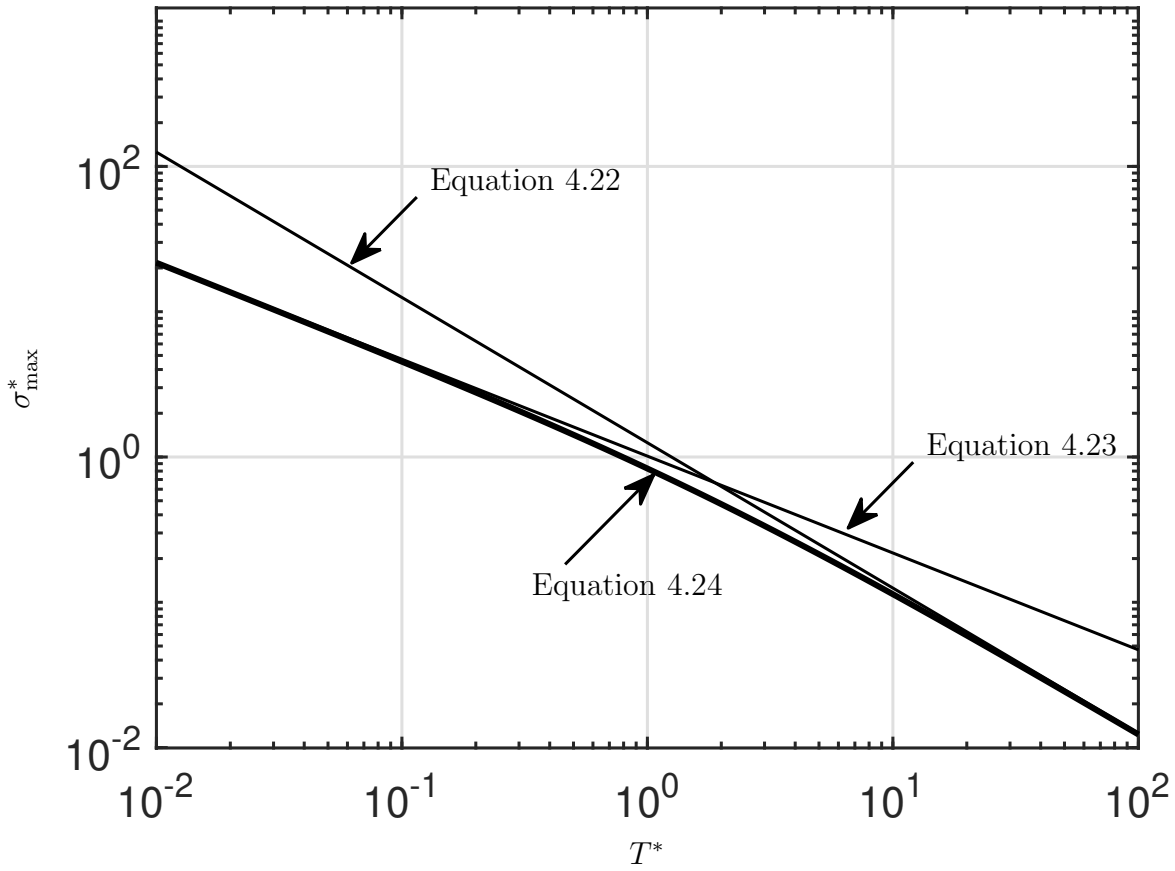

Figure 4.5: Dimensionless maximum distribution parameter of the heat source as a function of T^*.

Simple formulas and correction factors for the maximum heat source distribution parameter are obtained by bringing normalization expressions, Equation 4.7 and

Equation 4.8 into Equation 4.22 and Equation 4.23:

$$\widehat{\sigma}^{+}_{\max} = \widehat{\sigma}_{\max_{\mathrm{V}}} f_{\sigma_{\max_{\mathrm{V}}}}(T^*)$$
$$= \frac{\alpha}{\pi U}\left[\frac{qUI_m}{k\alpha(T-T_0)}\right]^{2/3} f_{\sigma_{\max_{\mathrm{V}}}}(T^*) \text{ For Regime V (large Ry, wide source)} \quad (4.25)$$
$$\widehat{\sigma}^{+}_{\max} = \widehat{\sigma}_{\max_{\mathrm{VI}}} f_{\sigma_{\max_{\mathrm{VI}}}}(T^*)$$
$$= \sqrt{\frac{1}{8\pi}}\frac{q}{k(T-T_0)} f_{\sigma_{\max_{\mathrm{VI}}}}(T^*) \text{ For Regime VI (small Ry, wide source)} \quad (4.26)$$

with correction factors in both regimes listed as the following:

$$f_{\sigma_{\max_{\mathrm{V\text{-}VI}}}}(T^*) = \left\{1 + \left[\left(\frac{\pi}{2}\right)^{\frac{5}{6}}\left({I_m}^2 T^*\right)^{-\frac{1}{3}}\right]^{\pm n}\right\}^{1/n} \quad (4.27)$$

where the exponent $+n$ corresponds to Regime V, and $-n$ corresponds to Regime VI.

The correction factors for maximum heat source distribution parameter of both asymptotic expressions are illustrated in Figure 4.6. The crossover point for the correction factors is $T^*_c = 1.888$ at $f_{\sigma^*_{\max_{\mathrm{V}}}} = f_{\sigma^*_{\max_{\mathrm{VI}}}} = 0.7493$, which means the error using two asymptotic expressions only without correction factors equals to 25% if used in their appropriate range. If a 10% relative error is considered (correction factor = 0.9), the critical value for Equation 4.22 and Equation 4.23 is $T^*_{\mathrm{VI}} = 8.994$ and $T^*_{\mathrm{V}} = 0.3960$, respectively. In Regime V, meaning $T^* < T^*_{\mathrm{V}} = 0.3960$, the maximum error of using Equation 4.22 without its correction factor is smaller than 10%. In Regime VI (when $T^* > T^*_{\mathrm{VI}} = 8.994$) the maximum error of using Equation 4.23 only is smaller than 10%.

4.8 Scaling Analysis of the Location of Peak Temperature $x_{\max}$

The magnitude $x_{\max}$ is the location of peak temperature at the plane $z = 0$. The dependence of $x^*_{\max}$ on σ^* is illustrated in Figure 4.7. When $\sigma^* = 0$, the peak temperature occurs at the location of the point heat source, and thus, the location of

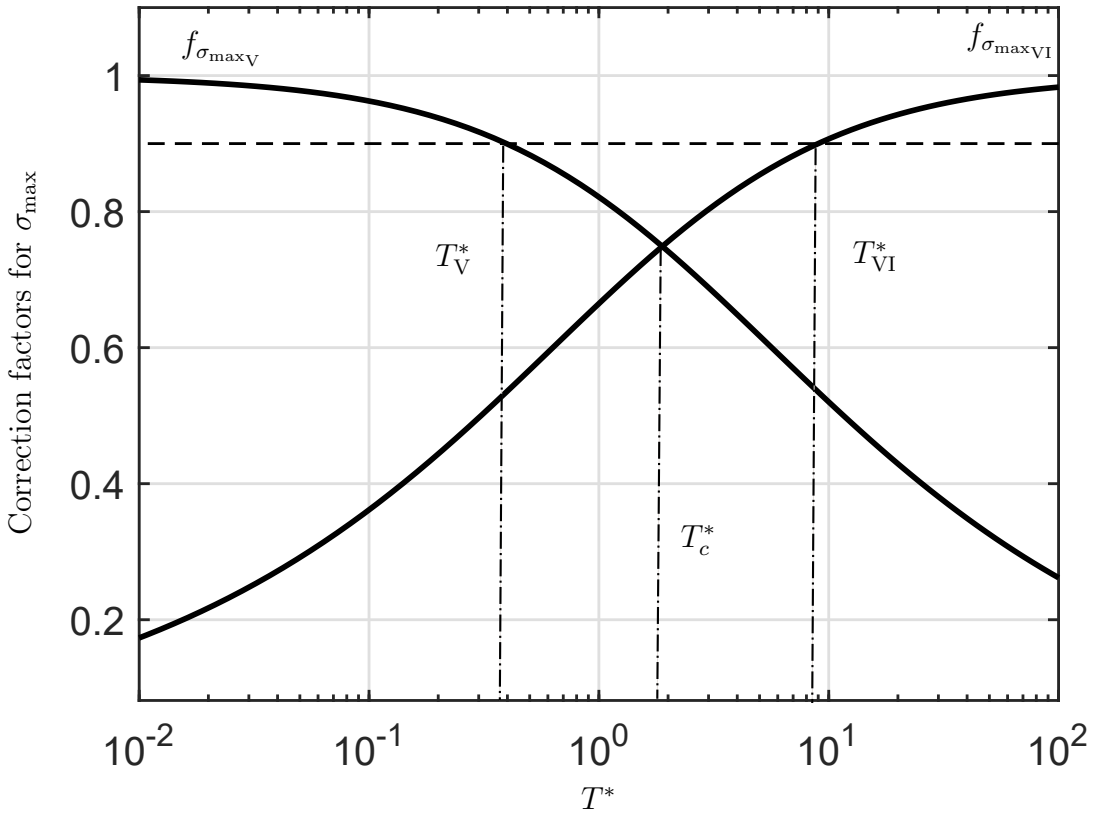

Figure 4.6: Correction factors to estimate the maximum distribution parameter. For $T^* < T_{\mathrm{V}}^* = 0.3960$ or $T^* > T_{\mathrm{VI}}^* = 8.994$, the maximum error of directly using simple formulas is less than 10%. The correction factors cross over at $T_c^* = 1.887$.

maximum temperature $x^*_{\max} = 0$. With increasing σ^*, $x^*_{\max}$ moves from the center to the edge of the heat source.

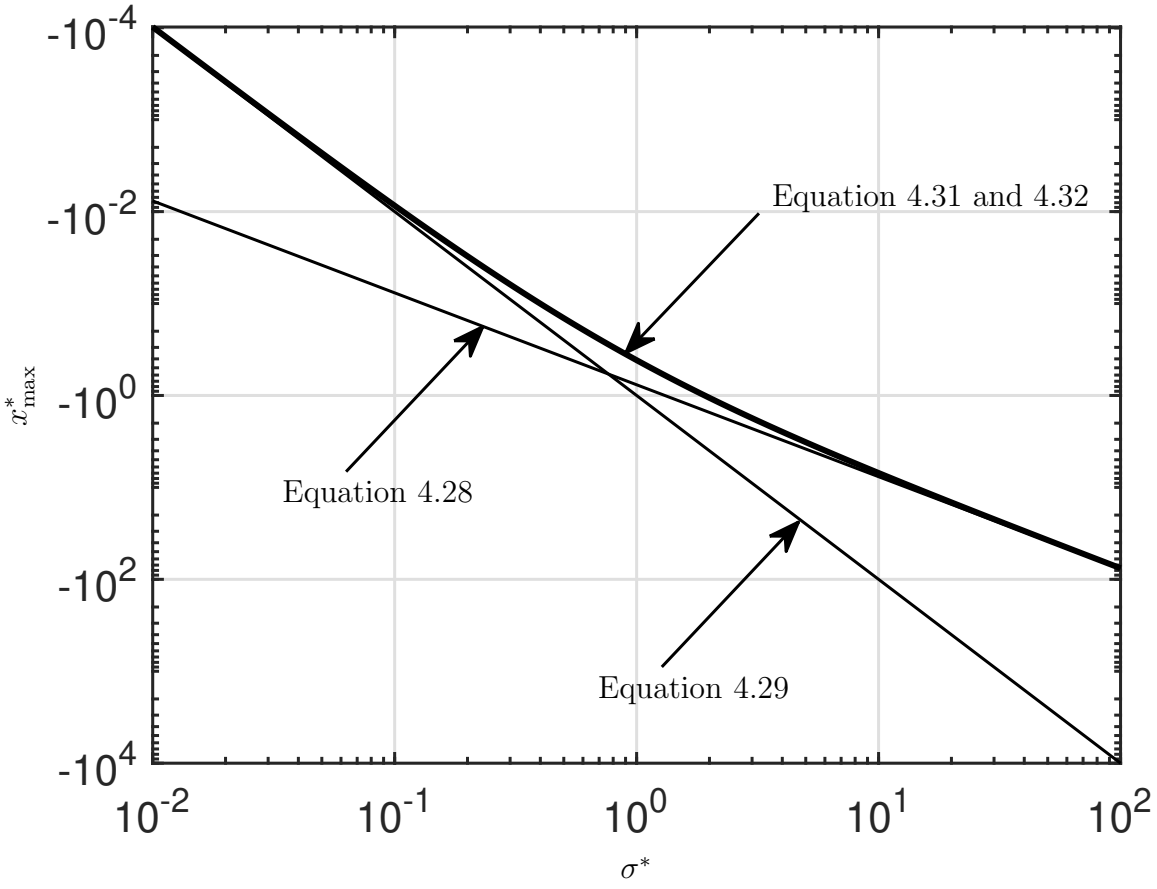

Figure 4.7: Dimensionless location of peak temperature $x^*_{\max}$ as a function of dimensionless heat source distribution parameter σ^*.

Asymptotic analysis of Equation 4.5, detailed in the Appendix, yields the following power laws:

$$\widehat{x^*}_{\max_{\mathrm{V}}}(\sigma^*) = -0.7650\sigma^* \quad \text{For Regime V (large Ry, wide source)} \tag{4.28}$$

$$\widehat{x^*}_{\max_{\mathrm{VI}}}(\sigma^*) = -\sigma^{*2} \quad \text{For Regime VI (small Ry, wide source)} \tag{4.29}$$

The blending expression for $\widehat{x}^+_{\max}(\sigma^*)$ is obtained with the same process used to obtain $\widehat{T}^+_{\max}(\sigma^*)$, yielding the following correction factors:

$$f_{x_{\max_{\text{V-VI}}}}(\sigma^*) = \left[1 + (1.307\sigma^*)^{\pm n}\right]^{1/n} \tag{4.30}$$

where the exponent $+n$ corresponds to Regime V, and $-n$ corresponds to Regime VI. The value of n for Equation 4.30 was determined using the same optimization as for $T_{\max}$. Figure 4.8 illustrates the error of approximation as a function of σ^* for three values of n around the optimal, and Figure 4.9 illustrates the variation of maximum error with blending parameter n. The minimax error is 0.47 %, corresponding to n = -0.9347.

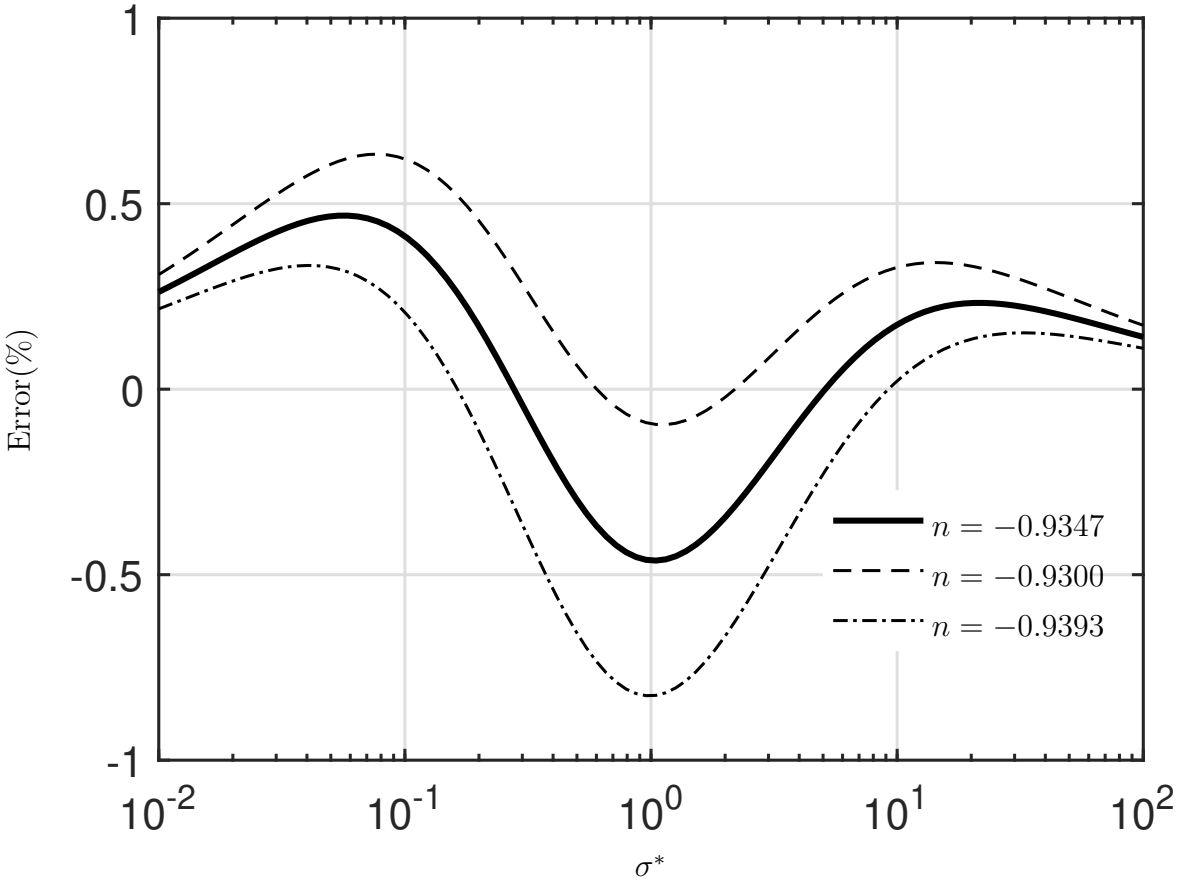

Figure 4.8: Relative error of blending for the location of peak temperature as a function of dimensionless heat source distribution parameter σ^* near the optimal value $n = -0.9347$.

Simple formulas and correction factors for the location of peak temperature are given by bringing normalization expressions, Equation 4.28 and Equation 4.29 into

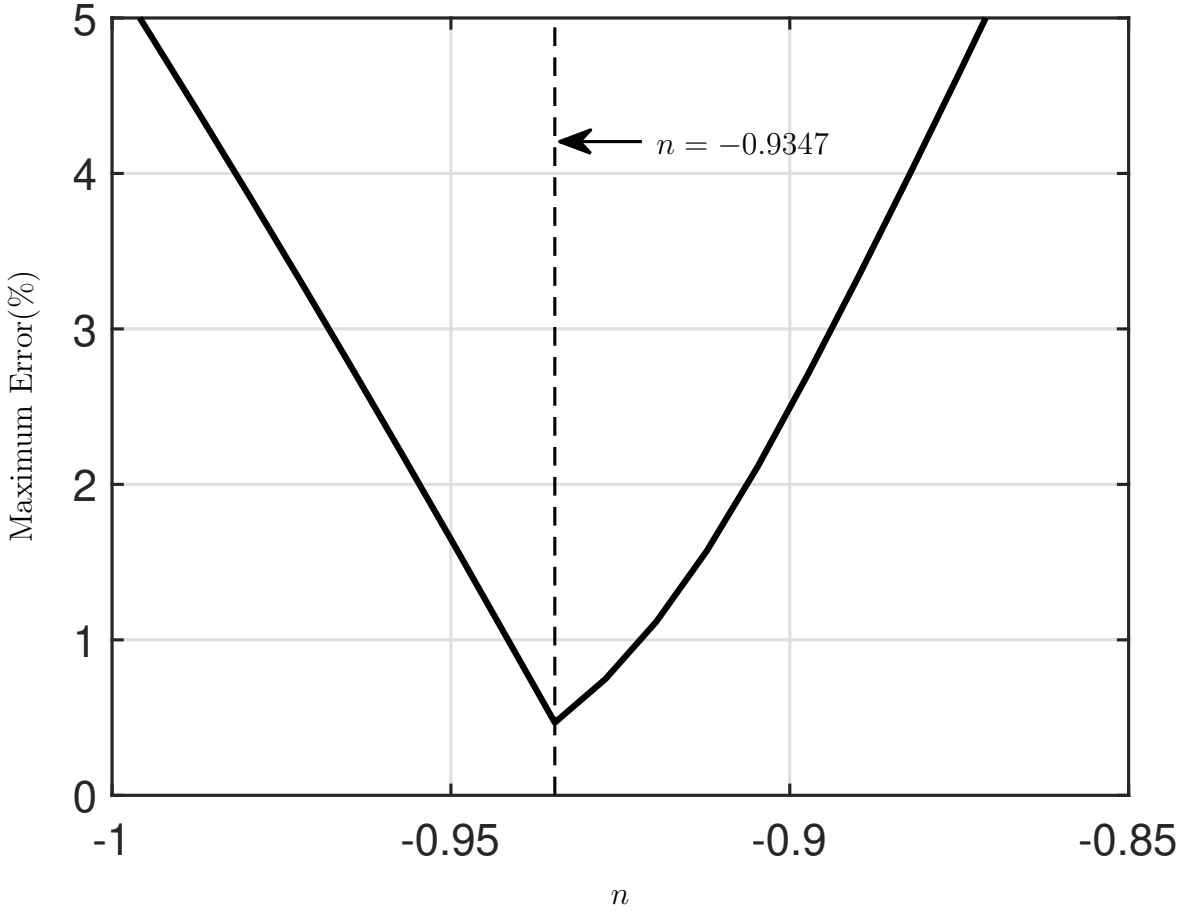

Figure 4.9: Maximum error for the location of peak temperature as a function of blending parameter n. Minimized maximum error is 0.47% at the optimal value $n = -0.9347$.

Equation 4.15 and Equation 4.16:

$$\begin{aligned}\widehat{x}^{+}_{\max} &= \widehat{x}_{\max_{\mathrm{V}}} f_{x_{\max_{\mathrm{V}}}}(\sigma^*) \\ &= -0.7650\sigma\ f_{x_{\max_{\mathrm{V}}}} \text{ For Regime V (large Ry, wide source)} \qquad (4.31) \\ \widehat{x}^{+}_{\max} &= \widehat{x}_{\max_{\mathrm{VI}}} f_{x_{\max_{\mathrm{VI}}}}(\sigma^*) \\ &= -\tfrac{U\sigma^2}{2\alpha}\ f_{x_{\max_{\mathrm{VI}}}} \text{ For Regime VI (small Ry, wide source)} \qquad (4.32)\end{aligned}$$

with correction factors expressed in Equation 4.30.

The correction factors for the location of peak temperature of both asymptotic expressions are illustrated in Figure 4.10. The crossover point for the correction factors is $\sigma_c^* = 0.7650$ with correction factor of $f_{x^*_{\max_{\mathrm{V}}}} = f_{x^*_{\max_{\mathrm{VI}}}} = 0.4743$, which means the maximum error using two asymptotic expressions without blending equals to 52.57%. At both ends, the asymptotics can be applied directly. If 10% relative error is considered, i.e. correction factor equals 0.9, the critical value for Equation 4.28 and Equation 4.29 is $\sigma^*_{\mathrm{V}} = 8.532$ and $\sigma^*_{\mathrm{VI}} = 0.07089$, respectively. In Regime V, meaning $\sigma^* > \sigma^*_{\mathrm{V}} = 8.532$, the maximum error of using Equation 4.28 is less than 10%. In Regime VI, meaning $\sigma^* < \sigma^*_{\mathrm{VI}} = 0.07089$, the maximum error of using Equation 4.29 is less than 10%.

4.9 Experimental Validation

The focus of this paper is on the peak temperature of the substrate in general, not restricted to any specific process. High-quality data available in the literature is in its vast majority for laser processing of materials, and it is the data that will be used for validation.

The validation of the proposed predictive expressions was made by comparison against published data and shown in Figure 4.11, spanning a range of σ^* of four orders of magnitude from 0.01 to 100. Measurements were collected for laser heat

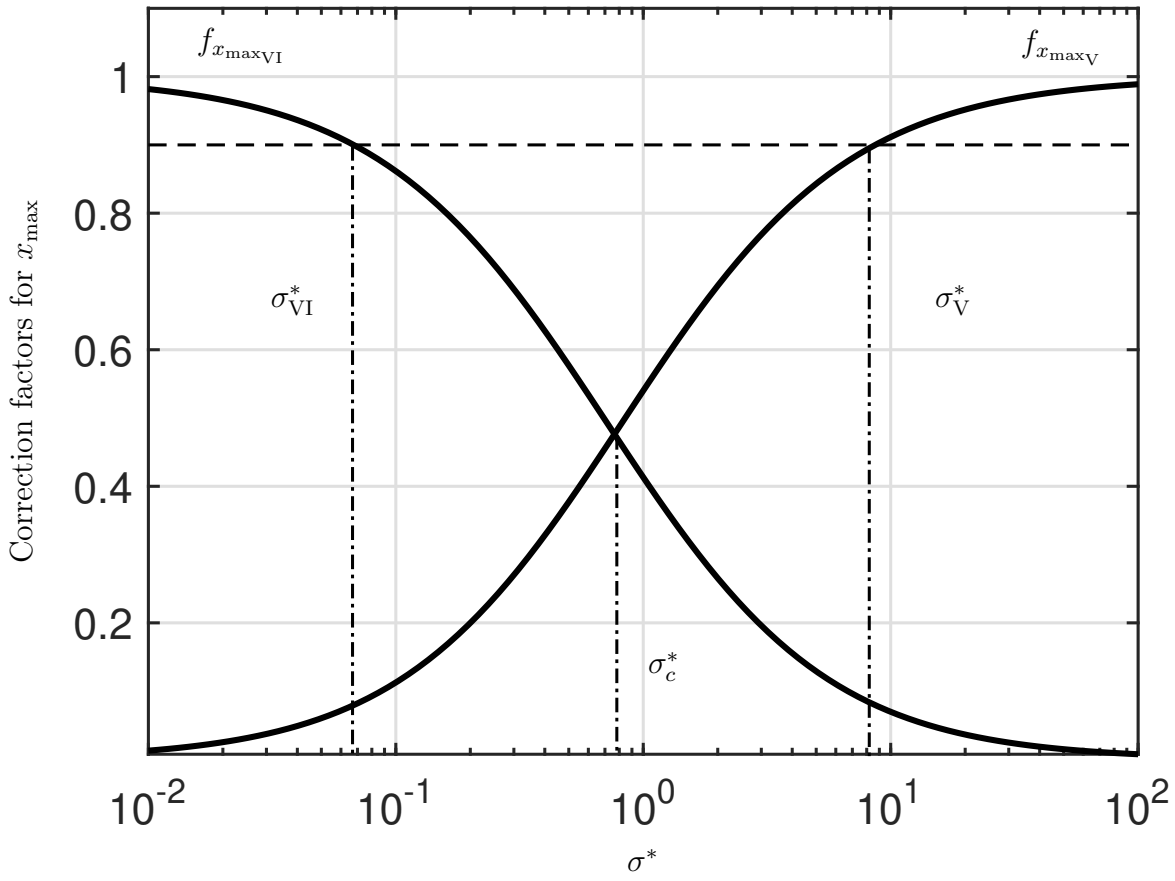

Figure 4.10: Correction factors of two simple formulas to estimate the location of peak temperature. For $\sigma^* < \sigma^*_{\mathrm{VI}} = 0.07089$ or $\sigma^* > \sigma^*_{\mathrm{V}} = 8.532$, the maximum error of directly using simple formulas is less than 10%. The correction factors cross over at $\sigma^*_c = 0.7650$.

treatment for a wide range of materials, including silicon, ZrO_2 ceramic, GaAs, Mn-Zn ferrite and low carbon steel.

The published values of peak temperature and measured heat distribution parameter were normalized using Equation 4.8 and Equation 4.7, respectively, and compared against the blended expression in Equation 4.21. The characteristic temperature used in these calculations (T_c) corresponds to the peak temperature on the surface (T_{max}) in all cases. The initial temperature T_0 was always assumed or given as 20°C except for [103], which was measured as 350°C.

When not listed in the original papers, the thermophysical properties were obtained from software JMatPro v11. When temperature-dependent properties were available [85, 103], effective values were calculated using the methodology of integral average introduced in [84]. Laser absorptivity was assessed from the original papers [21, 85, 103] or estimated as a constant of 0.67 based on the literature [116, 135] and the authors' experiences. The raw data from literature and all values used to calculate the points are listed in Table 4.2.

Figure 4.11 compares Equation 4.21 with published data for peak temperature in laser heat treatment. The results show a relatively narrow scatter and no obvious bias. The excellent agreement also supports the applicability of Eagar and Tsai's solution to moving Gaussian heat source and the small error caused by its simplifications.

The neglected secondary phenomena such as surface heat loss are a source of scatter in the comparisons. Other sources of scatter are uncertainties in the thermophysical properties used, uncertainties in the laser absorptivity, which varies in a very broad range for laser processes (0.3 to 0.75 depending on surface conditions and processing parameters [116]), and error in the measurements.

4.10 Example of Application

Consider the laser heat treatment of AISI1020 steel of 6.35 mm thickness performed by Farshidianfar [39]. The heat source was 225 W fiber laser, with a travel speed

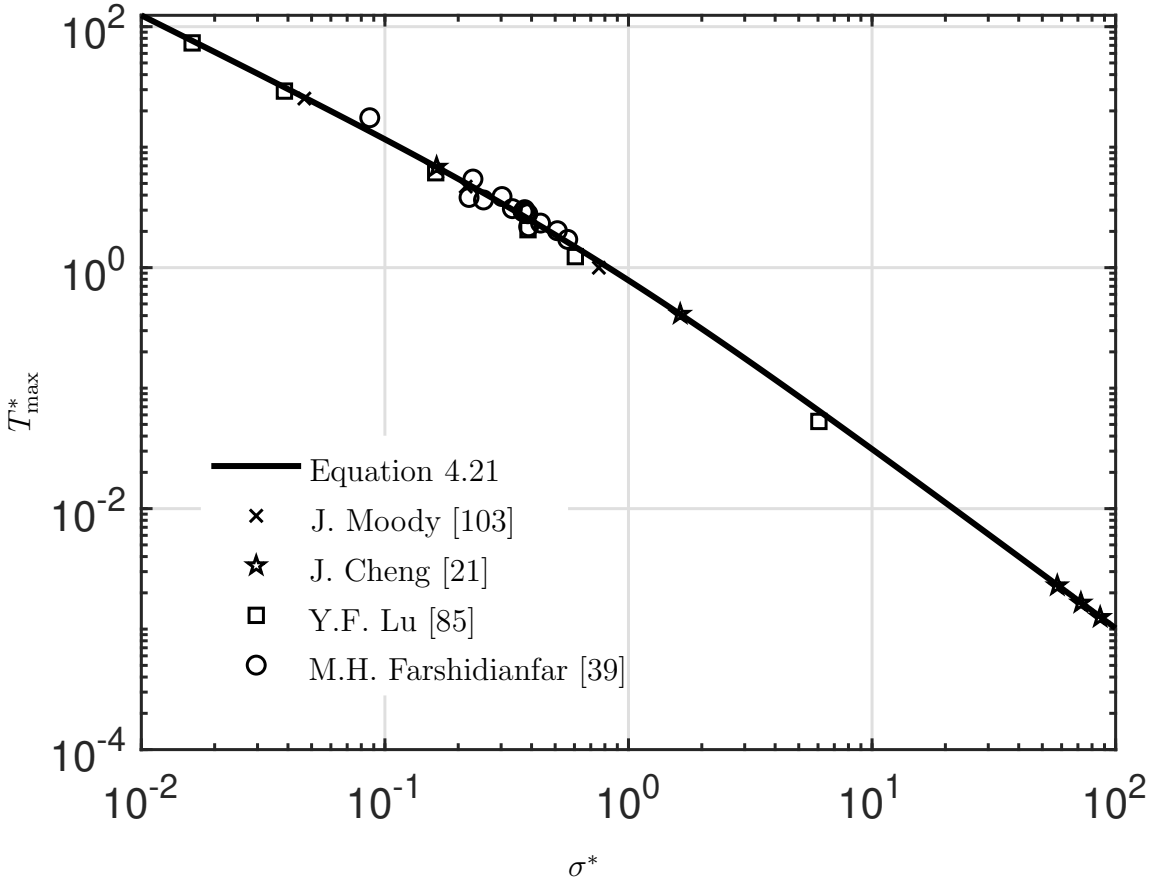

Figure 4.11: Comparison of explicit blending solution Equation 4.21 with published data for peak temperature in laser processing.

of 8.33 mm/s, a laser absorptivity of 0.67 estimated based on analysis of [116]. The laser beam radius measured at 1/e of the peak power intensity was 1 mm, and the corresponding standard deviation σ is 0.71 mm. Effective thermal conductivity and diffusivity of the substrate is 46.85 W/m $\cdot$ K and 8.83$\times$ 10^{-6}m^2/s, respectively. The measured peak temperature by the thermal infrared camera was 766°C.

For the case considered, the dimensionless standard deviation is $\sigma^* = 0.33$ (Equation 4.7), corresponding to the intermediate regime. The prediction of peak temperature is made using the appropriate equation for Regime VI (Equation 4.21), which yields $\widehat{T^*}_{\max_{\mathrm{VI}}} = 3.76$, and $f_{T_{\max_{\mathrm{VI}}}}(\sigma^*) = 0.81$ (Equation 4.19). The correction applied in this case is larger than 10%, consistently with the intermediate value of σ^*. Turning the dimensionless temperature into its dimensional counterpart with units (Equation 4.8), the predicted peak temperature is $\widehat{T}^+_{\max} = 754$°C, which is an underprediction with an error of -12°C compared to the measured value of 766°C.

4.11 Discussion

This paper presents closed-form expressions for maximum temperature, $T_{\max}$, location of peak temperature $x_{\max}$, and maximum distribution parameter of a Gaussian distributed heat source to reach a specific temperature, $\sigma_{\max}$. All predictions were obtained by a systematic methodology of asymptotic analysis and blending. Simple solutions were obtained by asymptotic analysis for extreme cases when the independent variable is asymptotically large or small. Blending functions were employed to construct a closed-form solution applicable to the domain by combining asymptotic solutions of broad and concentrated heat sources. Correction factors have been developed to extend the usefulness of asymptotes and determine intermediate regimes where the independent variable is either asymptotically large or small.

According to Equations 4.20 and 4.31, $x_{\max}$ tends to zero, and $T_{\max}$ tends to infinity, as σ tends to zero, which is consistent with the point heat source solution; while as σ tends to infinity, the heat source intensity is too small to heat the base metal, and peak

temperature tends to the initial temperature of the substrate T_0 as expected. The introduction of the Gaussian model avoids the singularity in Rosenthal's solution, and accuracy in the high-temperature region near the heat source is improved significantly without much complexity.

For moving heat source problems, the magnitude of temperature rise depends on several factors, including heat source intensity and its distribution parameter, velocity of the heat source, preheat and thermal properties of the substrate. For a given material, the interplay of heat source power q, moving speed U, and distribution parameter σ on the maximum surface temperature is explicitly reflected in Equations 4.20 and 4.21. The obtained equations can provide a quick estimation of the maximum temperature using parameters known before experiments by a calculator or spreadsheet, and can be embedded easily in higher order metamodels spanning multiple scales of detail. They are also helpful in the design of appropriate operating parameters to reach desired surface temperature.

A wide range of moving heat source configurations was studied in [107], although Gaussian heat sources were not included. If a similar calculation of dimensionless thermal resistance is performed based on the results presented here, the same dependence on $\sqrt{\sigma^*}$ is observed for wide sources, and a constant resistance is also observed for concentrated or stationary sources. Based on [107], it is to be expected these dimensionless resistances to be roughly applicable for broad gaussian heat sources of hyperelliptical shapes, using the geometric average of their distributions as the characteristic dimension.

Although the prediction of peak temperature has an excellent agreement with published measurements, they are valid within the range of validity of their hypotheses, such as large thickness of the substrate. Other simplifications that need further research are the effect of temperature-dependent materials properties, surface loss by convection and radiation, and latent heat of phase transformation. These factors are typically secondary and were reviewed in [84]. Also, heat intensity in practical cases

is seldom a perfect Gaussian distribution as assumed in the model. Efficiency of the heat source, such as laser absorptivity, is difficult to estimate because it depends on the surface preparation and temperature, and laser wavelength. Although all these factors influence the accuracy of prediction, the proposed expression still provides a functional relationship in closed form between the peak temperature, process and materials parameters. It can be applied to assess how changes in the process parameters or materials will affect the peak temperature of the workpiece.

Better accuracy of predictions can be achieved with additional correction factors. Intermediate plate thickness can be accounted for by introducing another correction factor pertinent to the plate thickness. Surface heat loss can be accounted for by a correction factor dependent on the heat transfer coefficient of the plate surface [83]. Conventional blending skills need to be extended into multiple parameters to apply to functions with more than one dimensionless degree of freedom, which is the focus of current research.

4.12 Conclusions

The use of asymptotic and blending is applied for the first time to predict with high accuracy the peak temperature rise $T_{\max}$ and its location $x_{\max}$, as well as the maximum distribution parameter $\sigma_{\max}$ to reach a certain peak temperature under a moving Gaussian heat source.

The dimensionless peak temperature and its location depend only on one dimensionless group, σ^*, which determines how broad or concentrated a heat source is. The parameter σ^* divides all possible solutions into two regimes: Regime V corresponding to large σ^* ("wide" heat sources) and Regime VI corresponding to small σ^* ("concentrated" heat sources).

The expressions proposed are written as simple formulas (asymptotes in extreme cases) multiplied by a correction factor (Equation 4.19 for $T_{\max}$, Equation 4.27 for $\sigma_{\max}$, and Equation 4.30 for $x_{\max}$). These expressions asymptotically approach the

exact solution for small and large independent variables, and the maximum error in the domain is 0.19 % for $T_{\max}$, 1.4 % for $\sigma_{\max}$ and 0.47 % for $x_{\max}$, respectively. For $\sigma^* > 20$ or $\sigma^* < 0.05$, the asymptotic expression alone, without correction, has an error below 10 %.

The proposed expressions do not present convergence issues and can be calculated using a calculator or a basic spreadsheet and can be readily embedded into multi-scale metamodels. The expressions presented here can be applied to design operating parameters (e.g. determine the onset of surface melting) in many processes or to verify numerical models. The results obtained support the applicability of asymptotics and blending to solve general moving heat source problems.

Acknowledgments

The authors wish to acknowledge support from the Natural Sciences and Engineering Research Council of Canada (NSERC). Student scholarships from the American Welding Society and the Canadian Welding Association Foundation were also gratefully received.

References

[4] S. Ahn and S. Kang, "Dissolution phenomena in the ti (c0. 7n0. 3)–wc–ni system," *International Journal of Refractory Metals and Hard Materials*, vol. 26, no. 4, pp. 340–345, 2008.

[15] J Blecher, T. Palmer, S. Kelly, and R. Martukanitz, "Identifying performance differences in transmissive and reflective laser optics using beam diagnostic tools," *Welding journal*, vol. 91, no. 7, 204S–214S, 2012.

[19] E. Buckingham, "On Physically Similar Systems; Illustrations of the Use of Dimensional Equations," *Physical Review*, vol. 4, no. 4, pp. 345–376, 1914, ISSN: 0031899X. arXiv: `arXiv:1011.1669v3`.

[21] J. Cheng and A. Kar, "Mathematical model for laser densification of ceramic coating," *Journal of materials science*, vol. 32, no. 23, pp. 6269–6278, 1997.

[22] N. Christensen, Davies, V. de L., and K. Gjermundsen, "Distribution of Temperatures in Arc Welding," *British Welding Journal*, vol. 12, no. 2, pp. 54–75, 1965.

[23] S. W. Churchill and R. Usagi, "A general expression for the correlation of rates of transfer and other phenomena," *AIChE Journal*, vol. 18, no. 6, pp. 1121–1128, 1972, ISSN: 15475905.

[27] H. E. Cline and T. R. Anthony, "Heat treating and melting material with a scanning laser or electron beam," *Journal of Applied Physics*, vol. 48, no. 9, 1977.

[32] D. Darmadi, J. Norrish, and A. K. Tieu, "Analytic and finite element solutions for temperature profiles in welding using varied heat source models," *World Academy of Science, Engineering and Technology*, vol. 81, pp. 154–162, 2011.

[36] T. W. Eagar and N. S. Tsai, "Temperature Fields Produced by Traveling Distributed Heat Sources," *Welding Journal*, vol. 62, no. 12, pp. 346–355, 1983, ISSN: 00432296.

[39] M. H. Farshidianfar, "Real-time closed-loop control of microstructure and geometry in laser materials processing," PhD thesis, University of Waterloo, 2017.

[47] J. Goldak, M. Asadi, and R. G. Alena, "Why Power per Unit Length of Weld Does Not Characterize a Weld?" *Computational Materials Science*, vol. 48, no. 2, pp. 390–401, 2010, ISSN: 09270256.

[60] Z. B. Hou and R. Komanduri, "General solutions for stationary/moving plane heat source problems in manufacturing and tribology," *International Journal of Heat and Mass Transfer*, vol. 43, no. 10, pp. 1679–1698, 2000, ISSN: 00179310.

[70] M. J. Kim, "Transient evaporative laser-cutting with boundary element method," *Applied Mathematical Modelling*, vol. 25, no. 1, pp. 25–39, 2000.

[73] R. Komanduri and Z. B. Hou, "Thermal analysis of the laser surface transformation hardening process," *International Journal of Heat and Mass Transfer*, vol. 44, no. 15, pp. 2845–2862, 2001, ISSN: 0017-9310.

[74] R Komanduri and Z. Hou, "Thermal analysis of the laser surface transformation hardening process," *International Journal of heat and mass transfer*, vol. 44, no. 15, pp. 2845–2862, 2001.

[76] S. Kou, D. K. Sun, and Y. P. Le, "A fundamental study of laser transformation hardening," *Metallurgical Transactions A*, vol. 14, no. 3, pp. 643–653, 1983.

[82] Y. Lu and P. F. Mendez, "Characteristic values of the temperature field induced by a moving line heat source," *International Journal of Heat and Mass Transfer*, p. 120 671, 2020.

[83] Y. Lu and P. F. Mendez, "The effect of surface heat losses on isotherm trailing length and cooling rate," 2021.

[84] Y. Lu, Y. Wang, and P. F. Mendez, "Width of thermal features induced by a 2-d moving heat source," *International Journal of Heat and Mass Transfer*, vol. 156, p. 119 793, 2020.

[85] Y.-F. Lu, "Heat flow in substrates induced by a scanning laser beam," *Journal of applied physics*, vol. 71, no. 8, pp. 3701–3712, 1992.

[88] K. Marcin, P. Wieslawa, and S. Sebastian, "Modelling of laser beam heat source based on experimental research of yb : Yag laser power distribution," *International Journal of Heat and Mass Transfer*, vol. 83, 2015.

[94] P. F. Mendez, N. Barnes, K. Bell, S. D. Borle, S. S. Gajapathi, S. D. Guest, H. Izadi, A. K. Gol, and G. Wood, "Welding processes for wear resistant overlays," *Journal of Manufacturing Processes*, vol. 16, no. 1, pp. 4–25, 2014.

[96] P. F. Mendez, Y. Lu, and Y. Wang, "Scaling Analysis of a Moving Point Heat Source in Steady- State on a Semi-Infinite Solid," *Journal of Heat Transfer*, vol. 140, no. 8, p. 081 301, 2018.

[103] J. E. Moody and R. H. Hendel, "Temperature profiles induced by a scanning cw laser beam," *Journal of Applied Physics*, vol. 53, no. 6, pp. 4364–4371, 1982.

[107] Y. S. Muzychka and M. M. Yovanovich, "Thermal Resistance Models for Non-Circular Moving Heat Sources on a Half Space," *Journal of Heat Transfer*, vol. 123, no. 4, pp. 624–632, 2001, ISSN: 00221481.

[109] O. R. Myhr and Ø. Grong, "Dimensionless Maps for Heat Flow Analyses in Fusion Welding," *Acta Metallurgica Et Materialia*, vol. 38, no. 3, pp. 449–460, 1990, ISSN: 09567151.

[111] N. T. Nguyen, A. Ohta, K. Matsuoka, N. Suzuki, and Y. Maeda, "Analytical Solutions for Transient Temperature of Semi-Infinite Body Subjected to 3-D Moving Heat Sources," *Welding Journal, Research Supplement*, vol. 78, no. August, 265s–274s, 1999.

[116] H. Pantsar and V. Kujanpää, "Diode laser beam absorption in laser transformation hardening of low alloy steel," *Journal of laser Applications*, vol. 16, no. 3, pp. 147–153, 2004.

[117] V. Pavelic, R. Tanbakuchi, O. A. Uyehara, and P. S. Myers, "Experimental and computed temperature histories in gas tungsten-arc welding of thin plates," *Welding Journal Research Supplement*, vol. 48, 1969.

[126] D. Rosenthal, "The Theory of Moving Sources of Heat and Its Application to Metal Treatments," *Transactions of the A.S.M.E.*, vol. 68, pp. 849–866, 1946.

[128] D. Rosenthal, "Mathematical Theory of Heat Distribution During Welding and Cutting," *Welding Journal*, vol. 20, no. 5, pp. 220–234, 1941.

[131] N. N. Rykalin, *Calculation of Heat Flow in Welding*. Moscow: Mashgis, 1951.

[134] P. S. Sheng and V. S. Joshi, "Analysis of heat-affected zone formation for laser cutting of stainless steel," *Journal of materials processing technology*, vol. 53, no. 3-4, pp. 879–892, 1995.

[135] S. Skvarenina and Y. C. Shin, "Predictive modeling and experimental results for laser hardening of aisi 1536 steel with complex geometric features by a high power diode laser," *Surface and Coatings Technology*, vol. 201, no. 6, pp. 2256–2269, 2006.

[141] S. M. Thompson, L. Bian, N. Shamsaei, and A. Yadollahi, "An overview of direct laser deposition for additive manufacturing; part i: Transport phenomena, modeling and diagnostics," *Additive Manufacturing*, vol. 8, pp. 36–62, 2015.

[143] X. Tian and F. E. Kennedy Jr, "Maximum and average flash temperatures in sliding contacts," *Journal of Tribology*, vol. 116, 1994.

[146] N. Tsai, "Heat distribution and weld bead geometry in arc welding," PhD thesis, Massachusetts Institute of Technology, 1983.

[149] Y. Wang, Y. Lu, and P. F. Mendez, "Scaling expressions of characteristic values for a moving point heat source in steady state on a semi-infinite solid," *International Journal of Heat and Mass Transfer*, vol. 135, pp. 1118–1129, 2019.

[152] T. Washio and H. Motoda, "Extension of Dimensional Analysis for Scale-types and its Application to Discovery of Admissible Models of Complex Processes," in *International Workshop on Similarity Method*, 1999, pp. 129–147.

[155] G. Wood and P. F. Mendez, "Disaggregated metal and carbide catchment efficiencies in laser cladding of nickel-tungsten carbide," *Welding Journal*, vol. 94, no. 11, pp. 343–350, 2015.

Appendix 4.A Derivation of Asymptotic Behaviors

Peak temperature locates at the surface of the base plate, defined by the equation $T^*_{\max} = \max[T(x^*, y^*, 0)]$. Due to the symmetry of temperature field in y, at the location of peak temperature, $y^* = 0$. Equation 4.12 turns into Equation 4.33, and the integrand has one peak at $\theta_{\max} = \arccos[\sigma^*(\sigma^{*2} - x^*)^{-1/2}]$:

$$T^* = \frac{2}{\sqrt{2\pi}\sigma^*} \cdot \int_0^{\frac{\pi}{2}} \exp\left\{-\frac{1}{2}\left[\sigma^{*2}\left(\cos^2\theta + \frac{1}{\cos^2\theta} - 2\right) + \frac{\cos^2\theta x^{*2}}{\sigma^{*2}} + 2x^*\sin^2\theta\right]\right\} d\theta \tag{4.33}$$

Regime VI: $\sigma^* \to 0$

In Regime VI, where $\sigma^* \to 0$, $|x^*_{\max_V}| << \sigma^* << 1$, by rearranging Equation 4.33, peak temperature in Regime VI equals:

$$\begin{aligned}
\widehat{T^*}_{\max_{VI}} &= \frac{2}{\sqrt{2\pi}\sigma^*}\int_0^{\frac{\pi}{2}} \exp\left(-\frac{1}{2}\frac{\sigma^{*2}}{\cos^2\theta}\right) \cdot \\
&\exp\left\{-\frac{1}{2}\left[\sigma^{*2}\left(\cos^2\theta - 2\right) + \frac{\cos^2\theta x^{*2}}{\sigma^{*2}} + \right.\right. \\
&\qquad\qquad \left.\left. 2x^*\sin^2\theta\right]\right\} d\theta \\
&\approx \frac{2}{\sqrt{2\pi}\sigma^*}\int_0^{\frac{\pi}{2}} \exp\left(-\frac{1}{2}\frac{\sigma^{*2}}{\cos^2\theta}\right) \cdot 1 d\theta \\
&\approx \frac{2}{\sqrt{2\pi}\sigma^*}\frac{\pi}{2} = \sqrt{\frac{\pi}{2}}\sigma^{*-1}
\end{aligned}$$

Location of the peak temperature in Regime VI is obtained by solving the partial derivative of $\partial\widehat{T^*}_{\max_{VI}}/\partial x^* = 0$:

$$\begin{aligned}
\frac{\partial\widehat{T^*}_{\max_{VI}}}{\partial x^*} = \frac{2}{\sqrt{2\pi}\sigma^*}\int_0^{\frac{\pi}{2}} -\frac{1}{2}\left(\frac{2x^*_{\max_{VI}}\cos^2\theta}{\sigma^{*2}} + 2\sin^2\theta\right) \cdot \\
\exp\left\{-\frac{1}{2}\left[\sigma^{*2}\left(\cos^2\theta + \frac{1}{\cos^2\theta} - 2\right) + \right.\right. \\
\left.\left.\frac{\cos^2 t x^{*}_{\max_{VI}}{}^2}{\sigma^{*2}} + 2x^*_{\max_{VI}}\sin^2\theta\right]\right\} d\theta = 0
\end{aligned}$$

We obtain

$$\frac{\pi}{2} + \left(\frac{^*_{\max_{VI}}}{\sigma^{*2}} - 1\right)\frac{\pi}{4} = 0$$

and thus $x^*_{\max_{\mathrm{VI}}} = -\sigma^{*2}$.

Regime V: $\sigma^* \to \infty$

In Regime V, when $\sigma^* \to \infty$, $x^*_{\max_{\mathrm{V}}} \sim \sigma^* \gg 1$. As mentioned before, the integrand $\exp[f(\theta)] = \exp\left\{-\frac{1}{2}\left[\sigma^{*2}\left(\cos^2\theta + \frac{1}{\cos^2\theta} - 2\right) + \frac{\cos^2\theta\, x^{*2}}{\sigma^{*2}} + 2x^*\sin^2\theta\right]\right\}$ has a single maxima at $\theta_{\max}$ over the interval of $[0, \frac{\pi}{2})$. As $\sigma^* \to \infty$, the integrand increases from 0 to $\theta_{\max}$ and then decreases exponentially with increasing θ. Also, as $x^*_{\max_{\mathrm{V}}} \sim \sigma^* \gg 1$, $\theta_{\max} = \arccos[\sigma^*(\sigma^{*2} - x^*)^{-1/2}] \approx \arccos[\sigma^*(\sigma^{*2})^{-1/2}] = 0$, which means the vicinity near $\theta_{\max}$ (near 0) contributes the most part of the integral, as shown in Figure 4.12:

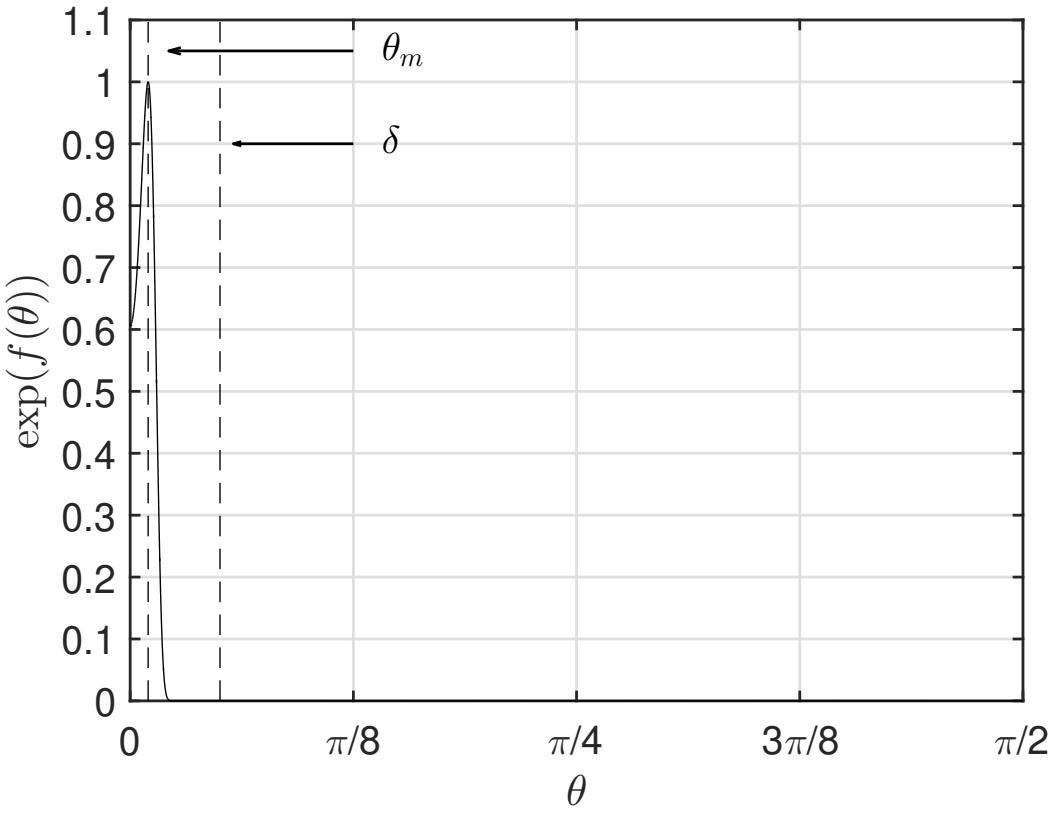

Figure 4.12: Plot of the integrand $\exp[f(\theta)]$ at $\sigma^* = 1000$, $x^* = -1000$, $y^* = 0$ over $[0, \frac{\pi}{2})$. $\exp[f(\theta)]$ increases with increasing θ until $\theta_{\max}$ and then decreases exponentially. Interval over $[0, \delta)$ where $\theta_{\max} \ll \delta \ll 1$, contributes the most part of the integral.

Therefore, the integral over the vicinity of the maxima δ, where $\theta_{\max} \ll \delta \ll 1$ can be estimated as the integral over the whole interval of $[0, \frac{\pi}{2})$:

$$\begin{aligned}\widehat{T^*}_{\max_V} &= \tfrac{2}{\sqrt{2\pi}\sigma^*} \int_0^{\frac{\pi}{2}} \exp\left\{-\frac{1}{2}\left[\sigma^{*2}\left(\cos^2\theta + \tfrac{1}{\cos^2\theta} - 2\right) + \right.\right. \\ &\qquad \left.\left. \tfrac{\cos^2\theta\, x^{*2}}{\sigma^{*2}} + 2x^* \sin^2\theta\right]\right\} d\theta \\ &\approx \tfrac{2}{\sqrt{2\pi}\sigma^*} \int_0^{\delta} \exp\left\{-\frac{1}{2}\left[\sigma^{*2}\left(\cos^2\theta + \tfrac{1}{\cos^2\theta} - 2\right) + \right.\right. \\ &\qquad \left.\left. \tfrac{\cos^2\theta\, x^{*2}}{\sigma^{*2}} + 2x^* \sin^2\theta\right]\right\} d\theta\end{aligned}$$

Performing a second-order Taylor expansion at $\theta = 0$, the integrand can be further simplified as:

$$\begin{aligned}\widehat{T^*}_{\max_V} &\approx \frac{2}{\sqrt{2\pi}\sigma^*} \int_0^{\delta} \exp\left\{-\frac{1}{2}\left[\sigma^{*2}\,\theta^4 + \frac{(1-\theta^2)x^{*2}}{\sigma^{*2}} + 2x^*\theta^2\right]\right\} d\theta \\ &\approx \frac{2}{\sqrt{2\pi}\sigma^*} \int_0^{\frac{\pi}{2}} \exp\left\{-\frac{1}{2}\left[\sigma^{*2}\,\theta^4 + \frac{(1-\theta^2)x^{*2}}{\sigma^{*2}} + 2x^*\theta^2\right]\right\} d\theta \\ &= \frac{2}{\sqrt{2\pi}\sigma^*} \int_0^{\frac{\pi}{2}} \exp\left\{-\frac{1}{2}\left[\sigma^{*2}\,\theta^4 + (2x^* - \frac{x^{*2}}{\sigma^{*2}})\theta^2 + \frac{x^{*2}}{\sigma^{*2}}\right]\right\} d\theta\end{aligned}$$

As $x^*_{\max_V} \sim \sigma^* \gg 1$, $\widehat{T^*}_{\max_V}$ can be rewritten as:

$$\begin{aligned}\widehat{T^*}_{\max_V} &\approx \frac{2}{\sqrt{2\pi}\sigma^*} \int_0^{\frac{\pi}{2}} \exp\left\{-\frac{1}{2}\left[\sigma^{*2}\,\theta^4 + 2x^*\theta^2 + \frac{x^{*2}}{\sigma^{*2}}\right]\right\} d\theta \\ &= \frac{2}{\sqrt{2\pi}\sigma^*} \int_0^{\frac{\pi}{2}} \exp\left[-\frac{1}{2}\left(\sigma^*\theta^2 + \frac{x^*}{\sigma^*}\right)^2\right] d\theta \\ &= \tfrac{2}{\sqrt{2\pi}\sigma^{*1.5}} \int_0^{\frac{\pi}{2}\sqrt{\sigma^*}} \exp\left\{-\tfrac{1}{2}\left[\left(\sqrt{\sigma^*}\theta\right)^2 + \tfrac{x^*}{\sigma^*}\right]^2\right\} d\left(\sqrt{\sigma^*}\theta\right) \\ &\approx \tfrac{2}{\sqrt{2\pi}\sigma^{*1.5}} \int_0^{\infty} \exp\left\{-\tfrac{1}{2}\left[\left(\sqrt{\sigma^*}\theta\right)^2 + \tfrac{x^*}{\sigma^*}\right]^2\right\} d\left(\sqrt{\sigma^*}\theta\right) \qquad (4.34)\end{aligned}$$

The integral part in Equation 4.34 ($\int_0^{\infty} \exp\left\{-\tfrac{1}{2}\left[\left(\sqrt{\sigma^*}\theta\right)^2 + \tfrac{x^*}{\sigma^*}\right]^2\right\} d\left(\sqrt{\sigma^*}\theta\right)$) depends only on the ratio of x^*/σ^*, and it increases with increasing x^*/σ^* to its maximum and then decreases until $x^* = 0$, as illustrated in Figure 4.13.

Traversing all values of x^*/σ^* from $-\infty$ to 0 with a Matlab script, when $x^*_{\max_V}/\sigma^* = -0.7650$, the integral reaches its maximum of a constant $I_m = 1.280$. Therefore,

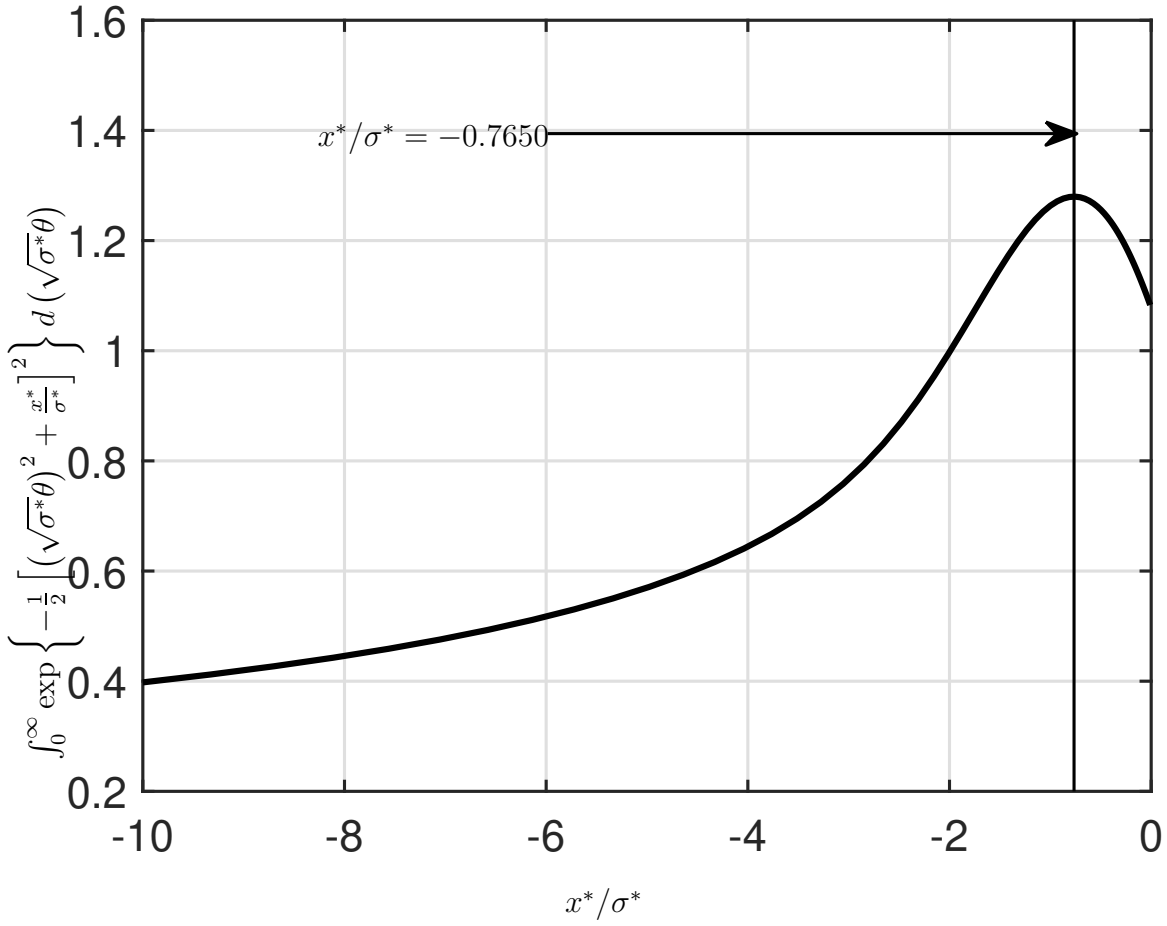

Figure 4.13: Plot of the integral in Equation 4.34 ($\int_0^\infty \exp\left\{-\frac{1}{2}\left[\left(\sqrt{\sigma^*}\theta\right)^2 + \frac{x^*}{\sigma^*}\right]^2\right\} d\left(\sqrt{\sigma^*}\theta\right)$) as a function of x^*/σ^*. When $x^*/\sigma^* =$ -0.7650, the integral reaches its maximum of $I_m = 1.280$.

dimensionless peak temperature in Regime V can be obtained:

$$\widehat{T^*}_{\max_{\mathrm{V}}} = \sqrt{\frac{2}{\pi}} I_m \ \sigma^{*-1.5}$$

Appendix 4.B Data Collected from the Literature Survey

Table 4.2: The laser absorptivity, heat distribution parameter, thermal properties, processing parameters and reported peak temperature used in the validation.

Process	Material	Power	Absoprtivity	Velocity	Conductivity	Diffusivity	T_0	Sigma	Tmax	Source
		W	1	mm/s	W/mK	m^2/s	°C	mm	°C	
LS	silicon	4	0.57 [103]	100	33.03*	1.5×10^{-5}*	350 [103]	0.01	1264	[103]
LS	silicon	4	0.57 [103]	500	35.69*	1.7×10^{-5}*	350 [103]	0.01	1083	[103]
LS	silicon	4	0.59 [103]	2000	40.17*	1.9×10^{-5}*	350 [103]	0.01	845	[103]
LS	silicon	4.1	0.56 [85]	100	46.34*	2.2×10^{-5}*	20 [85]	0.01	1350	[85]
LS	silicon	4.9	0.56 [85]	1000	46.34*	2.2×10^{-5}*	20 [85]	0.01	1350	[85]
LS	GaAs	1.28	0.61 [85]	100	14.93*	9.1×10^{-6}*	20 [85]	0.01	1350	[85]
LS	GaAs	1.81	0.61 [85]	1000	14.93*	9.1×10^{-6}*	20 [85]	0.01	1350	[85]
LS	Mn-Zn Fe	0.27	0.79 [85]	100	2.70*	5.8×10^{-7}*	20 [85]	0.01	1350	[85]
LS	Mn-Zn Fe	0.63	0.79 [85]	1000	2.70*	5.8×10^{-7}*	20 [85]	0.01	1350	[85]
LD	ZrO2	1000	0.6 [21]	0.1	2.7 [21]	4.6×10^{-7} [21]	20^+	1.50	26300	[21]
LD	ZrO2	1000	0.6 [21]	1.0	2.7 [21]	4.6×10^{-7} [21]	20^+	1.50	15836	[21]
LD	ZrO2	1000	0.6 [21]	53.0	2.7 [21]	4.6×10^{-7} [21]	20^+	1.50	2574	[21]
LD	ZrO2	1000	0.6 [21]	53.0	2.7 [21]	4.6×10^{-7} [21]	20^+	1.00	4695	[21]
LD	ZrO2	1000	0.6 [21]	53.0	2.7 [21]	4.6×10^{-7} [21]	20^+	1.25	3380	[21]
LHT	AISI1020	250	0.67^+ [116]	1.67	38.90*	6.8×10^{-6}*	20^+	0.71	1494	[39]
LHT	AISI1020	250	0.67^+ [116]	5.00	40.42*	7.7×10^{-6}*	20^+	0.71	1186	[39]
LHT	AISI1020	250	0.67^+ [116]	6.67	41.22*	7.8×10^{-6}*	20^+	0.71	1097	[39]
LHT	AISI1020	250	0.67^+ [116]	8.33	41.82*	7.9×10^{-6}*	20^+	0.71	1044	[39]
LHT	AISI1020	250	0.67^+ [116]	10.0	44.11*	8.1×10^{-6}*	20^+	0.71	892	[39]
LHT	AISI1020	250	0.67^+ [116]	11.7	43.76*	8.1×10^{-6}*	20^+	0.71	911	[39]
LHT	AISI1020	250	0.67^+ [116]	13.3	45.70*	8.4×10^{-6}*	20^+	0.71	817	[39]
LHT	AISI1020	175	0.67^+ [116]	8.33	55.10*	1.3×10^{-5}*	20^+	0.71	426	[39]
LHT	AISI1020	200	0.67^+ [116]	8.33	51.48*	1.2×10^{-5}*	20^+	0.71	562	[39]
LHT	AISI1020	225	0.67^+ [116]	8.33	46.85*	8.8×10^{-6}*	20^+	0.71	766	[39]
LHT	AISI1020	250	0.67^+ [116]	8.33	42.85*	8.0×10^{-6}*	20^+	0.71	967	[39]
LHT	AISI1020	275	0.67^+ [116]	8.33	40.95*	7.8×10^{-6}*	20^+	0.71	1125	[39]
LHT	AISI1020	300	0.67^+ [116]	8.33	40.01*	7.6×10^{-6}*	20^+	0.71	1243	[39]
LHT	AISI1020	400	0.67^+ [116]	8.33	39.58*	7.6×10^{-6}*	20^+	0.71	1316	[39]

* Properties calculated by JMatPro v11
+ Estimated
LS: Laser Scanning
LHT: Laser Heat Treatment
LD: Laser Densification

Chapter 5

Penetration Depth under a Moving Gaussian Surface Heat Source on a Thick Substrate

5.1 Abstract

This paper presents a systematic scaling analysis of a Gaussian distributed surface heat source moving on a semi-infinite solid. The dimensionless maximum isotherm depth depends on two dimensionless groups: the heat source distribution parameter and the Rykalin number associated with the velocity of the heat source. Maximum isotherm depth is determined for the first time with explicit closed-form expressions over a wide range of heat distributions and Rykalin numbers with an error below 9.7% against the exact solution. The methodology employed involves normalization, dimensional analysis, asymptotic analysis, and blending techniques. The proposed equations are validated against experiments reported in the literature. The expressions developed can be calculated using a handheld calculator or a basic spreadsheet and are also useful to optimize process parameters and verify numerical models.

Table 5.1: Notation

Variables	Unit	Description
f	1	Correction factor for a point source
g	1	Correction factor for a Gaussian source
I_m	1	Asymptotic constant $I_m = 1.280$
k	$\mathrm{W\,m^{-1}\,K^{-1}}$	Thermal conductivity of the substrate
q	W	Power absorbed by substrate
Ry	1	Rykalin number
t	s	Time
T	K	Temperature
T_0	K	Initial temperature or preheat
T_c	K	Temperature of interest
T_max	K	Maximum temperature of the substrate
U	$\mathrm{m\,s^{-1}}$	Travel speed of the moving heat source
x, y, z	m	Cartesian coordinates
z_max	m	Maximum isotherm depth
Greek symbols		
α	$\mathrm{m^2\,s^{-1}}$	Thermal diffusivity of the substrate
ρ	$\mathrm{kg\,m^{-3}}$	Density of the substrate
σ	m	Standard deviation of a Gaussian function
σ_max	m	Maximum distribution parameter to achieve a certain temperature
Superscripts		
*		Dimensionless value
$\widehat{\ }$		Asymptotic behaviour
$^+$		Improvement over asymptotic approximation

Continued on next page

Table 5.1 – continued from previous page

Variables	Unit	Description
Subscripts		
I		Regime I of concentrated heat sources and large Ry
II		Regime II of concentrated heat sources and small Ry
V		Regime V of wide heat sources and large Ry
VI		Regime VI of wide heat sources and small Ry
Acronyms		
GTAW		Gas Tungsten Arc Welding

5.2 Introduction

Moving heat source problems are central to a wide range of industrial applications such as cutting [142], welding [36, 145], heat treatment [27, 74, 137], additive manufacturing [71, 155] and many more. For example, for the case of surface hardening, operating parameters have to be carefully selected to obtain the depth of hardening (the maximum depth where structural transformation occurs) in the selective area without affecting the desirable mechanical properties of the substrate. Cost and effort in trial-and-error tests to optimize process parameters would be much saved if isotherm characteristics of interest such as isotherm width, depth, thermal history can be predicted in advance. There is substantial amount of published solutions to moving heat sources: empirical models [3, 137, 153], numerical simulations [48, 58, 76, 89] and analytical solutions [27, 36, 87, 96, 126]; however, current knowledge is often difficult to apply in procedure developments.

Empirical modelling is a convenient and reliable way of procedure development as

it is capable of generating simple expressions by statistical fitting of experimental results. However, empirical relationships seldom have a physical or analytical basis. Because their validity range is not clearly identified, empirical relationships can hardly be generalized to other processes or material systems that are substantially different from conditions where they were developed.

Numerical simulations are suitable to deal with the complexity of geometries and non-linearities. The accuracy of numerical predictions has been much improved with the rapid development of computer techniques. Due to the requirement of specialized software and computational skills, applications of numerical models are limited in industrial practice. Also, published solutions are valid for the particular parameters considered in each model and can hardly be summarized as general rules for different materials and processes.

Analytical solutions are inexpensive and useful at the early stage of the design. Derived from the heat conduction equation, analytical solutions have a solid theoretical backing; however, they are rather complicated involving series summations [20, 87] or improper integrals [36, 111], making it difficult to use and even more challenging to understand the relationship between process parameters and resulting isotherm characteristics. Therefore, it is essential to convert the analytical solution into a more straightforward explicit expression that is sufficiently close to the original solution.

Based on previous work of the point heat source model [82–84, 96, 148, 149], this paper presents an analytical solution to predict the maximum isotherm depth under a moving disk Gaussian distributed heat source on a semi-infinite plate. The introduction of a heat distribution parameter in the Gaussian model avoids the singularity in the point source solution and significantly improves the accuracy of prediction in the vicinity of the heat source [36, 146]. The proposed equation is written as an explicit function of operation parameters, e.g. heat source power, moving velocity, and thermal properties of the substrate. It can easily be applied to calculate the maximum isotherm depth of any given temperature or the critical moving velocity to achieve a

certain isotherm depth.

The conventional 1D blending technique, first proposed by Churchill and Usagi [23] has been applied and extended to a multidimensional domain in this paper to arrive at a general solution to the domain by combining asymptotes in the asymptotic extremes with constant blending parameters. In this way, asymptotic behaviour in each asymptotic extreme can be assured, and there is no convergence issue. The methodology of asymptotes and correction factors is often used in all engineering disciplines, and formal implementations are reported in [84, 96, 149] for the case of a moving point heat source.

The following sections introduce a mathematical formulation of a moving Gaussian heat source and a systematic methodology of asymptotes and blending. An explicit asymptotic in each regime is presented, and the blending technique is used to predict the maximum isotherm depth at the intermediate regime with high accuracy. The obtained expression was compared with results of a set of experiments [8, 79, 157, 158] and was found to be in excellent agreement. It can bring a deep understanding of moving heat source phenomena across different alloys and processes.

5.3 Mathematical Formulation

The model consists of a Gaussian distributed heat source moving along a straight line with constant velocity U on a semi-infinite solid. The thermal profile is considered steady relative to the position of the heat source. The material is isotropic and homogeneous, and thermophysical properties such as thermal conductivity are assumed constant. The governing equation is:

$$\frac{\partial^2 T}{\partial x^2} + \frac{\partial^2 T}{\partial y^2} + \frac{\partial^2 T}{\partial z^2} + \frac{U}{\alpha}\frac{\partial T}{\partial x} = 0 \tag{5.1}$$

where x, y and z are the independent spatial variables. This mathematical formulation involves an Eulerian coordinate frame, where the heat source is stationary, and the substrate moves in the $-x$ direction. The temperature, T, is the dependent

variable and also depends on problem parameters. α is the thermal diffusivity of the substrate.

Heat flux distribution is assumed as Gaussian distributed, and σ is the standard deviation of the Gaussian function [36]. σ varies in different processes. It can be as small as 0.1 mm for an electron beam [41] or as broad as 6 mm in laser beam additive manufacturing [155].

The boundary conditions for Equation 5.1 are:

$$\frac{\partial T}{\partial z} = \frac{q}{2\pi k\sigma^2} \exp\left(-\frac{x^2+y^2}{2\sigma^2}\right) \quad \text{for} \quad z = 0 \tag{5.2}$$

$$T \to T_0 \quad \text{for} \quad x^2+y^2+z^2 \to \infty \tag{5.3}$$

where q is the heat absorbed by the substrate, k is the thermal conductivity of the substrate, and T_0 is the preheat temperature. The temperature field to Equation 5.1 with boundary conditions from Equation 5.2 to 5.3 is:

$$T = T_0 + \frac{q\alpha^{\frac{1}{2}}}{2k\pi^{\frac{3}{2}}} \int_0^\infty dt \frac{t^{-\frac{1}{2}}}{2\alpha t+\sigma^2} \exp\left(-\frac{x^2+2xtU+U^2t^2+y^2}{4\alpha t+2\sigma^2} - \frac{z^2}{4\alpha t}\right) \tag{5.4}$$

Equation 5.4 was first proposed by Anthony and Cline in 1977 [27] and was then applied to the field of welding by Tsai and Eagar in 1983 [36]. In the limit when $\sigma \to 0$, Equation 5.4 converges to the analytical solution of a moving point heat source [126, 128]. The improper integral in Equation 5.4 requires substantial numerical calculations, making it difficult to apply to engineering practice.

5.4 Methodology of Asymptotic Analysis and Blending

The methodology was first described in [156] and has been successfully implemented for point heat source problems in [84, 96, 149]. It consists of finding an asymptotic solution to each regime where the independent variable is asymptotically large or small and then developing a correction factor that relates the asymptotic solution to the domain. The use of correction factors is common in engineering and allows for

the simultaneous benefits of practical expressions and accurate predictions within the validity of the correction factors.

5.4.1 Normalization

The original solution of temperature field is reduced to its dimensionless counterpart by normalization:

$$T^* = \frac{1}{\sqrt{2\pi}} \int_0^\infty dt^* \frac{t^{*-\frac{1}{2}}}{t^* + \sigma^{*2}} \exp\left(-\frac{x^{*2} + 2t^*x^* + t^{*2} + y^{*2}}{2t^* + 2\sigma^{*2}} - \frac{z^{*2}}{2t^*} \right) \tag{5.5}$$

Equation 5.6 and Equation 5.7 describe the dimensionless time and distribution parameter in terms of dimensional parameters:

$$t^* = \frac{U^2 t}{2\alpha} \tag{5.6}$$

$$\sigma^* = \frac{U\sigma}{2\alpha} \tag{5.7}$$

where t is the process time. Equation 5.8 to Equation 5.11 is the dimensionless temperature, and coordinates x^*, y^* and z^*, respectively.

$$T^* = \frac{4\pi k\alpha \left(T_c - T_0\right)}{qU} \tag{5.8}$$

$$x^* = \frac{Ux}{2\alpha} \tag{5.9}$$

$$y^* = \frac{Uy}{2\alpha} \tag{5.10}$$

$$z^* = \frac{Uz}{2\alpha} \tag{5.11}$$

where T_c is the temperature of interest. The * superscript in Equation 5.6 to Equation 5.11 represents a dimensionless quantity and it is consistent with [31, 84, 93, 96, 149].

Equation 5.5 has five dimensionless groups: three independent variables x^*, y^*, and z^*, distribution parameter σ^* and the dependent variable $T^*(x^*, y^*, z^*, \sigma^*)$. Dimensionless time t^* is integrated and also, in quasi-steady state, temperature field has no time dependence.

Using variable substitution method $\theta = \arctan\frac{\sqrt{t^*}}{\sigma}$, Equation 5.5 can be written as Equation 5.12 such that the zero-to-infinity intergration in Equation 5.5 can be converted to a proper one, saving much effort in computation:

$$T^* = \frac{2}{\sqrt{2\pi}\sigma^*}\int_0^{\frac{\pi}{2}} \exp\left\{-\frac{1}{2}\left[2x^*\sin^2\theta + \right.\right.$$
$$\left.\left.\sigma^{*2}\left(\tan^2\theta - \sin^2\theta\right) + \frac{\cos^2\theta}{\sigma^{*2}}\left(x^{*2} + y^{*2} + \frac{z^{*2}}{\sin^2\theta}\right)\right]\right\} d\theta \tag{5.12}$$

The number of dimensionless groups is consistent with the number expected from applying dimensional analysis theory [19]. Dimensional analysis theory states that the number of dimensionless groups in a problem is given by the number of magnitudes with dimension minus the number of independent units involved and minus one when the temperature is not measured in absolute terms [152]. Equation 5.4 involves ten magnitudes with units: three independent variables x, y, and z, the dependent variable $T(x, y, z, \sigma)$, heat source distribution parameter σ, and five problem parameters T_0, q, k, U, and thermal diffusivity α. There are four independent units for the magnitude with dimension: (m, kg, s, °C). The number of dimensionless groups is given by $10 - 4 - 1 = 5$.

The dimensionless maximum isotherm depth depends only on two dimensionless groups. Equation 5.5 involves five degree of freedom (DOFs), related to the five independent dimensionless groups (x^*, y^*, z^*, σ^*, T^*). One constraint is Equation 5.5, leaving only four DOFs between dimensionless groups. The definition of $z^*_{\max}$ involves two more constraints: $y^* = 0$, and $z^*_{\max} = \max(z^*)$, leaving two DOFs. A particular temperature of interest $T^* = T^*_c$ defines the Rykalin number (Ry) as:

$$\text{Ry} = \frac{1}{T^*_c} = \frac{qU}{4\pi k\alpha\left(T_c - T_0\right)} \tag{5.13}$$

Ry varies from zero to infinity, and it relates the effect of advection caused by the motion of the heat source relative to the conduction in the substrate. The dimensionless heat distribution parameter σ^* varies from zero to its maximum feasible value, $\sigma^*_{\max}$, above which the heat applied can not heat the substrate to the temperature

of interest, and the resultant maximum isotherm depth at T_c is zero. A closed-form expression to calculate $\sigma^*_{\max}$ was reported in [150], which is a function dependent only on Ry. Replacing σ^* with $\sigma^*/\sigma^*_{\max}$, the dependence on the heat distribution parameter of the solution domain of non-zero isotherm depth is transformed to a finite range from zero to one. Ry and $\sigma^*/\sigma^*_{\max}$ will be used to capture the remaining two DOFs, and four asymptotic regimes are identified as represented in Figure 5.3:

- Regime I ($\text{Ry} \to \infty, \sigma^*/\sigma^*_{\max} \to 0$), corresponding to fast heat sources with a concentrated heat distribution
- Regime II ($\text{Ry} \to 0, \sigma^*/\sigma^*_{\max} \to 0$), corresponding to slow heat sources with a concentrated heat distribution
- Regime V ($\text{Ry} \to \infty, \sigma^*/\sigma^*_{\max} \to 1$), corresponding to fast heat sources with a wide heat distribution
- Regime VI ($\text{Ry} \to 0, \sigma^*/\sigma^*_{\max} \to 1$), corresponding to slow heat sources with a wide heat distribution

Names for asymptotic regimes are consistent with [150]. These four asymptotic regimes yield simple asymptotes for the maximum isotherm depth, usually in the form of power laws.

5.4.2 Blending of Asymptotic Solutions

Blending technique was first proposed by Churchill and Usagi [23], and it is a rigorous approach to obtain approximate but accurate expressions in closed-form when the exact solution is implicit or when asymptotic behaviour in extreme cases is known from experiments or simulations. Correction factors can be developed as explicit functions of the independent variables to extend the range of validity of an asymptote, and often, they extend the validity of an asymptote into its opposite asymptotic regime [96].

For 1D blending, i.e., the independent variable depends only on one dimensionless variable, and the methodology is well understood [2, 23]. 1D blending has been applied successfully to develop explicit expressions for a moving point heat source on a thick substrate [96, 148–150] and a thin substrate [82, 84].

This paper faces an important challenge, in which the dimensionless exact solution (Equation 5.5) depends on two, not one parameter (2D blending): Ry and σ^*. The increase in complexity is enormous, comparable to the increase in complexity from single variable calculus to multivariate calculus. This paper attempts to construct a general solution applicable to a 2D domain by compositing Churchill's blending technique with two correction factors (instead of one) to extend the validity of asymptotes in extreme limits to other regimes.

For the case of dimensionless maximum isotherm depth $z^*_{\max}(\mathrm{Ry}, \sigma^*/\sigma^*_{\max})$, it has four asymptotic expressions and they are indicated with a $\widehat{\ }$ symbol. The associated asymptotic expression for Regime I to Regime VI is $\widehat{z^*}_{\max_{\mathrm{I}}}$, $\widehat{z^*}_{\max_{\mathrm{II}}}$, $\widehat{z^*}_{\max_{\mathrm{V}}}$, and $\widehat{z^*}_{\max_{\mathrm{VI}}}$, respectively. Asymptotes and correction factors for the maximum isotherm depth in Regime I and II were obtained in [96] and they are functions depend only on Ry. Using $\widehat{z^*}_{\max_{\mathrm{II}}}$, the asymptote in Regime II as an example, the blending function proposed for the maximum isotherm depth under a Gaussian source has the following expression:

$$\begin{aligned} {z^*}_{\max}(\mathrm{Ry}, \sigma^*/\sigma^*_{\max}) &\approx \widehat{z^*}^{+}_{\max}(\mathrm{Ry}, \sigma^*/\sigma^*_{\max}) \\ &= \widehat{z^*}_{\max,\mathrm{point}} \cdot g(\mathrm{Ry}, \sigma^*/\sigma^*_{\max}) \\ &\approx \widehat{z^*}_{\max_{\mathrm{II}}}(\mathrm{Ry}) \cdot f(\mathrm{Ry}) \cdot g(\mathrm{Ry}, \sigma^*/\sigma^*_{\max}) \end{aligned} \tag{5.14}$$

where $\widehat{z^*}_{\max,\mathrm{point}}$ is the blended solution based on a point heat source model. The $^+$ superscript indicates an improvement over the asymptotic approximations. f is the correction factor to extend the asymptote of a point heat source solution to its opposite regime. Function g is the correction factor for the heat distribution parameter, and it extends the validity of a point heat source solution to address

Gaussian distributed heat source issues.

Written in the form of asymptotic in an extreme case and correction factors, Equation 5.14 remains the exact asymptotic behaviour in all regimes. Compared to the exact analytical solution ($z^*_{\max}$ calculated by Equation 5.4), the error of approximation is defined as:

$$\text{error} = \ln \frac{\widehat{z^*}^{+}_{\max}}{z^*_{\max}} \tag{5.15}$$

The definition of error offers the advantage of yielding comparable magnitudes for large errors in excess or defect and convenient for power-law expressions. For small errors, Equation 5.15 is equivalent to the standard definition of relative error.

5.5 Asymptotic Analysis and Blending of Maximum Isotherm Depth

5.5.1 Asymptotic Analysis of Maximum Isotherm Depth

The maximum isotherm depth $z^*_{\max}$ requires a numerical optimization of Equation 5.4 to find the maximum for each point in the space domain considered. In the limit case where $\sigma^*/\sigma^*_{\max} = 0$, Equation 5.4 is consistent with that of a point source solution. Asymptotes of the maximum isotherm depth in Regime I and Regime II, which equals the isotherm width due to the symmetry of the point-source temperature field in y-z plane, have already been obtained in [96, 149] as power laws depend only on Ry:

$$\widehat{z^*}_{\max_{\mathrm{I}}}(\mathrm{Ry}) = \sqrt{\frac{2}{\mathrm{e}}\mathrm{Ry}} \qquad \text{For Regime I (large Ry, narrow source)} \tag{5.16}$$

$$\widehat{z^*}_{\max_{\mathrm{II}}}(\mathrm{Ry}) = \mathrm{Ry} \qquad \text{For Regime II (small Ry, narrow source)} \tag{5.17}$$

Asymptotic analysis of Equation 5.5, detailed in the Appendix, yields the following asymptotes in Regime V (large Ry under a wide heat source) and Regime VI (small

Ry under a wide heat source):

$$\widehat{z^*}_{\max_{\mathrm{V}}}(\mathrm{Ry}, \sigma^*/\sigma^*_{\max}) = 2.014\mathrm{Ry}^{\frac{1}{3}} \ln\left(\frac{\sigma^*_{\max}}{\sigma^*}\right) \text{ For Regime V (large Ry, wide source)} \tag{5.18}$$

$$\widehat{z^*}_{\max_{\mathrm{VI}}}(\mathrm{Ry}, \sigma^*/\sigma^*_{\max}) = \frac{\pi}{2}\mathrm{Ry} \ln\left(\frac{\sigma^*_{\max}}{\sigma^*}\right) \text{ For Regime VI (small Ry, wide source)} \tag{5.19}$$

5.5.2 1D blending in Contiguous Regimes

The asymptotes, Equations 5.16 to 5.19 are accurate in the corresponding asymptotic regime but less accurate at the intermediate regimes. 1D blending can be applied to obtain an accurate prediction at the intermediate regime by blending asymptotes of adjacent asymptotic regimes with an optimized blending constant.

In side Regime I-II, where $\sigma^*/\sigma^*_{\max} \to 0$ (concentrated heat sources), the dimensionless maximum isotherm depth depends only on Ry. A closed form equation applicable to both regimes is obtained by 1D blending of Equation 5.16 and Equation 5.17 [96, 149]:

$$\begin{aligned} z^*_{\max_{\text{I-II}}} \approx \widehat{z^*}^{+}_{\max_{\text{I-II}}} &= \widehat{z^*}_{\max_{\text{II}}} f_{z_{\max_{\text{I-II}}}}(\mathrm{Ry}) \\ &= \mathrm{Ry}\left[1 + \left(\sqrt{\frac{2}{\mathrm{eRy}}}\right)^n\right]^{1/n} \end{aligned} \tag{5.20}$$

The optimal value of the blending constant is determined by the same procedure of minimizing the approximation error (Equation 5.15) as detailed in [96, 149]. At the optimal value of $n = -1.731$, the maximum error of approximation compared to the analytical solution is 0.7% [96, 149].

In side Regime II-VI, where $\mathrm{Ry} \to 0$, under a slow heat source, the behaviour of $z^*_{\max}$ depends only on $\sigma^*/\sigma^*_{\max}$. 1D blending of the dimensionless maximum isotherm depth is obtained:

$$\begin{aligned} z^*_{\max_{\text{II-VI}}} \approx \widehat{z^*}^{+}_{\max_{\text{II-VI}}} &= \widehat{z^*}_{\max_{\text{II}}} f_{z_{\max_{\text{II-VI}}}}(\mathrm{Ry}, \sigma^*/\sigma^*_{\max}) \\ = \mathrm{Ry}\left\{1 + \left[\frac{\pi}{2}\ln\left(\frac{\sigma^*_{\max}}{\sigma^*}\right)\right]^n\right\}^{1/n} \end{aligned} \tag{5.21}$$

where the optimal blending constant $n = -1.656$, and the maximum error reaches 5.8%.

Dependence of dimensionless isotherm depth $z^*_{\max}$ on $\sigma^*/\sigma^*_{\max}$ in side Regime II-VI is illustrated in Figure 5.1. The dashed line and dotted line plots the dependence of asymptote in Regime II and Regime VI on $\sigma^*/\sigma^*_{\max}$, respectively. When $\sigma^* = 0$, $z^*_{\max}$ converges to the solution of a point heat source model. When $\sigma^*/\sigma^*_{\max} = 1$, the maximum isotherm depth at the temperature of interest equals 0.

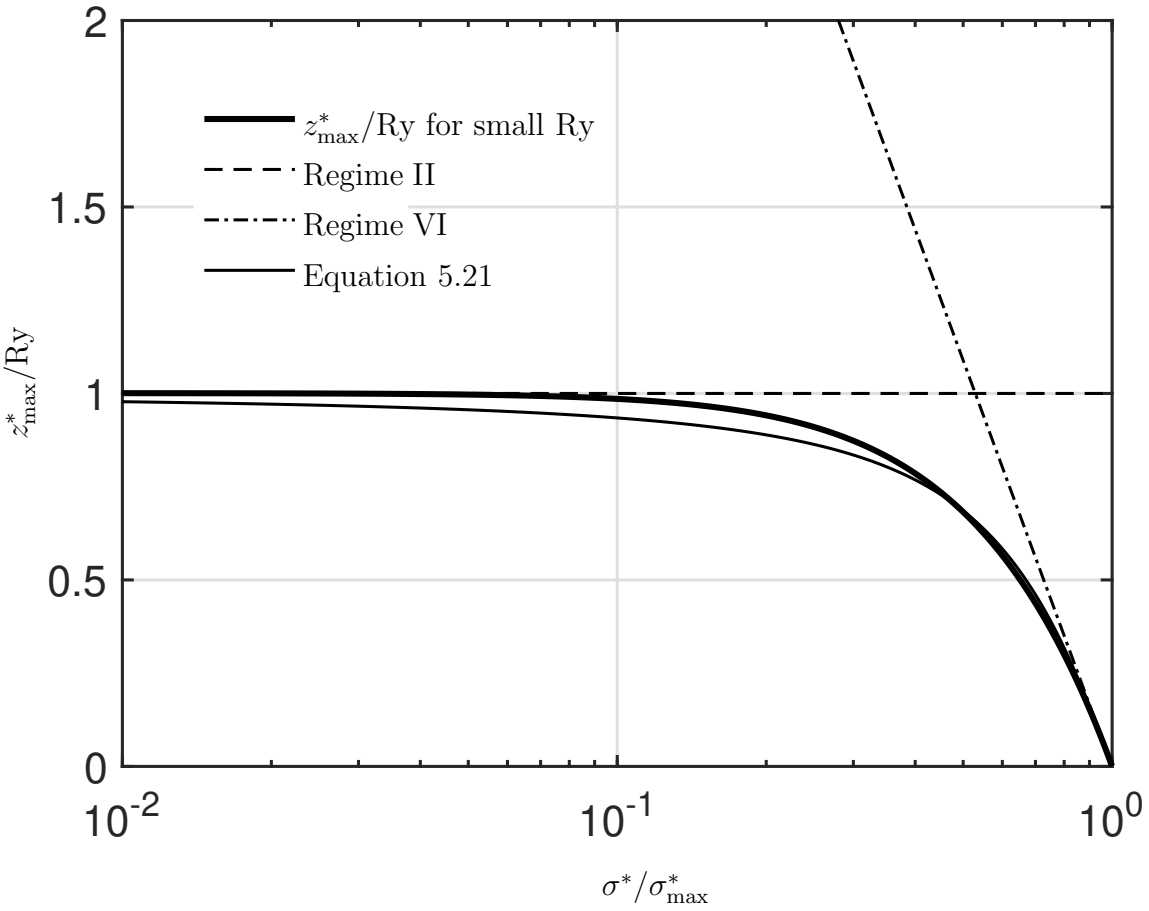

Figure 5.1: Dependence of dimensionless isotherm depth $z^*_{\max}$ on $\sigma^*/\sigma^*_{\max}$ in Regime II and VI. For a given Ry, $z^*_{\max}$ decreases with increasing $\sigma^*/\sigma^*_{\max}$. When $\sigma^* = 0$, $z^*_{\max}$ converges to the solution of a point heat source. The asymptote in Regime II and Regime VI shown by the dashed line and dotted line are derived from asymptotic analysis of Equation 5.12.

In side Regime V-VI, where $\sigma^*/\sigma^*_{\max} \to 1$ (wide heat sources), the behaviour of

$z^*_{\max}$ varies only with Ry. The 1D blending of $z^*_{\max}$ in Regime V-VI is obtained:

$$\begin{aligned} z^*_{\max_{\text{V-VI}}} &\approx \widehat{z^*}^{+}_{\max_{\text{V-VI}}} = \widehat{z^*}_{\max_{\text{V}}} f_{z_{\max_{\text{V}}}}(\text{Ry}, \sigma^*/\sigma^*_{\max}) \\ &= 2.014\text{Ry}^{\frac{1}{3}} \ln\left(\frac{\sigma^*_{\max}}{\sigma^*}\right)\left[1 + \left(0.7799\text{Ry}^{\frac{2}{3}}\right)^n\right]^{1/n} \end{aligned} \tag{5.22}$$

where the optimal blending constant $n = -1.113$, and the maximum error is 2.6%.

Figure 5.2 plots the dependence of $z^*_{\max}$ on Ry in side Regime V-VI where the heat distribution parameter tends to its maximum feasible size of $\sigma^*_{\max}$. $z^*_{\max}$ increases with increasing Ry. The dotted line represents how the asymptote in Regime V varies with Ry, and the dashed line plots the dependence of the asymptote in Regime VI on Ry. Due to the small approximation error, the blended equation (Equation 5.22) coincides with $z^*_{\max}$ calculated from the analytical temperature field as shown in Figure 5.2.

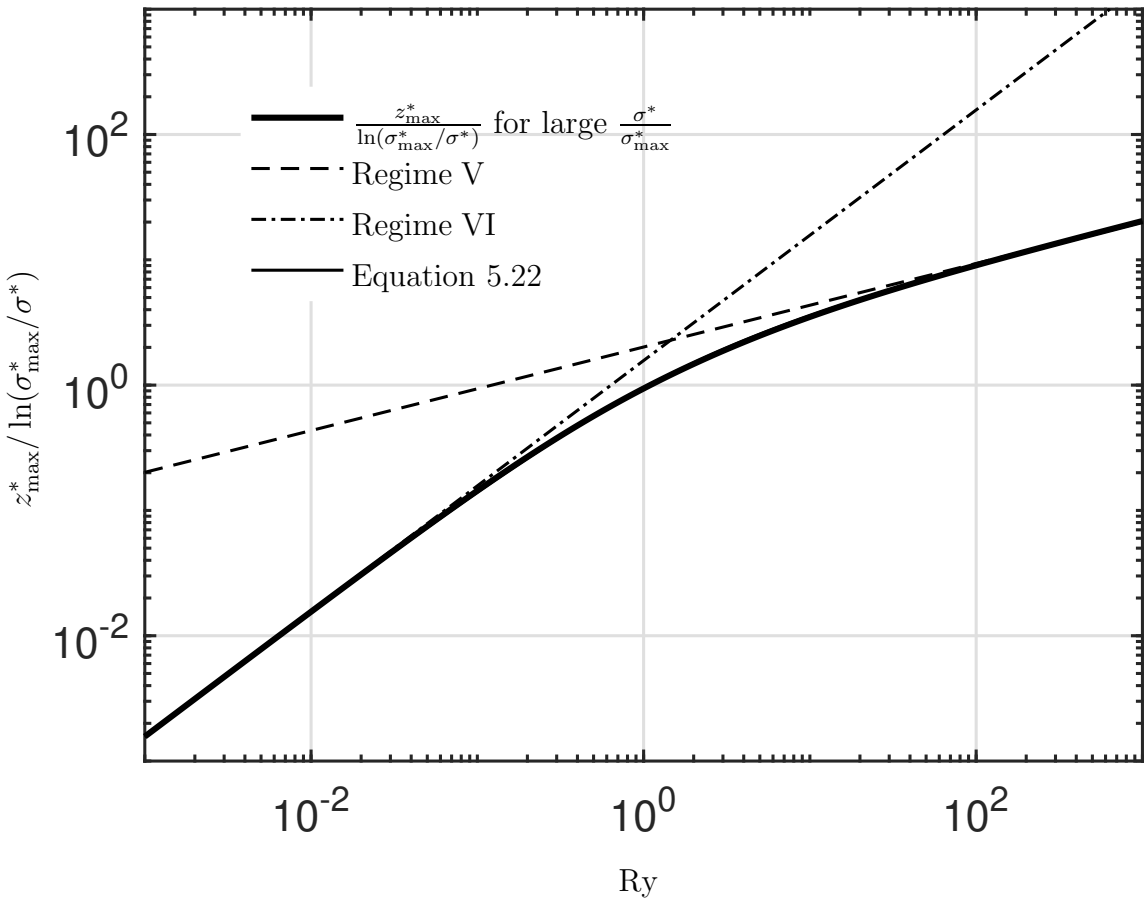

Figure 5.2: Dependence of dimensionless isotherm depth z^*_{max} on Ry in Regime V and VI. The asymptotes in Regime V and Regime VI are derived from asymptotic analysis of Equation 5.12. The exact solution and its blended counterpart are undistinguishable in this graph.

5.5.3 Blended Equation Applicable to all Regimes

Asymptotes in four asymptotic regimes and 1D blending in side Regimes I-II, II-IV and V-VI are proposed from Equation 5.16 to Equation 5.22. However, asymptotes in side Regime I-V where Ry $\to \infty$ have different dependence on Ry and σ^*/σ^*_{max}, and thus 1D blending is not applicable. Because typical Ry numbers in processes such as laser processing and welding ranges from 0.1 to 100, Ry = 1000 is chosen as the upper limit of the domain. A closed-form equation to predict the maximum isotherm depth can be obtained by compositing 1D blending in three side regimes with two

correction factors:

$$
\begin{aligned}
&{z^*}_{\max}(\mathrm{Ry}, \sigma^*/\sigma^*_{\max}) \approx \widehat{{z^*}^+}_{\max}(\mathrm{Ry}, \sigma^*/\sigma^*_{\max}) = \widehat{z^*}_{\max,\mathrm{point}} \cdot g(\mathrm{Ry}, \sigma^*/\sigma^*_{\max}) \\
&\approx \widehat{z^*}_{\max_{\mathrm{II}}}(\mathrm{Ry}) \cdot f_{z_{\max_{\text{I-II}}}}(\mathrm{Ry}) \cdot g(\mathrm{Ry}, \sigma^*/\sigma^*_{\max}) \\
&= \mathrm{Ry}\left[1 + \left(\sqrt{\frac{2}{\mathrm{eRy}}}\right)^{n_1}\right]^{1/n_1} \cdot g(\mathrm{Ry}, \sigma^*/\sigma^*_{\max})
\end{aligned} \tag{5.23}
$$

where the correction factor for the size of heat source $g(\mathrm{Ry}, \sigma^*/\sigma^*_{\max})$ can be rewritten as:

$$
g_{\text{I-II}}(\mathrm{Ry}, \sigma^*/\sigma^*_{\max}) = 1 \qquad \text{for } \sigma^*/\sigma^*_{\max} \to 0 \tag{5.24}
$$

$$
g_{\text{V-VI}}(\mathrm{Ry}, \sigma^*/\sigma^*_{\max}) = f_{\sigma_{\max}} \qquad \text{for } \sigma^*/\sigma^*_{\max} \to 1 \tag{5.25}
$$

Blending equation for $g(\mathrm{Ry}, \sigma^*)$ applicable for all regimes is then obtained:

$$
g(\mathrm{Ry}, \sigma^*/\sigma^*_{\max}) := \frac{z^*_{\max}}{\widehat{z^*}_{\max,\mathrm{point}}} = (1 + {f_{\sigma_{\max}}}^{n_2})^{1/n_2} \tag{5.26}
$$

where $f_{\sigma_{\max}}$ is the correction factor for the heat source size when $\sigma^*/\sigma^*_{\max} \to 1$. Substituting the obtained asymptotes in four regimes into Equation 5.25, $f_{\sigma_{\max}}$ has the following asymptotes:

$$
f_{\sigma_{\max}} = 2.348\mathrm{Ry}^{-\frac{1}{6}} \ln\left(\frac{\sigma^*_{\max}}{\sigma^*}\right) \qquad \text{for } \mathrm{Ry} \to \infty \tag{5.27}
$$

$$
f_{\sigma_{\max}} = \frac{\pi}{2} \ln\left(\frac{\sigma^*_{\max}}{\sigma^*}\right) \qquad \text{for } \mathrm{Ry} \to 0 \tag{5.28}
$$

As $f_{\sigma_{\max}}$ has the same dependence on $\ln(\sigma^*_{\max}/\sigma^*)$ for all Ry, 1D blending function can be applied to obtain:

$$
f_{\sigma_{\max}} = \frac{\pi}{2} \ln\left(\frac{\sigma^*_{\max}}{\sigma^*}\right) \left[1 + \left(1.495\mathrm{Ry}^{-\frac{1}{6}}\right)^{n_3}\right]^{1/n_3} \tag{5.29}
$$

Dimensionless expression to predict the maximum isotherm depth under a Gaussian distributed heat source on a semi-infinite solid valid for $\mathrm{Ry} \leq 1000$ can be obtained

by replacing Equation 5.26 and Equation 5.29 into Equation 5.23, obtaining:

$$
\begin{aligned}
&z^*{}_{\max}(\mathrm{Ry}, \sigma^*/\sigma^*_{\max}) \approx \widehat{z^*}^{+}_{\max}(\mathrm{Ry}, \sigma^*/\sigma^*_{\max}) = \widehat{z^*}_{\max,\mathrm{point}} \cdot g(\mathrm{Ry}, \sigma^*/\sigma^*_{\max}) \\
&\approx \widehat{z^*}_{\max_{\mathrm{II}}}(\mathrm{Ry}) \cdot f_{z_{\max_{\mathrm{I\text{-}II}}}}(\mathrm{Ry}) \cdot g(\mathrm{Ry}, \sigma^*/\sigma^*_{\max}) \\
&= \mathrm{Ry}\left[1 + \left(\sqrt{\frac{2}{\mathrm{eRy}}}\right)^{n_1}\right]^{1/n_1} \cdot \\
&\left\{1 + \left\{\tfrac{\pi}{2}\ln\left(\tfrac{\sigma^*_{\max}}{\sigma^*}\right)\left[1 + \left(1.495\mathrm{Ry}^{-\frac{1}{6}}\right)^{n_3}\right]^{1/n_3}\right\}^{n_2}\right\}^{1/n_2}
\end{aligned}
\tag{5.30}
$$

where $\sigma^*_{\max}$ can be estimated by the blended equation proposed in [150] as a function dependent only on Ry:

$$
\sigma^*_{\max} \approx \widehat{\sigma^*}^{+}_{\max} = \left[\left(1.014\mathrm{Ry}^{2/3}\right)^{n_4} + \left(\sqrt{\frac{\pi}{2}}\mathrm{Ry}\right)^{n_4}\right]^{1/n_4} \tag{5.31}
$$

In side regime V-VI where $\sigma^*/\sigma^*_{\max} \to 1$ and the resulting isotherm depth tends to zero, a small error in $\widehat{\sigma^*}^{+}_{\max}$ would result in a large approximation error in the logarithm term of $\ln(\sigma^*_{\max}/\sigma^*)$ in Equation 5.30. Therefore, optimal blending constants (n_1, n_2, n_3 and n_4) would be determined for $\sigma^*/\sigma^*_{\max} \leq 0.9$. Figure 5.3 illustrates the error of Equation 5.30 calculated by Equation 5.15 as a function of $\sigma^*/\sigma^*_{\max}$ (from 0 to 0.9) and Ry ≤ 1000. The transition between regimes is gradual. Different criteria can be used to divide regimes. A useful criterion to bound the regimes is to determine the boundary at which asymptotes of contiguous regimes have the same prediction, as shown by solid lines in Figure 5.3. Within area bounded by dashed lines, using asymptotes only yields an error smaller than 10% compared to the exact analytical solution.

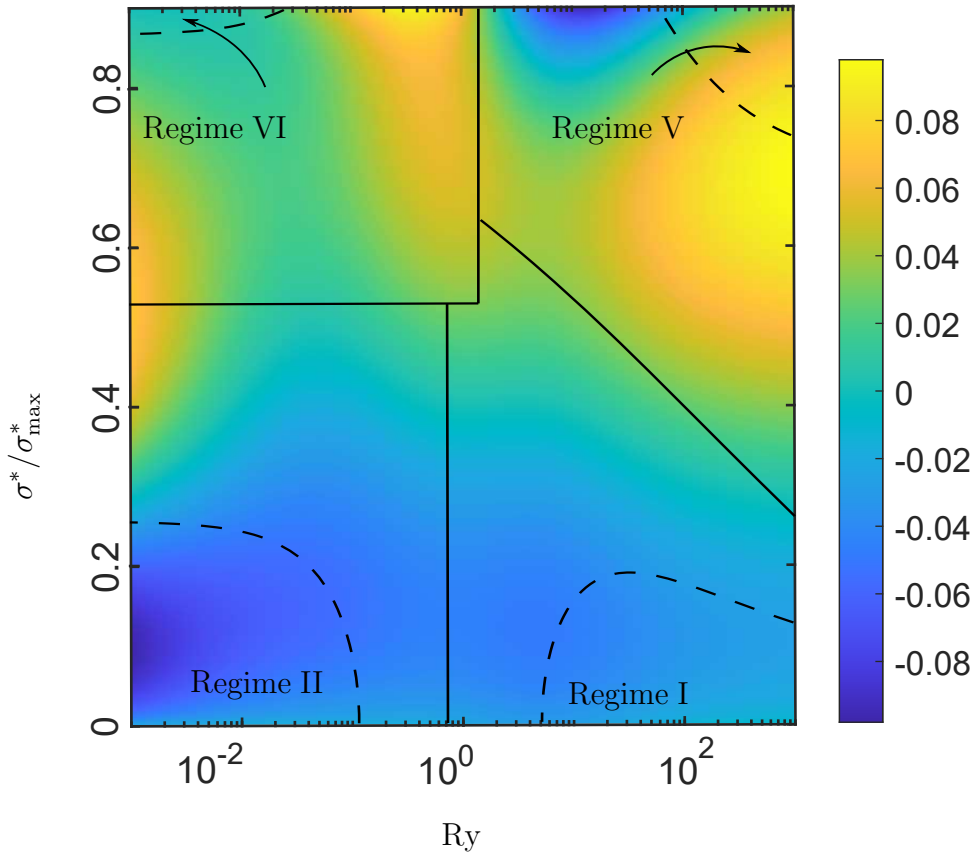

Figure 5.3: Error map of Equation 5.30 as a function of $\sigma^*/\sigma^*_{\max} \leq 0.9$ and $\mathrm{Ry} \leq 1000$. When $n_1 = -1.465$, $n_2 = -1.960$, $n_3 = -3.223$, $n_4 = -2.459$, the maximum error is below 9.7% compared to the exact analytical solution. Within area bounded by dash lines, using asymptotes only yields an error smaller than 10% compared to the analytical solution.

An explicit equation with units for the maximum isotherm depth under a moving Gaussian surface source can be obtained by substituting Equation 5.11 and Equation 5.13 into Equation 5.30:

$$\begin{aligned} z_{\max} \approx \widehat{z}^{+}_{\max} &= \widehat{z}_{\max,\mathrm{point}} \cdot g(\mathrm{Ry}, \sigma^*/\sigma^*_{\max}) \\ &= \frac{q}{2\pi k\,(T_c - T_0)} \left[1 + \left(\sqrt{\frac{2}{\mathrm{eRy}}}\right)^{n_1}\right]^{1/n_1} \cdot \\ &\left\{1 + \left\{\tfrac{\pi}{2} \ln\left(\tfrac{\sigma^*_{\max}}{\sigma^*}\right) \left[1 + \left(1.495\mathrm{Ry}^{-\frac{1}{6}}\right)^{n_3}\right]^{1/n_3}\right\}^{n_2}\right\}^{1/n_2} \end{aligned} \tag{5.32}$$

when $n_1 = -1.465$, $n_2 = -1.960$, $n_3 = -3.223$, $n_4 = -2.459$, the maximum error of Equation 5.30 is below 9.7% for $\sigma^*/\sigma^*_{\max} \leq 0.9$ and $\mathrm{Ry} \leq 1000$.

Equations 5.30 and 5.32 are novel. It is the first time to propose an explicit and accurate equation for the maximum isotherm depth applicable to a wide range of processes and materials. Determination of associated blending parameters needs be done just once. Written as simple formula and correction factors in explicit form, Equations 5.30 and 5.32 can reduce the design cycle by saving much time in computation and trial-and-error tests. It can be easily calculated by a handheld calculator or an Excel sheet in seconds compared to hours or days. Comparison of Equations 5.30 and 5.32 against experimental measurements in the literature will be discussed in the following section.

5.6 Experimental Validation

The focus of this paper is on the maximum depth of isotherms in general. The validation of the proposed predictive expression was made by comparison against published data as shown in Fig 5.5, spanning a range of $z^*_{\max}$ from 0.67 to 10. Measurements were collected for Gas Tungsten Arc Welding (GTAW), laser cladding and laser surface heat treating for various materials, including carbon steel, stainless steel, and alumina-based refractory.

The published values were normalized using Equation 5.7, Equation 5.11 and Equation 5.13, and compared against the prediction calculated by Equations 5.30 and 5.32. The characteristic temperature (T_c) used in these calculations corresponds to the melting temperature of the substrate in all cases except for [157] where T_c is used as the reported HAZ temperature. The preheat temperature T_0 was given by the original source [157] or otherwise assumed as 20°C.

Thermophysical properties were listed in the original sources for [8, 79, 157], and an effective thermal conductivity and diffusivity calculated based on temperature-dependent data from software JMatPro v11 were used for [158]. Thermal efficiency was assessed from original sources for [8, 157, 158], and an estimation of 0.7 was used for [79] as the absorptivity of CO_2 laser radiation on the surface of Al_2O_3 ceramics

according to [78]. Values of the heat distribution parameter (σ) were provided in [8, 157, 158]. For [79], σ was estimated as one fourth of the measured laser diameter. Thermal properties, heat source efficiencies, and processing parameters used in the literature survey are listed in Table 5.2.

Measured isotherm depth is compared with the point-source prediction (Equation 5.30 the without correction factor g) in Figure 5.4 and Gaussian-source prediction (Equation 5.30) in Figure 5.5. It can be seen that prediction by the Gaussian surface model has a better agreement with the measurements, and there is no obvious bias in Figure 5.5. The correction factor for heat intensity distribution can significantly improve the overprediction by the point-source solution. Despite the assumptions in the moving Gaussian surface heat source model, Equation 5.30 can still provide an accurate prediction for the maximum isotherm depth for various processes and materials.

The neglected secondary phenomena such as outward thermocapillary flows are a source of scatter in the comparisons. Other scatter sources are uncertainties in the thermophysical properties used, uncertainties in thermal efficiency, which is especially broad for laser processes, and of course, uncertainties in the measurements of heat distribution parameter and isotherm depth.

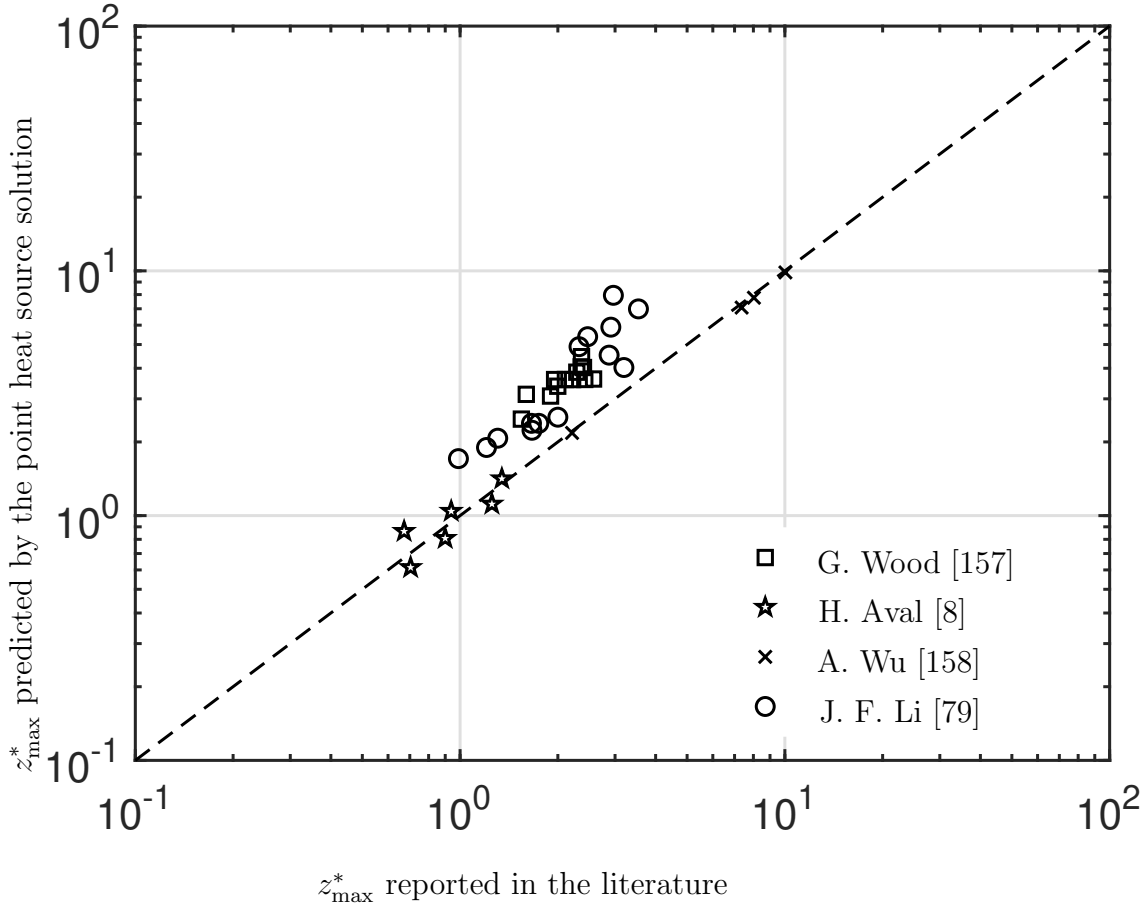

Figure 5.4: Comparison of a point heat source solution with published data for the maximum isotherm depth.

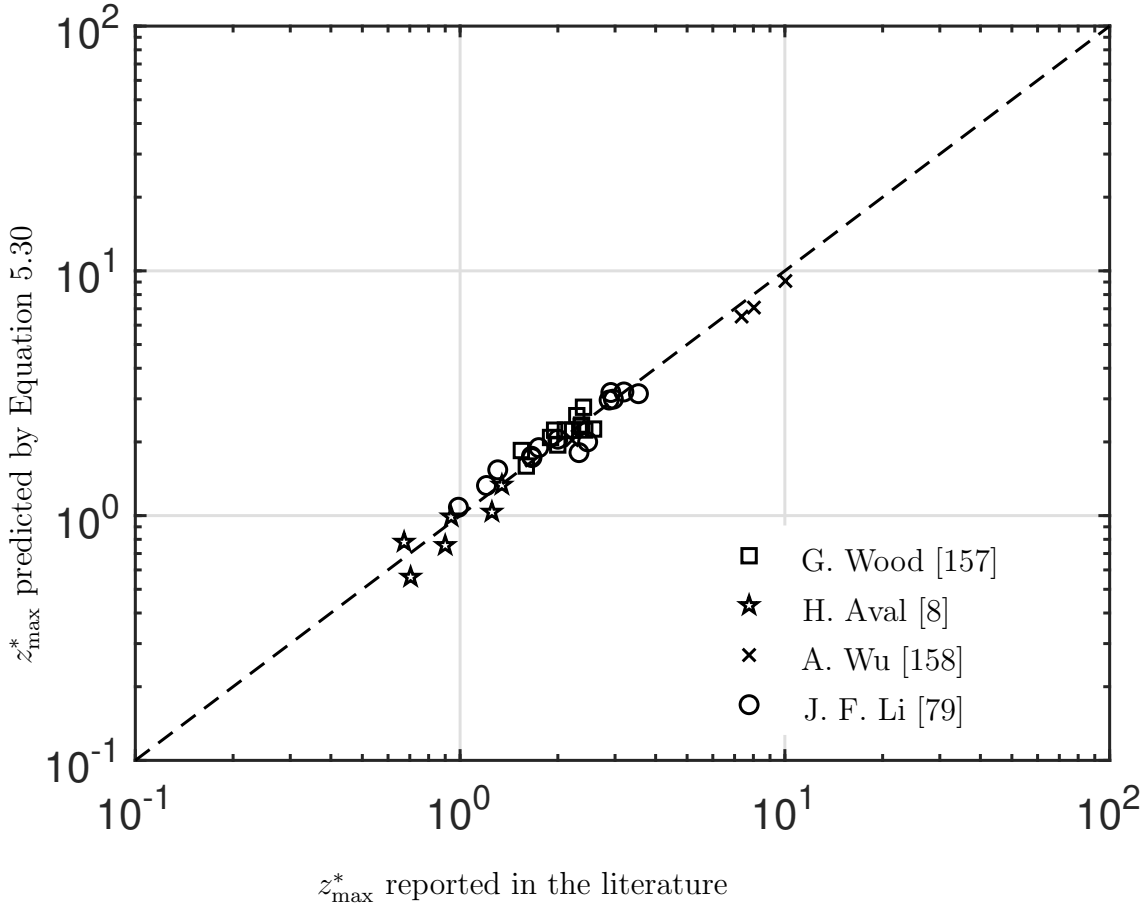

Figure 5.5: Validation of the blended expression for a Gaussian heat source (Equation 5.30) against published experimental data for the maximum isotherm depth.

5.7 Example of Application

Consider the laser cladding process of 4145 MOD carbon steel performed by Wood [157]. The laser power was 3990 W, with a beam diameter of 1.62 mm, a travel speed of 31.81 mm/s, a thermal efficiency of 0.3 as reported in the literature for CO_2 laser cladding [132]. Effective thermophysical properties are provided in [157]: $k = 32.52\text{W/mK}$ and $\alpha = 5.73 \times 10^{-6}\text{m}^2/\text{s}$. The measured melt depth was 0.85 mm.

For the bead considered, Ry = 23.5 (Equation 5.13), dimensionless distribution parameter is $\sigma^* = 4.5$ (Equation 5.7), the maximum feasible heat source size is $\sigma^*_{\max} = 8.2$ (Equation 5.31), resulting in a ratio of $\sigma^*/\sigma^*_{\max} = 0.55$. With Ry = 23.5, and $\sigma^*/\sigma^*_{\max} = 0.55$, the calculated example corresponds to Regime I, close to the

boundary between Regime I and Regime V.

The prediction of dimensionless melt depth is made using Equation 5.30, which yields $f(\mathrm{Ry}) = 0.1722$, and $g(\mathrm{Ry}, \sigma^*/\sigma^*_{\max}) = 0.5713$ (Equation 5.26). The predicted melt depth is $\widehat{z}^+_{\max} = 0.83$ mm, which is an underprediction with an error of 1.9% compared to the measured value of 0.85 mm. Neglecting the correction factor g, calculated melt depth by point source solution is overpredicted as $\widehat{z}^+_{\max} = 1.46$ mm, and the error compared to the measurement is 71%.

5.8 Discussion

Consistently with the foundations established in [96], the analysis presented here dispels old misconceptions and brings new insights. Similarly, the proper dimensional analysis of Equation 5.4 yields four regimes of the solution domain based on two dimensionless groups: Ry, associated with the temperature of interest, and the dimensionless heat distribution parameter, σ^*, an indicator that determines whether the heat source is concentrated or wide. The two dimensionless groups are defined using operating parameters and material properties, which are readily known before experiments.

The extended blending function proposed in this paper overcomes the limitations of the Churchill-Usagi blending technique and can be applied to problems other than moving heat sources. The correction factor $f(\mathrm{Ry})$ extends the usefulness of the asymptotic in Regime II to the side Regime I-II (point heat source domain) where $\sigma^*/\sigma^*_{\max} \to 0$. The correction factor for the heat intensity distribution, $g(\mathrm{Ry}, \sigma^*/\sigma^*_{\max})$ extends the applicability of a point heat source prediction to a moving Gaussian surface source with any finite heat distribution parameter. When $\sigma^* \to 0$, the obtained prediction coincides with that of a point heat source. Although the introduction of two correction factors would involve optimizing four blending constants, they need to be determined only once. The obtained predictive equation in explicit form can be calculated in seconds.

The conventional 1D blending does not apply to the side Regime I-V where Ry $\rightarrow \infty$ because the dimensionless isotherm depth does not converge to dependence on one dimensionless group, and there is no explicit asymptotic that can be derived from the analytical solution. Ry ≤ 1000 is thus chosen as the upper limit, which covers most typical Ry values in laser processing or welding. The error in the blending used here is always below 9.7%, for $\sigma^*/\sigma^*_{\max} \leq 0.9$ and Ry ≤ 1000. For a special case with Ry > 1000, only blending constants need to be redetermined without changing the format of Equations 5.30 and 5.32. To the best of the author's knowledge, there is no empirical solution or numerical simulation (without ad-hoc calibrations) in welding or surface hardening that can predict the maximum isotherm depth with similar applicability and accuracy.

Comparisons of the expressions proposed against experimental measurements show relatively low scatter and systematic error comparable with the experimental error in a broad range of processes and materials. It is difficult to tell at this stage how much of the discrepancy is due to the assumptions in the Gaussian model, how much is due to uncertainties in the measurements, and how much is due to error in the constants used for material properties [90]. Although the errors observed suggest room for improvement, the correction factor for the heat distribution parameter shows a significant improvement on the point-heat source prediction.

5.9 Conclusions

This work presents new practical and rigorous expressions for the maximum isotherm depth $z_{\max}$ under a moving Gaussian surface heat source (Equations 5.30 and 5.32). The dimensionless form of the isotherm depth depends on two dimensionless groups: Ry, and $\sigma^*/\sigma^*_{\max}$. These two dimensionless quantities divide all possible solutions in four regimes: Regime I corresponding to high Ry ("fast" heat sources) and small $\sigma^*/\sigma^*_{\max}$ ("concentrated" heat sources), Regime II corresponding to low Ry ("slow" heat sources) and small $\sigma^*/\sigma^*_{\max}$, Regime V corresponding to high Ry and large

$\sigma^*/\sigma^*_{\max}$ ("wide" heat sources), Regime VI corresponding to low Ry and large $\sigma^*/\sigma^*_{\max}$.

The expression proposed has the form of an asymptotic expression multiplied by two correction factors: a correction factor $f(\mathrm{Ry})$, which extends the usefulness of the asymptotic based on a point heat source solution to all values of Ry and correction factor $g(\mathrm{Ry}, \sigma^*/\sigma^*_{\max})$, which accounts for the effect of the heat intensity distribution. The proposed expression coincides with the exact solution in the asymptotic extremes, and the maximum error over the range of $\sigma^*/\sigma^*_{\max} \leq 0.9$ and $\mathrm{Ry} \leq 1000$ is smaller than 9.7%.

The predictive equation proposed can be calculated using a handheld calculator or a basic spreadsheet, requiring less computational time than simulations and without presenting convergence problems. It can also be used to design operating parameters in many processes or to verify numerical models. The results obtained support the applicability of asymptotics and blending techniques to tackle general moving heat source problems.

Acknowledgments

The authors wish to acknowledge support from the Natural Sciences and Engineering Research Council of Canada (NSERC). Student scholarships from the American Welding Society and the Canadian Welding Association Foundation were also gratefully received.

References

[2] A. Acrivos, "A Rapid Method for Estimating the Shear Stress and the Separation Point in Laminar Incompressible Boundary-Layer Flows," *Journal of the Aerospace Sciences*, vol. 27, no. 4, pp. 314–315, 1960.

[3] C. M. Adams, "Cooling Rates and Peak Temperatures in Fusion Welding," *Welding Journal*, vol. 37, no. 5, pp. 210–215, 1958.

[8] H. J. Aval, A. Farzadi, S. Serajzadeh, and A. H. Kokabi, "Theoretical and experimental study of microstructures and weld pool geometry during gtaw of 304 stainless steel," *The International Journal of Advanced Manufacturing Technology*, vol. 42, no. 11-12, pp. 1043–1051, 2009.

[19] E. Buckingham, "On Physically Similar Systems; Illustrations of the Use of Dimensional Equations," *Physical Review*, vol. 4, no. 4, pp. 345–376, 1914, ISSN: 0031899X. arXiv: `arXiv:1011.1669v3`.

[20] H. S. Carslaw and J. C. Jaeger, *Conduction of heat in solids*, Second. Oxford: Clarendon Press, 1959.

[23] S. W. Churchill and R. Usagi, "A general expression for the correlation of rates of transfer and other phenomena," *AIChE Journal*, vol. 18, no. 6, pp. 1121–1128, 1972, ISSN: 15475905.

[27] H. E. Cline and T. R. Anthony, "Heat treating and melting material with a scanning laser or electron beam," *Journal of Applied Physics*, vol. 48, no. 9, 1977.

[31] J. A. Dantzig and C. L. Tucker, *Modeling in Materials Processing*. Cambridge, England: Cambridge University Press, 2001, p. 384.

[36] T. W. Eagar and N. S. Tsai, "Temperature Fields Produced by Traveling Distributed Heat Sources," *Welding Journal*, vol. 62, no. 12, pp. 346–355, 1983, ISSN: 00432296.

[41] Z. R. Francis, "The effects of laser and electron beam spot size in additive manufacturing processes," PhD thesis, Carnegie Mellon University, 2017.

[48] J. Goldak, A. Chakravarti, and M. Bibby, "A New Finite Element Model for Welding Heat Sources," *Metallurgical Transactions B*, vol. 15, no. 2, pp. 299–305, 1984, ISSN: 03602141.

[58] A. Hoadley and M. Rappaz, "A thermal model of laser cladding by powder injection," *Metallurgical transactions B*, vol. 23, no. 5, pp. 631–642, 1992.

[71] W. E. King, A. T. Anderson, R. M. Ferencz, N. E. Hodge, C. Kamath, S. A. Khairallah, and A. M. Rubenchik, "Laser powder bed fusion additive manufacturing of metals; physics, computational, and materials challenges," *Applied Physics Reviews*, vol. 2, no. 4, p. 041 304, 2015.

[74] R Komanduri and Z. Hou, "Thermal analysis of the laser surface transformation hardening process," *International Journal of heat and mass transfer*, vol. 44, no. 15, pp. 2845–2862, 2001.

[76] S. Kou, D. K. Sun, and Y. P. Le, "A fundamental study of laser transformation hardening," *Metallurgical Transactions A*, vol. 14, no. 3, pp. 643–653, 1983.

[78] J. Lawrence, "An analysis of the beam interaction characteristics of selected lasers with an alpha-alumina bioceramic," *Optics and lasers in engineering*, vol. 41, no. 3, pp. 505–514, 2004.

[79] J. F. Li, L. Li, and F. H. Stott, "Comparison of volumetric and surface heating sources in the modeling of laser melting of ceramic materials," *International journal of heat and mass transfer*, vol. 47, no. 6-7, pp. 1159–1174, 2004.

[82] Y. Lu and P. F. Mendez, "Characteristic values of the temperature field induced by a moving line heat source," *International Journal of Heat and Mass Transfer*, p. 120 671, 2020.

[83] Y. Lu and P. F. Mendez, "The effect of surface heat losses on isotherm trailing length and cooling rate," 2021.

[84] Y. Lu, Y. Wang, and P. F. Mendez, "Width of thermal features induced by a 2-d moving heat source," *International Journal of Heat and Mass Transfer*, vol. 156, p. 119 793, 2020.

[87] O. Manca, B. Morrone, and V. Naso, "Quasi-steady-state three-dimensional temperature distribution induced by a moving circular gaussian heat source in a finite depth solid," *International Journal of Heat and Mass Transfer*, vol. 38, no. 7, pp. 1305–1315, 1995.

[89] J. Mazumder and W. M. Steen, "Heat transfer model for cw laser material processing," *Journal of Applied Physics*, vol. 51, no. 2, pp. 941–947, 1980.

[90] P. F. Mendez, "Synthesis and generalisation of welding fundamentals to design new welding technologies: status, challenges and a promising approach," *Science and Technology of Welding and Joining*, vol. 16, no. 4, pp. 348–356, 2011, ISSN: 1362-1718.

[93] P. F. Mendez, "Characteristic Values in the Scaling of Differential Equations in Engineering," *Journal of Applied Mechanics, Transactions ASME*, vol. 77, no. 6, 2010, ISSN: 00218936.

[96] P. F. Mendez, Y. Lu, and Y. Wang, "Scaling Analysis of a Moving Point Heat Source in Steady- State on a Semi-Infinite Solid," *Journal of Heat Transfer*, vol. 140, no. 8, p. 081 301, 2018.

[111] N. T. Nguyen, A. Ohta, K. Matsuoka, N. Suzuki, and Y. Maeda, "Analytical Solutions for Transient Temperature of Semi-Infinite Body Subjected to 3-D Moving Heat Sources," *Welding Journal, Research Supplement*, vol. 78, no. August, 265s–274s, 1999.

[126] D. Rosenthal, "The Theory of Moving Sources of Heat and Its Application to Metal Treatments," *Transactions of the A.S.M.E.*, vol. 68, pp. 849–866, 1946.

[128] D. Rosenthal, "Mathematical Theory of Heat Distribution During Welding and Cutting," *Welding Journal*, vol. 20, no. 5, pp. 220–234, 1941.

[132] M. F. Schneider and M. F. Schneider, "Laser cladding with powder," PhD thesis, University of Twente, 1998.

[137] W. M. Steen and C. Courtney, "Surface heat treatment of ens steel using a 2kw continuous-wave co2 laser," *Metals Technology*, vol. 6, no. 1, pp. 456–462, 1979.

[142] X. Tian, Y. Liu, W. Deng, and G. Liu, "Sensitivity analysis for process parameters influencing electric arc cutting," *The International Journal of Advanced Manufacturing Technology*, vol. 78, no. 1-4, pp. 481–492, 2015.

[145] N. S. Tsai and T. W. Eagar, "Distribution of the heat and current fluxes in gas tungsten arcs," *Metallurgical transactions B*, vol. 16, no. 4, pp. 841–846, 1985.

[146] N. Tsai, "Heat distribution and weld bead geometry in arc welding," PhD thesis, Massachusetts Institute of Technology, 1983.

[148] Y Wang, Y Lu, M Grams, A Cesaro, and P. Mendez, *Asymptotics and blending in the modeling of welding*, 2019.

[149] Y. Wang, Y. Lu, and P. F. Mendez, "Scaling expressions of characteristic values for a moving point heat source in steady state on a semi-infinite solid," *International Journal of Heat and Mass Transfer*, vol. 135, pp. 1118–1129, 2019.

[150] Y. Wang, Y. Lu, and P. F. Mendez, "Prediction of peak temperature under a moving gaussian surface heat source," 2021.

[152] T. Washio and H. Motoda, "Extension of Dimensional Analysis for Scale-types and its Application to Discovery of Admissible Models of Complex Processes," in *International Workshop on Similarity Method*, 1999, pp. 129–147.

[153] A. A. Wells, "Heat flow in welding," *Welding Journal Research Supplement*, vol. 31, no. 5, 1952.

[155] G. Wood and P. F. Mendez, "Disaggregated metal and carbide catchment efficiencies in laser cladding of nickel-tungsten carbide," *Welding Journal*, vol. 94, no. 11, pp. 343–350, 2015.

[156] G. Wood, S. A. Islam, and P. F. Mendez, "Calibrated expressions for welding and their application to isotherm width in a thick plate," *Soldagem & Inspeção*, vol. 19, no. 3, pp. 212–220, 2014.

[157] G. D. Wood, "Heat and mass transfer aspects of coaxial laser cladding and its application to nickel-tungsten carbide alloys," PhD thesis, University of Alberta, 2017.

[158] A. S. Wu, D. W. Brown, M. Kumar, G. F. Gallegos, and W. E. King, "An experimental investigation into additive manufacturing-induced residual stresses in 316l stainless steel," *Metallurgical and Materials Transactions A*, vol. 45, no. 13, pp. 6260–6270, 2014.

Appendix: Derivation of Asymptotic behaviours

Appendix 5.A Location of $z^*_{\max}$ in Regime V and VI

The maximum temperature at centerline and its location are notated in dimensionless form as $T^*{}_{\max,c}$ and $x^*_{\max,c}$. At the location of the maximum isotherm depth $(x^*_{\max,z}, y^* = 0, z_{\max})$, by definition, partial derivative of z to x equals zero:

$$\left.\frac{\partial z^*}{\partial x^*}\right|_{x^*_{\max,z},z_{\max}} = \left.\frac{\partial T^*/\partial x^*}{\partial T^*/\partial z^*}\right|_{x^*_{\max,z},z_{\max}} = 0$$

obtaining $\partial T^*/\partial x^*|_{x^*_{\max,z},z_{\max}} = 0$.

When $\sigma^*/\sigma^*_{\max}$ tends to 1, the maximum isotherm depth tends to zero. Assuming $x^*_{\max,z} = x^*_{\max,c} + \delta x$ and $z_{\max} = \delta z$ (both δx and δz are small value) such that $\frac{\partial T^*}{\partial x^*}$ at the location of the maximum isotherm depth can be expanded as follows:

$$\begin{aligned}\left.\frac{\partial T^*}{\partial x^*}\right|_{x^*_{\max,z},z_{\max}} \approx \Bigg[&\frac{\partial T^*}{\partial x^*} + \frac{\partial}{\partial x^*}\left(\frac{\partial T^*}{\partial x^*}\right)\delta x + \\ &\frac{\partial}{\partial z^*}\left(\frac{\partial T^*}{\partial x^*}\right)\delta z\Bigg]\Bigg|_{x^*_{\max,c},z^*=0} = 0\end{aligned} \tag{5.33}$$

where by definition, $\frac{\partial T^*}{\partial x^*}$ at the location of peak temperature equals 0:

$$\left.\frac{\partial T^*}{\partial x^*}\right|_{x^*_{\max,c},z^*=0} = 0 \tag{5.34}$$

Also, at $z^* = 0$, partial derivative calculation of Equation 5.12 yields:

$$\begin{aligned}&\frac{\partial}{\partial z^*}\left(\frac{\partial T^*}{\partial x^*}\right) = \sqrt{\frac{2}{\pi}}\frac{z^*}{\sigma^{*5}}\cdot \\ &\int_0^{\frac{\pi}{2}} \frac{\cos^2\theta\cot^2\theta\left(\sigma^{*2}\tan^2\theta + x^*\right)}{\exp\left[\frac{\left(\sigma^{*2}\sin\theta\tan\theta + x\cos\theta\right)^2 + z^{*2}\cot^2\theta}{2\sigma^{*2}}\right]}d\theta = 0\end{aligned} \tag{5.35}$$

Substituting Equation 5.34 and Equation 5.35 into Equation 5.33 to obtain $\delta x \approx 0$ and $x^*_{\max,z} = x^*_{\max,c}$, which means the location of peak temperature and the maximum isotherm depth are identical in Regime V and Regime VI when $\sigma^*/\sigma^*_{\max}$ tends to 1.

Asmptotics of the peak temperature and its location were derived in [150] and have the following power laws:

$$\widehat{T^*}_{\max_{\mathrm{V}}}(\sigma^*) = \sqrt{\frac{2}{\pi}} I_m \, \sigma^{*-1.5} \text{ For Regime V (large Ry, wide source)} \tag{5.36}$$

$$\widehat{T^*}_{\max_{\mathrm{VI}}}(\sigma^*) = \sqrt{\frac{\pi}{2}} \, \sigma^{*-1} \text{ For Regime VI (small Ry, wide source)} \tag{5.37}$$

where the asymptotic constant $I_m = 1.280$. For the location of the peak temperature:

$$\widehat{x^*}_{\max_{\mathrm{V}}}(\sigma^*) = -0.7650\sigma^* \qquad \text{For Regime V (large Ry, wide source)} \tag{5.38}$$

$$\widehat{x^*}_{\max_{\mathrm{VI}}}(\sigma^*) = -\sigma^{*2} \qquad \text{For Regime VI (small Ry, wide source)} \tag{5.39}$$

5.A.1 Regime VI Ry $\to 0$, $\sigma^*/\sigma^*_{\max} \to 1$

In Regime VI, as Ry $\to 0$, $\sigma^*_{\max} \to 0$, $\sigma^* \to 0$, substituting the location of the maximum isotherm depth (Equation 5.39) into Equation 5.12:

$$\begin{aligned}
T^* &= \sqrt{\frac{2}{\pi}} \frac{1}{\sigma^*} \int_0^{\frac{\pi}{2}} \exp\left[-\frac{\sigma^{*4}(\sin\theta\tan\theta - \cos\theta)^2 + \widehat{z^*}^2_{\max_{\mathrm{VI}}} \cot^2\theta}{2\sigma^{*2}} \right] d\theta \\
&\approx \sqrt{\frac{2}{\pi}} \frac{1}{\sigma^*} \int_0^{\frac{\pi}{2}} \exp\left[-\frac{\widehat{z^*}^2_{\max_{\mathrm{VI}}} \cot^2\theta}{2\sigma^{*2}} \right] d\theta \\
&= \sqrt{\frac{\pi}{2}} \frac{1}{\sigma^*} \exp\left(\frac{\widehat{z^*}^2_{\max_{\mathrm{VI}}}}{2\sigma^{*2}} \right) \mathrm{Erfc}\left(\frac{\widehat{z^*}_{\max_{\mathrm{VI}}}}{\sqrt{2}\sigma^*} \right) \\
&= \sqrt{\frac{\pi}{2}} \frac{1}{\sigma^*} - \frac{\widehat{z^*}_{\max_{\mathrm{VI}}}}{\sigma^{*2}} + O\left(z^*\right)^2 \\
&\approx \widehat{T^*}_{\max_{\mathrm{VI}}} - \frac{\widehat{z^*}_{\max_{\mathrm{VI}}}}{\sigma^{*2}}
\end{aligned} \tag{5.40}$$

Therefore, the maximum isotherm depth can be rewritten as:

$$\widehat{z^*}_{\max_{\mathrm{VI}}} = \sigma^{*2} \left(\widehat{T^*}_{\max_{\mathrm{VI}}} - T^* \right) \tag{5.41}$$

substituting Equation 5.37 into substituting Equation 5.41 to obtain:

$$\begin{aligned}
\widehat{z^*}_{\max_{\mathrm{VI}}} &= \sigma^{*2} \left(\sqrt{\frac{\pi}{2}} \frac{1}{\sigma^*} - \sqrt{\frac{\pi}{2}} \frac{1}{\sigma^*_{\max}} \right) \\
&= \sqrt{\frac{\pi}{2}} \sigma^*_{\max_{\mathrm{VI}}} \left(\frac{\sigma^*}{\sigma^*_{\max}} \right) \left[1 - \left(\frac{\sigma^*}{\sigma^*_{\max}} \right) \right] \\
&= \frac{\pi}{2} \mathrm{Ry} \left[1 - \left(\frac{\sigma^*}{\sigma^*_{\max}} \right) \right] \approx \frac{\pi}{2} \mathrm{Ry} \ln\left(\frac{\sigma^*_{\max}}{\sigma^*} \right) \quad \text{as } \tfrac{\sigma^*}{\sigma^*_{\max}} \to 1
\end{aligned}$$

5.A.2 Regime V Ry $\to \infty$, $\sigma^*/\sigma^*_{\mathbf{max}} \to 1$

As Ry $\to \infty$, $\sigma^*_{\max} \to \infty$, $x^*_{\max,c} = x^*_{\max,z} = -0.7650\sigma^*$. The integrand in Equation 5.12 is large for θ in the vicinity of $\theta = 0$ and decreases significantly until zero with increasing θ, as discussed in [150]. Taylor expansion of the integrand around $z^* = 0$ yields the following:

$$
\begin{aligned}
&-\frac{1}{2\sigma^{*2}}\left[\left(\sigma^{*2}\sin\theta\tan\theta + x^*_{\max,c}\cos\theta\right)^2 + z^{*2}\cot^2\theta\right] \\
&= -\frac{z^{*2}}{2\sigma^{*2}\theta^2} + \frac{2z^{*2}-3x^{*2}_{\max,c}}{6\sigma^{*2}} + \theta^2\left(\frac{x^{*2}_{\max,c}}{2\sigma^{*2}} - \frac{z^{*2}}{30\sigma^{*2}} - x^*_{\max,c}\right) \\
&+ \left(-\frac{\sigma^{*2}}{2} + \frac{x^*_{\max,c}}{3} - \frac{x^{*2}_{\max,c}}{6\sigma^{*2}} - \frac{z^{*2}}{189\sigma^{*2}}\right)\theta^4 + O\left(\theta^6\right) \\
&\approx -\frac{z^{*2}}{2\sigma^{*2}\theta^2} + \frac{2z^{*2}-3x^{*2}_{\max,c}}{6\sigma^{*2}} - \left(\frac{z^{*2}}{30\sigma^{*2}} + x^*_{\max,c}\right)\theta^2 \\
&- \left(\frac{\sigma^{*2}}{2} + \frac{z^{*2}}{189\sigma^{*2}}\right)\theta^4 \\
&\approx -\frac{z^{*2}}{2\sigma^{*2}\theta^2} - \frac{(x_{\max,c} + \sigma^{*2}\theta^2)^2}{2\sigma^{*2}}
\end{aligned}
\tag{5.42}
$$

Substituting Equation 5.42 and $x^*_{\max,c} = x^*_{\max,z} = -0.7650\sigma^*$ into Equation 5.12 to obtain:

$$
\begin{aligned}
T^* &= \sqrt{\frac{2}{\pi}}\frac{1}{\sigma^*}\int_0^{\frac{\pi}{2}} \exp\left[-\frac{\widehat{z^*}^2_{\max_V}}{2\sigma^{*2}\theta^2} - \frac{\left(\sigma^{*2}\theta^2 - 0.7650\sigma^*\right)^2}{2\sigma^{*2}}\right] d\theta \\
&= \sqrt{\frac{2}{\pi}}\sigma^{*-\frac{3}{2}}\int_0^{\frac{\pi}{2}\sqrt{\sigma^*}} \exp\left[-\frac{\widehat{z^*}^2_{\max_V}}{2\sigma^*\theta^2} - \frac{\left(\theta^2 - 0.7650\right)^2}{2}\right] d\theta \\
&= \sqrt{\frac{2}{\pi}}\sigma^{*-\frac{3}{2}}\int_0^{\infty} \exp\left[-\frac{\widehat{z^*}^2_{\max_V}}{2\sigma^*\theta^2} - \frac{\left(\theta^2 - 0.7650\right)^2}{2}\right] d\theta \\
&= \widehat{T^*}_{\max_V}\cdot\left\{\frac{1}{1.280}\int_0^{\infty} \exp\left[-\frac{\widehat{z^*}^2_{\max_V}}{2\sigma^*\theta^2} - \frac{\left(\theta^2 - 0.7650\right)^2}{2}\right] d\theta\right\} \\
&= \widehat{T^*}_{\max_V}\cdot f\left(\frac{\widehat{z^*}^2_{\max_V}}{2\sigma^*}\right)
\end{aligned}
$$

Therefore, $\widehat{z^*}_{\max_V}$ can be rewritten as a function of σ^*, dimensionless temperature T^*, and the peak temperature in Regime V, $\widehat{T^*}_{\max_V}$:

$$
\widehat{z^*}_{\max_V} = \sqrt{2\sigma^*\cdot f^{-1}\left(\frac{T^*}{\widehat{T^*}_{\max_V}}\right)}
\tag{5.43}
$$

where f^{-1} is inverse function of f and the independent variable $T^*/\widehat{T^*}_{\max V}$ varies from 0 to ∞. Numeric value of f^{-1} is plotted in Figure5.A.2:

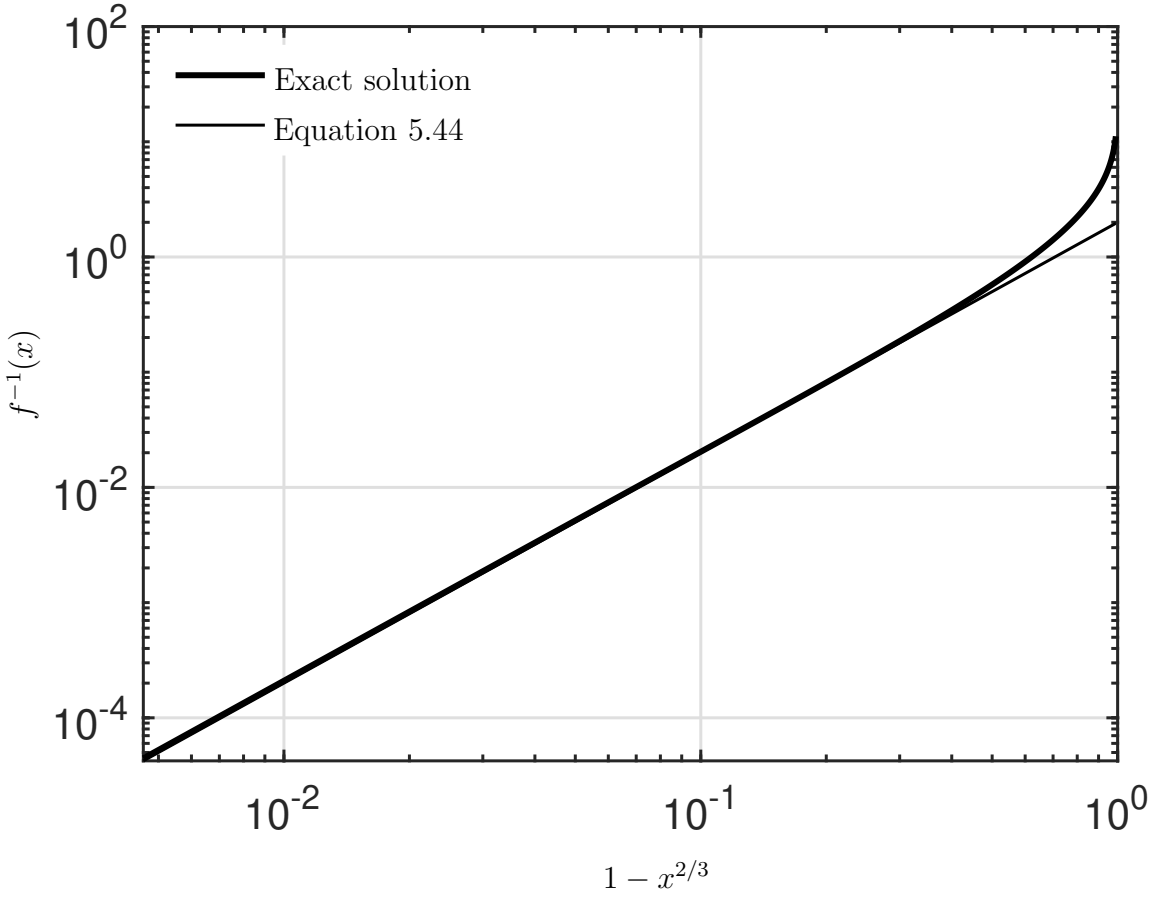

When $\sigma^*/\sigma^*_{\max} \to 1$, $T^*/T^*_{\max,c} \to 1$, the inverse function can be approximated by the following polynominal with high accuracy:

$$f^{-1}(x) = 2(1-x^{2/3})^2 \tag{5.44}$$

Substituting Equation 5.44 and Equation 5.36 to Equation 5.43 yields:

$$\begin{aligned}
\widehat{z^*}_{\max_{\mathrm{V}}} &= 2\sqrt{\sigma^*}\left[1-\left(\frac{T^*}{T^*_{\max,\mathrm{c}}}\right)^{\frac{2}{3}}\right] \\
&= 2\left(\frac{\sigma^*}{\sigma^*_{\max}}\right)^{\frac{1}{2}}\sqrt{\sigma^*_{\max}}\left(1-\frac{\sigma^*}{\sigma^*_{\max}}\right) \\
&\approx 2\left(\frac{2I}{\sqrt{2\pi}}\right)^{\frac{1}{3}}\mathrm{Ry}^{\frac{1}{3}}\left(1-\frac{\sigma^*}{\sigma^*_{\max}}\right) \\
&\approx 2.014\,\mathrm{Ry}^{1/3}\left(1-\frac{\sigma^*}{\sigma^*_{\max}}\right) \\
&\approx 2.014\,\mathrm{Ry}^{1/3}\ln\left(\frac{\sigma^*_{\max}}{\sigma^*}\right)
\end{aligned}$$

Appendix 5.B Data Collected from the Literature

Table 5.2: The heat source efficiency, heat distribution parameter, thermal properties, processing parameters and the maximum isotherm depth reported in the validation.

Process	Material	Power	Efficiency	Velocity	Conductivity	Diffusivity	T_c	T_0	σ	z_{max}	Source
		W	1	mm/s	W/mK	m^2/s	°C	°C	mm	mm	
LC	4145MOD	4980	0.3 [157]	25.45	32.52 [157]	5.7×10^{-6} [157]	955 [157]	257 [157]	1.62 [157]	1.08	[157]
LC	4145MOD	3090	0.3 [157]	25.45	32.52 [157]	5.7×10^{-6} [157]	955 [157]	257 [157]	1.62 [157]	0.72	[157]
LC	4145MOD	3990	0.3 [157]	25.45	32.52 [157]	5.7×10^{-6} [157]	955 [157]	261 [157]	1.62 [157]	1	[157]
LC	4145MOD	3990	0.3 [157]	19.09	32.52 [157]	5.7×10^{-6} [157]	955 [157]	258 [157]	1.62 [157]	1.14	[157]
LC	4145MOD	3990	0.3 [157]	25.45	32.52 [157]	5.7×10^{-6} [157]	955 [157]	268 [157]	1.62 [157]	1.16	[157]
LC	4145MOD	3990	0.3 [157]	31.81	32.52 [157]	5.7×10^{-6} [157]	955 [157]	264 [157]	1.62 [157]	0.85	[157]
LC	4145MOD	4540	0.3 [157]	25.45	32.52 [157]	5.7×10^{-6} [157]	955 [157]	263 [157]	1.62 [157]	1.03	[157]
LC	4145MOD	3530	0.3 [157]	25.45	32.52 [157]	5.7×10^{-6} [157]	955 [157]	264 [157]	1.62 [157]	0.9	[157]
LC	4145MOD	3980	0.3 [157]	12.73	32.52 [157]	5.7×10^{-6} [157]	955 [157]	263 [157]	1.62 [157]	1.39	[157]
LC	4145MOD	3980	0.3 [157]	25.45	32.52 [157]	5.7×10^{-6} [157]	955 [157]	264 [157]	1.62 [157]	0.95	[157]
LC	4145MOD	3980	0.3 [157]	25.45	32.52 [157]	5.7×10^{-6} [157]	955 [157]	264 [157]	1.62 [157]	1.09	[157]
LC	4145MOD	3980	0.3 [157]	38.18	32.52 [157]	5.7×10^{-6} [157]	955 [157]	267 [157]	1.62 [157]	0.71	[157]
LC	4145MOD	3980	0.3 [157]	25.45	32.52 [157]	5.7×10^{-6} [157]	955 [157]	263 [157]	1.62 [157]	0.88	[157]
LC	316L stainless	100	0.4 [158]	400	22.95*	5.4×10^{-6} [158]	1410*	20+	0.013 [158]	0.0595	[158]
LC	316L stainless	250	0.4 [158]	1500	22.95*	5.4×10^{-6} [158]	1410*	20+	0.013 [158]	0.0528	[158]
LC	316L stainless	250	0.4 [158]	1800	22.95*	5.4×10^{-6} [158]	1410*	20+	0.013 [158]	0.0480	[158]
LC	316L stainless	400	0.4 [158]	1800	22.95*	5.4×10^{-6} [158]	1410*	20+	0.013 [158]	0.0600	[158]
GTAW	304 stainless	1265	0.62 [8]	1.6	17.64 [8]	4.1×10^{-6} [8]	1424 [8]	20+	0.89 [8]	3.6	[8]
GTAW	304 stainless	1265	0.65 [8]	2.5	17.64 [8]	4.1×10^{-6} [8]	1424 [8]	20+	0.89 [8]	2.2	[8]
GTAW	304 stainless	1890	0.61 [8]	1.6	17.64 [8]	4.1×10^{-6} [8]	1424 [8]	20+	0.89 [8]	4.6	[8]
GTAW	304 stainless	1890	0.64 [8]	2.5	17.64 [8]	4.1×10^{-6} [8]	1424 [8]	20+	0.89 [8]	4.1	[8]
GTAW	304 stainless	2760	0.62 [8]	1.6	17.64 [8]	4.1×10^{-6} [8]	1424 [8]	20+	0.89 [8]	4.8	[8]
GTAW	304 stainless	2760	0.65 [8]	2.5	17.64 [8]	4.1×10^{-6} [8]	1424 [8]	20+	0.89 [8]	4.4	[8]
LHT	ABR	500	0.7 [78]	1	3.25 [79]	8.5×10^{-7} [79]	2100 [79]	20+	2.5 [79]	1.68	[79]
LHT	ABR	600	0.7 [78]	1	3.25 [79]	8.5×10^{-7} [79]	2100 [79]	20+	2.5 [79]	2.05	[79]
LHT	ABR	700	0.7 [78]	1	3.25 [79]	8.5×10^{-7} [79]	2100 [79]	20+	2.5 [79]	2.22	[79]
LHT	ABR	800	0.7 [78]	1	3.25 [79]	8.5×10^{-7} [79]	2100 [79]	20+	2.5 [79]	2.83	[79]
LHT	ABR	900	0.7 [78]	1	3.25 [79]	8.5×10^{-7} [79]	2100 [79]	20+	2.5 [79]	2.97	[79]
LHT	ABR	1000	0.7 [78]	1	3.25 [79]	8.5×10^{-7} [79]	2100 [79]	20+	2.5 [79]	3.40	[79]
LHT	ABR	1000	0.7 [78]	3	3.25 [79]	8.5×10^{-7} [79]	2100 [79]	20+	2.5 [79]	1.63	[79]
LHT	ABR	1000	0.7 [78]	5	3.25 [79]	8.5×10^{-7} [79]	2100 [79]	20+	2.5 [79]	0.99	[79]
LHT	ABR	1000	0.7 [78]	7	3.25 [79]	8.5×10^{-7} [79]	2100 [79]	20+	2.5 [79]	0.86	[79]
LHT	ABR	1000	0.7 [78]	9	3.25 [79]	8.5×10^{-7} [79]	2100 [79]	20+	2.5 [79]	0.56	[79]
LHT	ABR	600	0.7 [78]	7	3.25 [79]	8.5×10^{-7} [79]	2100 [79]	20+	2 [79]	0.60	[79]
LHT	ABR	700	0.7 [78]	5	3.25 [79]	8.5×10^{-7} [79]	2100 [79]	20+	2.5 [79]	0.79	[79]
LHT	ABR	800	0.7 [78]	3	3.25 [79]	8.5×10^{-7} [79]	2100 [79]	20+	1.5 [79]	1.81	[79]
LHT	ABR	900	0.7 [78]	1	3.25 [79]	8.5×10^{-7} [79]	2100 [79]	20+	3.0 [79]	2.82	[79]

* Properties calculated by JMatPro v11
\+ Estimated
LC: Laser Cladding
LHT: Laser Heat Treatment
ABR: Alumina-based Refractory

Chapter 6

Conclusions and Future Work

6.1 Conclusions

This research focuses on developing a set of design rules in the form of simple formula and its correction factors to understand the relationship between general welding conditions and thermal characteristics of heat flow in welds. A few of these design rules exist in welding, and current ones are typically material-specific or process-specific with a limited range of applicability. A systematic methodology of asymptotic analysis and blending has been employed to construct closed-form solutions by combining asymptotes in asymptotic regimes and blending constants determined with a systematic optimization procedure. The obtained design rules approach the exact analytical solutions in asymptotic regimes and provide accurate estimation in the intermediate regimes.

As listed in Table 6.1, design rules based on the moving point heat source model are developed for 13 thermal characteristics: maximum bead width and its location, leading and trailing lengths of the isotherm, centreline heating and cooling rate, maximum temperature and its gradient, aspect ratio of isotherms, melting efficiency, cooling time $t_{8/5}$, solidification time, thickness of the heat affected zone, and modification coefficient for joint preparation geometry. In dimensionless form, the design rules developed depend on a single dimensionless parameter, the Rykalin number (Ry), and are accurate to within 7% of the exact analytical solutions. As a rule of thumb, for

Ry $< 1/20$ or Ry > 20, asymptotic solutions alone yield an error below 10% for all listed characteristics. The design rules obtained can provide welding operators and engineers with the knowledge and understanding necessary to produce high-quality, sound, and economic welded joints.

To avoid the singularity caused by the point heat source assumption, a moving Gaussian distributed heat source model is employed as the theoretical basis to improve the accuracy of prediction for the peak temperature around the heat source. The methodology of asymptotic and 1D blending is applied to predict with high accuracy the peak temperature and its location and the maximum feasible heat distribution parameter to reach a certain peak temperature. The dimensionless peak temperature and its location depend only the dimensionless heat distribution parameter (σ^*). For a given Ry, σ^* ranges from zero to the dimensionless maximum feasible heat distribution parameter $\sigma^*_{\max}$, above which the heat intensity is too small to heat the substrate to the desired temperature ($T^*_c = 1/\text{Ry}$). The ratio of $\sigma^*/\sigma^*_{\max}$ transforms the solution domain to a finite range from zero (corresponding to "concentrated" heat sources) to one (corresponding to "wide" heat sources). The maximum error of approximation is 0.19 % for the dimensionless peak temperature, 1.4 % for the maximum feasible heat distribution parameter and 0.47 % for the location of the peak temperature, respectively. For $\sigma^* > 20$ or $\sigma^* < 0.05$, the asymptotics alone, without correction, has an error below 10 % compared to the exact solutions. The design rules presented can be applied to optimize operating parameters (e.g. determine the onset of surface melting) in many processes and materials. The excellent agreement of the obtained design rules with experimental measurements and simulation data collected from the literature supports the applicability of the methodology of asymptotics and blending to solve general moving heat source problems.

In the feasible region defined by Ry and $\sigma^*/\sigma^*_{\max}$, a novel, practical and rigorous expression for the maximum isotherm depth $z_{\max}$ is obtained by asymptotic analysis and blending of the analytical temperature field under a moving Gaussian sur-

face heat source. These two dimensionless quantities divide the solution domain into four regimes: Regime I corresponding to high Ry ("fast" heat sources) and small $\sigma^*/\sigma^*_{\max}$ ("concentrated" heat sources), Regime II corresponding to low Ry ("slow" heat sources) and small $\sigma^*/\sigma^*_{\max}$, Regime V corresponding to high Ry and large $\sigma^*/\sigma^*_{\max}$ ("wide" heat sources), Regime VI corresponding to low Ry and large $\sigma^*/\sigma^*_{\max}$. The convectional 1D blending technique is extended to two dimensionless groups. Dimensionless isotherm depth is written as an asymptote multiplied by two correction factors: correction factor $f(\mathrm{Ry})$, which extends the usefulness of the asymptotic derived from a point heat source solution to all values of Ry, and correction factor $g(\mathrm{Ry}, \sigma^*/\sigma^*_{\max})$, which accounts for the effect of the heat intensity distribution. The maximum error over the range of $\sigma^*/\sigma^*_{\max} \leq 0.9$ and $\mathrm{Ry} \leq 1000$ is smaller than 9.7% compared to the exact analytical solution. The obtained design rules for the penetration depth has an excellent agreement with experimental measurements and simulation data collected from the literature. All design rules derived from the moving Gaussian surface heat source model are summarized in Table 6.2.

The methodology of asymptotic analysis and blending and the design rules obtained can be applied to other phenomena besides welding, such as surface heat treatment and additive manufacturing. The proposed design rules do not present convergence issues and can be calculated using a calculator or a basic spreadsheet. All obtained design rules are written in a closed form, and they can be readily embedded into multi-scale metamodels. Systematic errors in the modelling captured by the secondary terms can be calibrated by comparisons with experimental measurements or numerical simulation results.

Table 6.1: Summary of thermal characteristics and correction factors derived from a moving point heat source model.

Variable	Regime	Asymptotic	Correction factor	n	Error[%]
$y_{\max}$	I	$\sqrt{\frac{2}{\pi \mathrm{e}} \frac{\alpha q}{k U \left(T_{\mathrm{c}} - T_0\right)}}$	$\left[1 + \left(\sqrt{\frac{\mathrm{eRy}}{2}}\right)^{n}\right]^{\frac{1}{n}}$	-1.73	0.7
	II	$\frac{1}{2\pi} \frac{q}{k \left(T_{\mathrm{c}} - T_0\right)}$	$\left[1 + \left(\sqrt{\frac{\mathrm{eRy}}{2}}\right)^{-n}\right]^{\frac{1}{n}}$		
$x_{\max}$	I	$-\frac{q}{2\pi \mathrm{e} k \left(T_{\mathrm{c}} - T_0\right)}$	$\left[1 + (\mathrm{eRy})^{n}\right]^{\frac{1}{n}}$	-1.00	1.9
	II	$-\frac{2U}{\alpha}\left[\frac{q}{4\pi k \left(T_{\mathrm{c}} - T_0\right)}\right]^2$	$\left[1 + (\mathrm{eRy})^{-n}\right]^{\frac{1}{n}}$		
x_{b}	I and II	$-\frac{q}{2\pi k \left(T_{\mathrm{c}} - T_0\right)}$			
$\dot{T}_{\mathrm{b}}$	I and II	$-\frac{2\pi k U \left(T[c] - T_0\right)^2}{q}$			
x_{f}	I and II	$\frac{\alpha}{U} W_0\left[\frac{qU}{2\pi k \alpha \left(T_{\mathrm{c}} - T_0\right)}\right]$			
$\dot{T}_{\mathrm{f}}$	I and II	$\frac{U^2 \left(T_{\mathrm{c}} - T_0\right)}{\alpha}\left[\frac{1}{W_0\left(2Ry\right)} + 1\right]$			
$T_{\max}$	I	$T_0 + \frac{2\alpha q}{\mathrm{e}\pi k U {y_{\mathrm{c}}}^2}$	$\left[1 + \left(\frac{\mathrm{e} U y_{\mathrm{c}}}{4\alpha}\right)^{n}\right]^{\frac{1}{n}}$	-1.25	3.9
	II	$T_0 + \frac{q}{2\pi k y_{\mathrm{c}}}$	$\left[1 + \left(\frac{\mathrm{e} U y_{\mathrm{c}}}{4\alpha}\right)^{-n}\right]^{\frac{1}{n}}$		
$dT_{\max}/dy$	I	$-\sqrt{\frac{2\mathrm{e}\pi k U}{q\alpha}}\left(T_{\mathrm{m}} - T_0\right)^{\frac{3}{2}}$	$\left[1 + \left(\sqrt{\frac{1}{2\mathrm{eRy}}}\right)^{n}\right]^{\frac{1}{n}}$	3.08	6.1
	II	$-\frac{2\pi k}{q}\left(T_{\mathrm{m}} - T_0\right)^2$	$\left[1 + \left(\sqrt{\frac{1}{2\mathrm{eRy}}}\right)^{-n}\right]^{\frac{1}{n}}$		
A_R	I	$\sqrt{\frac{\mathrm{e} q U}{32\pi k \alpha \left(T - T_0\right)}}$	$\left[1 + \left(\sqrt{\frac{8}{\mathrm{eRy}}}\right)^{n}\right]^{\frac{1}{n}}$	1.90	2.0
	II	1	$\left[1 + \left(\sqrt{\frac{8}{\mathrm{eRy}}}\right)^{-n}\right]^{\frac{1}{n}}$		
η_{m}	I	$\frac{1}{\mathrm{e}}$	$\left[1 + \left(\frac{\mathrm{eRy}}{2}\right)^{n}\right]^{\frac{1}{n}}$	-0.87	1.4
	II	$\frac{qU}{8\pi k \alpha \left(T_{\mathrm{m}} - T_0\right)}$	$\left[1 + \left(\frac{\mathrm{eRy}}{2}\right)^{-n}\right]^{\frac{1}{n}}$		
$t_{8/5}$	N/A	$\frac{q}{2\pi k U}\left(\frac{1}{T_{500} - T_0} - \frac{1}{T_{800} - T_0}\right)$			
$t_{8/5}$	N/A	$\frac{q\left(T_{800} - T_{500}\right)}{2\pi k U \left(T_{\mathrm{i}} - T_0\right)^2}$			
		$T_{\mathrm{i}} - T_0 = \sqrt{\left(T_{800} - T_0\right)\left(T_{500} - T_0\right)}$			*
t_{sl}	N/A	$\frac{q i_{\mathrm{sl}}}{2\pi k c_{\mathrm{p}} U \left(T_{\mathrm{m}} - T_0\right)^2}$			
Δy_{HAZ}	I	$\sqrt{\frac{2\alpha q}{\pi \mathrm{e} k U}}\left[\frac{f_{y_{\max_{\mathrm{I}}}}(\mathrm{Ry}_{T_{\mathrm{HAZ}}})}{\sqrt{T_{\mathrm{HAZ}} - T_0}} - \frac{f_{y_{\max_{\mathrm{I}}}}(\mathrm{Ry}_{T_{\mathrm{m}}})}{\sqrt{T_{\mathrm{m}} - T_0}}\right]$	$\left[1 + \left(\sqrt{\frac{\mathrm{eRy}}{2}}\right)^{n}\right]^{\frac{1}{n}}$	-1.73	0.7
	II	$\frac{q}{2\pi k}\left[\frac{f_{y_{\max_{\mathrm{II}}}}(\mathrm{Ry}_{T_{\mathrm{HAZ}}})}{T_{\mathrm{HAZ}} - T_0} - \frac{f_{y_{\max_{\mathrm{II}}}}(\mathrm{Ry}_{T_{\mathrm{m}}})}{T_{\mathrm{m}} - T_0}\right]$	$\left[1 + \left(\sqrt{\frac{\mathrm{eRy}}{2}}\right)^{-n}\right]^{\frac{1}{n}}$		
Δy_{HAZ}	I	$\Delta y_{\mathrm{HAZ}} \approx \sqrt{\frac{q\alpha}{2\mathrm{e}\pi k U}} \frac{T_{\mathrm{m}} - T_{\mathrm{HAZ}}}{\left(T_{\mathrm{i}} - T_0\right)^{\frac{3}{2}}}$	$\left[1 + \left(\sqrt{\frac{1}{2\mathrm{eRy}}}\right)^{n}\right]^{\frac{1}{n}}$	3.08	6.1
		$T_{\mathrm{i}} - T_0 = \left[\sqrt{\left(T_{\mathrm{HAZ}} - T_0\right)\left(T_{\mathrm{m}} - T_0\right)} \frac{\sqrt{T_{\mathrm{HAZ}} - T_0} + \sqrt{T_{\mathrm{m}} - T_0}}{2}\right]^{2/3}$			*
	II	$\Delta y_{\mathrm{HAZ}} \approx \frac{q\left(T_{\mathrm{m}} - T_{\mathrm{HAZ}}\right)}{2\pi k (T_{\mathrm{i}} - T_0)}$	$\left[1 + \left(\sqrt{\frac{1}{2\mathrm{eRy}}}\right)^{-n}\right]^{\frac{1}{n}}$	3.08	6.1
		$T_{\mathrm{i}} - T_0 = \sqrt{\left(T_{\mathrm{HAZ}} - T_0\right)\left(T_{\mathrm{m}} - T_0\right)}$			*

* using these intermediate temperatures the calculation using the derivative is exactly the same as that using differences

Table 6.2: Summary of thermal characteristics and correction factors derived from a moving Gaussian surface source model.

Variable	Regime	Asymptotic	Correction factor	n	Error[%]
$T_{\max} - T_0$	V	$\sqrt{\frac{1}{8\pi}}\frac{I_m q U}{\pi k \alpha}\left(\frac{U\sigma}{2\alpha}\right)^{-1.5}$	$\left[1+\left(\frac{\pi}{T_m}\sqrt{\frac{U\sigma}{8\alpha}}\right)^{n}\right]^{\frac{1}{n}}$	-1.95	1.9
	VI	$\frac{1}{8\pi}\frac{q}{k\sigma}$	$\left[1+\left(\frac{\pi}{T_m}\sqrt{\frac{U\sigma}{8\alpha}}\right)^{-n}\right]^{\frac{1}{n}}$		
$x_{\max}$	V	-0.7650σ	$\left[1+\left(\frac{1.307U\sigma}{2\alpha}\right)^{n}\right]^{\frac{1}{n}}$	-0.935	0.47
	VI	$-\frac{U\sigma^2}{2\alpha}$	$\left[1+\left(\frac{1.307U\sigma}{2\alpha}\right)^{-n}\right]^{\frac{1}{n}}$		
$\sigma_{\max}$	V	$\frac{\alpha}{\pi U}\left[\frac{qUI_m}{k\alpha\,(T-T_0)}\right]^{2/3}$	$\left\{1+\left[\left(\frac{\pi}{2}\right)^{\frac{5}{6}}\left({I_m}^2 T^*\right)^{-\frac{1}{3}}\right]^{n}\right\}^{1/n}$	-2.40	1.40
	VI	$\sqrt{\frac{1}{8\pi}}\frac{q}{k\,(T-T_0)}$	$\left\{1+\left[\left(\frac{\pi}{2}\right)^{\frac{5}{6}}\left({I_m}^2 T^*\right)^{-\frac{1}{3}}\right]^{-n}\right\}^{1/n}$		
$z_{\max}$	II	$\frac{q}{2\pi k\,(T_c-T_0)}$	$f(\mathrm{Ry})\cdot g(\mathrm{Ry},\sigma^*)$	$n_1=-1.47$	
f		$\left[1+\left(\sqrt{\frac{2}{\mathrm{eRy}}}\right)^{n_1}\right]^{1/n_1}$		$n_2=-1.96$	9.7
				$n_3=-3.22$	***
g		$\left\{1+\left\{\frac{\pi}{2}\ln\left(\frac{\sigma^*_{\max}}{\sigma^*}\right)\left[1+\left(1.495\mathrm{Ry}^{-\frac{1}{6}}\right)^{n_3}\right]^{1/n_3}\right\}^{n_2}\right\}^{1/n_2}$		**	

* Asymptotic constant $I_m = 1.280$.

** n for $\sigma_{\max}$ is adjusted to -2.46.

*** Valid for $\sigma^*/\sigma^*_{\max} \leq 0.9$ and $\mathrm{Ry} \leq 1000$.

6.2 Future Work

The following analysis can continue this research to develop correction factors for other potential secondary phenomena:

- The consideration of an intermediate plate thickness can be addressed by blending Rosenthal's thick plate solution with the 2D solution of a moving point heat source (often called as Rosenthal's thin plate solution). 2D blending technique is required to blend functions dependent on two or more dimensionless groups.

- Address the role of phase transformations in the temperature field and quantify

its effect on isotherm characteristics with an additional correction factor.

- Apply the methodology of asymptotic analysis and blending to distributed heat sources other than Gaussian surface source. For example, a uniform distributed rectangle source is a more realistic representation of a top-hat (or flat top) beam profile in the laser scanning or drilling process.

Bibliography

[1] A. Acrivos, "On the Solution of the Convection Equation in Laminar Boundary Layer Flows," *Chemical Engineering Science*, vol. 17, no. 6, pp. 457–465, 1962.

[2] A. Acrivos, "A Rapid Method for Estimating the Shear Stress and the Separation Point in Laminar Incompressible Boundary-Layer Flows," *Journal of the Aerospace Sciences*, vol. 27, no. 4, pp. 314–315, 1960.

[3] C. M. Adams, "Cooling Rates and Peak Temperatures in Fusion Welding," *Welding Journal*, vol. 37, no. 5, pp. 210–215, 1958.

[4] S. Ahn and S. Kang, "Dissolution phenomena in the ti (c0. 7n0. 3)–wc–ni system," *International Journal of Refractory Metals and Hard Materials*, vol. 26, no. 4, pp. 340–345, 2008.

[5] O. M. Akselsen and G. Sagmo, "Technical Report STF34 A89147," Sintef-Division of Metallurgy, Trondheim(Norway), Tech. Rep., 1989.

[6] Y. Arata, K. Nishiguchi, T. Ohji, and N. Kohsai, "Weldability Concept on Hardness Prediction (Materials, Metallurgy, Weldability)," *Transactions of JWRI*, vol. 8, no. 1, pp. 43–52, 1979.

[7] ASME Section IX: Boiler and Pressure Vessel Code, *Qualification Standard for Welding and Brazing Procedures, Welders, Brazers, and Welding and Brazing Operators*. New York: American Society of Mechanical Engineers, 2010.

[8] H. J. Aval, A. Farzadi, S. Serajzadeh, and A. H. Kokabi, "Theoretical and experimental study of microstructures and weld pool geometry during gtaw of 304 stainless steel," *The International Journal of Advanced Manufacturing Technology*, vol. 42, no. 11-12, pp. 1043–1051, 2009.

[9] AWS D1.1/D1.1M:2015, *Structural Welding Code–Steel*. the United States of America: American Welding Society, 2015.

[10] A. Bahrami and D. K. Aidun, "Modeling of Carbon Steel-Duplex Stainless Steel GTA Weld Pool," *Welding Journal*, vol. 93, no. 7, 262s–270s, 2014.

[11] E. J. Barnhouse and J. C. Lippold, "Microstructure/Property Relationships in Dissimilar Welds between Duplex Stainless Steels and Carbon Steels," *Welding Journal, Research Supplement*, vol. 77, no. 12, 477s–487s, 1998.

[12] D. A. Barry, J. Parlange, L. Li, H. Prommer, C. J. Cunningham, and F. Stagnitti, "Analytical Approximations for Real Values of the Lambert W - function," *Mathematics and Computers in Simulation*, vol. 53, pp. 95–103, 2000.

[13] A. Bejan, *Convection Heat Transfer*. Hoboken, New Jersey: John Wiley & Sons, Inc., 2013.

[14] H. K.D. H. Bhadeshia, L. E. Svensson, and B. Gretoft, "A Model for the Development of Microstructure in Low-Alloy Steel (Fe-Mn-Si-C) Weld Deposits," *Acta Metallurgica*, vol. 33, no. 7, pp. 1271–1283, 1985.

[15] J Blecher, T. Palmer, S. Kelly, and R. Martukanitz, "Identifying performance differences in transmissive and reflective laser optics using beam diagnostic tools," *Welding journal*, vol. 91, no. 7, 204S–214S, 2012.

[16] S. D. Borle, I. Le Gall, and P. F. Mendez, "Primary Chromium Carbide Fraction Control with Variable Polarity SAW," *Welding Journal*, vol. 94, no. January, pp. 1–7, 2015.

[17] N. S. Boulton and H. E. Lance-Martin, "Residual Stresses in Arc Welded Plates.," in *Proceedings of the Institution of Mechanical Engineers*, 1936, pp. 295–347.

[18] BS EN 1011-2:2001, *Welding–Recommendations for Welding of Metallic Materials–Part 2: Arc Welding of Ferritic Steels*. London: British Standards Institution, 2001.

[19] E. Buckingham, "On Physically Similar Systems; Illustrations of the Use of Dimensional Equations," *Physical Review*, vol. 4, no. 4, pp. 345–376, 1914, ISSN: 0031899X. arXiv: `arXiv:1011.1669v3`.

[20] H. S. Carslaw and J. C. Jaeger, *Conduction of heat in solids*, Second. Oxford: Clarendon Press, 1959.

[21] J. Cheng and A. Kar, "Mathematical model for laser densification of ceramic coating," *Journal of materials science*, vol. 32, no. 23, pp. 6269–6278, 1997.

[22] N. Christensen, Davies, V. de L., and K. Gjermundsen, "Distribution of Temperatures in Arc Welding," *British Welding Journal*, vol. 12, no. 2, pp. 54–75, 1965.

[23] S. W. Churchill and R. Usagi, "A general expression for the correlation of rates of transfer and other phenomena," *AIChE Journal*, vol. 18, no. 6, pp. 1121–1128, 1972, ISSN: 15475905.

[24] S. W. Churchill, "Comprehensive Correlating Equations For Heat, Mass and Momentum Transfer in Fully Developed Flow in Smooth Tubes," *Industrial & Engineering Chemistry Fundamentals*, vol. 16, no. 1, pp. 109–116, 1977.

[25] S. W. Churchill and H. H. S. Chu, "Correlating Equations for Laminar and Turbulent Free Convection From a Vertical Plate," *International Journal of Heat and Mass Transfer*, vol. 18, no. 11, pp. 1323–1329, 1975.

[26] S. W. Churchill and R. Usagi, "A Standardized Procedure for the Production of Correlations in the Form of a Common Empirical Equation," *Industrial & Engineering Chemistry Fundamentals*, vol. 13, no. 1, pp. 39–44, 1974.

[27] H. E. Cline and T. R. Anthony, "Heat treating and melting material with a scanning laser or electron beam," *Journal of Applied Physics*, vol. 48, no. 9, 1977.

[28] N. Coniglio, C. E. Cross, T. Michael, and M. Lammers, "Defining a Critical Weld Dilution to Avoid Solidification Cracking in Aluminum," *Welding Journal*, vol. 87, no. 8, 237s–247s, 2008.

[29] R. M. Corless, G. H. Gonnet, D. E. G. Hare, D. J. Jeffrey, and D. E. Knuth, "On the Lambert W function," *Advances in Computational Mathematics*, vol. 5, no. 1, pp. 329–359, 1996.

[30] CSA W59–13, *Welded Steel Construction (Metal Arc Welding)*. Canada: Canadian Standards Association, 2013.

[31] J. A. Dantzig and C. L. Tucker, *Modeling in Materials Processing*. Cambridge, England: Cambridge University Press, 2001, p. 384.

[32] D. Darmadi, J. Norrish, and A. K. Tieu, "Analytic and finite element solutions for temperature profiles in welding using varied heat source models," *World Academy of Science, Engineering and Technology*, vol. 81, pp. 154–162, 2011.

[33] J. N. DuPont, "Solidification of an Alloy 625 Weld Overlay," *Metallurgical and Materials Transactions A*, vol. 27A, no. 11, pp. 3612–3620, 1996.

[34] J. N. DuPont and A. R. Marder, "Thermal Efficiency of Arc Welding Processes," *Welding Journal-Including Welding Research Supplement*, vol. 74, no. 12, 406s–416s, 1995.

[35] F. Durst, S. Ray, B. Ünsal, and O. A. Bayoumi, "The Development Lengths of Laminar Pipe and Channel Flows," *Journal of Fluids Engineering*, vol. 127, no. 6, pp. 1154–1160, 2005.

[36] T. W. Eagar and N. S. Tsai, "Temperature Fields Produced by Traveling Distributed Heat Sources," *Welding Journal*, vol. 62, no. 12, pp. 346–355, 1983, ISSN: 00432296.

[37] K. E. Easterling, *Introduction to the physical metallurgy of welding*. Butterworth Heinemann, 1992, p. 270.

[38] J. W. Elmer, W. H. Giedt, and T. W. Eagar, "The Transition from Shallow to Deep Penetration during Electron Beam Welding," *Welding Journal, Research Supplement*, vol. 69, no. 5, 167s–176s, 1990.

[39] M. H. Farshidianfar, "Real-time closed-loop control of microstructure and geometry in laser materials processing," PhD thesis, University of Waterloo, 2017.

[40] P. S. Fedkiw and J. Newman, "Mass-Transfer Coefficients in Packed Beds at Very Low Reynolds Numbers," *International Journal of Heat and Mass Transfer*, vol. 25, no. 7, pp. 935–943, 1982.

[41] Z. R. Francis, "The effects of laser and electron beam spot size in additive manufacturing processes," PhD thesis, Carnegie Mellon University, 2017.

[42] E. Friedman, "Thermomechanical Analysis of the Welding Process Using the Finite Element Method," *Journal of Pressure Vessel Technology*, vol. 97, no. 3, pp. 206–213, 1975.

[43] P. W. Fuerschbach, "Measurement and Prediction of Energy Transfer Efficiency in Laser Beam Welding," *Welding Journal, Research Supplement*, vol. 75, no. 1, pp. 24–34, 1996.

[44] P. W. Fuerschbach and G. A. Knorovsky, "A Study of Melting Efficiency in Plasma Arc and Gas Tungsten Arc Welding," *Welding Journal*, vol. 70, no. 11, pp. 287–297, 1991.

[45] P. W. Fuerschbach and G. R. Eisler, "Determination of Material Properties for Welding Models by Means of Arc Weld Experiments," in *6th Intl. Trends in Welding Research*, Pine Mountain, Georgia, 2002.

[46] J. W. Gibbs, C. Schlacher, A. Kamyabi-Gol, P. Mayr, and P. F. Mendez, "Cooling Curve Analysis as an Alternative to Dilatometry in Continuous Cooling Transformations," *Metallurgical and Materials Transactions A*, vol. 46A, no. 1, pp. 148–155, 2015.

[47] J. Goldak, M. Asadi, and R. G. Alena, "Why Power per Unit Length of Weld Does Not Characterize a Weld?" *Computational Materials Science*, vol. 48, no. 2, pp. 390–401, 2010, ISSN: 09270256.

[48] J. Goldak, A. Chakravarti, and M. Bibby, "A New Finite Element Model for Welding Heat Sources," *Metallurgical Transactions B*, vol. 15, no. 2, pp. 299–305, 1984, ISSN: 03602141.

[49] M. Grams and P. F. Mendez, "Quantification of root pass residual stresses in pipeline girth welds," in *Fabtech/AWS Annual Meeting*, 2017.

[50] B. A. Graville, "Weld Cooling Rates and Heat-Affected Zone Hardness in a Carbon Steel," *Welding Journal, Research Supplement*, vol. 52, no. 9, 377s–385s, 1973.

[51] G. N. Greaves, A. L. Greer, R. S. Lakes, and T. Rouxel, "Poisson's ratio and modern materials," *Nat Mater*, vol. 10, no. 11, pp. 823–837, 2011, ISSN: 1476-1122.

[52] M. L. Greeff and M. d. Toit, "Looking at the Sensitization of 11-12 % Chromium EN 1.4003 Stainless Steels during Welding," *Welding Journal*, vol. 85, no. 11, 243s–251s, 2006.

[53] D. Grewell and A. Benatar, "Modeling Heat Flow For A Moving Heat Source To Describe Scan Micro-Laser Welding," in *ANTEC*, 2003, pp. 1045–1050.

[54] R. J. Grosh, E. A. Trabant, and G. A. Hawkins, "Temperature Distribution in Solids of Variable Thermal Properties Heated by Moving Heat Sources," *Quarterly of Applied Mathematics*, vol. 13, no. 2, pp. 161–167, 1955.

[55] X. He, P. W. Fuerschbach, and T. DebRoy, "Heat Transfer and Fluid Flow during Laser Spot Welding of 304 Stainless Steel," *Journal of Physics D: Applied Physics*, vol. 36, no. 12, pp. 1388–1398, 2003.

[56] K. Heller, S. Kessler, F. Dorsch, P. Berger, and T. Graf, "Analytical Description of the Surface Temperature for the Characterization of Laser Welding Processes," *International Journal of Heat and Mass Transfer*, vol. 106, pp. 958–969, 2017.

[57] W. F. Hess, L. L. Merrill, E. F. Nippes, and A. P. Bunk, "The Measurement of Cooling Rates Associated with Arc Welding and Their Application to the Selection of Optimum Welding Conditions," *Welding Journal*, vol. 22, no. 9, pp. 377–422, 1943.

[58] A. Hoadley and M. Rappaz, "A thermal model of laser cladding by powder injection," *Metallurgical transactions B*, vol. 23, no. 5, pp. 631–642, 1992.

[59] W. Hofmeister, M. Griffith, M. Ensz, and J. Smugeresky, "Solidification in Direct Metal Deposition by LENS Processing," *The Journal of The Minerals, Metals & Materials Society*, vol. 53, no. 9, pp. 30–34, 2001.

[60] Z. B. Hou and R. Komanduri, "General solutions for stationary/moving plane heat source problems in manufacturing and tribology," *International Journal of Heat and Mass Transfer*, vol. 43, no. 10, pp. 1679–1698, 2000, ISSN: 00179310.

[61] M. Inagaki, "Welding Conditions of Steels and Cooling Time near the Fusion Line (Report 1)," *Journal of the Japan Welding Society*, vol. 27, no. 12, pp. 716–722, 1958.

[62] M. Inagaki, H. Nakamura, and A. Okada, "Studies of Cooling Processes in the Cases of Welding with Coated Electrode and Submerged Arc Welding," *Journal of the Japan Welding Society*, vol. 34, no. 10, pp. 1064–1075, 1965.

[63] J. C. Ion, *Laser Processing of Engineering Materials: Principles, Procedure and Industrial Application*. Butterworth-Heinemann, Oxford: Elsevier, 2005.

[64] F Jackson, "Moving Heat Sources With Change of Phase," *Journal of Heat Transfer*, vol. 87, no. 3, pp. 329–332, 1965.

[65] J. C. Jaeger, "Moving Sources of Heat and the Temperature of Sliding Contacts," *Proceeding of the Royal Society of New South Wales*, vol. 76, pp. 203–224, 1942.

[66] C. L. Jenney and A. O'Brien, *Welding Handbook, Volume 1 - Welding Science and Technology (9th Edition)*. American Welding Society (AWS), 2001.

[67] P. Jhaveri, W. G. Moffatt, and C. M. Adams, "The Effect of Plate Thickness and Radiation on Heat Flow in Welding and Cutting," *Welding Journal, Research Supplement*, vol. 41, no. 1, pp. 12–16, 1962.

[68] A. T. A. Kamyabi-Gol and P. F. Mendez, "The Evolution of the Fraction of Individual Phases During a Simultaneous Multiphase Transformation from Time – Temperature Data," *Metallurgical and Materials Transactions A*, vol. 46, no. 2, pp. 622–638, 2015.

[69] T. Kasuya and N. Yurioka, "Prediction of Welding Thermal History by a Comprehensive Solution," *Welding Journal*, vol. 72, no. 3, pp. 107–115, 1993.

[70] M. J. Kim, "Transient evaporative laser-cutting with boundary element method," *Applied Mathematical Modelling*, vol. 25, no. 1, pp. 25–39, 2000.

[71] W. E. King, A. T. Anderson, R. M. Ferencz, N. E. Hodge, C. Kamath, S. A. Khairallah, and A. M. Rubenchik, "Laser powder bed fusion additive manufacturing of metals; physics, computational, and materials challenges," *Applied Physics Reviews*, vol. 2, no. 4, p. 041 304, 2015.

[72] R Komanduri and Z. B Hou, "Thermal Analysis of the Arc Welding Process : Part I . General Solutions," *Metallurgical and Materials Transactions B*, vol. 31, no. 6, pp. 1353–1370, 2000.

[73] R. Komanduri and Z. B. Hou, "Thermal analysis of the laser surface transformation hardening process," *International Journal of Heat and Mass Transfer*, vol. 44, no. 15, pp. 2845–2862, 2001, ISSN: 0017-9310.

[74] R Komanduri and Z. Hou, "Thermal analysis of the laser surface transformation hardening process," *International Journal of heat and mass transfer*, vol. 44, no. 15, pp. 2845–2862, 2001.

[75] S. Kou, *Welding Metallurgy*, 2nd ed. Hoboken, New Jersey: John Wiley & Sons, Inc., 2003, pp. 234–235.

[76] S. Kou, D. K. Sun, and Y. P. Le, "A fundamental study of laser transformation hardening," *Metallurgical Transactions A*, vol. 14, no. 3, pp. 643–653, 1983.

[77] W. B. Krantz, *Scaling Analysis in Modeling Transport and Reaction Processes: A Systematic Approach to Model Building and the Art of Approximation*. New York: John Wiley & Sons, 2007.

[78] J. Lawrence, "An analysis of the beam interaction characteristics of selected lasers with an alpha-alumina bioceramic," *Optics and lasers in engineering*, vol. 41, no. 3, pp. 505–514, 2004.

[79] J. F. Li, L. Li, and F. H. Stott, "Comparison of volumetric and surface heating sources in the modeling of laser melting of ceramic materials," *International journal of heat and mass transfer*, vol. 47, no. 6-7, pp. 1159–1174, 2004.

[80] T. J. Lienert, S. S. Badu, T. A. Siewert, and V. L. Acoff, *ASM Handbook*, ser. Volume 06A Welding Fundamentals and Processes. Materials Park, Ohio: ASM International, 2011.

[81] W. Liu and J. N. DuPont, "Effects of Melt-Pool Geometry on Crystal Growth and Microstructure Development in Laser Surface-Melted Superalloy Single Crystals . Mathematical Modeling of Single-Crystal Growth in a Melt Pool (Part I)," *Acta Materialia*, vol. 52, no. 16, pp. 4833–4847, 2004.

[82] Y. Lu and P. F. Mendez, "Characteristic values of the temperature field induced by a moving line heat source," *International Journal of Heat and Mass Transfer*, p. 120 671, 2020.

[83] Y. Lu and P. F. Mendez, "The effect of surface heat losses on isotherm trailing length and cooling rate," 2021.

[84] Y. Lu, Y. Wang, and P. F. Mendez, "Width of thermal features induced by a 2-d moving heat source," *International Journal of Heat and Mass Transfer*, vol. 156, p. 119 793, 2020.

[85] Y.-F. Lu, "Heat flow in substrates induced by a scanning laser beam," *Journal of applied physics*, vol. 71, no. 8, pp. 3701–3712, 1992.

[86] N. D. Malmuth, W. F. Hall, B. I. Davis, and C. D. Rosen, "Transient Thermal Phenomena and Weld Geometry in GTAW," *Welding Journal, Research Supplement*, vol. 53, no. 9, pp. 388–400, 1974.

[87] O. Manca, B. Morrone, and V. Naso, "Quasi-steady-state three-dimensional temperature distribution induced by a moving circular gaussian heat source in a finite depth solid," *International Journal of Heat and Mass Transfer*, vol. 38, no. 7, pp. 1305–1315, 1995.

[88] K. Marcin, P. Wieslawa, and S. Sebastian, "Modelling of laser beam heat source based on experimental research of yb : Yag laser power distribution," *International Journal of Heat and Mass Transfer*, vol. 83, 2015.

[89] J. Mazumder and W. M. Steen, "Heat transfer model for cw laser material processing," *Journal of Applied Physics*, vol. 51, no. 2, pp. 941–947, 1980.

[90] P. F. Mendez, "Synthesis and generalisation of welding fundamentals to design new welding technologies: status, challenges and a promising approach," *Science and Technology of Welding and Joining*, vol. 16, no. 4, pp. 348–356, 2011, ISSN: 1362-1718.

[91] P. F. Mendez and T. W. Eagar, "Order of Magnitude Scaling: A Systematic Approach to Approximation and Asymptotic Scaling of Equations in Engineering," *Journal of Applied Mechanics*, vol. 80, no. 1, p. 011 009, 2013, ISSN: 0021-8936.

[92] P. F. Mendez, K. E. Tello, and S. S. Gajapathi, "Generalization and communication of welding simulations and experiments using scaling analysis," in *9th International Conference on Trends in Welding Research*, vol. 1, Chicago, Illinois, USA: ASM International, 2012, pp. 249–258.

[93] P. F. Mendez, "Characteristic Values in the Scaling of Differential Equations in Engineering," *Journal of Applied Mechanics, Transactions ASME*, vol. 77, no. 6, 2010, ISSN: 00218936.

[94] P. F. Mendez, N. Barnes, K. Bell, S. D. Borle, S. S. Gajapathi, S. D. Guest, H. Izadi, A. K. Gol, and G. Wood, "Welding processes for wear resistant overlays," *Journal of Manufacturing Processes*, vol. 16, no. 1, pp. 4–25, 2014.

[95] P. F. Mendez, R. Furrer, R. Ford, and F. Ordóñez, "Scaling Laws as a Tool of Materials Informatics," *JOM*, vol. 60, no. 3, pp. 60–66, 2008.

[96] P. F. Mendez, Y. Lu, and Y. Wang, "Scaling Analysis of a Moving Point Heat Source in Steady- State on a Semi-Infinite Solid," *Journal of Heat Transfer*, vol. 140, no. 8, p. 081 301, 2018.

[97] P. F. Mendez, Y. Lu, and Y. Wang, "Scaling Analysis of a Moving Point Heat Source in Steady-State on a Semi-Infinite Solid," *Journal of Heat Transfer*, vol. 140, no. 8, p. 081 301, 2018.

[98] P. F. Mendez and F. Ordonez, "Scaling Laws from Statistical Data and Dimensional Analysis," *Journal of Applied Mechanics, Transactions ASME*, vol. 72, no. 5, pp. 648–657, 2005, ISSN: 00218936.

[99] P. F. Mendez, K. E. Tello, and T. J. Lienert, "Scaling of Coupled Heat Transfer and Plastic Deformation around the Pin in Friction Stir Welding," *Acta Materialia*, vol. 58, no. 18, pp. 6012–6026, 2010, ISSN: 1359-6454.

[100] P. Mendez, "Reduced order models for welding and solidification processes," in *IOP Conference Series: Materials Science and Engineering*, IOP Publishing, vol. 861, 2020, p. 012 003.

[101] R. W. Messler Jr, *Principles of welding: processes, physics, chemistry, and metallurgy*. New York: John Wiley & Sons, 2004.

[102] J. Miettinen, "Calculation of Solidification-Related Thermophysical Properties for Steels," *Metallurgical and Materials Transactions B*, vol. 28, no. 2, pp. 281–297, 1997.

[103] J. E. Moody and R. H. Hendel, "Temperature profiles induced by a scanning cw laser beam," *Journal of Applied Physics*, vol. 53, no. 6, pp. 4364–4371, 1982.

[104] P. E. Murray, "Stability of Droplets in Gas Metal Arc Welding," *Science and Technology of Welding and Joining*, vol. 5, no. 4, pp. 221–226, 2000.

[105] P. E. Murray, "Selecting Parameters for GMAW Using Dimensional Analysis," *Welding Journal*, vol. 81, no. 7, pp. 125–131, 2002.

[106] P. E. Murray and A. Scotti, "Depth of Penetration in Gas Metal Arc Welding," *Science and Technology of Welding and Joining*, vol. 4, no. 2, pp. 112–117, 1999.

[107] Y. S. Muzychka and M. M. Yovanovich, "Thermal Resistance Models for Non-Circular Moving Heat Sources on a Half Space," *Journal of Heat Transfer*, vol. 123, no. 4, pp. 624–632, 2001, ISSN: 00221481.

[108] P. S. Myers, O. A. Uyehara, and G. L. Borman, "Fundamentals of Heat Flow in Welding," *Welding Research Council Bulletin*, no. 123, pp. 1–46, 1967.

[109] O. R. Myhr and Ø. Grong, "Dimensionless Maps for Heat Flow Analyses in Fusion Welding," *Acta Metallurgica Et Materialia*, vol. 38, no. 3, pp. 449–460, 1990, ISSN: 09567151.

[110] O. R. Myhr and Ø. Grong, "Process Modelling Applied to 6082-T6 Aluminium Weldments–II. Applications of Model," *Acta Metallurgica et Materialia*, vol. 39, no. 11, pp. 2703–2708, 1991.

[111] N. T. Nguyen, A. Ohta, K. Matsuoka, N. Suzuki, and Y. Maeda, "Analytical Solutions for Transient Temperature of Semi-Infinite Body Subjected to 3-D Moving Heat Sources," *Welding Journal, Research Supplement*, vol. 78, no. August, 265s–274s, 1999.

[112] R. W. Niles and C. E. Jackson, "Weld Thermal Efficiency of the GTAW Process," *Welding Journal*, vol. 54, no. 1, pp. 25–32, 1975.

[113] F. F. Noecker II and J. N. DuPont, "Microstructural Development and Solidification Cracking Susceptibility of Cu Deposits on Steel : Part I," *Journal of Materials Science*, vol. 42, no. 2, pp. 495–509, 2007.

[114] A. C. Nunes, "An Extended Rosenthal Weld Model," *Welding Journal, Research Supplement*, vol. 62, no. 6, pp. 165–170, 1983.

[115] A. Okada, "Application of Melting Efficiency Welding and its Problems," *Journal of the Japan Welding Society*, vol. 46, no. 2, pp. 53–61, 1977.

[116] H. Pantsar and V. Kujanpää, "Diode laser beam absorption in laser transformation hardening of low alloy steel," *Journal of laser Applications*, vol. 16, no. 3, pp. 147–153, 2004.

[117] V. Pavelic, R. Tanbakuchi, O. A. Uyehara, and P. S. Myers, "Experimental and computed temperature histories in gas tungsten-arc welding of thin plates," *Welding Journal Research Supplement*, vol. 48, 1969.

[118] W. Perret, C. Schwenk, and M. Rethmeier, "Comparison of Analytical and Numerical Welding Temperature Field Calculation," *Computational Materials Science*, vol. 47, no. 4, pp. 1005–1015, 2010, ISSN: 0927-0256.

[119] P. Peyre, P. Aubry, R. Fabbro, R. Neveu, and A. Longuet, "Analytical and Numerical Modelling of the Direct Metal Deposition Laser Process," *Journal of Physics D: Applied Physics*, vol. 41, no. 2, p. 025 403, 2008.

[120] A. J. Pinkerton and L. Li, "Modelling the Geometry of a Moving Laser Melt Pool and Deposition Track via Energy and Mass Balances," *Journal of Physics D: Applied Physics*, vol. 37, no. 14, pp. 1885–1895, 2004.

[121] K. Poorhaydari, B. M. Patchett, and D. G. Ivey, "Estimation of Cooling Rate in the Welding of Plates with Intermediate Thickness," *Welding Journal*, vol. 84, no. 10, 149–s–155–s, 2005.

[122] K. Rajan, C. Suh, and P. F. Mendez, "Principal Component Analysis and Dimensional Analysis as Materials Informatics Tools to Reduce Dimensionality in Materials Science and Engineering," *Statistical Analysis and Data Mining*, vol. 1, no. 6, pp. 362–371, 2009.

[123] D. Rivas and S. Ostrach, "Scaling of Low-Prandtl-Number Thermocapillary Flows," *International Journal of Heat and Mass Transfer*, vol. 35, no. 6, pp. 1469–1479, 1992.

[124] A. Robert and T. DebRoy, "Geometry of Laser Spot Welds from Dimensionless Numbers," *Metallurgical and Materials Transactions B*, vol. 32, no. 5, pp. 941–947, 2001.

[125] O. F. T. Roberts, "The Theoretical Scattering of Smoke in a Turbulent Atmosphere," *Proceedings of the Royal Society of London. Series A, Containing Papers of a Mathematical and Physical Character*, vol. 104, no. 728, pp. 640–654, 1923.

[126] D. Rosenthal, "The Theory of Moving Sources of Heat and Its Application to Metal Treatments," *Transactions of the A.S.M.E.*, vol. 68, pp. 849–866, 1946.

[127] D. Rosenthal, "Etude Théorique du Régime Thermique Pendant La Soudure à L'Arc," in *Comptes Rendus (2eme Congres National des Sciences)*, 1935, pp. 1277–1292.

[128] D. Rosenthal, "Mathematical Theory of Heat Distribution During Welding and Cutting," *Welding Journal*, vol. 20, no. 5, pp. 220–234, 1941.

[129] D. Rosenthal and R. Schmerber, "Thermal Study of Arc Welding. Experimental Verification of Theoretical Formulas.," *The Welding Journal*, vol. 17, no. 4, pp. 2–8, 1938.

[130] G. G. Roy, R. Nandan, and T. DebRoy, "Dimensionless Correlation to Estimate Peak Temperature during Friction Stir Welding," *Science and Technology of Welding and Joining*, vol. 11, no. 5, pp. 606–608, 2006.

[131] N. N. Rykalin, *Calculation of Heat Flow in Welding*. Moscow: Mashgis, 1951.

[132] M. F. Schneider and M. F. Schneider, "Laser cladding with powder," PhD thesis, University of Twente, 1998.

[133] P. Seyffarth, B. Meyer, and A. Scharff, *Grosser Atlas Schweiss-ZTU-Schaubilder*, ser. Fachbuchreihe Schweisstechnik. Düsseldorf: Deutscher Verlag für Schweisstechnik, 1992, p. 175.

[134] P. S. Sheng and V. S. Joshi, "Analysis of heat-affected zone formation for laser cutting of stainless steel," *Journal of materials processing technology*, vol. 53, no. 3-4, pp. 879–892, 1995.

[135] S. Skvarenina and Y. C. Shin, "Predictive modeling and experimental results for laser hardening of aisi 1536 steel with complex geometric features by a high power diode laser," *Surface and Coatings Technology*, vol. 201, no. 6, pp. 2256–2269, 2006.

[136] E. Soylemez, J. L. Beuth, and K. Taminger, "Controlling Melt Pool Dimensions over a Wide Range of Material Deposition Rates in Electron Beam Additive Manufacturing," in *Proceedings of 21st Solid Freeform Fabrication Symposium, Austin, TX, Aug*, 2010, pp. 571–582.

[137] W. M. Steen and C. Courtney, "Surface heat treatment of ens steel using a 2kw continuous-wave co2 laser," *Metals Technology*, vol. 6, no. 1, pp. 456–462, 1979.

[138] L. E. Svensson, B. Gretoft, and H. K.D. H. Bhadeshia, "An Analysis of Cooling Curves from the Fusion Zone of Steel Weld Deposits," *Scandinavian Journal of Metallurgy*, vol. 15, no. 97, pp. 97–103, 1986.

[139] P Tekriwal and J Mazumder, "Finite Element Analysis of Three-Dimensional Transient Heat Transfer in GMA Welding," *Welding Journal, Research Supplement*, vol. 67, no. 7, pp. 150–156, 1988.

[140] K. Tello, U. Duman, and P. Mendez, "Scaling Laws for the Welding Arc, Weld Penetration and Friction Stir Welding," in *Trends in Welding Research, Proceedings of the 8th International Conference*, 2009, pp. 172–181.

[141] S. M. Thompson, L. Bian, N. Shamsaei, and A. Yadollahi, "An overview of direct laser deposition for additive manufacturing; part i: Transport phenomena, modeling and diagnostics," *Additive Manufacturing*, vol. 8, pp. 36–62, 2015.

[142] X. Tian, Y. Liu, W. Deng, and G. Liu, "Sensitivity analysis for process parameters influencing electric arc cutting," *The International Journal of Advanced Manufacturing Technology*, vol. 78, no. 1-4, pp. 481–492, 2015.

[143] X. Tian and F. E. Kennedy Jr, "Maximum and average flash temperatures in sliding contacts," *Journal of Tribology*, vol. 116, 1994.

[144] C. L. Tsai, "Heat Flow in Fusion Welding," *Welding, Brazing, and Soldering, ASM Handbook, ASM International*, vol. 6, pp. 7–18, 1993.

[145] N. S. Tsai and T. W. Eagar, "Distribution of the heat and current fluxes in gas tungsten arcs," *Metallurgical transactions B*, vol. 16, no. 4, pp. 841–846, 1985.

[146] N. Tsai, "Heat distribution and weld bead geometry in arc welding," PhD thesis, Massachusetts Institute of Technology, 1983.

[147] M. Ushio, T. Ishimura, F. Matsuda, and Y. Arata, "Theoretical Calculation on Shape of Fusion Boundary and Temperature Distribution around Moving Heat Source (Report I)," *Transactions of JWRI*, vol. 6, no. 1, pp. 1–6, 1977.

[148] Y Wang, Y Lu, M Grams, A Cesaro, and P. Mendez, *Asymptotics and blending in the modeling of welding*, 2019.

[149] Y. Wang, Y. Lu, and P. F. Mendez, "Scaling expressions of characteristic values for a moving point heat source in steady state on a semi-infinite solid," *International Journal of Heat and Mass Transfer*, vol. 135, pp. 1118–1129, 2019.

[150] Y. Wang, Y. Lu, and P. F. Mendez, "Prediction of peak temperature under a moving gaussian surface heat source," 2021.

[151] Y. Wang and J. Lin, "Characterization of the Laser Cleaving on Glass Sheets with a Line-Shape Laser Beam," *Optics & Laser Technology*, vol. 39, no. 5, pp. 892–899, 2007.

[152] T. Washio and H. Motoda, "Extension of Dimensional Analysis for Scale-types and its Application to Discovery of Admissible Models of Complex Processes," in *International Workshop on Similarity Method*, 1999, pp. 129–147.

[153] A. A. Wells, "Heat flow in welding," *Welding Journal Research Supplement*, vol. 31, no. 5, 1952.

[154] H. A. Wilson, "On Convection of Heat," *Proceedings of the Cambridge Philosophical Society*, vol. 12, pp. 406–423, 1904.

[155] G. Wood and P. F. Mendez, "Disaggregated metal and carbide catchment efficiencies in laser cladding of nickel-tungsten carbide," *Welding Journal*, vol. 94, no. 11, pp. 343–350, 2015.

[156] G. Wood, S. A. Islam, and P. F. Mendez, "Calibrated expressions for welding and their application to isotherm width in a thick plate," *Soldagem & Inspeção*, vol. 19, no. 3, pp. 212–220, 2014.

[157] G. D. Wood, "Heat and mass transfer aspects of coaxial laser cladding and its application to nickel-tungsten carbide alloys," PhD thesis, University of Alberta, 2017.

[158] A. S. Wu, D. W. Brown, M. Kumar, G. F. Gallegos, and W. E. King, "An experimental investigation into additive manufacturing-induced residual stresses in 316l stainless steel," *Metallurgical and Materials Transactions A*, vol. 45, no. 13, pp. 6260–6270, 2014.

[159] K. M.-k. Yip, "Model Simplification by Asymptotic Order of Magnitude Reasoning," *Artificial Intelligence*, vol. 80, no. 2, pp. 309–348, 1996.

[160] N. Yurioka, O. Makoto, K. Tadashi, and C. Harry, "Prediction of HAZ Hardness of Transformable Steels," *Metal Construction*, vol. 19, no. 4, 217R–223R, 1987.

[161] W. Zhang, C. H. Kim, and T. DebRoy, "Heat and Fluid Flow in Complex Joints during Gas Metal Arc Welding ? Part I : Numerical Model of Fillet Welding," *Journal of Applied Physics*, vol. 95, no. 9, pp. 5210–5219, 2004.

Appendix A: MATLAB Codes

A.1 Calculating the peak temperature induced by a moving Gaussian surface source

```
clear;clc;close all
%% pick 100 points between 0.01 to 100 in log scale
   linearly
sigma =  logspace(-2,2,100);
%% calculate peak temperature and its location for each
   value in sigma
close all
tic
sigma =  logspace(-10,10,1000);
[Tmax,xmax] = arrayfun(@(x) fun_TmaxSigma(x),sigma);
toc

figure
loglog(sigma,Tmax);
figure
loglog(sigma,xmax);
format long
%% Tmax
Tmax1 = 2*1.280./sqrt(2*pi)*sigma.^(-1.5);
Tmax2 =sqrt(pi/2)*sigma.^(-1);
[N_Tmax,ME_Tmax]= blending(sigma,Tmax,Tmax1,Tmax2,-2)

%% sigmam
sigmam1 = (sqrt(2*pi)/(2*1.280)*Tmax).^(-2/3);
sigmam2 =sqrt(pi/2)*Tmax.^(-1);
[N_sigma,ME_sigma]= blending(Tmax,sigma,sigmam1,sigmam2
   ,-2)

%% xmax
xmax1 = 0.7650*sigma;
xmax2 = sigma.^(2);
```

```
[N_xmax,ME_xmax]= blending(sigma,-xmax,xmax1,xmax2,-1)

%%
function [TmaxCenter,xmaxCenter] = fun_TmaxSigma(sigma)
% Tstar is the dimensionless Gaussian temp field
% Tstar=@(x,o) 1/sqrt(2*pi)*quadgk(@(t) t.^(-1/2)./(t+o
   .^2).*exp(-0.5*(x.^2+t.^2+2.*t.*x)./(t+o.^2)),0,inf,'
   RelTol',1e-300,'AbsTol',1e-300);
%
% % xm1 and xm2 are the two asymps (negative value). Seed
   is a defined interval vector where true xmax locates
% xm1=-0.7650*sigma; xm2=-sigma.^2;
% seed=[1.1*min(xm1,xm2),0.2*max(xm1,xm2)];
%
% % seed(1) is the first item in vector seed and seed (2)
   is the second item in seed.
% [xmax,Tmax]=fminbnd(@(x) -Tstar(x,sigma),seed(1),seed(2)
   ,optimset('TolFun',1e-200,'TolX',1e-200,'MaxFunEvals
   ',100000,'MaxIter',5000));
% Tmax=-Tmax;

T = @(x,z,sigma) sqrt(2/pi)./sigma.*( ...
          integral(@(theta) exp(-((z.^2.*cot(theta).^2+cos
             (theta).^2.*(x+sigma.^2.*tan(theta).^2).^2)
             ./(2.*sigma.^2))),0,fun_theta0(x,z,sigma),'
             AbsTol',1e-300,'RelTol',1e-50) + ...
          integral(@(theta) exp(-((z.^2.*cot(theta).^2+cos
             (theta).^2.*(x+sigma.^2.*tan(theta).^2).^2)
             ./(2.*sigma.^2))),fun_theta0(x,z,sigma),pi/2,
             'AbsTol',1e-300,'RelTol',1e-50));
mdTdx =@(x,z,sigma)   integral(@(theta) (1+(-1+x./sigma
   .^2).*cos(theta).^2).*exp(-((z.^2.*cot(theta).^2+(x.*
   cos(theta)+sigma.^2.*sin(theta) .*tan(theta)).^2)./(2.*
   sigma.^2))),0,fun_theta0(x,z,sigma),'AbsTol',1e-30,'
   RelTol',1e-20) + ...
          integral(@(theta) (1+(-1+x./sigma.^2).*cos(theta
             ).^2).*exp(-((z.^2.*cot(theta).^2+(x.*cos(
             theta)+sigma.^2.*sin(theta) .*tan(theta)).^2)
             ./(2.*sigma.^2))),fun_theta0(x,z,sigma),pi/2,
             'AbsTol',1e-30,'RelTol',1e-20);
xmaxCenterSeed=[5*max(-0.7650*sigma,-sigma.^2),0.2*max
   (-0.7650*sigma,-sigma.^2)];
xmaxCenter= fzero(@(x) (mdTdx(x,0,sigma)),[xmaxCenterSeed
   (1),xmaxCenterSeed(2)],optimset('MaxFunEvals',1e10,'
   MaxIter',1e10,'TolX',1e-30,'TolFun',1e-10));
```

```
TmaxCenter = T(xmaxCenter,0,sigma);

end

%% Function to define blending with indep varible x,depend
    variable y,asymp y1,asymp y2,initial guess seed and
   output optimal blending parameter N and the mimimum max
    absolute error ME
function [optimalN,optimalME]= blending(x,y,y1,y2,seed)

fun_y =  @(n) (y1.^n+y2.^n).^(1./n);
fun_error = @(n) log(y./fun_y(n));
fun_me = @(n) max(abs(fun_error(n)));

[optimalN,optimalME]=fminsearch(@(n) fun_me(n),seed);
%% plot indep variable x, depend variable y and two asymps
    y1 and y2
figure
loglog(x,fun_y(optimalN),'-k','linewidth',2); hold on
loglog(x,y1,'-k','linewidth',1); hold on
loglog(x,y2,'-k','linewidth',1); hold on
xlabel('x')
ylabel('y')
axis([1e-10,1e10,-inf,inf])
DefaultGca
%% plot error with optimal blending parameter n against
   indep variable x in log
figure
semilogx(x,100*fun_error(optimalN),'-k','linewidth',2);
   hold on
semilogx(x,100*fun_error(0.995*optimalN),'--k','linewidth'
   ,1); hold on
semilogx(x,100*fun_error(1.005*optimalN),'-.k','linewidth'
   ,1); hold on
legend(num2str(optimalN),num2str(0.995*optimalN),num2str
   (1.005*optimalN))
xlabel('x')
ylabel('e')
axis([1e-2,1e2,-inf,inf])
DefaultGca
%% plot correction factors based on asymp y1 and y2
figure
semilogx(x,fun_y(optimalN)./y1,'-k','linewidth',2); hold
   on
semilogx(x,fun_y(optimalN)./y2,'-k','linewidth',2); hold
```

```
   on
semilogx(x,x./x*0.9,'--k','linewidth',1);
xlabel('x')
ylabel('cf')
axis([1e-2,1e2,-inf,inf])
DefaultGca
%% pick 25 n linearly from 0.7*optimal n to 1.3* optimal n
    and plot minimum max absolute error against each n in
   the list
figure
n_list =  linspace(0.8*optimalN,1.2*optimalN,51);
me_list=100*arrayfun(@(x) fun_me(x),n_list);
plot(n_list,me_list,'-k','linewidth',2);  hold on
plot([optimalN,optimalN],[0,1],'--k','linewidth',1);
xlabel('x')
ylabel('me')
DefaultGca
end


function  theta0 = fun_theta0(x,z,sigma)
% theta0 is the location of maximum exp
% solve  -1+ct.^4 .*(1-x./sigma.^2).^2+ct.^4
% .*(z./sigma.^2).^2/(1-ct.^2).^2 == 0 where  t= cos(theta
   );
% [ct0]=arrayfun(@(x,z,sigma) fminsearchbnd(@(ct) abs(-1+
   ct.^4 .*(1-x./sigma.^2).^2+ct.^4 .*(z./sigma.^2).^2/(1-
   ct.^2).^2),0.5,0,1,optimset('MaxFunEvals',1e50,'MaxIter
   ',1e50,'TolX',1e-300,'TolFun',1e-300)),x,z,sigma);
[ct0]=arrayfun(@(x,z,sigma) fminbnd(@(ct) abs(-1+ct.^4
   .*(1-x./sigma.^2).^2+ct.^4 .*(z./sigma.^2).^2/(1-ct.^2)
   .^2),0,1,optimset('TolX',1e-300)),x,z,sigma);
%     [t0,fval0]=fzero(@(t) -1+ct.^4 .*(1-x./sigma.^2)
   .;^2+ct.^4 .*(z./sigma.^2).^2/(1-ct.^2).^2,0.5);
theta0 =  acos(ct0);
end
```

A.2 Calculating the maximum isotherm depth under a moving Gaussian surface source

```
clear;clc;close all
warning off
%% Initialization
s1 = 250; s2 = 500; filename='GaussianZmaxCorse';
```

```
mul = [logspace(-3,-0.1,s1/2),logspace(-0.09,0,s1/2+1)]; %
    mul $sigma / sigma_max$
mul = mul(1:s1);
Ry = logspace(-3,3,s2);
%% Functions
% Theta0 is the location of maximum exp, solve  $$-1+ct.^4
    .*(1-x./sigma.^2).^2+ct.^4.*(z./sigma.^2).^2/(1-ct.^2)
   .^2 == 0 $$ where $$ t= cos(theta)$$;
% [t0,fval0]=fzero(@(t) -1+ct.^4 .*(1-x./sigma.^2).;^2+ct
   .^4 .*(z./sigma.^2).^2/(1-ct.^2).^2,0.5);
fun_theta0 = @(x,z,sigma)   acos(fminbnd(@(ct) abs(-1+ct
   .^4 .*(1-x./sigma.^2).^2+ct.^4 .*(z./sigma.^2).^2/(1-ct
   .^2).^2),0,1,optimset('MaxFunEvals',1e50,'MaxIter',1e50
   ,'TolX',1e-50,'TolFun',1e-30)));
% Temerpature field as function of x,z,sigma
fun_T = @(x,z,sigma) sqrt(2/pi)./sigma.*(integral(@(theta)
    exp(-((z.^2.*cot(theta).^2+cos(theta).^2.*(x+sigma
   .^2.*tan(theta).^2).^2)./(2.*sigma.^2))),0,pi/2,'
   Waypoints',fun_theta0(x,z,sigma),'AbsTol',1e-10,'RelTol
   ',1e-10));
% Negative value to dTdx
% NdTdx =  - dTdx * sigma*sqrt(pi/2). It is just for
   simiplicity.
fun_NdTdx =@(x,z,sigma)   integral(@(theta) (1+(-1+x./
   sigma.^2).*cos(theta).^2).*exp(-((z.^2.*cot(theta).^2+(
   x.*cos(theta)+sigma.^2.*sin(theta) .*tan(theta)).^2)
   ./(2.*sigma.^2))),0,pi/2,'Waypoints',fun_theta0(x,z,
   sigma),'AbsTol',1e-10,'RelTol',1e-10);

%% Variables
MaxSigma = arrayfun(@(Ry) fun_sigma_max(Ry,fun_T,fun_NdTdx
   ),Ry);
[~,MRy]  = meshgrid(mul,Ry) ;
Msigma = bsxfun(@times,mul,MaxSigma') ;
Vsigma =  reshape(Msigma,s1*s2,1);   VRy =  reshape(MRy,s1
   *s2,1);
[Vxmax,Vzmax,Vxb,VxmaxCenter,VTmaxCenter,VToldTdx,VTolT] =
    deal(nan*VRy);
parfor i =1:s1*s2
    disp(num2str(i))
    [Vxmax(i),Vzmax(i),Vxb(i),VxmaxCenter(i),VTmaxCenter(i
       ),VToldTdx(i),VTolT(i)] = fun_zmax(VRy(i),Vsigma(i)
       );
end
Mxmax   = reshape( Vxmax,s2,s1);
```

```
Mzmax   = reshape( Vzmax,s2,s1);
Mxb = reshape( Vxb ,s2,s1);
MxmaxCenter   = reshape( VxmaxCenter,s2,s1);
MTmaxCenter   = reshape( VTmaxCenter,s2,s1);
MToldTdx = reshape( VToldTdx ,s2,s1);
MTolT   = reshape( VTolT,s2,s1);
%% Plot zmax
surf(mul,Ry,Mzmax)
set(gca,'xscale','log','yscale','log','zscale','log')
%% Save Data
save(filename);

%% Maximum depth
function [xmax,zmax,xb,xmaxCenter,TmaxCenter,ToldTdx,TolT]
    = fun_zmax(Ry,sigma)
try
    % Theta0 is the location of maximum exp, solve  $$-1+
       ct.^4 .*(1-x./sigma.^2).^2+ct.^4.*(z./sigma.^2)
       .^2/(1-ct.^2).^2 == 0 $$ where $$ t= cos(theta)$$;
    fun_theta0 = @(x,z,sigma)   acos(fminbnd(@(ct) abs(-1+
       ct.^4 .*(1-x./sigma.^2).^2+ct.^4 .*(z./sigma.^2)
       .^2/(1-ct.^2).^2),0,1,optimset('MaxFunEvals',1e50,'
       MaxIter',1e50,'TolX',1e-50,'TolFun',1e-30)));
    % Temerpature field as function of x,z,sigma
    fun_T = @(x,z,sigma) sqrt(2/pi)./sigma.*(integral(@(
       theta) exp(-((z.^2.*cot(theta).^2+cos(theta).^2.*(x
       +sigma.^2.*tan(theta).^2).^2)./(2.*sigma.^2))),0,pi
       /2,'Waypoints',fun_theta0(x,z,sigma),'AbsTol',1e
       -10,'RelTol',1e-10));
    % Negative value to dTdx, NdTdx =  - dTdx * sigma*sqrt
       (pi/2). It is just for simiplicity.
    fun_NdTdx =@(x,z,sigma)   integral(@(theta) (1+(-1+x./
       sigma.^2).*cos(theta).^2).*exp(-((z.^2.*cot(theta)
       .^2+(x.*cos(theta)+sigma.^2.*sin(theta) .*tan(theta
       )).^2)./(2.*sigma.^2))),0,pi/2,'Waypoints',
       fun_theta0(x,z,sigma),'AbsTol',1e-10,'RelTol',1e
       -10);

    % Point heat source
    % FunZmaxPoint = @(Ry) (Ry.^(-1.7312) + (sqrt(2*Ry./
       exp(1))).^(-1.7312) ).^(-1/1.7312);
    % FunXmaxPoint= @(Ry) - ((Ry./exp(1)).^(-0.9990) + (Ry
       .^2).^(-0.9990) ).^(-1/0.9990);
    % FunXbPoint = @(Ry)  -Ry;
    % SigmaMax=((2*1.2798/sqrt(2*pi)*Ry).^(-2.3975*2/3)+(
```

```
        sqrt(pi/2)*Ry).^(-2.3975)).^(-1/2.3975);
    zmaxPoint =  (Ry.^(-1.7312) + (sqrt(2*Ry./exp(1)))
        .^(-1.7312) ).^(-1/1.7312);
    % Maximum temerpature at centerline
    xmaxCenterSeed=[5*max(-0.7650*sigma,-sigma.^2),0.2*max
        (-0.7650*sigma,-sigma.^2)];
    xmaxCenter= fzero(@(x) (fun_NdTdx(x,0,sigma)),[
        xmaxCenterSeed(1),xmaxCenterSeed(2)],optimset('
        MaxFunEvals',1e10,'MaxIter',1e10,'TolX',1e-30,'
        TolFun',1e-10));
    TmaxCenter = fun_T(xmaxCenter,0,sigma);
    if 1/Ry > TmaxCenter
        disp(['Temperature is too high for Ry = ',num2str(
            Ry),', sigma=',num2str(sigma)])
    end

    % Find upper and lower bounds of xmax for zmax
    xmax_ub = 0.999*xmaxCenter;
    [xb,~] = fzero(@(x) (fun_T(x,0,sigma) .*Ry - 1), [- 2*
        Ry+2*xmax_ub ,xmax_ub],optimset('MaxFunEvals',1e10,
        'MaxIter',1e10,'TolX',1e-10));
    xmax_lb = 0.99*xb + 0.01 * xmaxCenter;
    % Find xmax and zmax
    Fun_z_x_iso  = @(x) fzero(@(z) fun_T (x ,z,sigma ).*Ry
        - 1,[0,1.1*zmaxPoint],optimset('MaxFunEvals',1e10,
        'MaxIter',1e10,'TolX',1e-10));
    xmax = fzero(@(x) fun_NdTdx(x,Fun_z_x_iso(x),sigma),[
        xmax_lb,xmax_ub]);
    zmax = Fun_z_x_iso(xmax);
    % Error of T and dTdx
    ToldTdx =  fun_NdTdx(xmax,abs(zmax),sigma);
    TolT = fun_T(xmax,zmax,sigma).*Ry - 1 ;

catch
    xmax=nan;
    zmax=nan;
    xb=nan;
    xmaxCenter=nan;
    TmaxCenter=nan;
    ToldTdx=nan;
    TolT=nan;
    disp(['Fail for Ry = ',num2str(Ry),', sigma = ',
        num2str(sigma)])
end
end
```

```
%% Maximum sigma
function [sigmaMax] = fun_sigma_max(Ry,fun_T,fun_NdTdx)
SeedSigmaMax=((2*1.2798/sqrt(2*pi)*Ry).^(-2.3975*2/3)+(
   sqrt(pi/2)*Ry).^(-2.3975)).^(-1/2.3975);
xmaxCenter=@(sigma) fzero(@(x) (fun_NdTdx(x,0,sigma)),[5*
   max(-0.7650*sigma,-sigma.^2),0.2*max(-0.7650*sigma,-
   sigma.^2)],optimset('MaxFunEvals',1e10,'MaxIter',1e10,'
   TolX',1e-30,'TolFun',1e-10));
TmaxCenter=@(sigma) fun_T(xmaxCenter(sigma),0,sigma);
sigmaMax = fzero(@(sigma) TmaxCenter(sigma)*Ry - 1,[0.9*
   SeedSigmaMax,1.1*SeedSigmaMax]) ;
end
```

```
clear;clc;close all
ph = pwd;
cd ./Coarse
load('GaussianZmaxCoarse.mat')
cd(ph);
FunZmax  =  @(Ry,mul) @(p)  (Ry.^(p(1)) + (sqrt(2*Ry./exp
   (1))).^(p(1)) ).^(1/p(1)).* ...
    (1+(pi/2.*(1+(1.495*Ry.^(-1/6) ).^p(3)).^(1./p(3)).*
       log(1./mul)).^(p(2))).^(1./p(2));
[Mmul,MRy]  = meshgrid(mul,Ry) ;
FunSigmaMax =@(Ry) ((2*1.2798/sqrt(2*pi)*Ry)
   .^(-2.3975*2/3)+(sqrt(pi/2)*Ry).^(-2.3975))
   .^(-1/2.3975);
MsigmaMaxCal = FunSigmaMax(MRy);
MulCal  = Msigma./MsigmaMaxCal;
MulCal(Mmul>0.9) =nan;
FunZmaxP = FunZmax(MRy,MulCal);
FunE =@(p) log(FunZmaxP(p)./Mzmax);
FunME =@(p) max(max(abs(FunE(p))));
[pval,fval] = fminsearch(@(p) FunME(p),[-1.7,-1.6,-20])
surf(mul,Ry,FunE(pval))
set(gca,'yscale','log')
xlabel('sigma/sigmam')
axis([0,0.9,1e-3,1e3])
ylabel('Ry')
shading interp
```

Appendix B: Supporting figures for blending results in Chapter 3

B.1 Asymptotes, error map and correction factors for the maximum temperature at y_c^*

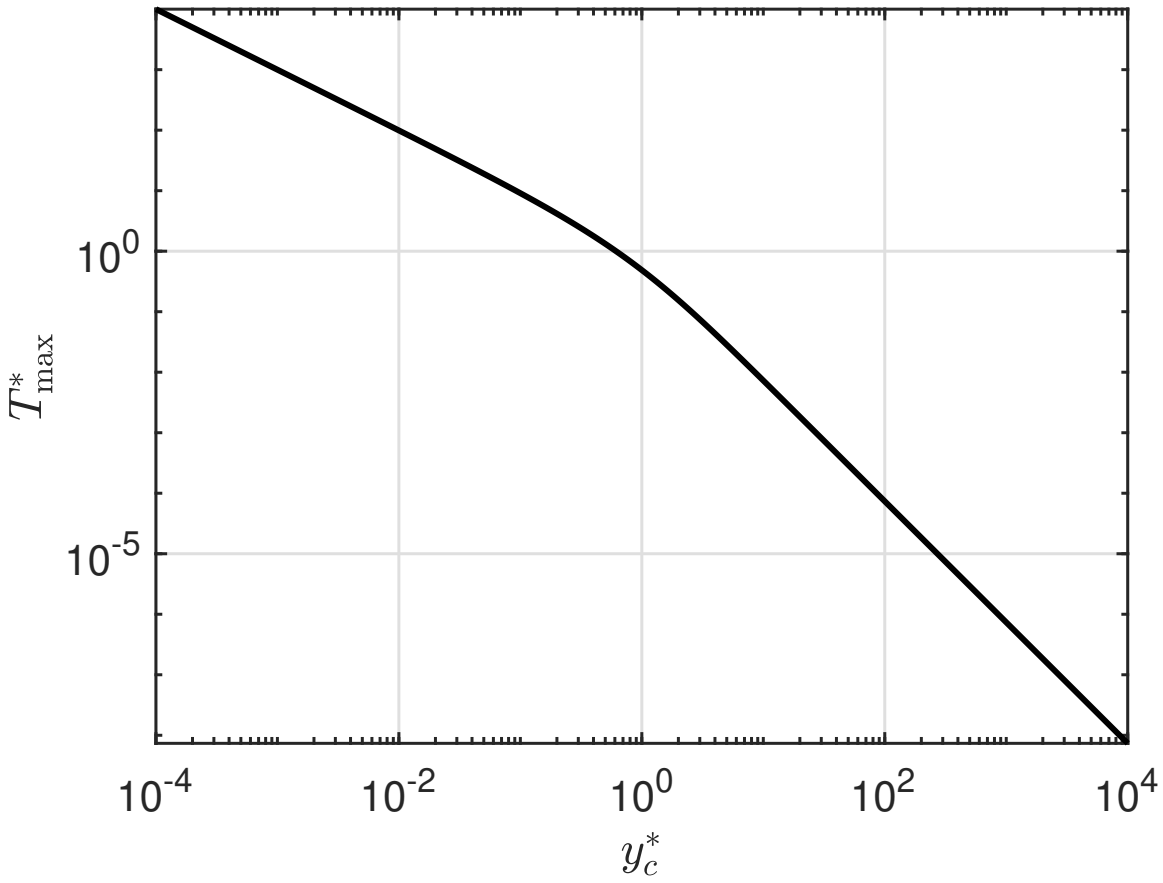

Figure B.1: Dimensionless maximum temperature as a function of y_c^*

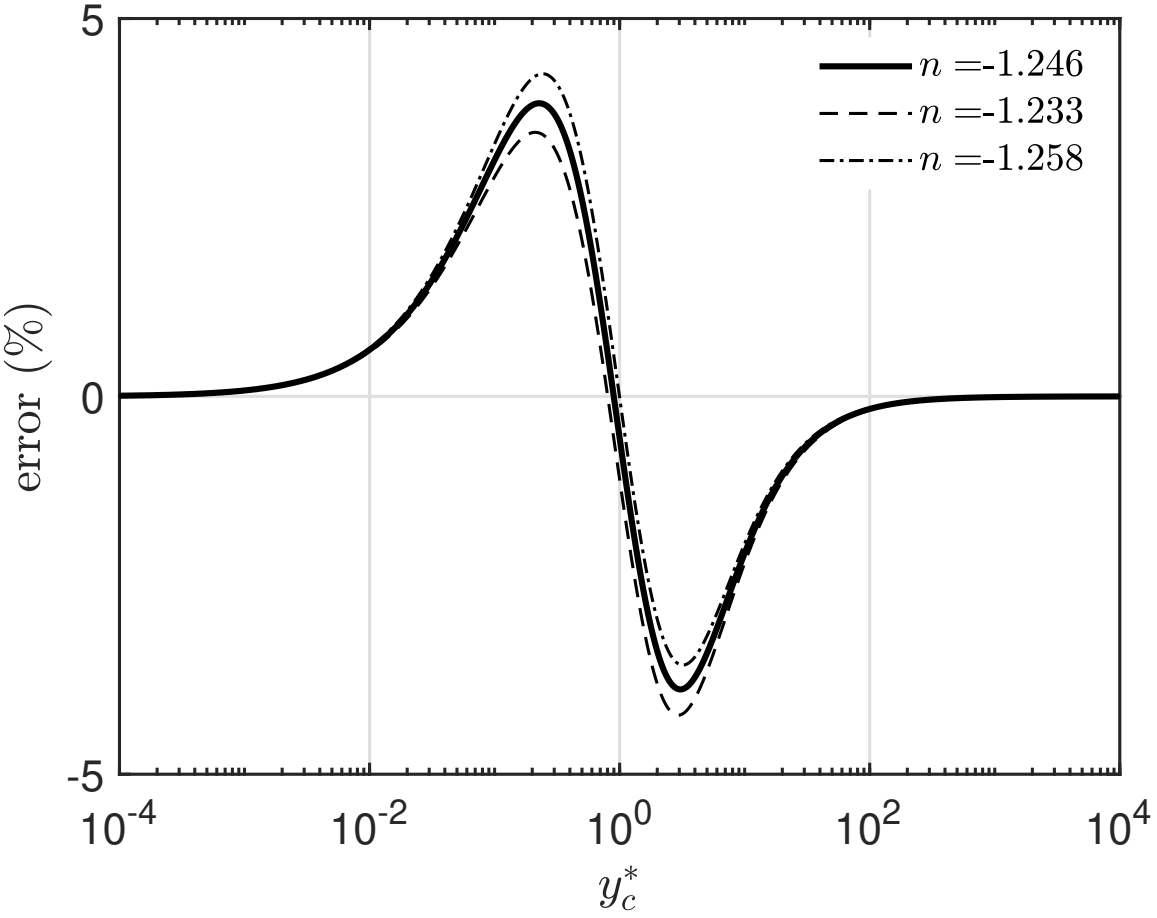

Figure B.2: Blending error for the maximum temperature as a function of y_c^* for exponents n at or near the optimal value

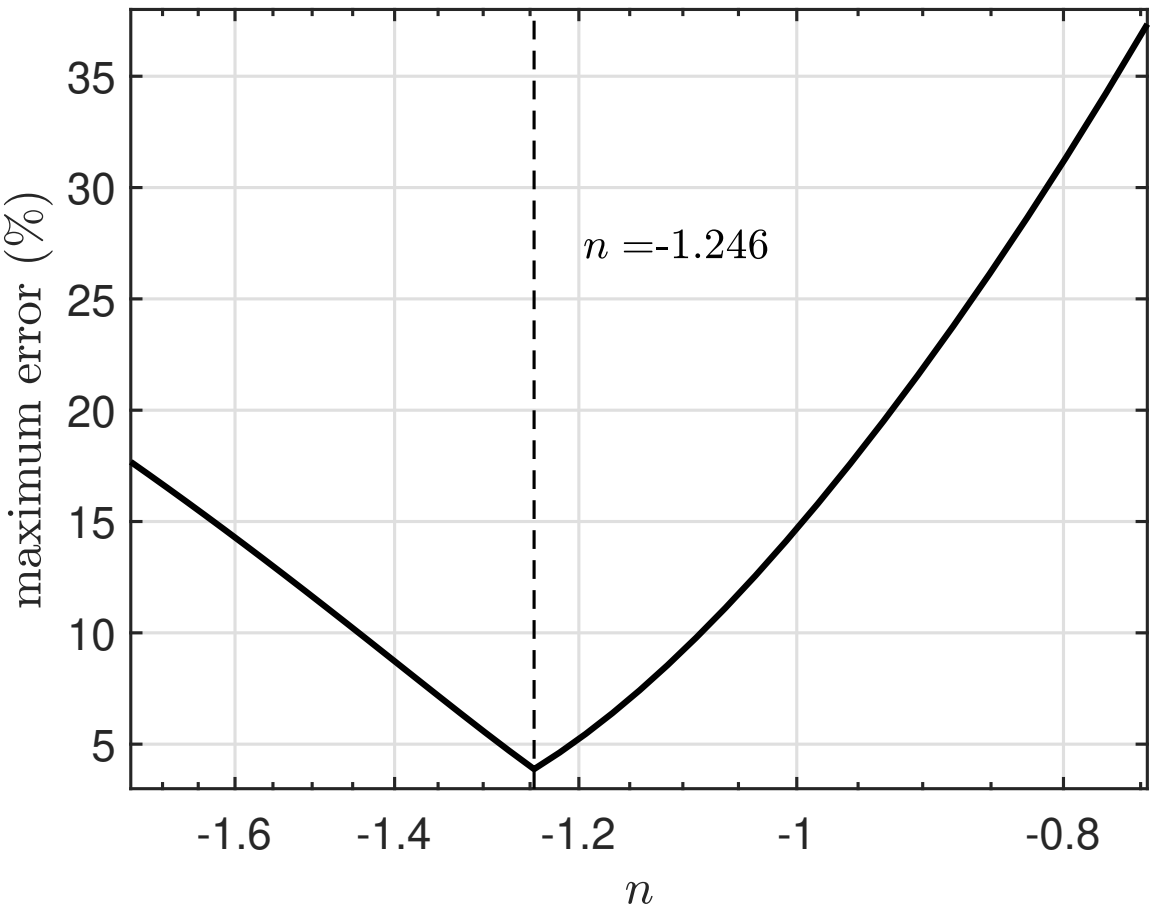

Figure B.3: Maximum blending error for the maximum temperature as a function of blending parameter n

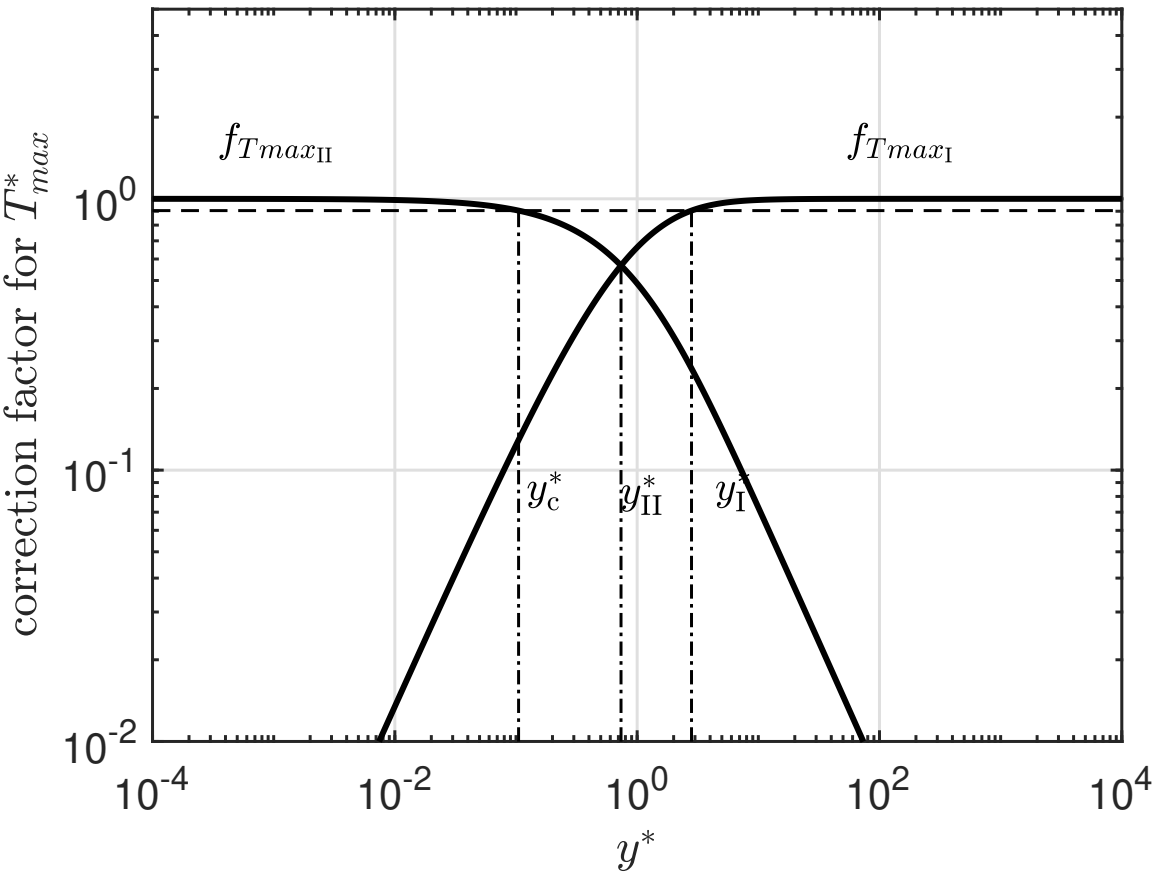

Figure B.4: Correction factors for the maximum temperature

B.2 Asymptotes, error map and correction factors for the gradient of maximum temperature

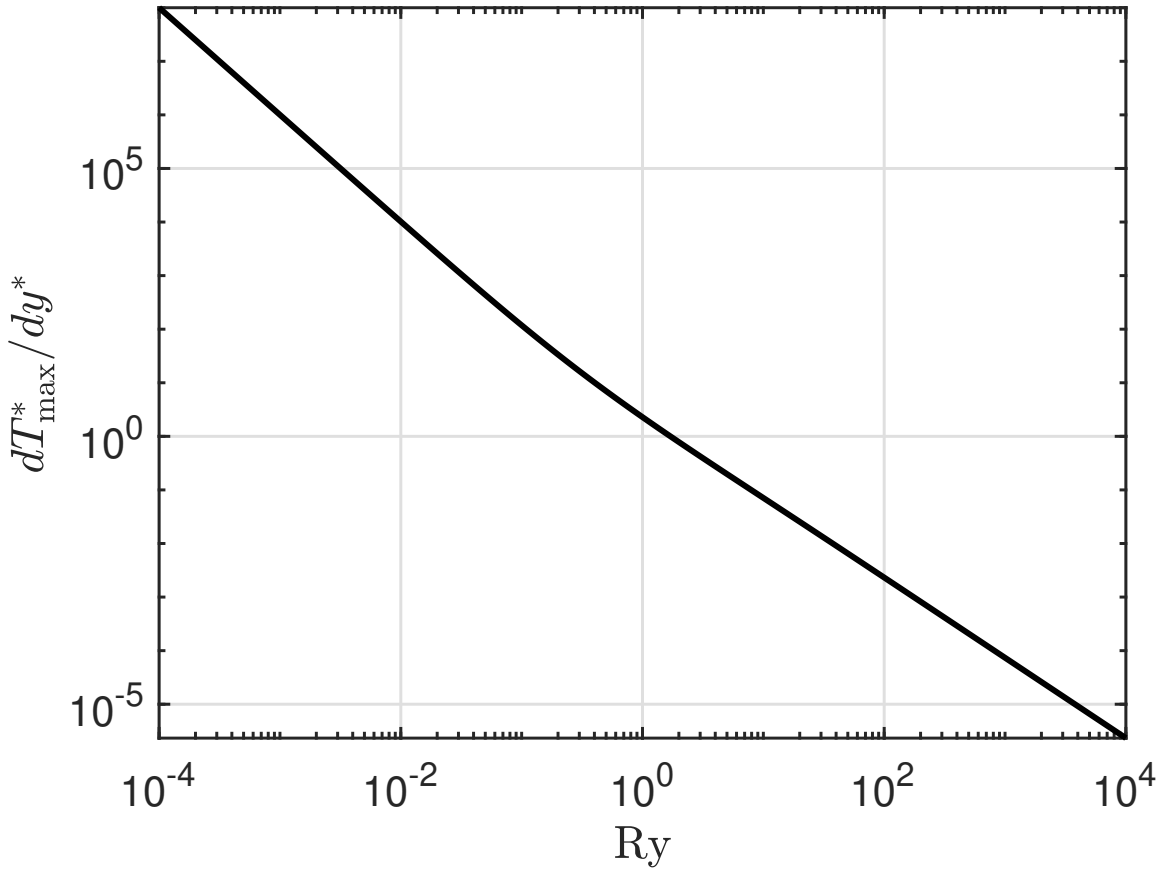

Figure B.5: Dimensionless gradient of maximum temperature as a function of Ry

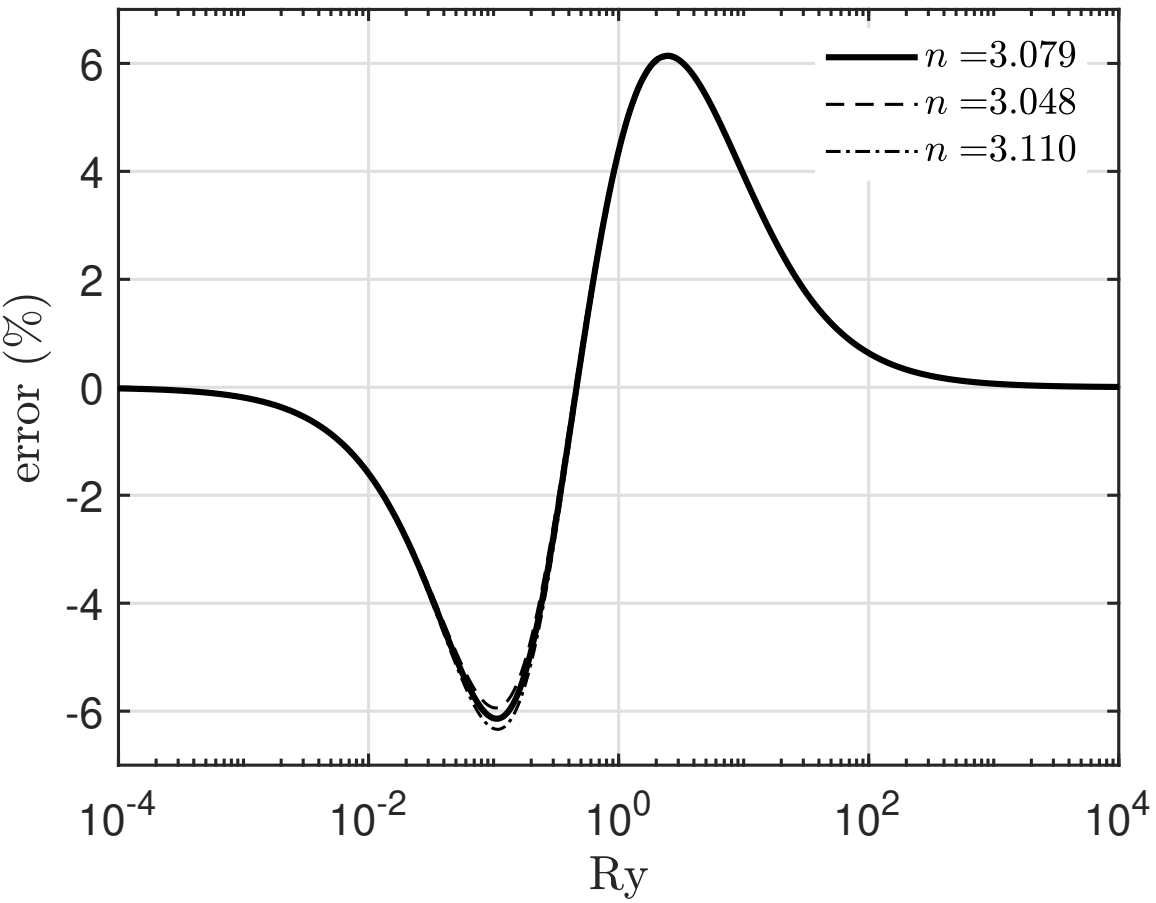

Figure B.6: Blending error for the gradient of maximum temperature as a function of Ry for exponents n at or near the optimal value

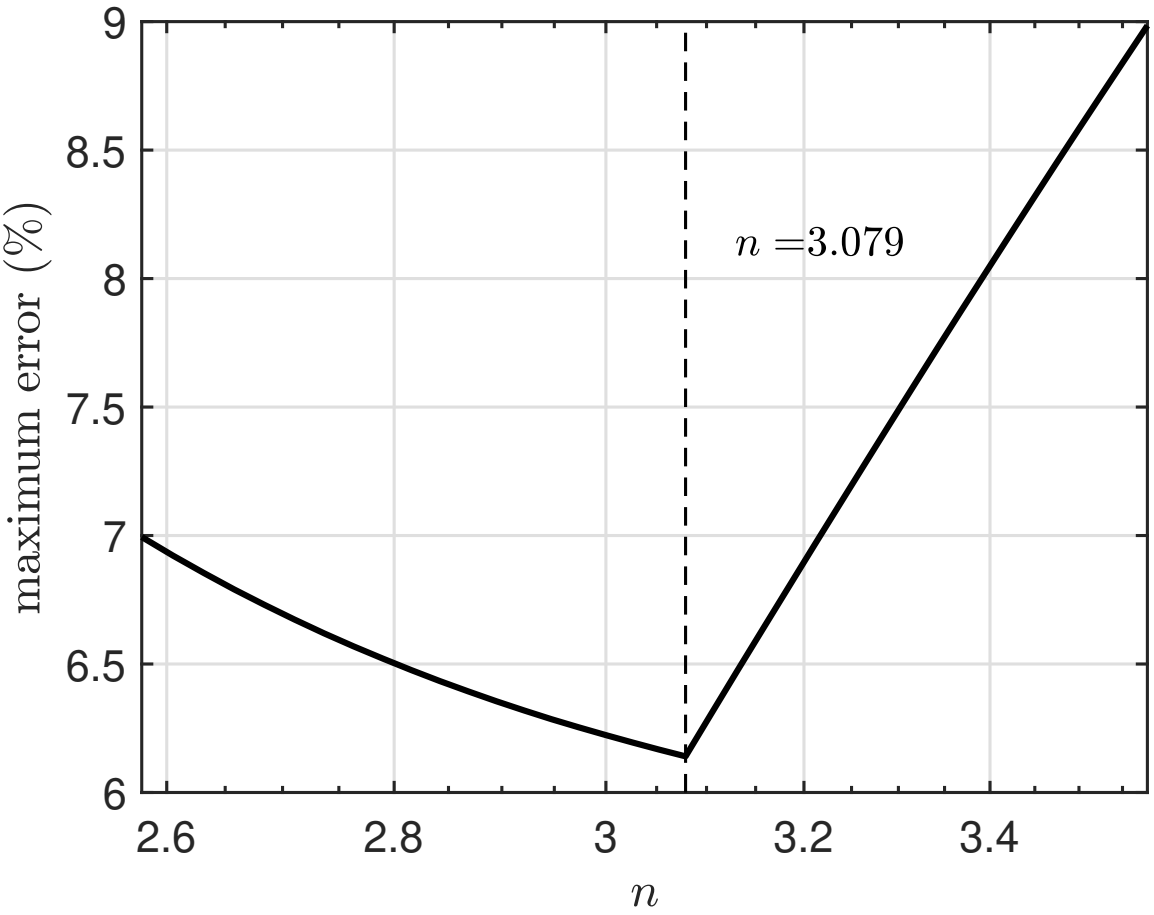

Figure B.7: Maximum blending error for the gradient of maximum temperature as a function of blending parameter n

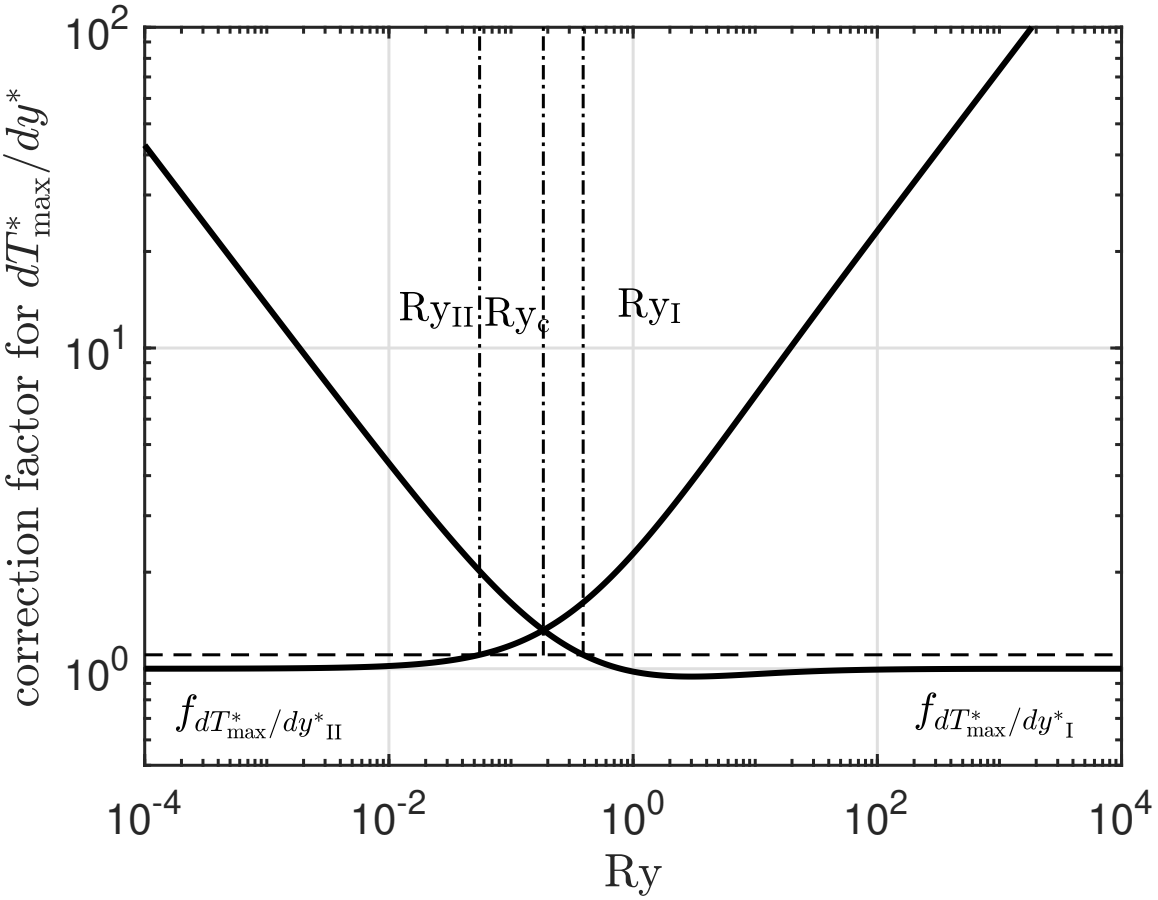

Figure B.8: Correction factors for the gradient of maximum temperature

B.3 Asymptotes, error map and correction factors for aspect ratio of isotherms

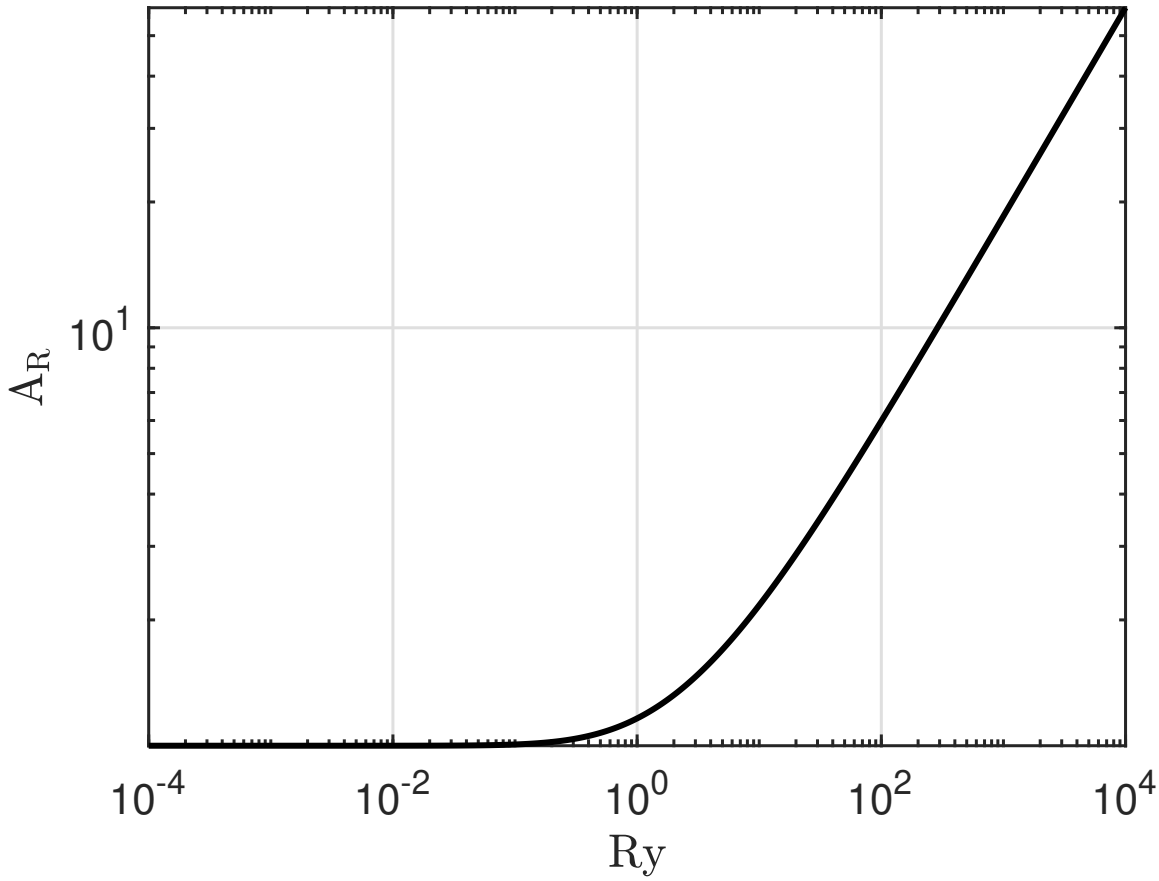

Figure B.9: Aspect ratio of isotherms as a function of Ry

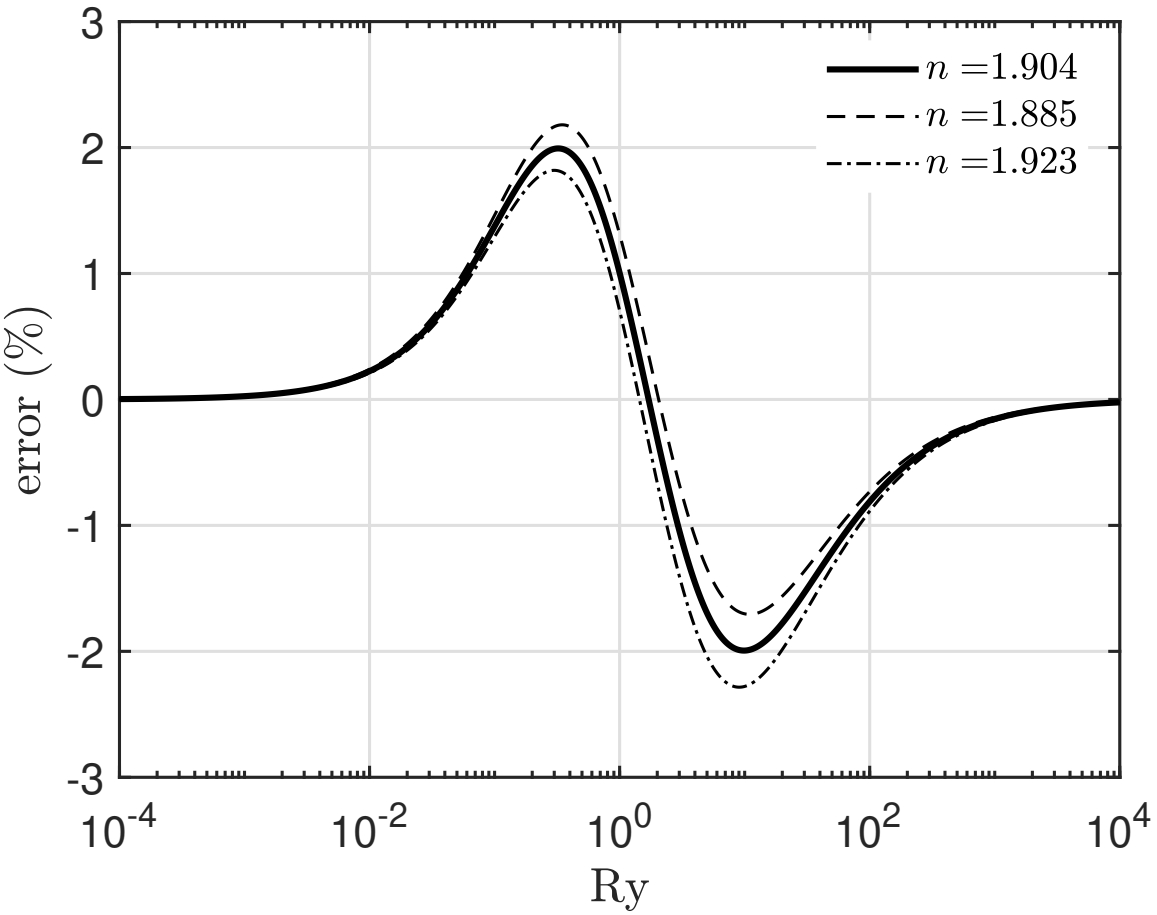

Figure B.10: Blending error for aspect ratio of isotherms as a function of Ry for exponents n at or near the optimal value

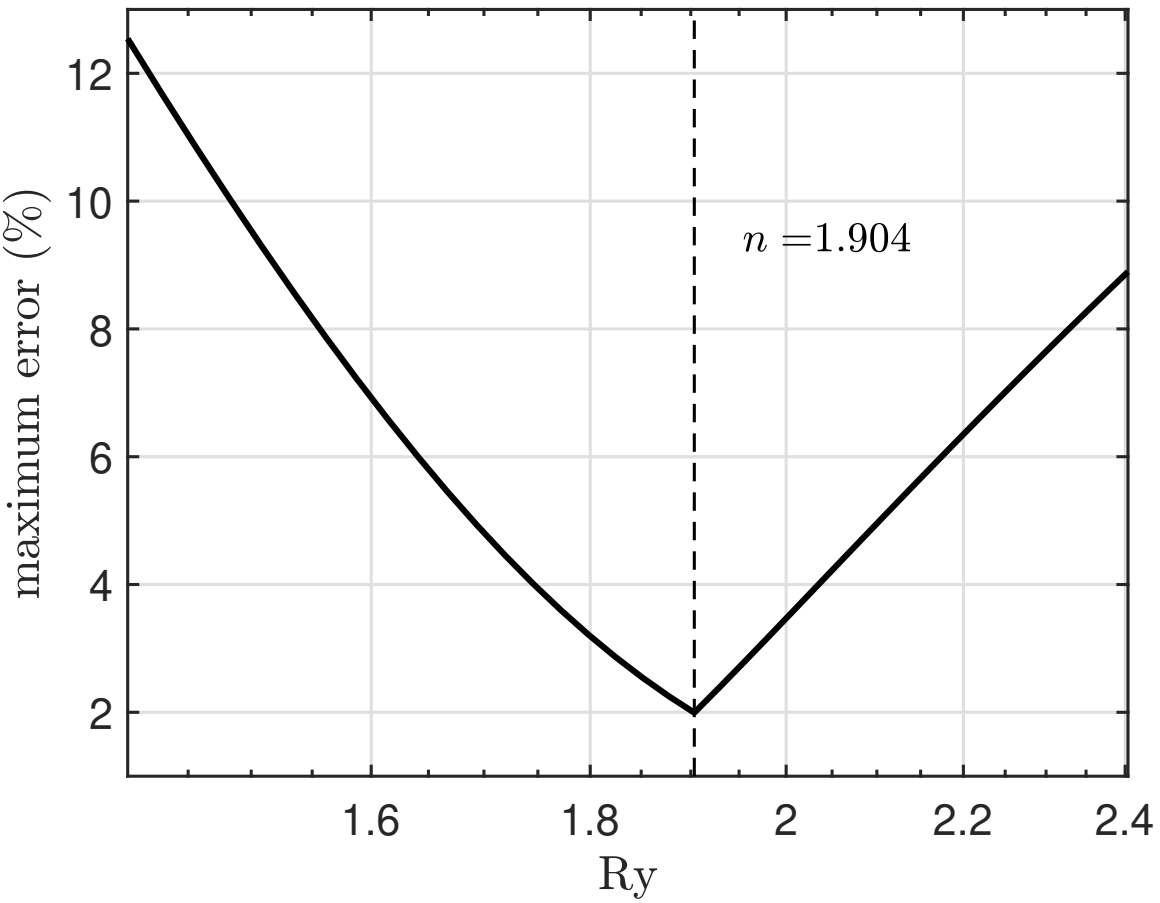

Figure B.11: Maximum blending error for aspect ratio of isotherms as a function of blending parameter n

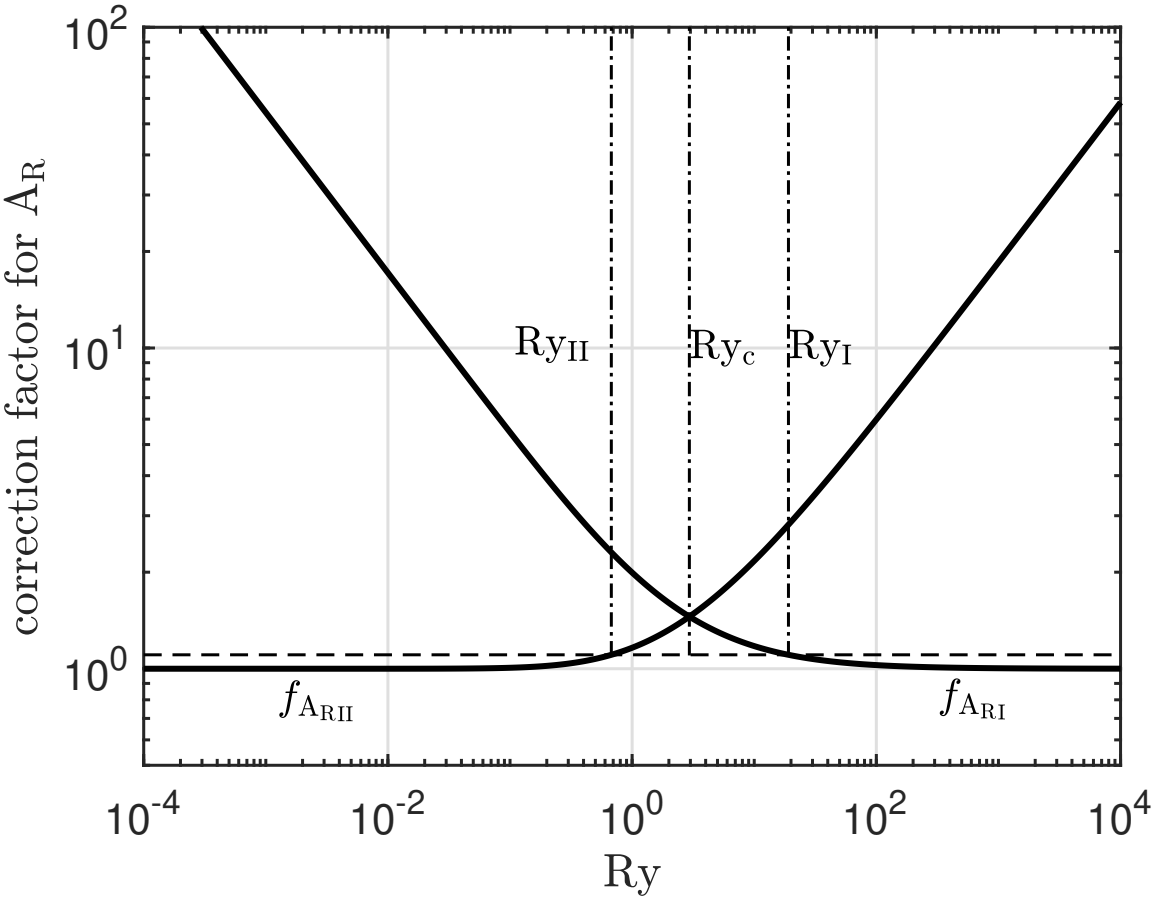

Figure B.12: Correction factors for aspect ratio of isotherms

B.4 Asymptotes, error map and correction factors for melting efficiency

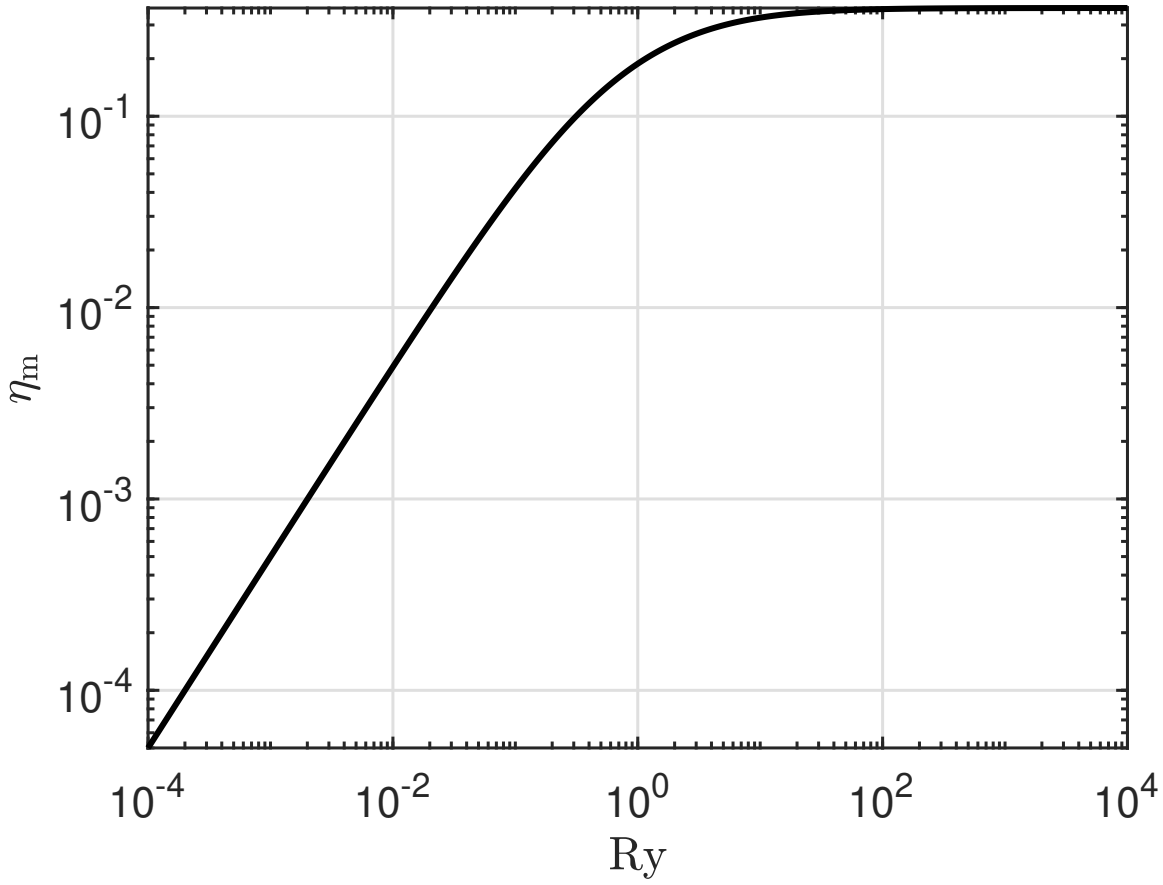

Figure B.13: Melting efficiency as a function of Ry

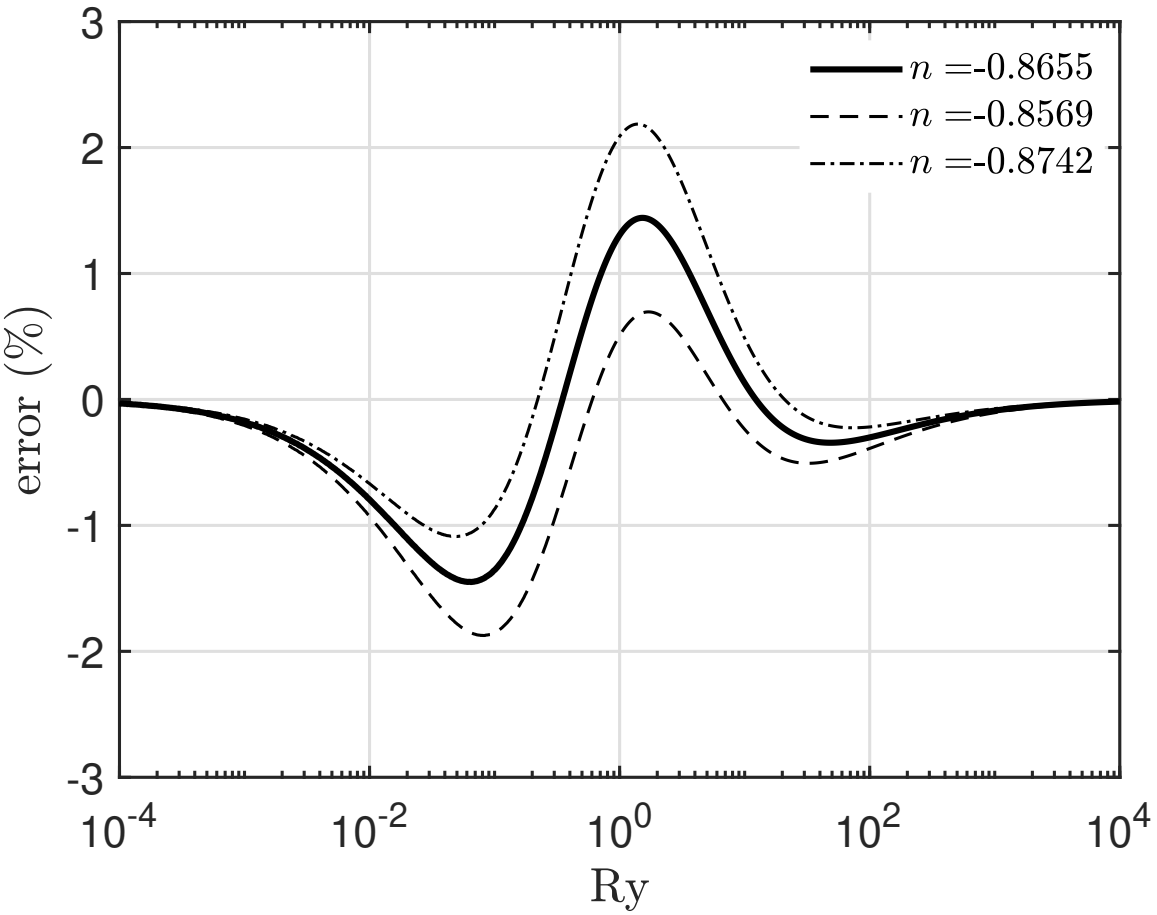

Figure B.14: Blending error for melting efficiency as a function of Ry for exponents n at or near the optimal value

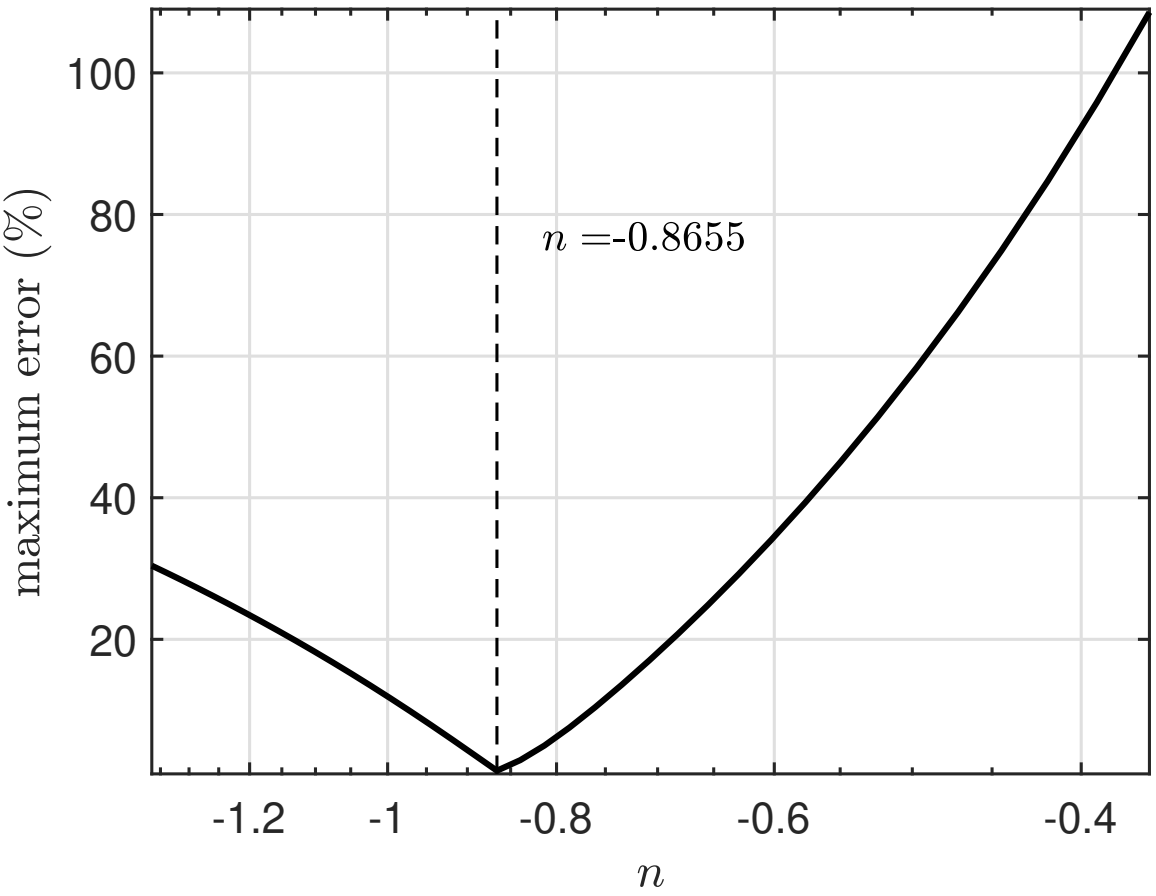

Figure B.15: Maximum blending error for melting efficiency as a function of blending parameter n

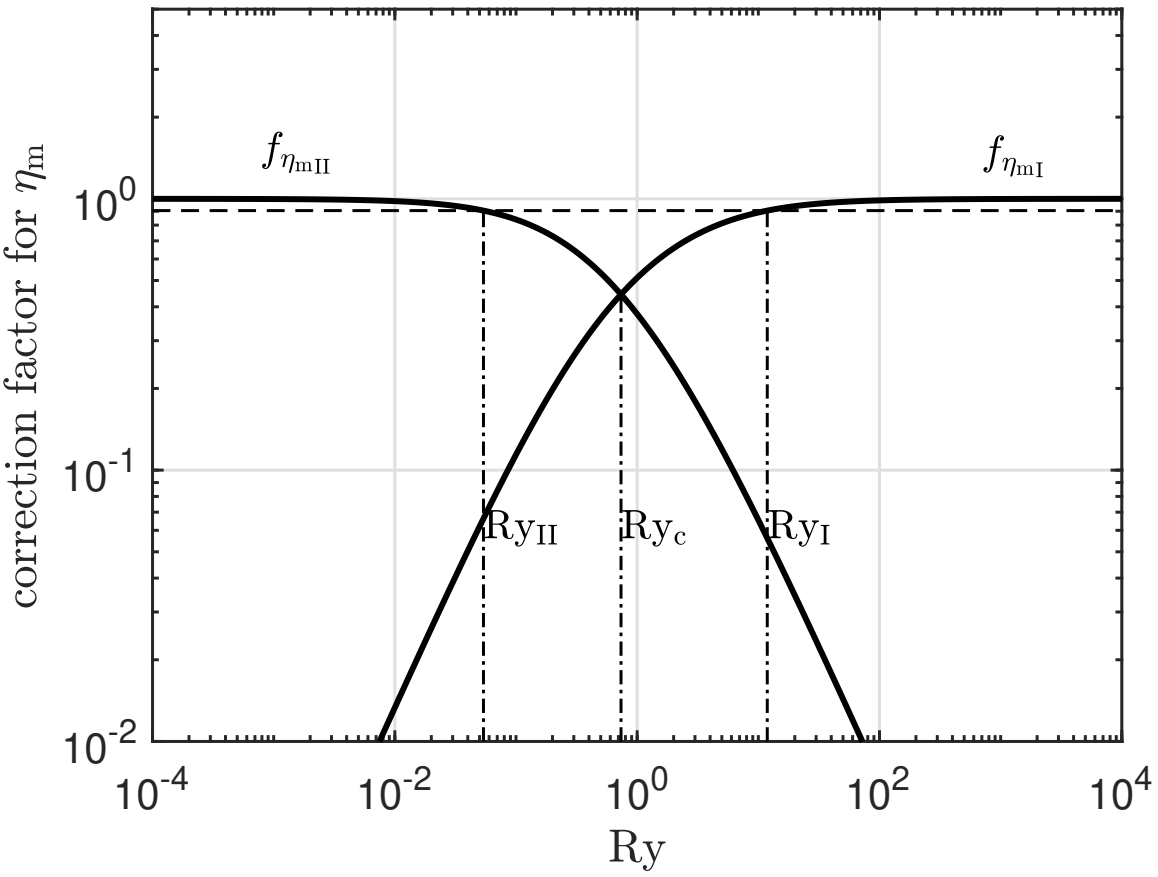

Figure B.16: Correction factors for melting efficiency